

Design, Synthesis, and Reactivity of High-Valent Nickel and Palladium Complexes

by

Nicole Marie Camasso

A dissertation submitted in partial fulfillment
of the requirements for the degree of
Doctor of Philosophy
(Chemistry)
in the University of Michigan
2017

Doctoral Committee:

Professor Melanie S. Sanford, Chair
Professor Kenichi Kuroda
Professor Anne J. McNeil
Professor Nathaniel K. Szymczak

Nicole M. Camasso

camasso@umich.edu

ORCID iD: 0000-0003-3845-1627

© Nicole M. Camasso
2017

For my Grandma Jean

ACKNOWLEDGEMENTS

I am very fortunate to have been surrounded by so many supportive people during my time at the University of Michigan. First and foremost, I would like to thank my advisor, Melanie, for the opportunity to work in her lab and for her constant encouragement and support throughout the past five years. During my first semester of graduate school I took Melanie's Physical Organic Chemistry class and was so impressed with her style of teaching and contagious enthusiasm for chemistry. I knew I wanted to work in her lab, but I was worried I didn't make enough of an impression in her class. Gratefully, Melanie took a chance on the shy student that sat in the back of the lecture hall and allowed me to rotate in the winter semester and ultimately join her lab. Thank you, Melanie, for the opportunity to work on some amazing projects and for recognizing my need for positive reinforcement (even if it wasn't always warranted). I have learned so much from you and I thank you for pushing me to go beyond my comfort zones and become a better person and scientist.

I would also like to thank my dissertation committee members, Prof. Ann McNeil, Prof. Nathaniel Szymczak, and Prof. Kenichi Kuroda. I appreciate all of your suggestions and insight throughout my candidacy, data meeting, and defense. I'd also like to thank Prof. Allan Canty for hosting me at the University of Tasmania during my exchange and for collaborating with us on a number of projects throughout my time here. Jeff Kampf, thank you for solving all of my crystals (even those of the poorest quality) in such a timely manner. Also, I'd like to acknowledge Eugenio Alvarado for helping with so many NMR spectroscopy experiments and analyses.

I would like to acknowledge Prof. Pavel Nagorny for being my rotation advisor during my first semester of grad school. I learned so much about organic chemistry during my time there and I appreciate the opportunity to have worked on such an exciting project. My first mentor, Enoch Mensah, was instrumental in the success of my first semester at U of M. His constant positivity and encouragement helped me to get through all of my classes and difficult sugar separations. His mantra was "whenever things fail, that's when you work harder" and I have always tried to remember that throughout my five years.

When I joined the Sanford lab in the winter of 2013, I was welcomed by a number of great labmates that I continue to look up to and seek advice from. Mónica was assigned as my mentor during my rotation. As a first year graduate student who previously worked on photocatalysis and sugar chemistry, I had no idea how to even isolate a metal complex. Mónica introduced me to organometallic chemistry and taught me important skills that I have used throughout my time in the lab. Even more than that, Mónica took me under her wing and got me through the first two years of grad school. She listened to all of my problems and encouraged me to be a better person. She told me: “If there’s something you don’t like about yourself, then change it.” Mónica, I am forever grateful for everything you’ve done for me and continue to do for me. I am so glad that you’re still always there to listen, to give me advice, and to be a true friend.

To my deskmate Doug: No one truly knows how deep the crazy goes like you. You always knew how to calm me down when I would stress about presentations, sub-group meetings, passing cumes, knocking on Melanie’s door, answering the phone, making a phone call, writing an email...unfortunately the list goes on. Even though I miss our hourly conversations (with topics ranging from man or woman polls to the life and legacy of Paul Walker), I am so glad that we are still in touch. Even though “I’m no Doug” I always try to be. Love, Nicolette Camichi.

I would like to thank a few other mentors and friends that were so helpful throughout my early years in the Sanford Lab and made coming to “work” so much fun. To Rachel, James, Laura, Joe, Christo, Amanda, Ansis, Monica, and Naoko thank you for never hesitating to answer my questions, for never making me feel dumb for asking them, and for being great chemistry role models. Naoko, you are an incredible person who will drop everything you’re doing to help anyone. You are also an amazing friend and I am so glad that we are still close. I’ll “never forget” our great times together over the years.

If MVPs were given out at the end of a PhD mine would go to James Bour. James is one of the smartest and hardest working people I have ever met and I am very fortunate to have worked alongside him. What James lacks in aesthetic skills and simple jack haircuts he makes up for in just about everything else. Thanks for being an all-star cowboy chemist and team nickel leader and for teaching me so much over the years. To my other organometallic subgroup/best subgroup members Devin, Eugene, Liz, and Eric, thank you for your suggestions and constant entertainment. Liz, I am so lucky to have been your mentor. I have learned so much from you that I feel like most of the time you’re mentoring me. I hope you realize how amazing of a chemist, person, and friend you are.

It says a lot when the people you see every day in lab are the same people you want to spend time with outside of lab. In particular, Danielle, BJ, Sharmila, and Courtney you are all amazing friends that I am so lucky to have met. I am forever grateful to you all for being a part of “Team Nicole” and for being constant sources of happiness in my life. I hope there are many reunion cruises in our future.

To my fellow fifth years, Nomaan, Sydonie, Pablo, and Ian, it has been great to go on this journey together. Nomaan, when we first met in Rochester over five years ago I didn’t think we’d become such good friends at Michigan. I will be sending you pictures of sour cream for many years to come.

I would like to acknowledge Andrew, James, Eric, Liz, Courtney, and Christo for reading through chapters of this thesis. Andrew, you are the founding member of team nickel and I am so happy to have you around the lab. I appreciate all of your advice, your great sense of humor, and for providing me with some much needed dog therapy. Christian, you are one of the sweetest people I know and you have been an amazing person to share a bay with over the past few months. To all of the current and past Sanford group members that I have been fortunate enough to share a lab with, thank you for being great people and for helping me to become a better chemist.

I would also like to thank my undergrad advisor Emily McLaughlin who pushed me to apply to graduate school. She believed in my abilities even when I didn’t and continues to be an amazing source of encouragement for me. I have always admired and (still admire) you.

Finally, I would like to dedicate this thesis to my Grandma Jean. Although she never got to see me finish graduate school, I would not have gotten through my first three years here (or the first 25 years of my life) without her love and support. I will never be a Nobel Peace Prize Winner but I hope I have made you proud.

TABLE OF CONTENTS

DEDICATION	ii
ACKNOWLEDGEMENTS	iii
LIST OF SCHEMES	ix
LIST OF FIGURES	xii
LIST OF TABLES	xvi
ABSTRACT	xvii
CHAPTER 1. Introduction	1
1.1. Palladium-Catalyzed Carbon–Carbon and Carbon–Heteroatom Bond-Forming Reactions	1
1.2. High-Valent Organometallic Chemistry of Palladium	3
1.3. Nickel-Catalyzed Carbon–Carbon and Carbon–Heteroatom Bond-Forming Reactions	5
1.4. High-Valent Organometallic Chemistry of Nickel	7
1.5. References	10
CHAPTER 2. Carbon–Heteroatom Bond-Forming Reductive Elimination from Pd^{IV} Complexes	15
2.1. Introduction	15
2.2. Results and Discussion	16
2.2.1. C(sp ³)–O Bond-Forming Reductive Elimination from Pd ^{IV} with Diverse Oxygen Nucleophiles	16
2.2.2. Carbon–Halogen Bond-Forming Reductive Elimination from Pd ^{IV} : Evidence for Re-Oxidative Addition Pathways with Non-Traditional Nucleophiles	33
2.2.3. Exploring the Synthesis and Reactivity of a Model Pd ^{IV} (biphenyl) System	37
2.3. Conclusions	40
2.4. Experimental Procedures and Characterization of Compounds	41

2.4.1. General Procedures and Materials and Methods	41
2.4.2. Synthesis and Characterization of Compounds	42
2.4.3. General Procedures for Mechanistic Experiments.....	55
2.4.4. X-ray Structural Determination	59
2.4.5. Computational Details	61
2.5. References.....	62

CHAPTER 3. Design, Synthesis, and Reactivity of Organometallic Ni^{IV} Complexes..... 66

3.1. Introduction	66
3.2. Results and Discussion	67
3.2.1. Design, Synthesis, and Carbon–Heteroatom Coupling Reactions of Organometallic Ni ^{IV} Complexes	67
3.2.2. Aryl–CF ₃ Bond-Forming Reductive Elimination from Ni ^{IV}	80
3.3. Conclusions	91
3.4. Experimental Procedures and Characterization of Compounds	92
3.4.1. General Procedures and Materials and Methods	92
3.4.2. Synthesis and Characterization of Compounds	93
3.4.3. NMR Oxidation Studies.....	105
3.4.4. Reductive Elimination Studies.....	109
3.4.5. Cyclic Voltammetry Studies.....	116
3.4.6. X-ray Structural Determination	117
3.5. References.....	120

CHAPTER 4. Reactivity Studies of Organometallic Ni^{III} and Ni^{IV} Complexes..... 124

4.1. Introduction	124
4.2. Results and Discussion	125
4.2.1. Carbon–Carbon Coupling Reactions from Diorgano-Ni ^{III} Complexes.....	125
4.2.2. Comparing the Stability, Reactivity, and Selectivity of Ni ^{III} and Ni ^{IV} Complexes in Coupling Reactions	134
4.3. Conclusions	141
4.4. Experimental Procedures and Characterization of Compounds	142
4.4.1. General Procedures and Materials and Methods	142

4.4.2. Synthesis and Characterization of Compounds	143
4.4.3. EPR Studies	147
4.4.4. Cyclic Voltammetry Studies	148
4.4.5. Reactivity Studies	148
4.4.6. X-ray Structural Determination	159
4.5. References.....	160

CHAPTER 5. Investigation of the Accessibility, Reactivity, and Mechanisms of High-Valent Ni and Pd Complexes 163

5.1. Introduction	163
5.2. Results and Discussion	165
5.3. Conclusions	182
5.4. Experimental Procedures and Characterization of Compounds	183
5.4.1. General Procedures and Materials and Methods	183
5.4.2. Synthesis and Characterization of Compounds	184
5.4.3. Cyclic Voltammetry Studies	188
5.4.4. NMR Oxidation Studies	189
5.4.5. Reductive Elimination Studies.....	192
5.4.6. X-ray Structural Determination	200
5.4.7. Computational Details	201
5.5. References.....	203

LIST OF SCHEMES

Scheme 1.1. (a) Low-valent Pd Catalysis (b) Pd-catalyzed Cross-Coupling Reactions	1
Scheme 1.2. (a) High-Valent Pd Catalysis (b) Pd-catalyzed C–H Functionalization Reactions	2
Scheme 1.3. Pd ^{II/IV} -catalyzed (a) C–H iodination (b) Allylic Acetoxylation and (c) Aminoacetoxylation	2
Scheme 1.4. Synthesis and Reactivity of the First Structurally Characterized Pd ^{IV} Complex	3
Scheme 1.5. Pd-catalyzed C–H Acetoxylation via a Proposed Pd ^{IV} Intermediate.....	4
Scheme 1.6. Ni-catalyzed Cross-Coupling Reactions of (a) Tertiary Alkyl Bromides and (b) Aryl Ethers.....	6
Scheme 1.7. Ni-mediated Carbon–Carbon and C–Heteroatom Bond-Forming Reactions via Proposed Ni ^{III} intermediates	8
Scheme 1.8. Examples of Characterized Ni ^{III} Complexes and their Reactivity towards (a) Carbon–Bromine and (b) Carbon–Carbon Bond-Forming Reactions	9
Scheme 2.1. Proposed Mechanism for Pd ^{II/IV} -catalyzed Ligand-directed C–H Functionalization	15
Scheme 2.2. The Design of a Model System for Studying C–O Coupling from Pd ^{IV}	17
Scheme 2.3. Competitive C–N vs. C–F Reductive Elimination from Pd ^{IV}	18
Scheme 2.4. Synthesis and Reactivity of Phenoxide-Ligated Pd ^{IV} Complex 2a	18
Scheme 2.5. Optimized Conditions for the Isolation of Pd ^{II} Product 5a	20
Scheme 2.6. Scope of C–O Bond-Forming Reductive Elimination from Pd ^{IV}	20
Scheme 2.7. Chemoselectivity of Reductive Elimination as a Function of the Cation.....	22
Scheme 2.8. Proposed Mechanism for C(sp ³)–O Bond Formation.....	25
Scheme 2.9. Equilibria and Reaction Pathway for Reductive Elimination from 2d	33
Scheme 2.10. Competitive C–Halogen Reductive Elimination from <i>in situ</i> Generated Complexes 7a-c	34
Scheme 2.11. Proposed Mechanism for the Observed Reactivity Depicted in Scheme 2.10	35
Scheme 2.12. Synthesis of Pd ^{IV} Model System 12	38
Scheme 2.13. Difference in Stability/Reactivity of Model Complexes 3 and 12 Towards C–O Coupling with Acetate and Nitrate as Coupling Partners	39

Scheme 2.14. Reactivity of Diacetate Complex 13	40
Scheme 3.1. Ni-Catalyzed C(sp ³)-H Functionalization via Proposed Ni ^{IV} Intermediate	66
Scheme 3.2. Previous Studies by Hillhouse Demonstrating C-X Coupling via Proposed Ni ^{III} and Ni ^{IV} intermediates	67
Scheme 3.3. Initial Chemical Oxidation Studies with Complex 1	69
Scheme 3.4. Formation of a Detectable Ni ^{IV} Intermediate by the Oxidation of Complex 1 with Umemoto's Reagent	70
Scheme 3.5. Synthesis of the Stable Ni ^{IV} Complex [(Py ₃ CH)Ni ^{IV} (CH ₂ CMe ₂ - <i>o</i> -C ₆ H ₄)(CF ₃)]OTf	72
Scheme 3.6. Reactivity of Complex 6 Towards: (a) C(sp ²)-C(sp ³) Reductive Elimination and (b) C(sp ³)-O Coupling	73
Scheme 3.7. Synthesis of [(Tp)Ni ^{IV} (CH ₂ CMe ₂ - <i>o</i> -C ₆ H ₄)(CF ₃)] (9)	75
Scheme 3.8. Selective C(sp ³)-O, C(sp ³)-S, and C(sp ³)-N bond formation from 9	76
Scheme 3.9. Distinct Reactivity of Ni ^{IV} Complex 9 with Azide as the Nucleophile	77
Scheme 3.10. Targeted Model System for Studying Ar-CF ₃ Coupling from Ni ^{IV}	81
Scheme 3.11. Synthesis of [TpNi ^{IV} (Ph)(CF ₃) ₂] (13) via the Oxidation of 12 with Umemoto's Reagent (Pathway a)	82
Scheme 3.12. Scope of Oxidants for the Formation of 13	83
Scheme 3.13. Reductive Elimination from Complex 13 to Form Benzotrifluoride	84
Scheme 3.14. Rationalizing the Electronic Effect	87
Scheme 3.15. The Reactivity of 13 with NMe ₄ SPh, Demonstrating Pyrazole Lability at Ni ^{IV}	89
Scheme 3.16. Oxidation and Subsequent Aryl-CF ₃ Coupling from (dtbpy)Ni ^{II} Complexes 16 and 17	90
Scheme 4.1. Synthesis of Ni ^{II} Complex 1c	127
Scheme 4.2. The <i>in situ</i> Generation of Ni ^{III} Complexes 2a and 2b	128
Scheme 4.3. One Electron Oxidation Studies of Complex 1c	131
Scheme 4.4. Ni-CF ₃ Bond Homolysis from Unstable Ni ^{III} Intermediate 2c	131
Scheme 4.5. Plausible Decomposition Pathways of Unstable Ni ^{III} Intermediate 2c	132
Scheme 4.6. The Oxidation of 1c with CH ₃ I to Generate Proposed Ni ^{IV} Complex 2c'	132
Scheme 4.7. Thermolysis of Ni ^{III} Complex 2b	133
Scheme 4.8. Reactivity of Ni ^{III} Complex 2a Towards C-C Coupling in the (a) Absence and (b) Presence of the Weak Oxidant Additive, Cp [*] FeBF ₄	134
Scheme 4.9. Synthesis and Isolation of Ni ^{III} Complex 2a and Ni ^{IV} Complex 3a	136
Scheme 4.10. C(sp ³)-C(sp ²) Coupling to form 1,1-dimethyl benzocyclobutane Product 4 from (a) Ni ^{III} Complex 2a and (b) Ni ^{IV} Complex 3a Conducted at 55 °C	137

Scheme 4.11. Selectivity Differences as a Function of Oxidation State Demonstrating Preferential (a) C–O Coupling from 3a and (b) C–C Coupling from 2a in the Presence of Tetramethyl Ammonium Acetate	139
Scheme 4.12. Recent Report by Mirica Demonstrating Low-yielding Benzocyclobutane Formation from an Octahedral Ni ^{III} Center.	140
Scheme 5.1. Synthesis of M ^{II} Precursors (a) K[(Tp)Ni ^{II} (CH ₂ CMe ₂ - <i>o</i> -C ₆ H ₄)] (1-Ni) and (b) NMe ₄ [(Tp)Pd ^{II} (CH ₂ CMe ₂ - <i>o</i> -C ₆ H ₄)] (1-Pd).....	165
Scheme 5.2. Synthesis of TpNi ^{IV} CF ₃ (CH ₂ CMe ₂ - <i>o</i> -C ₆ H ₄) (4-Ni)	170
Scheme 5.3. Synthesis of TpPd ^{IV} CF ₃ (CH ₂ CMe ₂ - <i>o</i> -C ₆ H ₄) (4-Pd).....	170
Scheme 5.4. Stability of 4-Pd towards C–C Reductive Elimination	173
Scheme 5.5. C(sp ³)-heteroatom Coupling from M ^{IV} Complexes 4-Ni/Pd to Form Reductive Elimination Products 6a-e	174
Scheme 5.6. Distinct Reactivity of M ^{II} -alkyl Azides 6e-Ni and 6e-Pd	180

LIST OF FIGURES

Figure 1.1. Proposed Mechanism for Pd ^{II/IV} -catalyzed C–H Functionalization	4
Figure 1.2. (a-b) Commonly Proposed Ni-catalyzed Mechanisms via Ni ⁰ , Ni ^I , Ni ^{II} , and Ni ^{III} Intermediates and (c) Rarely Invoked Ni ^{II/IV} Mechanism.....	7
Figure 1.3. Representative Examples of Structurally-Characterized Ni ^{IV} Complexes	9
Figure 2.1. ORTEP Structure of Reductive Elimination Product 5d	21
Figure 2.2. Job Plot of $\Delta\delta_F \times \chi$ vs. χ at 25 °C, where χ is the mol fraction of Substrate 1	23
Figure 2.3. The Effect of the Cation (Y ⁺) on the ¹⁹ F NMR Chemical Shift of Complex 1 in the Presence of 5 equiv of (a) LiOTf, (b) NaOTf, (c) KOTf, (d) CsOTf (e) NBu ₄ OTf	23
Figure 2.4. Representative EXSY NMR Spectrum of 2a at 15 °C Showing Exchange of Phenoxide Ligand	26
Figure 2.5. Reaction Profile for Reductive Elimination from 2a to form 3a at 35 °C	27
Figure 2.6. The Effect of Water on the Rate of C–O Coupling from 2b	28
Figure 2.7. The Effect of the Counterion on the Rate of C–O Coupling from 2a	30
Figure 2.8. Energy Profile for Reductive Elimination from 2a , Together with Gaussview Diagrams	31
Figure 2.9. Identification of an Equilibrium Between 1d and 2d in the Presence of (a) 1 equiv of NBu ₄ NO ₃ (b) 20 equiv of NBu ₄ NO ₃ and (c) 50 equiv of NBu ₄ NO ₃ at –40 °C	33
Figure 2.10. Monitoring the Reactivity of Complex 7a by ¹ H NMR spectroscopy	35
Figure 2.11. ¹ H NMR Spectra of (a) complex 5d at 25 °C (b) treatment of 5d with 1 equiv of NMe ₄ Cl at 50 °C for 36 h to form complex 8c	37
Figure 2.12. ORTEP Representation of Pd ^{IV} Complex 12b	38
Figure 2.13: (ln[2a]) vs. time plot.....	56
Figure 2.14: Plot of k_{obs} vs. [free ⁻ OPh]. $y = 0.00059 + 0.0014x$, $R^2 = 0.9712$	57
Figure 2.15. Plot of concentration vs. time for reductive elimination from 2a (generated <i>in situ</i>) to form 3a under anhydrous conditions	58
Figure 3.1. Cyclic Voltammogram of (bpy)Ni ^{II} (CH ₂ CM _e ₂ - <i>o</i> -C ₆ H ₄).....	68
Figure 3.2. Computed Natural Atomic Charges for Rh–CH ₃ and Rh–CF ₃ Complexes Illustrating the Unique Electronic Effects of a Trifluoromethyl Group on a Metal System ...	69
Figure 3.3. Synthesis and Cyclic Voltammogram of Ni ^{II} Complex 5	71
Figure 3.4. ORTEP Diagram of Cationic Complex 6	72
Figure 3.5. Evidence for Ligand-Anion Interactions in Complex 6	74

Figure 3.6. ORTEP Diagram of Complex 9	75
Figure 3.7. ¹ H NMR Spectra Showing the Reaction Progress for the Formation of 3,3-dimethyl indoline from Complex 9 and Azide Intermediate 10e after (a) 2 h, 23 °C and (b) 15 h, 23 °C	77
Figure 3.8. ¹⁹ F NMR Spectra Showing the Reaction Progress for the Formation of Ni ^{II} (MeCN) ₂ (CF ₃) ₂ from Complex 9 and Azide Intermediate 10e after (a) 2 h, 23 °C and (b) 15 h, 23 °C	77
Figure 3.9. ORTEP Diagram of Tp ₂ Ni	78
Figure 3.10. Correlation Between Experimental Initial Rates (r ₀) of Reductive Elimination from Complex 9 and Swain-Scott Nucleophilicity Values (n _X)	79
Figure 3.11. Design Features of Model Ni ^{IV} System	80
Figure 3.12. ORTEP Diagram of Complex 13	82
Figure 3.13. Plot of Concentration vs. Time Data for Reductive Elimination from 13-H to Form Benzotrifluoride (Ar-CF ₃) at 55 °C	85
Figure 3.14. Hammett Plot for Reductive Elimination from 13-R	86
Figure 3.15. ¹ H/ ¹ H ROESY Spectrum of 13-OMe at 40 °C Showing No Chemical Exchange Between the Pyrazole Rings on the NMR Time Scale	88
Figure 3.16. ¹⁹ F NMR Resonances of Proposed Complex 15'	89
Figure 3.17. ¹⁹ F NMR Spectrum at -25 °C Showing the Two Signals Assigned to the CF ₃ Resonances of Ni ^{IV} Intermediate 18	90
Figure 3.18. ¹⁹ F NMR Spectra Monitoring the Reaction Progress of 12 in the Presence of CF ₃ I.....	106
Figure 3.19. ¹⁹ F NMR Spectra at -25 °C Showing the Two Signals Assigned to the CF ₃ Resonances of Ni ^{IV} Intermediate 18 via (a) Pathway A; CF ₃ ⁺ Oxidant and (b) Pathway B; Aryl ⁺ Oxidant	107
Figure 3.20. Plot of Concentration versus Time for Reductive Elimination from 9 to form 10a with 5 equiv of NMe ₄ OAc at 50 °C.	109
Figure 3.21. Initial Rates Plot of Concentration versus Time for Reductive Elimination from 9 to form 10a at 50 °C.....	110
Figure 3.22. Plot of ln(r ₀) versus ln([OAc]).....	110
Figure 3.23. Initial Rates Plot of Concentration versus Time for Reductive Elimination from 9 to form 10a at 23 °C	112
Figure 3.24. Hammett Plot for Reductive Elimination from Ni ^{IV} Complexes 13-R to form the Corresponding Ar-CF ₃ Coupled Product at 55 °C	114
Figure 4.1. (a) Kochi Mechanism for Biaryl Coupling and (b) Stoichiometric Studies by Mirica Demonstrating C-C Coupling from <i>in situ</i> -generated Ni ^{III}	124
Figure 4.2. Targeted Model System for Studying C-C Coupling from Isolable Ni ^{III} Complexes.....	126
Figure 4.3. Cyclic Voltammograms of 1a-c in MeCN.	128
Figure 4.4. EPR Spectrum of 2a at 98 K in PrCN:MeCN (3:1)	129

Figure 4.5. Synthesis and ORTEP Structure of Ni ^{III} Complex 2a	130
Figure 4.6. Synthesis and ORTEP Structure of Ni ^{III} Complex 2b	130
Figure 4.7. ¹ H NMR Spectra Providing Evidence for the Formation of Ni ^{IV} -Me Species 2c'	133
Figure 4.8. Cyclic Voltammogram of 1a in MeCN	135
Figure 4.9. Initial Rates Plot for the C–C Coupling Event from 2a and 3a Conducted at 25 °C.	137
Figure 4.10. Cyclic Voltammograms of 1a with NMe ₄ OAc as the Supporting Electrolyte in MeCN.....	138
Figure 4.11. Atomic Point Charges on the Methylene Carbon of Complexes 2a , 2a-Tpm , 3a , 3a-Tpm	141
Figure 4.12. EPR Spectrum of 2a (bottom/blue) and the Simulated Spectrum (top/red).....	147
Figure 4.13. ¹ H NMR Spectrum of the Crude Reaction Mixture after Oxidation of 1c with FcBF ₄	149
Figure 4.14. ¹ H NMR Spectra Showing the Treatment of Complex 1c with FcBF ₄ and MeI, Generating Proposed Ni ^{IV} -Me Complex, 2c' in Both Experiments.....	150
Figure 4.15. (a) ¹ H NMR Spectrum of the Crude Reaction Mixture after Heating 2a at 70 °C for 8 h. (b) ¹¹ B NMR Spectrum of the Ni ^{II} Byproduct NiTp ₂ after Heating for 70 °C for 8 h	152
Figure 4.16. ¹ H NMR Spectrum of the Crude Reaction Mixture after Heating 2a at 70 °C for 8 h with the Additive Cp* ₂ FeBF ₄	153
Figure 4.17. ¹ H NMR Spectra of (a) Unreacted Ni ^{IV} Complex 3a and the Standard 1,3,5- trimethoxybenzene (b) Dimethyl Benzocyclobutane Formation after 5 h at 55 °C	154
Figure 4.18. Plot of Concentration vs. Time Data for the Formation of C–C Coupled Product dimethyl benzocyclobutane from 3a and 2a	155
Figure 4.19. ¹ H NMR Spectra of (a) Unreacted Ni ^{IV} Starting Material 3a (b) the Reaction of 3a with 2 equiv of NMe ₄ OAc after 10 min at rt to Generate 5 (c) Organic Product 6 Formed after 12 h at 23 °C	157
Figure 4.20. ¹ H NMR Spectrum of the Reaction between 2a and 2 equiv of NMe ₄ OAc after 15 h at 70 °C and Treatment with Trifluoroacetic Acid (TFA)	158
Figure 5.1. (a) High-Valent Pd Catalysis and (b) Representative Organometallic Pd ^{III} and Pd ^{IV} Complexes	163
Figure 5.2. (a) High-Valent Ni Catalysis and (b) Representative Organometallic Ni ^{III} and Ni ^{IV} Complexes.....	164
Figure 5.3. Cyclic Voltammograms of M ^{II} Precursors 1-Ni and 1-Pd	166
Figure 5.4. ¹ H NMR Oxidation Studies of 1-Ni with 1 or 2 equiv of AcFcBF ₄ , Generating the Paramagnetic Ni ^{III} Complex 2-Ni or Diamagnetic Ni ^{IV} Complex 3-Ni	168
Figure 5.5. ¹ H NMR Oxidation Studies of 1-Pd with 1 or 2 equiv of AcFcBF ₄	169
Figure 5.6. ¹ H NMR Spectra of 4-Ni and 4-Pd in Acetonitrile- <i>d</i> ₃ , Highlighting the Methylene Protons in Both Complexes	171
Figure 5.7. ORTEP Diagrams of (a) 4-Ni and (b) 4-Pd	172

Figure 5.8. Initial Rate Data for C–C Coupling from Ni ^{IV} –CF ₃ 4-Ni and Cationic Ni ^{IV} 3-Ni to form Benzocyclobutane 5 at 70 °C, Demonstrating Stabilization of the CF ₃ Ligand	173
Figure 5.9. Swain-Scott Plot Relating the Relative Nucleophilicities (n_x) with the Initial Rate of C–Heteroatom Coupling.....	174
Figure 5.10. Eyring Plot for C(sp ³)–heteroatom Coupling from M ^{IV} Complexes 4-Ni and 4-Pd	175
Figure 5.11. Possible S _N 2 Mechanisms for Carbon–Heteroatom Coupling from M ^{IV} Complexes 4-Ni/Pd	177
Figure 5.12. Energy Profiles for the Reaction of Phenoxide with (a) 4-Ni and (b) 4-Pd via a Five-coordinate Intermediate (mechanism A, blue), or Direct Nucleophilic Attack (mechanism B, black).	178
Figure 5.13. Energy Schemes for the Reaction of Thiophenoxide with 4-Ni and 4-Pd via a Five-coordinate Intermediate (pathway A), or Direct Nucleophilic Attack (pathway B). ...	179
Figure 5.14. Energy Profiles Computed for the Formation of Ni ^{II} indolinide Complexes from 6e-Ni via Singlet (blue) and Triplet States (black)	181
Figure 5.15. Transition Structures Computed for Loss of N ₂ from Ni ^{II} Intermediate 6e-Ni and Pd ^{II} Complex 6e-Pd	182
Figure 5.16. CV of 1-Pd in the Absence of Added Pyridine	188
Figure 5.17. CV of 1-Pd with Added Pyridine.	189
Figure 5.18. ¹ H NMR Spectra of 1-Ni and the Treatment of 1-Ni with 1 or 2 equiv of AcFcBF ₄	190
Figure 5.19. ¹ H NMR Spectra of 1-Pd and the Treatment of 1-Pd with 1 or 2 equiv of AcFcBF ₄	191
Figure 5.20. Concentration vs. Time Data for Reductive Elimination of 4-Ni to form 5	192
Figure 5.21. Concentration vs. Time Data for the Reductive Elimination of 4-Pd to form 6a-Pd in the Presence of 1.2, 2.5, 5, and 10 equiv of NMe ₄ OPh.....	194
Figure 5.22. (ln[OPh]) vs. (ln[r ₀]) Plot.....	194
Figure 5.23. Concentration vs. Time Data for Reductive Elimination from 4-Pd to Form 6a-Pd	195
Figure 5.24. Concentration vs. Time Data for Reductive Elimination from 4-Pd to Form 6b-Pd	196
Figure 5.25. Concentration vs. Time Data for Reductive Elimination from 4-Pd to Form 6c-Pd	196
Figure 5.26. Concentration vs. Time Data for Reductive Elimination from 4-Pd to Form 6d-Pd	196
Figure 5.27. Concentration vs. Time Data for Reductive Elimination from 4-Pd to Form 6e-Pd	197
Figure 5.28. Plot of Nucleophilicity Parameters vs. Initial Rate of C–X Coupling from 4-Pd to Form 6a-e-Pd	198

LIST OF TABLES

Table 1.1. Estimated Prices of Group 10 Metal Salts and Metal–Carbon Bond Dissociation Energies (BDE) in $L_2(X)M^{II}-CH_3$ Complexes	6
Table 2.1. Product Distribution of C–O and C–F Reductive Elimination from 1 as a Function of Cation	24
Table 2.2. Summary of Experimental Mechanistic Data for Reductive Elimination from Complexes 2a-c to form 3a-c	25
Table 2.3. Summary of DFT Data for Reductive Elimination from 2a-c	32
Table 2.4. Chemical Shift Data for Job Plot at 25 °C	55
Table 2.5. Selected Bond Lengths (Å) and Angles (°) for 3d	60
Table 2.6. Selected Bond Lengths (Å) and Angles (°) for 12b	61
Table 3.1. Reductive Elimination from Ni^{IV} Complexes 13-R at 55 °C	84
Table 3.2. Nucleophilicity Parameters and Initial Rate Values for C–X Bond-Formation Reactions from Complex 9 to form 10a-e	113
Table 3.3. Summary of Kinetic Data for Reductive Elimination from Complexes 13-R at 55 °C	114
Table 3.4. Comparison of Ar–CF ₃ Yields from the Reductive Elimination of 13 in the Absence and Presence of Radical Traps	115
Table 3.5. Selected Bond Lengths (Å) and Angles (°) for 6	118
Table 3.6. Selected Bond Lengths (Å) and Angles (°) for 9	119
Table 4.1. Selected Bond Lengths (Å) and Angles (°) for 2a	160
Table 5.1. Activation Parameters for C(sp ³)–O coupling from 4-Ni and 4-Pd	176
Table 5.2. Nucleophilicity parameters and Initial Rate Values for C–X Bond-Formation Reactions from Complex 4-Pd to Form 6a-e-Pd	197
Table 5.3. Eyring Plot Data for the Reductive Elimination of 4-Ni to Form 6a-Ni	199
Table 5.4. Eyring Plot Data for the Reductive Elimination of 4-Pd to Form 6a-Pd	200
Table 5.5. Selected Bond Lengths (Å) and Angles (°) for 4-Pd	201

ABSTRACT

Fundamental organometallic studies at well-defined metal centers provide important insight into the reactivity and selectivity profiles of catalytically relevant systems. Of particular interest are high oxidation state nickel and palladium complexes (i.e. Pd^{IV}, Ni^{IV}, Ni^{III}). These species have been implicated as reactive intermediates in a variety of catalytic transformations including C–H bond functionalization, alkene difunctionalization, and carbon-carbon coupling reactions. However, the transient nature of these intermediates has hindered definitive characterization and confirmation of their roles in catalysis. Ultimately, a fundamental understanding of catalytically relevant organometallic complexes will inform the optimization of known transformations and the development of new catalytic reactions. This thesis describes the design, synthesis, and isolation of high-valent nickel and palladium complexes and studies of their reactivity towards challenging bond-forming reactions.

Chapter 1 describes in detail the roles of palladium and nickel catalysts in carbon–carbon and carbon–heteroatom bond-forming reactions, as well as the relevant history and precedent for the work detailed herein.

Chapter 2 is focused on reactivity studies of well-defined Pd^{IV} complexes supported by bipyridines and cyclometallated carbon-donor ligands. These design strategies enable the direct study of C(sp³)–heteroatom bond-forming reductive elimination from Pd^{IV}. We demonstrate that a diverse set of oxygen nucleophiles participate as coupling partners in C(sp³)–O coupling from Pd^{IV} and that cationic additives play an important role in the chemoselectivity of competing C(sp³)–O and C(sp³)–F bond-forming reactions. Experimental

and computational studies provide insight into the mechanism of these reductive elimination reactions.

Chapter 3 details our systematic investigation into the organometallic chemistry of high-valent nickel. We demonstrate that a series of isolable Ni^{IV} complexes can be accessed by the treatment of Ni^{II} precursors with common two-electron oxidants. The importance of the trifluoromethyl (CF₃) ligand and tris(pyrazolyl)borate (Tp) scaffold in stabilizing these traditionally transient species is highlighted. Furthermore, reactivity studies show that these Ni^{IV} complexes participate in highly selective carbon–carbon and carbon–heteroatom bond-forming reactions that remain extremely challenging to achieve at lower oxidation states of nickel.

In Chapter 4, the reactivity profiles of diorgano-Ni^{III} complexes are evaluated and compared to the Ni^{IV} counterparts. Throughout these studies, Ni^{IV} was shown to promote reductive elimination events more readily than analogous Ni^{III} complexes. In addition, selective carbon–carbon or carbon–heteroatom coupling could be achieved depending on the oxidation state of the nickel center.

Finally, Chapter 5 details a comparative study between high-valent nickel and palladium complexes. Electrochemical analyses, kinetic studies, and computational insights demonstrate the remarkable similarities in the chemistry of Ni^{IV} and Pd^{IV}, but an enhanced role for Ni^{III} in enabling reactivity that is distinct from palladium.

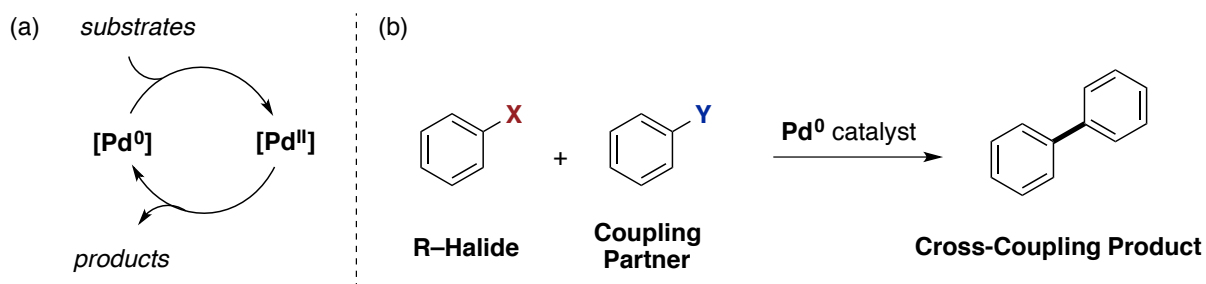
CHAPTER 1

Introduction

1.1. Palladium-Catalyzed Carbon–Carbon and Carbon–Heteroatom Bond-Forming Reactions

The selective formation of carbon–carbon and carbon–heteroatom bonds is an essential chemical transformation in organic synthesis. Over the past several decades, transition metal-catalyzed reactions that utilize palladium catalysts have served as one of the most powerful and reliable methods for achieving these bond connections.¹ The vast majority of Pd-catalyzed cross-coupling reactions involve Pd^{0/II} catalytic cycles (low-valent Pd catalysis, Scheme 1.1).¹ This area of research has been the subject of more than four decades of development and mechanistic study, culminating in the 2010 Nobel Prize in Chemistry.²

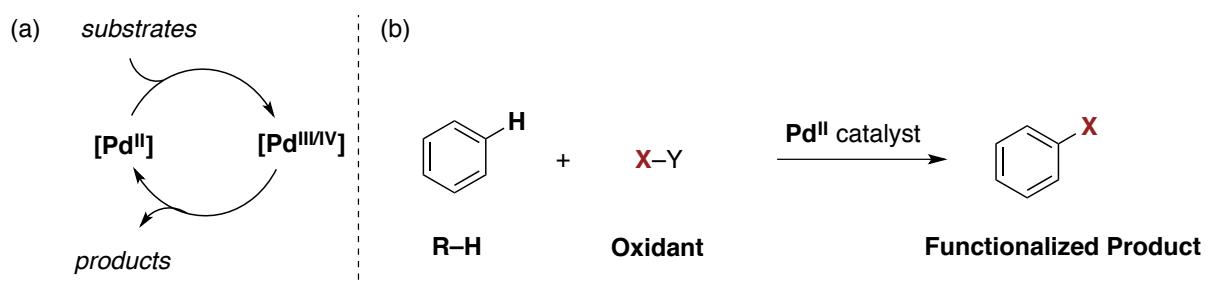
Scheme 1.1. (a) Low-valent Pd Catalysis (b) Pd-catalyzed Cross-Coupling Reactions



Despite the ubiquity and synthetic importance of low-valent Pd catalysis, certain classes of transformations have yet to be realized through the Pd^{0/II} manifold. Reactions such as C(sp³)–heteroatom and C–CF₃ bond-formation remain prohibitively challenging through low-valent Pd mechanisms.^{3–5} In these reactions, high kinetic barriers to reductive elimination are thought to impede efficient catalysis. These limitations to the remarkable scope of Pd^{0/II} cross-

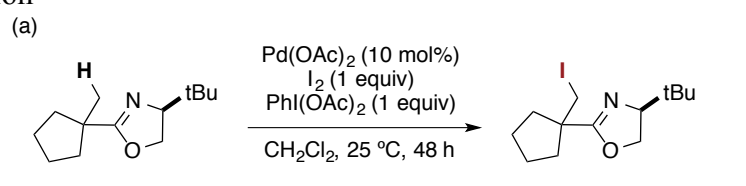
coupling reactions have driven the field of high-valent Pd catalysis, which involve Pd intermediates in the +3 and/or +4 oxidation state (Scheme 1.2).⁶ Reductive elimination from these species generally has a high thermodynamic driving force and relatively low activation barrier.⁷ Consequently, the rate of reductive elimination from high-valent Pd centers is often faster than analogous transformations at low-valent Pd.⁸ This leads to a broader scope of viable coupling reactions as well as different mechanisms and selectivities.^{9,10} As a result, high-valent Pd catalysis has emerged as a highly complementary method to low-valent Pd catalysis in terms of both substrate scope and the types of bonds that can be formed.

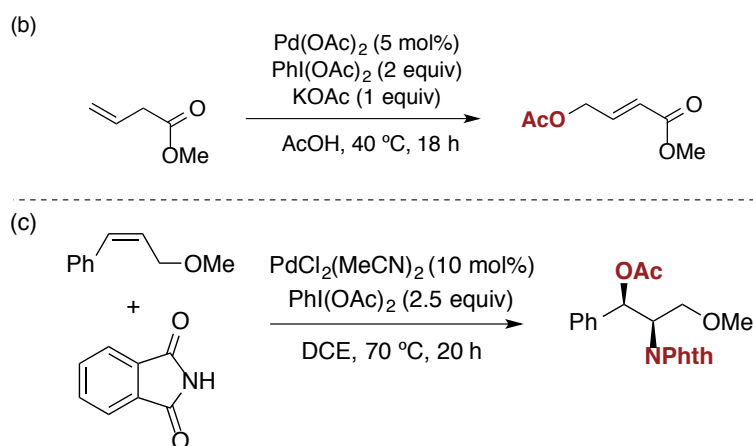
Scheme 1.2. (a) High-Valent Pd Catalysis (b) Pd-catalyzed C–H Functionalization Reactions



The unique reactivity and selectivity of high-valent Pd intermediates have increasingly been recognized and exploited in catalysis.^{6,11} In particular, carbon–carbon and carbon–heteroatom bond-forming reductive elimination from transient Pd^{IV} species is commonly proposed as the product forming step in Pd^{II/IV} catalyzed reactions, including C–H functionalization,¹² allylic acetoxylation,¹³ and alkene difunctionalization¹⁴ (Scheme 1.3a-c). While low-valent Pd catalysts dominated early developments of cross-coupling reactions, the emergence of high-valent Pd catalysis has led to unique transformations that were previously inaccessible from more traditional Pd centers.¹⁵

Scheme 1.3. Pd^{II/IV}-catalyzed (a) C–H iodination (b) allylic acetoxylation and (c) aminoacetoxylation

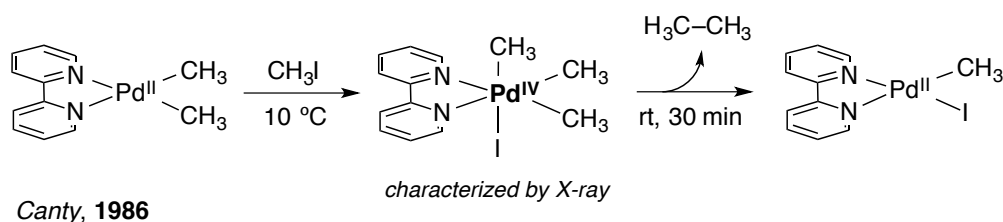




1.2. High-Valent Organometallic Chemistry of Palladium

Fundamental organometallic studies of well-defined Pd^{IV} and Pd^{III} complexes have provided insight into the reactivity profiles and mechanistic pathways of catalytically-relevant Pd intermediates.^{9,10,16} In 1986, Canty reported the first example of a structurally characterized Pd^{IV} complex [(bpy)Pd^{IV}(CH₃)₃I] (bpy = 2,2'-bipyridine), which was accessed by the net two-electron oxidation of a Pd^{II} precursor with methyl iodide (Scheme 1.4).^{16b} This complex underwent rapid carbon–carbon reductive elimination to release ethane, demonstrating the competency of Pd^{IV} in mediating important bond-forming reactions.

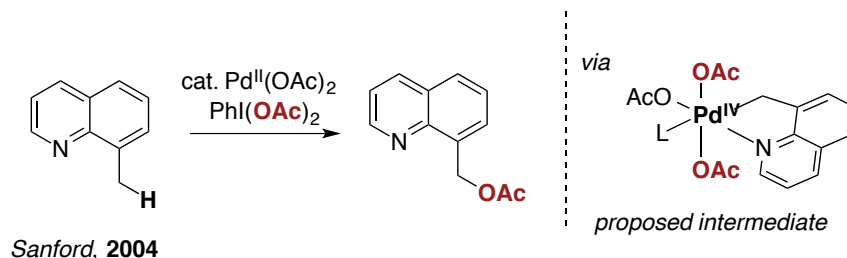
Scheme 1.4. Synthesis and Reactivity of the First Structurally Characterized Pd^{IV} Complex



After this seminal discovery, the field of high-valent Pd catalysis did not greatly advance until almost twenty years later. The renaissance of Pd^{III/IV} catalysis in the mid-2000s is largely attributed to the development of ligand-directed C–H functionalization reactions.^{6,11,12} These reactions convert ubiquitous C–H bonds into functionalized products in

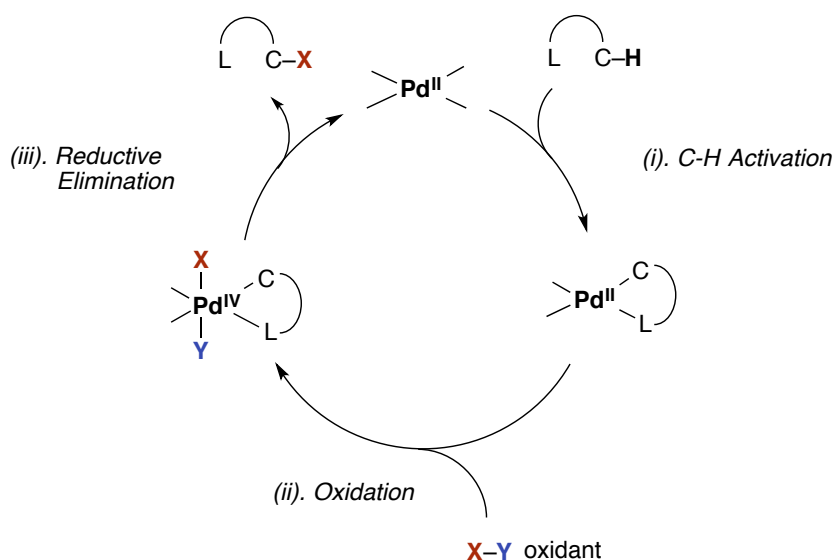
the presence of a directing group, a terminal oxidant, and a Pd^{II} catalyst (representative example shown in Scheme 1.5).¹⁷

Scheme 1.5. Pd-catalyzed C–H acetoxylation via a Proposed Pd^{IV} Intermediate



The rapid development of high-valent palladium catalysis in recent years has been accompanied by extensive systematic investigations of reaction mechanisms at well-defined Pd^{IV} centers.^{16,18} These studies have provided support for the following mechanism for Pd^{II/IV}-catalyzed C–H functionalization: (i) ligand-directed C–H activation at a Pd^{II} center; (ii) the two-electron oxidation of Pd^{II} to Pd^{IV} in the presence of a terminal oxidant (X–Y); and (iii) C–X bond-forming reductive elimination from the Pd^{IV} center, regenerating Pd^{II} and releasing the functionalized product (where X = carbon, heteroatom).

Figure 1.1. Proposed Mechanism for Pd^{II/IV}-catalyzed C–H Functionalization



Stoichiometric studies by our lab, Canty,^{9a,b,16b,d,19} Vedernikov,^{9f,16l,20} Mirica,^{16n,p,21} Ritter,^{10,15c,18a,22} and others have provided insight about the scope of oxidants capable of

accessing Pd^{IV}, the ability of these species to participate in carbon–carbon and carbon–heteroatom coupling reactions, and the mechanistic profiles of these transformations. In particular, the two-electron oxidation of Pd^{II} to Pd^{IV} with a number of catalytically-relevant oxidants (i.e., alkyl halides, hypervalent iodine reagents, electrophilic halogenating reagents) has been well-documented.⁹ Moreover, it has been demonstrated that reductive elimination from Pd^{IV} often proceeds with high selectivity for C(sp³)–X (X = heteroatom) bond-formation over competing C(sp²)–X coupling, which contrasts with the selectivity typically observed at Pd^{II} centers.^{9,16s} Overall, fundamental organometallic studies have led to tremendous advancements in the field of Pd-catalyzed cross-coupling, providing mild and complementary access to important bond formations that remain challenging to achieve at low-valent Pd centers.

Chapter 2 of this thesis is focused on the systematic investigation of C(sp³)–heteroatom bond-forming reductive elimination from well-characterized Pd^{IV} centers, with a focus on the scope, selectivity, and mechanism of these transformations.²³

1.3. Nickel-Catalyzed Carbon–Carbon and Carbon–Heteroatom Bond-Forming Reactions

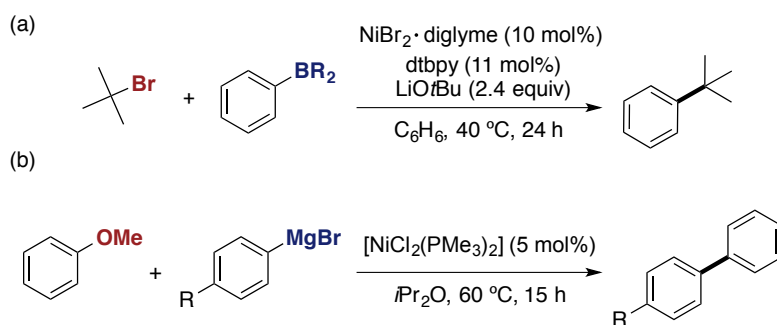
Over the past decade, tremendous progress has been made in the field of nickel catalysis.²⁴ For one, nickel catalysts offer the advantage of being more sustainable and cost-effective than their palladium analogues (Table 1).²⁵ Nickel can also readily perform many of the same elementary reactions as palladium (i.e., oxidative addition and reductive elimination). However, the fundamental properties of nickel have enabled its use as an effective catalyst for a variety of challenging bond-forming reactions, including transformations that are not accessible with palladium systems.²⁴

Table 1.1. Estimated Prices of Group 10 Metal Salts and Metal–Carbon Bond Dissociation Energies (BDE) in $L_2(X)M^{II}-CH_3$ Complexes

MCl_2	Price (USD/mmol)	Bond	BDE (kcal/mol)
NiCl ₂	0.1	Ni–C	38–51
PdCl ₂	5.8	Pd–C	48–55
PtCl ₂	32.2	Pt–C	61–66

As a first-row transition metal, it is anticipated that organonickel complexes are most reactive among the platinum group metals (Table 1.1).^{26,27} Moreover, while palladium and platinum complexes generally prefer two-electron processes (with M^{III} intermediates¹⁰ being less common), nickel species readily undergo single electron transfer reactions.²⁴ The reactivity of nickel species is therefore enriched (and also complicated) by the availability of the Ni^I and Ni^{III} states as well as the possible involvement of outer-sphere radical processes. These characteristics have enabled unique cross-coupling reactions that utilize tertiary alkyl halides²⁸ and phenol derivatives as electrophiles²⁹ (Scheme 1.6).

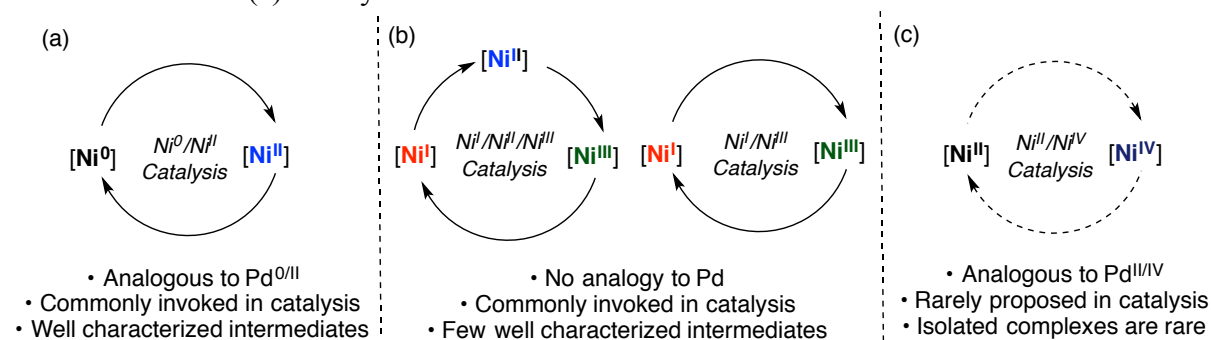
Scheme 1.6. Ni-catalyzed Cross-Coupling Reactions of (a) Tertiary Alkyl Bromides and (b) Aryl Ethers



Mechanistic studies have shown that Ni-catalyzed reactions can occur via organometallic Ni^0 , Ni^I , Ni^{II} , and Ni^{III} intermediates (Figure 1.2a-b).²⁴ These pathways have enabled transformations such as the reductive coupling of alkynes,³⁰ the cross-coupling of alcohols,³¹ and photocatalytic bond-forming reactions.²⁴ⁱ In marked contrast, the accessibility of Ni^{IV} in catalysis has not been established (Figure 1.2c). A few reports³² have proposed the

intermediacy of Ni^{IV} , for example in Ni-catalyzed C–H functionalization. However, the transient nature of these species has hindered characterization and confirmation of their mechanistic roles.

Figure 1.2. (a-b) Commonly Proposed Ni-catalyzed Mechanisms via Ni^0 , Ni^{I} , Ni^{II} , and Ni^{III} Intermediates and (c) Rarely Invoked $\text{Ni}^{\text{II/IV}}$ Mechanism

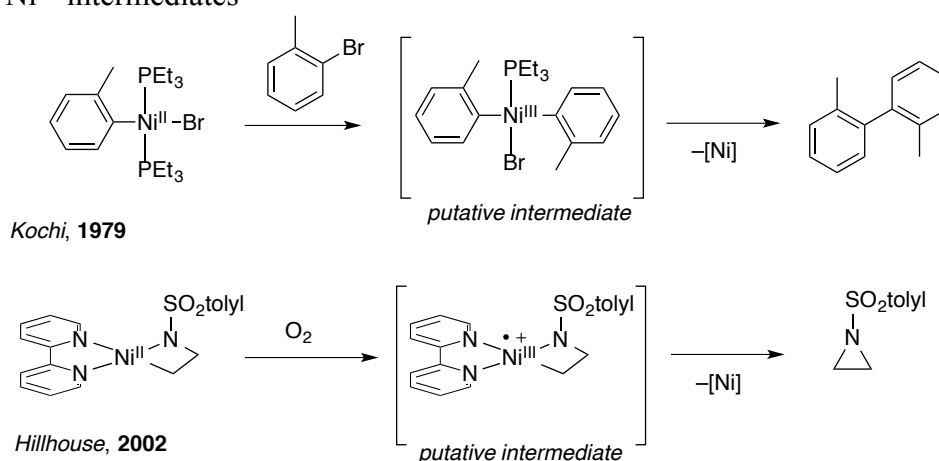


Although the field of nickel catalysis has rapidly expanded over the past decade, challenges in controlling or predicting the operative pathways remain. It is anticipated that systematic studies of organometallic Ni complexes will facilitate mechanistic understanding and ultimately aid in the development of new transformations that promote even more difficult bond-forming reactions.

1.4. High-Valent Organometallic Chemistry of Nickel

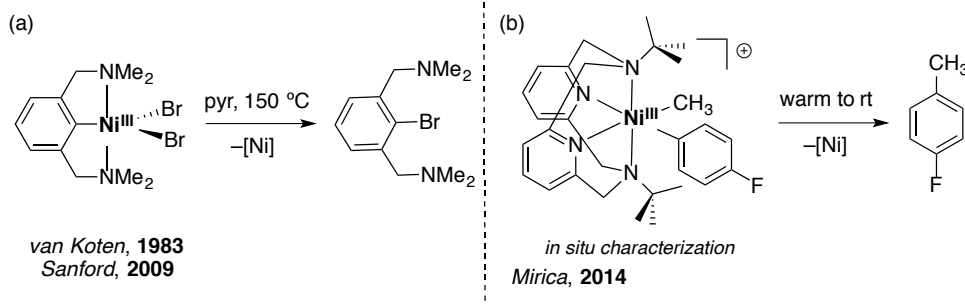
In comparison to palladium, the organometallic chemistry of high-valent nickel is far less developed. Early stoichiometric studies first suggested nickel's enhanced ability to mediate carbon–carbon and carbon–heteroatom bond-forming reactions in the presence of external oxidants. For example, Kochi demonstrated oxidatively–induced carbon–carbon coupling reactions at Ni to form biaryl linkages (Scheme 1.7).³³ Hillhouse and co-workers later showed carbon–heteroatom bond-forming reactions from cyclometallated Ni^{II} precursors (Scheme 1.7).³⁴ High-oxidation state Ni^{III} intermediates (rather than Ni^{IV}) were generally proposed as the operative species in these reactions; however, no intermediates were structurally characterized.

Scheme 1.7. Ni-mediated Carbon–Carbon and C–Heteroatom Bond-Forming Reactions via Proposed Ni^{III} intermediates



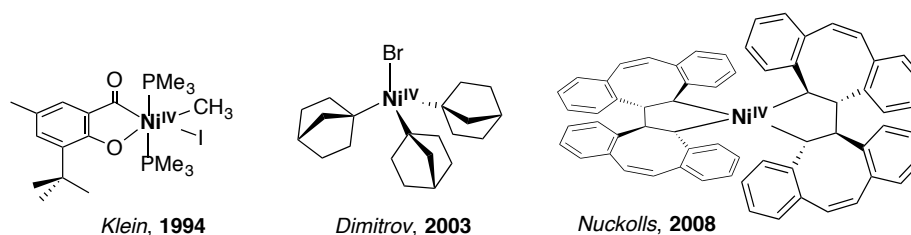
While a large amount of indirect evidence supports the transient formation of organoNi^{III} species,³⁵ examples of isolable Ni^{III} complexes remain rare.³⁶ In the early 1980s, van Koten employed a pincer ligand to stabilize and ultimately isolate an organometallic Ni^{III} complex (Figure 1.8a).^{36a} Later studies by our lab demonstrated the ability of this species to mediate C–Br reductive elimination.³⁷ Most recently, Mirica and co-workers reported the first example of C–C coupling from a Ni^{III} center (Figure 1.8b).³⁸ This complex was supported by a tetradentate nitrogen donor ligand but could only be characterized by *in situ* EPR studies. Because of the well-documented challenges associated with stabilizing highly reactive Ni^{III} intermediates, systematic studies investigating the formation, reactivity, and mechanism of these species are lacking. It is anticipated that a fundamental understanding of the organometallic chemistry of Ni^{III} will aid in the development of high-valent Ni-catalyzed reactions.

Scheme 1.8. Examples of Characterized Ni^{III} Complexes and their Reactivity towards (a) Carbon–Bromine and (b) Carbon–Carbon Bond-Forming Reactions



While Ni^{III} intermediates are commonly implicated in catalysis, the feasibility of the +4 oxidation state is less certain. In the early 1990s, Klein and co-workers reported the first example of a structurally characterized Ni^{IV} species, which was accessed by the two-electron oxidation of a Ni^{II} precursor with methyl iodide (Figure 1.3).³⁹ More recent studies by Dimitrov⁴⁰ and later Nuckolls,⁴¹ demonstrated the use of exotic carbon-donor ligands to stabilize the highly reactive metal centers (Figure 1.3). However, in all cases, these complexes contained highly specialized ligands that did not allow catalytically-relevant bond-forming reactions to be directly investigated. Overall, the uncertainty of Ni^{IV} in catalysis can be attributed, in part, to the limited examples of well-characterized Ni^{IV} complexes and the inability to directly investigate their reactivity thus far.⁴²

Figure 1.3. Representative Examples of Structurally-Characterized Ni^{IV} Complexes



Our interest in the design and synthesis of organometallic Ni^{IV} complexes stems from the hypothesis that such complexes could possess distinct reactivity from the more common oxidation states of Ni. This hypothesis is predicated on the organometallic chemistry of Pd^{IV}, in which fundamental studies have demonstrated its complementary reactivity to low-valent

Pd centers.⁹ Moreover, the intrinsic properties of Ni could provide access to challenging transformations that are not accessible with Pd.

Chapter 3 of this thesis is focused on our design strategies for synthesizing isolable organometallic Ni^{IV} complexes.^{42c,d} We demonstrate that the use of stabilizing tridentate ligands, trifluoromethyl groups, and chelating carbon-donor ligands support catalytically-relevant Ni^{IV} centers. Systematic studies provide insight into the reactivity of these complexes towards carbon–carbon and carbon–heteroatom bond-forming reactions. In Chapter 4, the formation and reactivity of Ni^{III} complexes are directly investigated and compared to the reactivity of their Ni^{IV} analogues.⁴³ These studies offer preliminary evidence that complementary selectivity can be achieved by accessing distinct oxidation states of nickel. These chapters are followed by a comparative investigation into the formation, reactivity, and mechanism of well-characterized Ni^{IV} and Pd^{IV} complexes (Chapter 5), which concludes the work detailed herein.

1.5. References

-
- (1) (a) Stille, J. K. *Angew. Chem. Int. Ed.* **1986**, *25*, 508. (b) Miyaura, N.; Suzuki, A. *Chem. Rev.* **1995**, *95*, 2457. (c) Littke, A. F.; Fu, G. C. *Angew. Chem. Int. Ed.* **2002**, *41*, 4176. (d) Tsuji, J. *Modern Palladium Catalysis: New Perspectives for the 21st Century*. John Wiley & Sons: Chichester, 2004. (e) Nicolaou, K. C.; Bulger, P. G.; Sarlah, D. *Angew. Chem. Int. Ed.* **2005**, *44*, 4442. (f) Hartwig, J. *Organotransition Metal Chemistry: From Bonding to Catalysis*. University Science Books: Sausalito, 2010. (g) Johansson Seechurn, C. C. C.; Kitching, M. O.; Colacot, T. J.; Snieckus, V. *Angew. Chem., Int. Ed.* **2012**, *51*, 5062.
 - (2) (a) Amatore, C.; Jutand, A. *J. Organomet. Chem.* **1999**, *576*, 254. (b) Beletskaya, I. P.; Cheprakov, A. V. *Chem. Rev.* **2000**, *100*, 3009. (c) Espinet, P.; Echavarren, A. M. *Angew. Chem., Int. Ed.* **2004**, *43*, 4704. (d) Casares, J. A.; Espinet, P.; Fuentes, B.; Salas, G. *J. Am. Chem. Soc.* **2007**, *129*, 3508. (e) Carrow, B. P.; Hartwig, J. F. *J. Am. Chem. Soc.* **2011**, *133*, 2116.
 - (3) (a) Watson, D. A.; Su, M.; Teverovskiy, G.; Zhang, Y.; Garcia-Fortanet, J.; Kinzel, T.; Buchwald, S. L. *Science* **2009**, *325*, 1661. (b) Cho, E. J.; Senecal, T. D.; Kinzel, T.; Zhang, Y.; Watson, D. A.; Buchwald, S. L. *Science* **2010**, *328*, 1679. (c) Grushin, V. V. *Acc. Chem. Res.* **2010**, *43*, 160.
 - (4) Tomashenko, O. A.; Grushin, V. V. *Chem. Rev.* **2011**, *111*, 4475.
 - (5) Stoichiometric example of C(sp³)-O coupling from Pd^{II}: Marquard, S. L.; Hartwig, J. F. *Angew. Chem. Int. Ed.* **2011**, *50*, 7119.
 - (6) For select reviews on Pd^{IV} in catalysis, see: (a) Muñiz, K. *Angew. Chem. Int. Ed.* **2009**,

- 48, 9412. (b) Lyons, T.; Sanford, M. S. *Chem. Rev.* **2010**, *110*, 1147. (c) Hickman, A. J.; Sanford, M. S. *Nature* **2012**, *484*, 177. (d) Engle, K. M.; Mei, T.-S.; Wasa, M.; Yu, J.-Q. *Acc. Chem. Res.* **2012**, *45*, 788. (e) Topczewski, J. T.; Sanford, M. S. *Chem. Sci.*, **2015**, *6*, 70.
- (7) Hartwig, J. F. Reductive Elimination. In *The Organotransition Metal Chemistry: From Bonding to Catalysis*; University Science Books: Sausalito, CA, 2010; pp 321.
- (8) Hartwig, J. F. *Nature* **2008**, *455*, 314.
- (9) For select reviews on fundamental studies at Pd^{IV}, see: (a) Canty, A. J. *Acc. Chem. Res.* **1992**, *25*, 83. (b) Canty, A. J. *Dalton Trans.* **2009**, 10409. (c) Muñiz, K. *Angew. Chem. Int. Ed.* **2009**, *48*, 9412. (d) Xu, L. M.; Li, B. J.; Yang, Z.; Shi, Z. *J. Chem. Soc. Rev.* **2010**, *39*, 712. (e) Sehnal, P.; Taylor, R. J. K.; Fairlamb, I. J. S. *Chem. Rev.* **2010**, *110*, 824. (f) Vedernikov, A. N. *Top. Organomet. Chem.* **2010**, *31*, 101. (g) Racowski, J. M.; Sanford, M. S. *Top. Organomet. Chem.* **2011**, *35*, 61. (h) Vigalok, A. *Acc. Chem. Res.*, **2015**, *48*, 238. (i) Desnoyer, A.; Love, J. A. *Chem. Soc. Rev.* **2017**, *46*, 197.
- (10) For a review on Pd^{III}, see: Powers, D. C.; Ritter, T. *Top. Organomet. Chem.* **2011**, *35*, 129.
- (11) Chen, X.; Engle, K. M.; Wang, D.-H.; Yu, J.-Q. *Angew. Chem. Int. Ed.* **2009**, *48*, 5094.
- (12) For select early examples, see: (a) Desai, L. V.; Hull, K. L.; Sanford, M. S. *J. Am. Chem. Soc.*, **2004**, *126*, 9542. (b) Giri, R.; Chen, X.; Yu, J. Q. *Angew. Chem., Int. Ed.* **2005**, *44*, 2112. (c) Kalyani, D.; Deprez, N. R.; Desai, L. V.; Sanford, M. S. *J. Am. Chem. Soc.*, **2005**, *127*, 7330. (d) Chen, X.; Goodhue, C. E.; Yu, J.-Q. *J. Am. Chem. Soc.* **2006**, *128*, 12634.
- (13) For select examples, see: (a) Pilarski, L. T.; Selander, N.; Böse, D.; Szabó, K. *J. Org. Lett.* **2009**, *11*, 5518. (c) Pilarski, L. T.; Janson, P. G.; Szabó, K. *J. Org. Chem.* **2011**, *76*, 1503. (d) Check, C. T.; Henderson, W. H.; Wray, B. C.; Vanden Eynden, M. J.; Stambuli, J. P. *J. Am. Chem. Soc.* **2011**, *133*, 18503 (d) Alam, R.; Pilarski, L. T.; Pershagen, E.; Szabó, K. *J. Am. Chem. Soc.* **2012**, *134*, 8778.
- (14) For select examples, see: (a) Alexanian, E. J.; Lee, C.; Sorensen, E. J. *J. Am. Chem. Soc.* **2005**, *127*, 7690. (b) Liu, G.; Stahl, S. S. *J. Am. Chem. Soc.* **2006**, *128*, 7179. (c) Sibbald, P. A.; Rosewall, C. F.; Swartz, R. D.; Michael, F. E. *J. Am. Chem. Soc.* **2009**, *131*, 15945. (d) Rosewall, C. F.; Sibbald, P. A.; Liskin, D. V.; Michael, F. E. *J. Am. Chem. Soc.* **2009**, *131*, 9488. (e) Sibbald, P. A.; Michael, F. E. *Org. Lett.* **2009**, *11*, 1147 (f) Kalyani, D.; Satterfield, A. D.; Sanford, M. S. *J. Am. Chem. Soc.* **2010**, *132*, 8419. (g) Neufeldt, S. R.; Sanford, M. S. *Org. Lett.* **2012**, *15*, 46. (h) Muñiz, K.; Martinez, C. *J. Org. Chem.* **2012**, *78*, 2168.
- (15) (a) Ye, Y.; Ball, N. D.; Kampf, J. W.; Sanford, M. S. *J. Am. Chem. Soc.* **2010**, *132*, 14682 (b) Ball, N. D.; Kampf, J. W.; Sanford, M. S. *J. Am. Chem. Soc.* **2010**, *132*, 2878. (c) Furuya, T.; Benitez, D.; Tkatchouk, E.; Strom, A. E.; Tang, P. Goddard, III, W. A.; Ritter, T. *J. Am. Chem. Soc.* **2010**, *132*, 3793.
- (16) For select fundamental organometallic studies at Pd^{IV}, see: (a) Uson, R.; Fornies, J.; Navarro, R. *J. Organomet. Chem.* **1975**, *96*, 307. (b) Byers, P. K.; Canty, A. J.; Skelton, B. W.; White, A. H. *J. Chem. Soc., Chem. Commun.* **1986**, 1722. (c) Alsters, P. L.; Engel, P. F.; Hogerheide, M. P.; Copijn, M.; Spek, A. L.; van Koten, G. *Organometallics* **1993**, *12*, 1831. (d) Markies, B. A.; Canty, A. J.; Boersma, J.; van Koten, G. *Organometallics* **1994**, *13*, 2053. (e) van Asselt, R.; Rijnberg, E.; Elsevier, C. J. *Organometallics* **1994**, *13*, 706. (f) van Belzen, R.; Hoffmann, H.; Elsevier, C. J. *Angew. Chem., Int. Ed.* **1997**, *36*, 1743. (g) Cotton, F. A.; Gu, J.; Murillo, C. A.; Timmons, D. J. *J. Am. Chem. Soc.* **1998**, *120*, 13280. (h) Dick, A. R.; Kampf, J. W.; Sanford, M. S. *J. Am. Chem. Soc.* **2005**, *127*, 12790. (i) Cotton, F. A.; Koshevoy, I. O.; Lahuerta, P.; Murillo, C. A.; Sanau, M.; Ubeda, M. A.; Zhao, Q. *J. Am. Chem. Soc.* **2006**, *128*, 13674. (j) Whitfield, S. R.; Sanford, M. S. *J. Am. Chem. Soc.* **2007**, *129*, 15142. (k) Racowski, J. M.; Dick, A. R.; Sanford, M. S. J.

- Am. Chem. Soc.* **2009**, *131*, 10974. (l) Oloo, W.; Zavalij, P. Y.; Zhang, J.; Khaskin, E.; Vedernikov, A. N. *J. Am. Chem. Soc.* **2010**, *132*, 14400. (m) Vicente, J.; Arcas, A.; Julia-Hernandez, F.; Bautista, D. *Chem. Commun.* **2010**, 7253. (n) Khusnutdinova, J. R.; Rath, N. P.; Mirica, L. M. *J. Am. Chem. Soc.* **2010**, *132*, 7303. (o) Bercaw, J. E.; Durrell, A. C.; Gray, H. B.; Green, J. C.; Hazari, N.; Labinger, J. A.; Winkler, J. R. *Inorg. Chem.* **2010**, *49*, 1801. (p) Khusnutdinova, J. R.; Rath, N. P.; Mirica, L. M. *Angew. Chem. Int. Ed.* **2011**, *50*, 5532. (q) Vicente, J.; Arcas, A.; Julia-Hernandez, F.; Bautista, D. *Angew. Chem. Int. Ed.* **2011**, *50*, 6896. (r) Zhao, X.; Dong, V. M. *Angew. Chem. Int. Ed.* **2011**, *50*, 932. (s) Racowski, J. M.; Gary, J. B.; Sanford, M. S. *Angew. Chem. Int. Ed.* **2012**, *51*, 3414.
- (17) Dick, A. R.; Hull, K. L.; Sanford, M. S. *J. Am. Chem. Soc.* **2004**, *126*, 2300.
- (18) (a) Powers, D. C.; Xiao, D. Y.; Geibel, M. A. L.; Ritter, T. *J. Am. Chem. Soc.* **2010**, *132*, 14530. (b) Nielsen, M. C.; Lyngvi, E.; Schoenebeck, F. *J. Am. Chem. Soc.* **2013**, *135*, 1978 (c) Pérez-Temprano, M. H.; Racowski, J. M.; Kampf, J. W.; Sanford, M. S. *J. Am. Chem. Soc.* **2014**, *136*, 4097 (d) Cook, A. K.; Sanford, M. S. *J. Am. Chem. Soc.*, **2015**, *137*, 3109. (e) Haines, B. E.; Xu, H.; Verma, P.; Wang, X.-C.; Yu, J.-Q.; Musaev, D. G. *J. Am. Chem. Soc.* **2015**, *137*, 9022. (f) Pendleton, I. M.; Pérez-Temprano, M. H.; Sanford, M. S.; Zimmerman, P. M. *J. Am. Chem. Soc.* **2016**, *138*, 6049.
- (19) (a) Canty, A. J.; Done, M. C.; Skelton, B. W.; White, A. H. *Inorg. Chem. Commun.* **2001**, *4*, 648. (b) Canty, A. J.; Denney, M. C.; Skelton, B. W.; White, A. H. *Organometallics* **2004**, *23*, 1122. (c) Canty, A. J.; Denney, M. C.; van Koten, G.; Skelton, B. W.; White, A. H. *Organometallics* **2004**, *23*, 5432. (d) Canty, A. J.; Ariaford, A.; Sanford, M. S.; Yates, B. F. *Organometallics* **2013**, *32*, 544.
- (20) (a) Vedernikov, A. N. *Acc. Chem. Res.* **2012**, *45*, 803. (b) Abada, E.; Zavalij, P. Y.; Vedernikov, A. N. *J. Am. Chem. Soc.* **2017**, *139*, 643.
- (21) (a) Khusnutdinova, J. R.; Rath, N. P.; Mirica, L. M. *J. Am. Chem. Soc.*, **2012**, *134*, 2414. (b) Khusnutdinova, J. R.; Qu, F.; Zhang, Y.; Rath, N. P.; Mirica, L. M. *Organometallics*, **2012**, *31*, 4627. (c) Tang, F.; Zhang, Y.; Rath, N. P.; Mirica, L. M. *Organometallics*, **2012**, *31*, 6690. (d) Tang, F.; Qu, F.; Khusnutdinova, J. R.; Rath, N. P.; Mirica, L. M. *Dalton Trans.* **2012**, *41*, 14046. (e) Luo, J.; Rath, N. P.; Mirica, L. M. *Organometallics* **2013**, *32*, 3343. (f) Luo, J.; Rath, N. P.; Mirica, L. M. *Organometallics* **2013**, *32*, 3343. (g) Qu, F.; Khusnutdinova, J. R.; Rath, N. P.; Mirica, L. M. *Chem. Comm.* **2014**, *50*, 3036.
- (22) (a) Powers, D. C.; Ritter, T. *Nat. Chem.* **2009**, *1*, 302. (b) Powers, D. C.; Ritter, T. *Acc. Chem. Res.* **2012**, *45*, 840 (c) Powers, D. C.; Lee, E.; Ariafard, A.; Sanford, M. S.; Yates, B. F.; Canty, A. J.; Ritter, T. *J. Am. Chem. Soc.* **2012**, *134*, 12002.
- (23) (a) Camasso, N. M.; Pérez-Temprano, M. H.; Sanford, M. S. *J. Am. Chem. Soc.* **2014**, *136*, 12771. (b) Canty, A. J.; Ariafard, A.; Camasso, N. M.; Higgs, A. T.; Yates, B. F.; Sanford, M. S. *Dalton Trans.* **2017**, *46*, 3742.
- (24) (a) Meijere, A. d.; Diederich, F. *Metal-Catalyzed Cross-Coupling Reactions*; Wiley-VCH: Weinheim, 2004. (b) Hu, X. *Chem. Sci.* **2011**, *2*, 1867. (c) Rosen, B. M.; Quasdorf, K. W.; Wilson, D. A.; Zhang, N.; Resmerita, A.-M.; Garg, N. K.; Percec, V. *Chem. Rev.* **2011**, *111*, 1346. (d) Montgomery, J. "Organonickel Chemistry" in *Organometallics in Synthesis: Fourth Manual* Lipshutz, B. H. (Ed.) Wiley, Hoboken, N.J., **2013**, pp. 319-428. (e) Tasker, S. Z.; Standley, E. A.; Jamison, T. F. *Nature* **2014**, *509*, 299. (f) Everson, D. A.; Weix, D. J. *J. Org. Chem.* **2014**, *79*, 4793. (g) Standley, E. A.; Tasker, S. Z.; Jensen, K. L.; Jamison, T. F. *Acc. Chem. Res.* **2015**, *48*, 1503. (h) Ananikov, V. *ACS Catal.* **2015**, *5*, 1964. (i) Cavalcanti, L. N.; Molander, G. A. *Top. Curr. Chem.* **2016**, *374*, 39. (j) Yamaguchi, J.; Muto, K.; Itami, K. *Top. Curr. Chem.* **2016**, *374*, 55.
- (25) Sigma-Aldrich Co, <http://www.sigmaaldrich.com> (prices depend on many factors; the numbers given should be considered as an estimate only).

-
- (26) Macgregor, S. A.; Neave, G. W.; Smith, C. *Faraday Discuss.* **2003**, *124*, 111.
- (27) Ananikov, V. P.; Musaev, D. G.; Morokuma, K. *Organometallics* **2005**, *24*, 715.
- (28) (a) Zultanski, S. L.; Fu, G. C. *J. Am. Chem. Soc.* **2013**, *135*, 624. (b) Iwasaki, T.; Kambe, N. *Top. Curr. Chem.* **2016**, *374*, 66. (c) Serrano, E.; Martin, R. *Angew. Chem. Int. Ed.* **2016**, *55*, 11207. (d) Chu, C. K.; Liang, Y.; Fu, G. C. *J. Am. Chem. Soc.*, **2016**, *138*, 6404.
- (29) (a) Dankwardt, J. W. *Angew. Chem. Int. Ed.* **2004**, *43*, 2428. (b) Rosen, B. M.; Quasdorf, K. W.; Wilson, D. A.; Zhang, N.; Resmerita, A.-M.; Garg, N. K.; Percec, V. *Chem. Rev.* **2011**, *111*, 1346. (c) Li, B.-J.; Yu, D.-G.; Sun, C.-L.; Shi, Z.-J. *Chem. Eur. J.* **2011**, *17*, 1728. (d) Chatani, N. *Top. Curr. Chem.* **2016**, *374*, 41.
- (30) Mahandru, G. M.; Liu, G.; Montgomery, J. *J. Am. Chem. Soc.* **2004**, *126*, 3698.
- (31) Yu, D.-G.; Wang, X.; Zhu, R.-Y.; Luo, S.; Zhang, X.-B.; Wang, B.-Q.; Wang, L.; Shi, Z.-J. *J. Am. Chem. Soc.* **2012**, *134*, 14638.
- (32) (a) Terao, J.; Kambe, N. *Acc. Chem. Res.* **2008**, *41*, 1545. (b) Aihara, Y.; Chatani, N. *J. Am. Chem. Soc.* **2013**, *136*, 898. (c) Aihara, Y.; Chatani, N. *J. Am. Chem. Soc.* **2013**, *135*, 5308. (d) Iyanaga, M.; Aihara, Y.; Chatani, N. *J. Org. Chem.* **2014**, *79*, 11933. (e) Yan, S.-Y.; Liu, Y.-J.; Liu, B.; Liu, Y.-H.; Zhang, Z.-Z.; Shi, B.-F. *Chem. Commun.* **2015**, *51*, 7341.
- (33) (a) Tsou, T. T.; Kochi, J. K. *J. Am. Chem. Soc.* **1978**, *100*, 1634. (b) Tsou, T. T.; Kochi, J. K. *J. Am. Chem. Soc.* **1979**, *101*, 7547.
- (34) (a) Matsunaga, P. T.; Hillhouse, G. L.; Rheingold, A. L. *J. Am. Chem. Soc.* **1993**, *115*, 2075. (b) Koo, K.; Hillhouse, G. L. *Organometallics* **1995**, *14*, 4421. (c) Koo, K.; Hillhouse, G. L.; Rheingold, A. L. *Organometallics* **1995**, *14*, 456. (d) Koo, K.; Hillhouse, G. L. *Organometallics* **1996**, *15*, 2669. (e) Han, R.; Hillhouse, G. L. *J. Am. Chem. Soc.* **1997**, *119*, 8135. (f) Koo, K.; Hillhouse, G. L. *Organometallics* **1998**, *17*, 2924. (g) Lin, B. L.; Clough, C. R.; Hillhouse, G. L. *J. Am. Chem. Soc.* **2002**, *124*, 2890.
- (35) For select examples of nickel catalyzed C–C and C–heteroatom coupling reactions invoking Ni^{III} intermediates, see: (a) Jones, G. D.; Martin, J. L.; McFarland, C.; Allen, O. R.; Hall, R. E.; Haley, A. D.; Brandon, R. J.; Konovalova, T.; Desrochers, P. J.; Pulay, P.; Vicic, D. A. *J. Am. Chem. Soc.* **2006**, *128*, 13175. (b) Zultanski, S.; Fu, G. C. *J. Am. Chem. Soc.* **2011**, *133*, 15362. (c) Hu, X. *Chem. Sci.* **2011**, *2*, 1867. (d) Joshi-Pangu, A.; Wang, C.-Y.; Biscoe, M. R. *J. Am. Chem. Soc.* **2011**, *133*, 847. (e) Dudnik, A. S.; Fu, G. C. *J. Am. Chem. Soc.* **2012**, *134*, 10693. (f) Dai, Y. J.; Wu, F.; Zang, Z. H.; You, H. Z.; Gong, H. G. *Chem. Eur. J.* **2012**, *18*, 808. (g) Schley, N. D.; Fu, G. C. *J. Am. Chem. Soc.* **2014**, *136*, 16588. (h) Aihara, Y.; Tobisu, M.; Fukumoto, Y.; Chatani, N. *J. Am. Chem. Soc.* **2014**, *136*, 15509. (i) Wu, X.; Zhao, Y.; Ge, H. *J. Am. Chem. Soc.* **2014**, *136*, 1789. (j) Tellis, J. C.; Primer, D. N.; Molander, G. A. *Science* **2014**, *345*, 433. (k) Zuo, Z.; Ahneman, D. T.; Chu, L.; Terrett, J. A.; Doyle, A. G.; MacMillan, D. W. C. *Science* **2014**, *345*, 437. (l) Cornella, J.; Edwards, J. T.; Qin, T.; Kawamura, S.; Wang, J.; Pan, C.-M.; Gianatassio, R.; Schmidt, M. A.; Eastgate, M. D.; Baran, P. S. *J. Am. Chem. Soc.* **2016**, *138*, 2174. (m) Gui, Y.-Y.; Sun, L.; Lu, Z.-P.; Yu, D.-G. *Org. Chem. Front.* **2016**, *3*, 522. (n) Shields, B. J.; Doyle, A. G. *J. Am. Chem. Soc.* **2016**, *138*, 12719.
- (36) For select examples of structurally characterized Ni^{III} complexes, see: (a) Grove, D. M.; van Koten, G.; Zoet, R.; Murrall, N. W.; Welch, A. J. *J. Am. Chem. Soc.* **1983**, *105*, 1379. (b) Grove, D. M.; van Koten, G.; Mul, W. P.; van der Zeijden, A. A. H.; Terheijden, J. *Organometallics* **1986**, *5*, 322. (c) Grove, D. M.; van Koten, G.; Mul, P.; Zoet, R.; van der Linden, J. G. M.; Letgers, J.; Schmitz, J. E. J.; Murrall, N. W.; Welch, A. J. *Inorg. Chem.* **1988**, *27*, 2466. (d) van de Kuil, V. A.; Veldhuizen, Y. S. J.; Grove, D. M.; Zwikker, J. L.; Jenneskens, L. W.; Drenth, W.; Smeets, W. J. J.; Spek, A. L.; van Koten, G. *J. Organomet. Chem.* **1995**, *488*, 191. (e) Pandarus, V.; Zargarian, D. *Organometallics* **2007**, *26*, 4321. (f) Castonguay, A.; Beauchamp, A.; Zargarian, D. *Organometallics* **2008**, *27*, 5723. (f) Lee,

-
- C. M.; Chen, C. H.; Liao, F. X.; Hu, C. H.; Lee, G. H. *J. Am. Chem. Soc.* **2010**, *132*, 9256. (g) Tang, F.; Rath, N. P.; Mirica, L. M. *Chem. Commun.* **2015**, *51*, 3113. (h) Yu, S.; Dudkina, Y.; Wang, H.; Kholin, K. V.; Budnikova, V.; Vivic, D. A. *Dalton Trans.* **2015**, *44*, 19443.
- (37) Higgs, A. T.; Zinn, P. J.; Sanford, M. S. *Organometallics* **2009**, *28*, 6142.
- (38) Zheng, B.; Tang, F.; Luo, J.; Schultz, J. W.; Rath, N. P.; Mirica, L. M. *J. Am. Chem. Soc.* **2014**, *136*, 6499.
- (39) Klein, H.-F.; Bickelhaupt, A.; Jung, T.; Cordier, G. *Organometallics* **1994**, *13*, 2557.
- (40) Dimitrov, V.; Linden, A. *Angew. Chem., Int. Ed.* **2003**, *42*, 2631.
- (41) Carnes, M.; Buccella, D.; Chen, J. Y. C.; Ramirez, A. P.; Turro, N. J.; Nuckolls, C.; Steigerwald, M. *Angew. Chem. Int. Ed.* **2009**, *48*, 290.
- (42) See 39-41, also: (a) Klein, H. F.; Bickelhaupt, A.; Lemke, M.; Sun, H. J.; Brand, A.; Jung, T.; Rohr, C.; Florke, U.; Haupt, H. J. *Organometallics* **1997**, *16*, 668. (b) Shimada, S.; Rao, M. L. N.; Tanaka, N. *Organometallics* **1999**, *18*, 291. (c) Camasso, N. M.; Sanford, M. S. *Science* **2015**, *136*, 12771. (d) Bour, J. R.; Camasso, N. M.; Sanford, M. S. *J. Am. Chem. Soc.* **2015**, *137*, 8034. (e) Martinez, G. E.; Ocampo, C.; Park, Y. J.; Fout, A. R. *J. Am. Chem. Soc.* **2016**, *138*, 4290. Schultz, J. W.; Fuchigami, K.; Zheng, B.; Rath, N. P.; Mirica, L. M. *J. Am. Chem. Soc.* **2016**, *138*, 12928. (f) Watson, M. B.; Rath, N. P.; Mirica, L. M. *J. Am. Chem. Soc.* **2017**, *139*, 35. (g) Meucci, E. A.; Camasso, N. M.; Sanford, M. S. *Organometallics*, **2017**, *36*, 247.
- (43) Bour, J. R.; Camasso, N. M.; Meucci, E. A.; Kampf, J. W.; Canty, A. J.; Sanford, M. S. *J. Am. Chem. Soc.* **2016**, *138*, 16105.

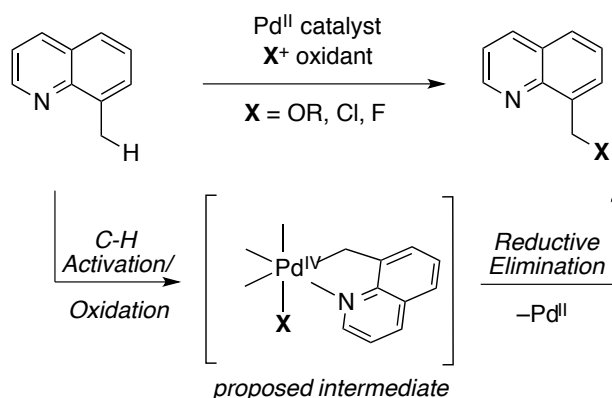
CHAPTER 2

Carbon–Heteroatom Bond-Forming Reductive Elimination from Pd^{IV} Complexes¹

2.1. Introduction

Carbon–heteroatom bond-forming reductive elimination from Pd^{IV} centers is a key elementary step in numerous high-valent Pd-catalyzed reactions,² including ligand-directed C–H functionalization,^{3,4} alkene difunctionalization,⁵ and allylic acetoxylation.⁶ Studies by our group^{7,8} and others^{9–12} have probed the mechanism of C(sp²)–heteroatom bond-forming reductive elimination reactions from high-valent Pd complexes. In turn, these studies have helped to inform the design and development of new catalytic processes.^{3–6}

Scheme 2.1. Proposed mechanism for Pd^{II/IV}-catalyzed ligand-directed C–H functionalization



In marked contrast, much less is known about the corresponding C(sp³)–heteroatom coupling processes at high-valent Pd (Scheme 2.1).^{13,14} Previous attempts to investigate these transformations have been plagued by the low stability of high-valent Pd intermediates and by side reactions, such as competing methyl group transfer from Pd^{IV} intermediates to Pd^{II} reactants, as well as C–C coupling at Pd^{IV}.¹⁵ As a result, the mechanisms of these

transformations remain opaque, and the scope of nucleophiles that can serve as coupling partners has not been well studied. Furthermore, the chemoselectivity of C–heteroatom bond-forming reductive elimination is poorly understood in systems where multiple competing reductive elimination processes could take place.

This chapter describes the design of a model system that enables a detailed exploration of the scope, chemoselectivity, and mechanism of C(sp³)–heteroatom bond-forming reductive elimination from Pd^{IV}. Throughout our studies, C(sp³)–heteroatom bond formation was found to proceed selectively over potentially competing C(sp²)–heteroatom coupling, which is in contrast to the selectivity typically observed at lower oxidation states of Pd.¹⁶ We have also found that these transformations can proceed with weak oxygen nucleophiles such as nitrate and tosylate. In addition, we demonstrate that cationic additives (i.e., Li⁺ versus NBu₄⁺) play an important role in the chemoselectivity of competing C(sp³)–O and C(sp³)–F coupling at Pd^{IV} centers. Finally, studies suggest the reversibility of this reductive elimination process when electron deficient nucleophiles such as nitrate, tosylate, and iodide participate as coupling partners.

2.2. Results and Discussion

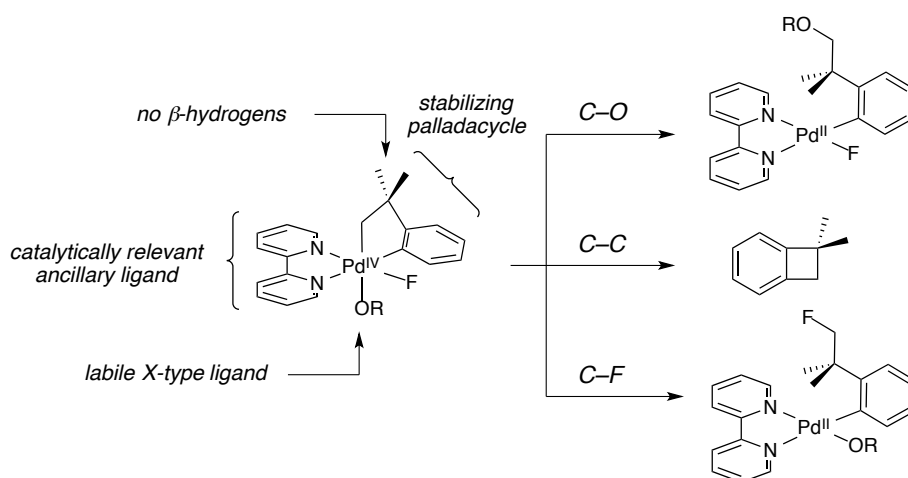
2.2.1. C(sp³)–O Bond-Forming Reductive Elimination from Pd^{IV} with Diverse Oxygen Nucleophiles

Design of a Model System

Several considerations went into the design of a model system for studying C(sp³)–O bond-forming reductive elimination from Pd^{IV} (Scheme 2.2). First, a Pd^{IV}-alkyl complex that does not contain β-hydrogens was selected to avoid competing β-hydride elimination. Second, a ligand environment was targeted that would render the Pd^{IV} intermediates isolable and still be highly modular to allow for the introduction of diverse oxygen nucleophiles. Finally, a system that would enable the investigation of competing C–O, C–F, and C–C bond-

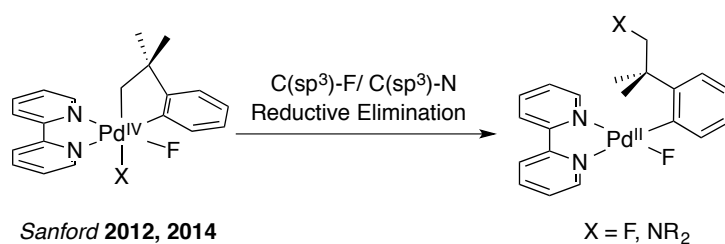
forming reductive elimination was sought to mimic important elementary steps in catalytic methodologies. For instance, prior work in our lab has shown that competing C(sp³)–O and C(sp³)–F bond-formation occurs from a putative high-valent Pd center in catalytic fluorination reactions of 8-methylquinoline with AgF/PhI(OPiv)₂.¹⁷ Achieving the selective formation of a single product remains a major challenge in this and related Pd^{II/IV}-catalyzed methods.

Scheme 2.2. The Design of a Model System for Studying C–O Coupling from Pd^{IV}



Our group has previously demonstrated that cyclometallated Pd^{IV} derivatives of the general structure (bpy)Pd(CH₂CMe₂-*o*-C₆H₄)(F)(X) can be stable and often isolable complexes (Scheme 2.3).¹⁸ When X = OTf, this ligand can be readily displaced by other anions or Lewis bases (e.g., TsNH[−], pyridine). Some of these complexes have been shown to participate in selective reductive elimination at the sp³-carbon ligand. Furthermore, depending on the conditions, competing reductive eliminations can be observed.^{18b} Thus, this system was selected to probe the scope, mechanism, and selectivity of C(sp³)–O bond-forming reductive elimination at Pd^{IV}.

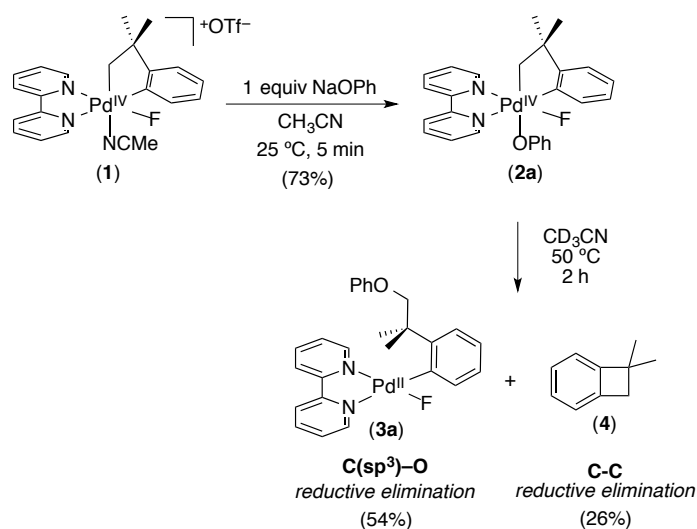
Scheme 2.3. Competitive C–N vs. C–F Reductive Elimination from Pd^{IV}



Initial Studies with Phenoxide as the Nucleophile

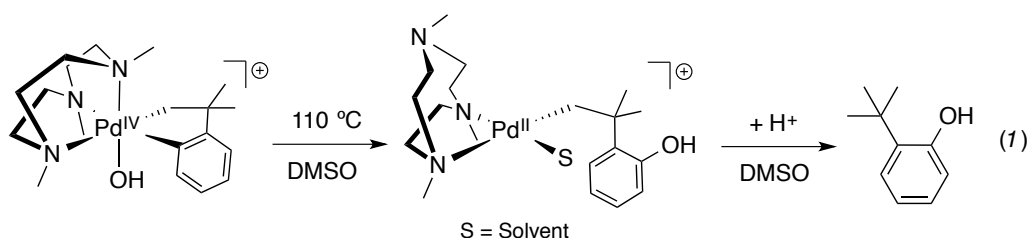
Phenoxide ligands are known to serve as coupling partners in numerous reductive elimination reactions, including both C(sp²)-O¹⁹ and C(sp³)-O¹⁴ coupling at Pd^{II} centers and C(sp³)-O bond formation at Pt^{IV}.^{13b} Based on these precedents, we targeted Pd^{IV} phenoxide complex **2a** for our initial investigations. Complex **2a** was obtained in 73% isolated yield by treatment of the Pd^{IV} triflate complex **1**^{18a} with 1 equiv of sodium phenoxide in CH₃CN at room temperature (Scheme 2.4). Complex **2a**²⁰ was fully characterized by one- and two-dimensional ¹H, ¹³C, and ¹⁹F NMR spectroscopy.

Scheme 2.4. Synthesis and Reactivity of Phenoxide-Ligated Pd^{IV} Complex **2a**



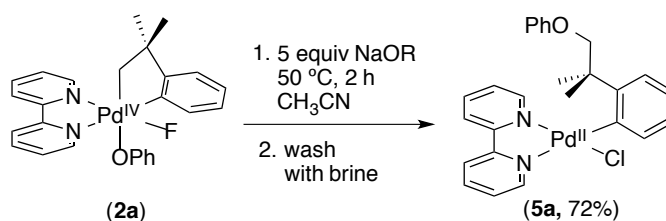
When **2a** was heated at 50 °C for 2 h in CD₃CN it underwent C(sp³)-O bond-forming reductive elimination to form **3a** in 54% yield as determined by ¹H NMR spectroscopy (Scheme 2.4). The main by-product in this reaction was cyclobutane **4** (derived from C(sp³)-C(sp²) coupling),^{18b} which was formed in 26% yield. Importantly, no C(sp³)-F or C(sp²)-O/F

reductive elimination products were observed under these conditions. This is in notable contrast to a recent report by Mirica, who showed that a closely related $\text{Pd}^{\text{IV}}(\text{CH}_2\text{CMe}_2\text{-}o\text{-C}_6\text{H}_4)(\text{OH})$ complex undergoes clean $\text{C}(\text{sp}^2)\text{-OH}$ coupling upon thermolysis (eq. 1).^{11,21} We rationalize the difference in reactivity between the two systems based on the comparatively stronger nucleophilicity of OH^- . This would inhibit dissociation from the Pd^{IV} center, favoring a concerted or quasi-concerted intramolecular reductive elimination processes. DFT calculations carried out by the authors suggest that this intramolecular $\text{C}(\text{sp}^2)\text{-O}$ bond formation is favored over intramolecular $\text{S}_{\text{N}}2$ -type $\text{C}(\text{sp}^3)\text{-O}$ reductive elimination in their model system.



Based on some of the prior studies in our group,^{18b} we hypothesized that the addition of exogenous OPh^- to reductive elimination reactions from **2a** might enhance the selectivity for $\text{C}(\text{sp}^3)\text{-O}$ coupling. Indeed, the addition of 2-5 equiv of NaOPh resulted in the quantitative formation of **3a** as determined by NMR spectroscopic analysis. This Pd^{II} fluoride product was challenging to isolate because of the highly hygroscopic fluoride ligand. It is well documented that hydrogen bond donors such as water can interact with the fluoride ligand in $\text{Pd}^{\text{II}}\text{-F}$ complexes.²² This interaction facilitates rapid ionization of the $\text{Pd}\text{-F}$ bond, making it susceptible to ligand substitution and decomposition pathways.^{22,23} However, washing dichloromethane solutions of **3a** with brine resulted in substitution of the fluoride ligand for chloride to form **5a**, which was isolated in 72% yield (Scheme 2.5).

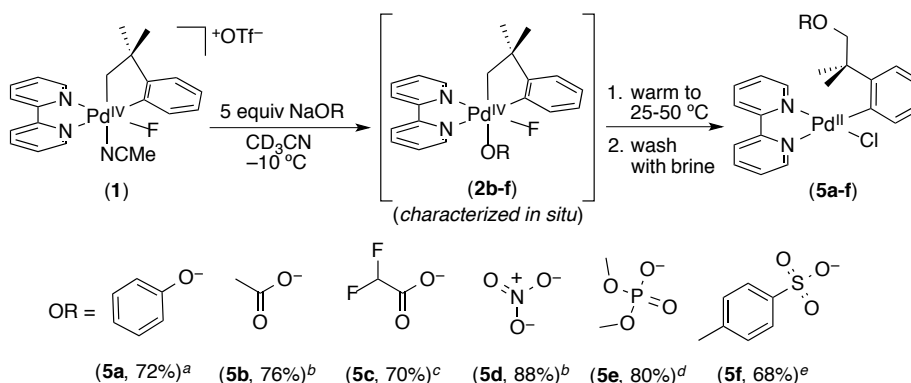
Scheme 2.5. Optimized Conditions for the Isolation of Pd^{II} Product **5a**



Scope of Oxygen Nucleophiles for C–O Coupling from Pd^{IV}

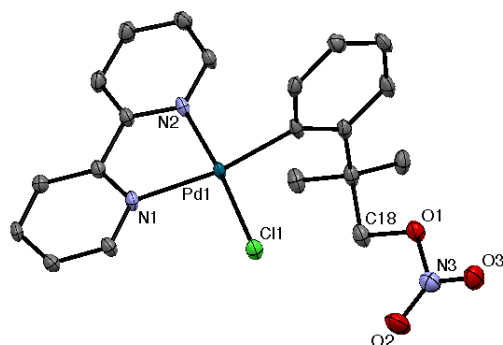
We next explored the scope of oxygen nucleophiles that participate in this transformation, with a focus on weakly nucleophilic oxyanions. The treatment of **1** with 1 equiv of NaOR (OR = acetate, difluoroacetate, nitrate, dimethyl phosphate, and tosylate) at –10 °C resulted in the quantitative formation of new Pd^{IV} complexes, as determined by ¹H and ¹⁹F NMR spectroscopic analyses.²⁴ Unlike the phenoxide adduct **2a**, these complexes (**2b–f**) were not sufficiently stable for isolation; however, they were all characterized *in situ* using one and two-dimensional ¹H, ¹³C, and ¹⁹F NMR spectroscopy.²⁵ Warming solutions of **2b–f** to between 25 and 50 °C in the presence of 4 equiv of exogenous NaOR resulted in clean C(sp³)–O coupling, and the products **5b–e** were isolated in high yield after washing with aqueous brine (Scheme 2.6).^{26,27} The structure of the Pd^{II} nitrate product **5d** was confirmed by X-ray crystallography, and an ORTEP representation of this structure is shown in Figure 2.1.

Scheme 2.6. Scope of C–O Bond-Forming Reductive Elimination from Pd^{IV}



^a50 °C, 2 h. ^b25 °C, 5 h. ^cNMe₄DFA, 40 °C, 1 h. ^dDMSO, 50 °C, 1 h. ^eNaOTs/NMe₄OTs, 25 °C, 12 h

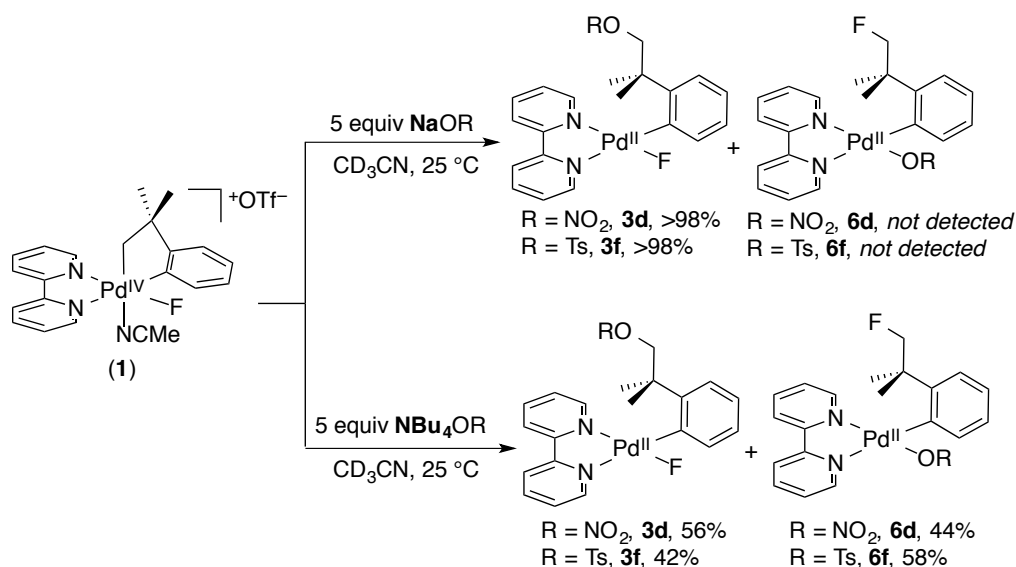
Figure 2.1. ORTEP Structure of Reductive Elimination Product **5d**. Thermal ellipsoids are drawn at 50% probability. Hydrogen atoms are omitted for clarity.



Influence of the Cation on Chemoselectivity

Selectivity for C–O versus C–F reductive elimination in catalysis is often rationalized based on the relative nucleophilicity of F^- versus RO^- , with the more nucleophilic anion dominating the reductive elimination process.²⁸ As such, we were intrigued that products of C–F coupling were not observed in any of the reactions in Scheme 2.6, even with the very weakly nucleophilic $NaNO_3$ and $NaOTs$. However, changing the nitrate/tosylate source from $NaOR$ to NBu_4OR under otherwise identical conditions resulted in a dramatic change in product distribution. For instance, as shown in Scheme 2.7, the treatment of **1** with 5 equiv of NBu_4NO_3 resulted in competitive formation of products derived from $C(sp^3)$ –O (**3d**, 56% yield) and $C(sp^3)$ –F (**6d**, 44% yield) bond-forming reductive elimination. Similarly, the use of NMe_4OTs resulted in 42% yield of $C(sp^3)$ –O coupled product **3f** and 58% of the corresponding alkyl fluoride **6f**.

Scheme 2.7. Chemoselectivity of Reductive Elimination as a Function of the Cation



We hypothesize that these counterion effects are due to interactions between the Lewis acidic cation and the Lewis basic fluoride ligand.²⁹ Consistent with this proposal, the ^{19}F NMR signal for the fluoride ligand in **1** (-336 ppm in CD_3CN) shifts in a concentration dependent manner upon the addition of Lewis acidic cations. For instance, in the presence of 5 equiv (0.11 M) of NaOTf, this signal appears at -338 ppm, while with 20 equiv (0.44 M) of NaOTf the resonance appears at -341 ppm. This effect is cation-specific; for instance, no analogous shift was observed upon the addition of 5 equiv of NBu₄OTf. The stoichiometry of this interaction was assessed by evaluation of a series of solutions with a constant total concentration of **1** and NaOTf ($[\mathbf{1}] + [\text{NaOTf}] = 36 \text{ mM}$), but with varied molar ratios of the two components. The resulting Job Plot (Figure 2.2) shows a maximum at $\chi = 0.5$, indicative of a 1:1 interaction between **1** and NaOTf.³⁰

Figure 2.2. Job Plot of $\Delta\delta_F \times \chi$ vs. χ at 25 °C, where χ is the mol fraction of Substrate **1**

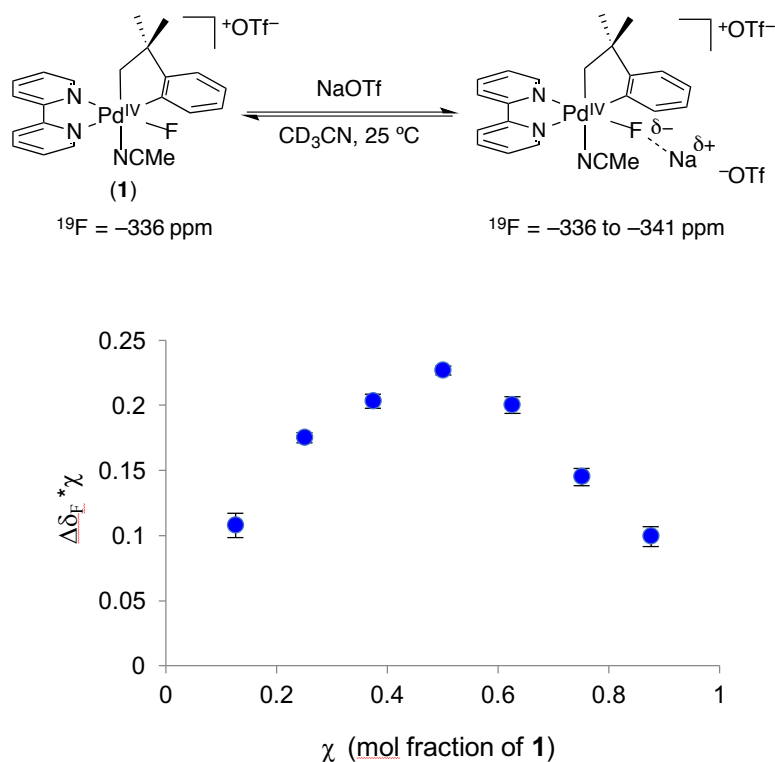
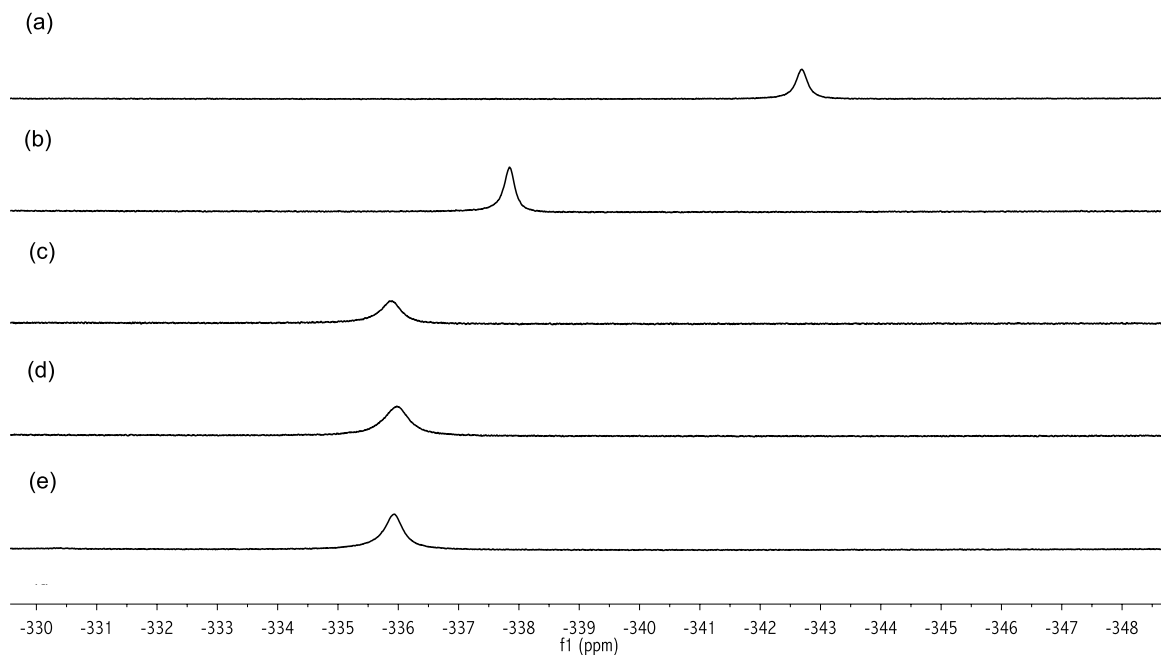
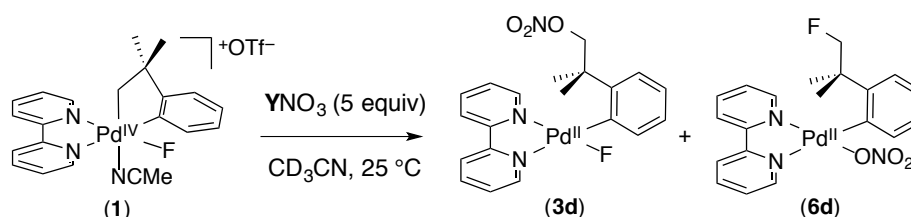


Figure 2.3. The Effect of the Cation (Y^+) on the ¹⁹F NMR Chemical Shift of Complex **1** in the Presence of 5 equiv of (a) LiOTf, (b) NaOTf, (c) KOTf, (d) CsOTf (e) NBu₄OTf



LiOTf, a stronger Lewis acid than NaOTf,³¹ has an even greater impact on the ¹⁹F NMR chemical shift of **1** (−343 ppm with 5 equiv (0.11 M) of LiOTf; Figure 2.3a). In contrast, the weaker Lewis acids KOTf and CsOTf produced negligible changes in the chemical shift (−336 ppm; Figure 2.3c, d). Subjecting **1** to 5 equiv of KNO₃ and CsNO₃ led to 29% and 53% yield of the C–F reductive elimination product, respectively, while the addition of LiNO₃ resulted in exclusive formation of the C(sp³)–O coupling product **3d** (Table 2.1). Taken together, these data suggest that interactions between the Pd^{IV}–F and the Lewis acidic cation decrease the accessibility of C–F bond-forming pathway(s). These results provide unprecedented new information about the role of cations in reductive elimination reactions from Pd^{IV}, and, as such, they have numerous potential applications in catalysis.³²

Table 2.1. Product Distribution of C–O and C–F Reductive Elimination from **1** as a Function of Cation



Cation (Y ⁺)	C–O (%)	C–F (%)
Li	>98	<2
Na	>98	<2
K	71	29
Cs	47	53
NBu ₄	56	44

Yields determined by ¹H NMR analysis of the crude reaction

Mechanistic Investigations

A variety of experimental and computational studies were conducted to gain further insights into the mechanism of these C(sp³)–O bond-forming reductive elimination reactions. Complexes **2a-c** were selected for detailed mechanistic study because they all undergo high

yielding C(sp³)-O bond-formation under a standard set of conditions, thereby enabling the direct comparison of reaction rates. Unless otherwise stated, these studies were conducted using tetramethylammonium salts of the oxyanions to render the CH₃CN solutions completely homogeneous for kinetic measurements. As described in detail below, the data are all consistent with the mechanism presented in Scheme 2.8. Here, pre-equilibrium dissociation of ⁻OR is followed by rate-limiting C(sp³)-O bond formation proceeding via an S_N2-type pathway. The rate expression for the proposed mechanism is shown in Scheme 2.8, and a summary of the mechanistic data is provided in Table 2.2.

Scheme 2.8. Proposed Mechanism for C(sp³)-O Bond Formation

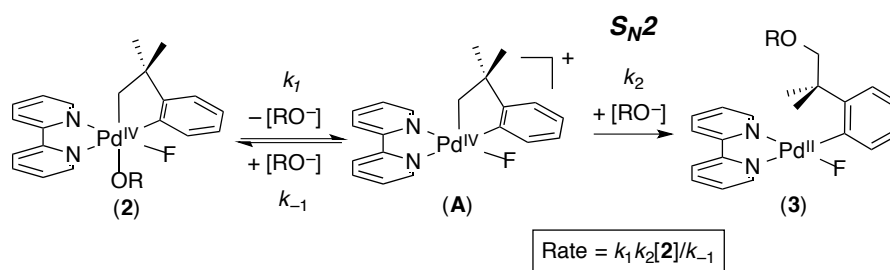
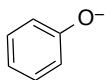
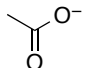
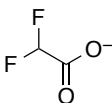
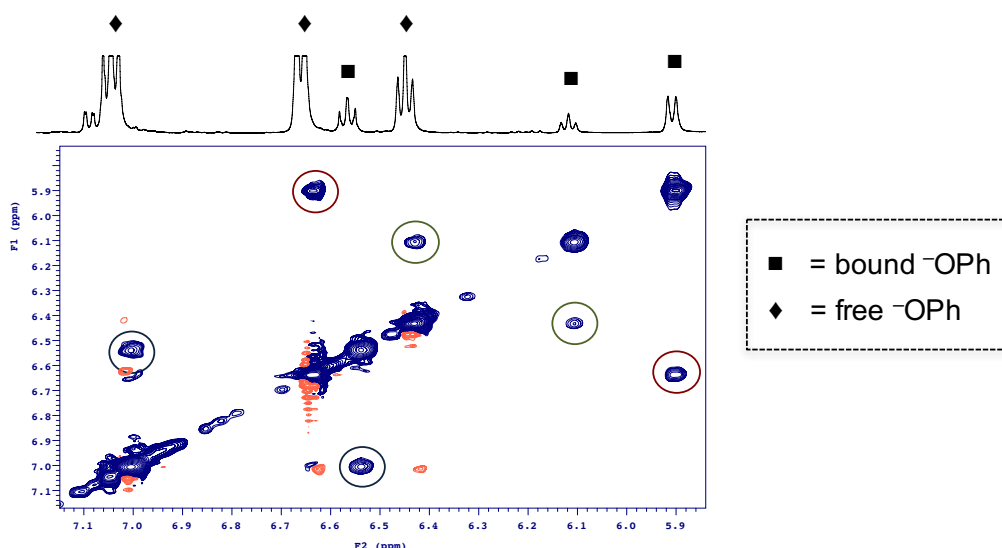


Table 2.2. Summary of Experimental Mechanistic Data for Reductive Elimination from Complexes **2a-c** to form **3a-c**

complex	RO ⁻	pK _a (conj acid)	EXSY (minimum temp for exchange)	k _{obs} at 35 °C (10 ⁻⁴ s ⁻¹)
2a		10	15 °C	8.1 ± 1.6
2b		4.7	10 °C	8.1 ± 1.2
2c		1.3	-10 °C	8.0 ± 0.2

Exchange Studies. We first examined the lability of the OR^- ligands in Pd^{IV} complexes **2a-c** using EXSY NMR experiments (Figure 2.4). In all cases, ^1H and ^{19}F EXSY studies show exchange between free and bound oxyanions at temperatures where complexes **2a-c** are stable to reductive elimination (-10 to 15 $^\circ\text{C}$). As shown in Table 2.2, the minimum temperature for exchange parallels the basicity of the oxyanion, with more basic (and therefore presumably more coordinating) ligands requiring higher temperatures for exchange. These results support the feasibility of rapid pre-equilibrium dissociation of OR^- to form a cationic intermediate prior to C–O bond formation.

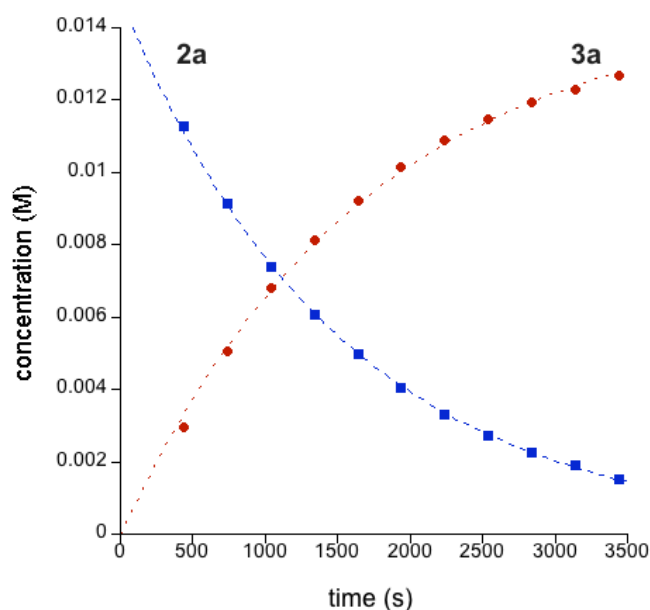
Figure 2.4. Representative EXSY NMR Spectrum of **2a** at 15 $^\circ\text{C}$ Showing Exchange of Phenoxide Ligand



Rate Studies. Rate studies were next carried out to probe the kinetic order of $\text{C}(\text{sp}^3)\text{--O}$ bond-formation from **2a-c** in both $[\text{Pd}]$ and $[\text{OR}^-]$. First, the reactions of **1** with 5 equiv of NMe_4OR (0.071 M) ($\text{OR}^- = \text{phenoxide, acetate, difluoroacetate}$) at 35 $^\circ\text{C}$ in CD_3CN were monitored by ^1H NMR spectroscopy. Under these conditions, the decay of *in situ*-generated **2a-c** proceeded with clean first-order kinetic behavior over 3 half-lives, and a representative kinetics plot is shown in Figure 2.5. The value of k_{obs} for reductive elimination was determined over a range of concentrations of exogenous $[\text{NMe}_4\text{OR}]$ (0.021 M to 0.13 M, 1.5-

9.0 equiv). In all cases, a zeroth-order dependence on $[\text{NMe}_4\text{OR}]$ was observed. These data rule out a mechanism involving direct attack of an external oxyanion nucleophile on complexes **2a-c**, as such a process would be expected to display a first-order dependence on $[\text{NMe}_4\text{OR}]$. Instead, the zeroth-order dependence on the nucleophile is fully consistent with the proposed mechanism (see rate expression in Scheme 2.8).

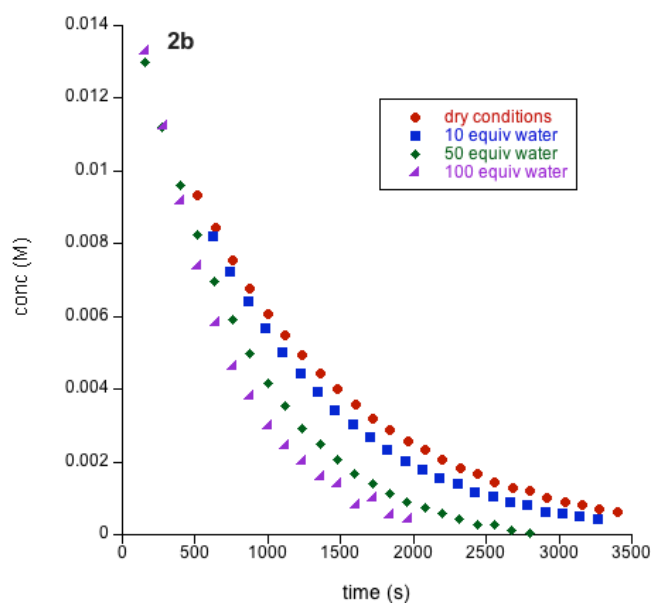
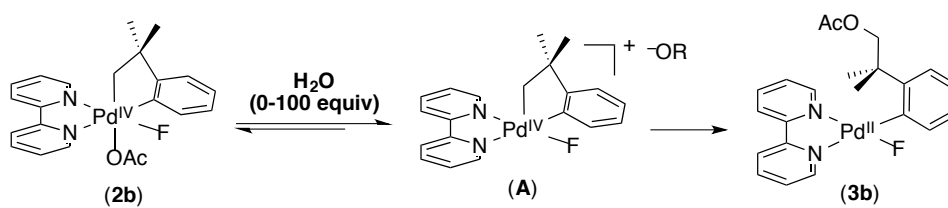
Figure 2.5. Reaction Profile for Reductive Elimination from **2a** to form **3a** at 35 °C



The value of k_{obs} for this reaction was nearly identical for complexes **2a-c** (ranging between 8.0 and $8.1 \times 10^{-4} \text{ s}^{-1}$). There is no correlation between the $\text{p}K_{\text{a}}$ of the conjugate acid of the oxyanion and the rate of reductive elimination, over a $\text{p}K_{\text{a}}$ range of >8 . Hartwig has reported a similar observation in studies of $\text{C}(\text{sp}^3)\text{-O}$ bond-forming reductive elimination from Pd^{II} centers.¹⁴ These data are consistent with a mechanism involving two sequential steps that have opposing electronic requirements. In our system, the pre-equilibrium OR^- dissociation is fastest with the most electron deficient oxyanions. In contrast, $\text{S}_{\text{N}}2$ -type attack of RO^- on the $\text{Pd}^{\text{IV}}\text{-C}$ bond is expected to be fastest with more electron rich oxyanions. In both our system and in Hartwig's, the electronic requirements of these two steps appear to essentially cancel one another out.

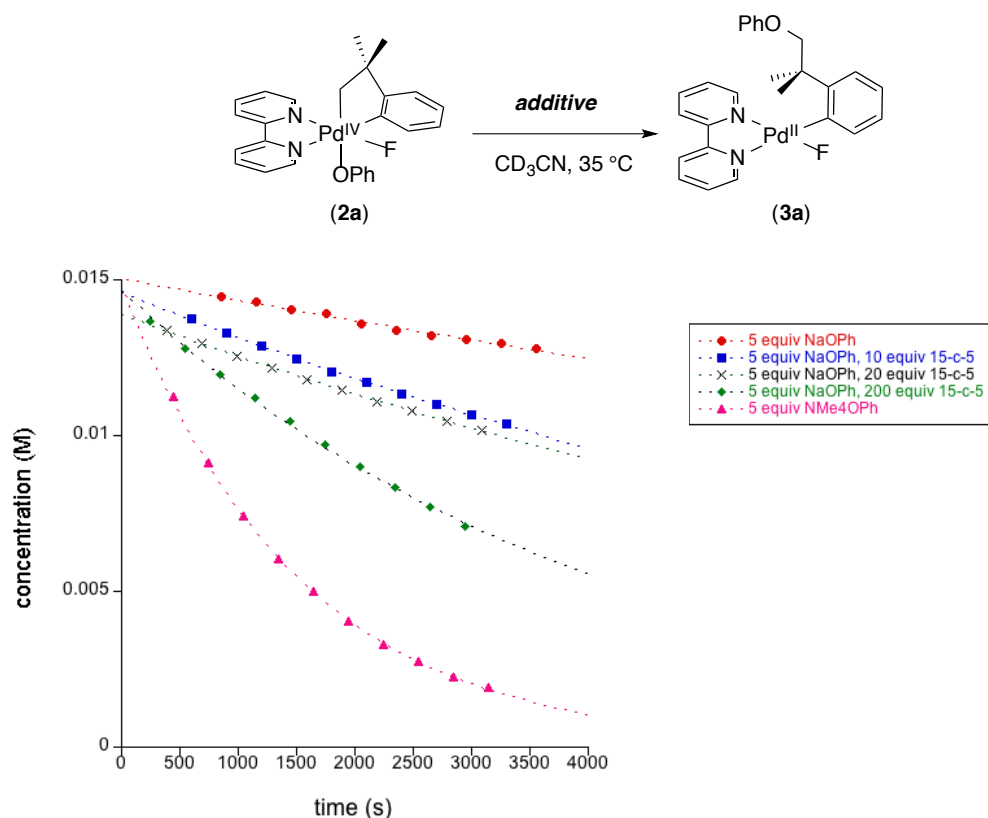
Additive Effects. While the electronic properties of ^-OR had a negligible effect on the rate of reductive elimination, the addition of water impacted the kinetics of reductive elimination. In the presence of 100 equiv of water, k_{obs} for reductive elimination from complex **2b** was approximately 2-fold faster ($18 \times 10^{-4} \text{ s}^{-1}$ at $35 \text{ }^\circ\text{C}$) than under anhydrous conditions ($8.1 \times 10^{-4} \text{ s}^{-1}$ at $35 \text{ }^\circ\text{C}$).³³ Protic additives have been previously reported to increase the rate of reductive elimination for reactions proceeding through an ionic intermediate, presumably by facilitating pre-equilibrium dissociation of X^- .^{13b,14,34} Consistent with this proposal, EXSY experiments for complex **2b** in the presence of 100 equiv of water show that exchange of free and bound acetate occurs at a lower temperature ($0 \text{ }^\circ\text{C}$) than observed under anhydrous conditions ($10 \text{ }^\circ\text{C}$, Table 2.2). Thus, the addition of water may also shift the pre-equilibrium proposed in Scheme 2.8 and Figure 2.6 towards the cationic intermediate **A**.

Figure 2.6. The Effect of Water on the Rate of C–O Coupling from **2b**



Finally, the cation was found to dramatically impact the rate of reductive elimination. For instance, k_{obs} for reductive elimination from **2a** was more than an order of magnitude faster for reactions conducted in the presence of 4 equiv of NMe₄O⁻Ph than with 4 equiv of NaO⁻Ph ($k_{\text{obs}} = 81 \times 10^{-5}$ vs. $4.2 \times 10^{-5} \text{ s}^{-1}$, respectively). Notably, solubility is not the origin of this effect as both salts are completely soluble under the experimental conditions. Moreover, no competing C–F reductive elimination was observed under any of the conditions examined when the comparatively stronger nucleophile ⁻O⁻Ph served as the coupling partner. We thus rationalize these observations based on the relative strengths of the ion pairs in these two species, with NaO⁻Ph existing as a much tighter ion pair in CH₃CN than NMe₄O⁻Ph. Tight ion pairing is expected to render PhO⁻ less accessible as a nucleophile, which is expected to slow the S_N2-type reductive elimination step. Consistent with this hypothesis, the addition of 15-crown-5 to the reactions with NaO⁻Ph led to a seven-fold increase in the observed rate constant ($k_{\text{obs}} = 27 \times 10^{-5} \text{ s}^{-1}$), presumably by decreasing the tightness of the NaO⁻Ph ion pair.³⁵

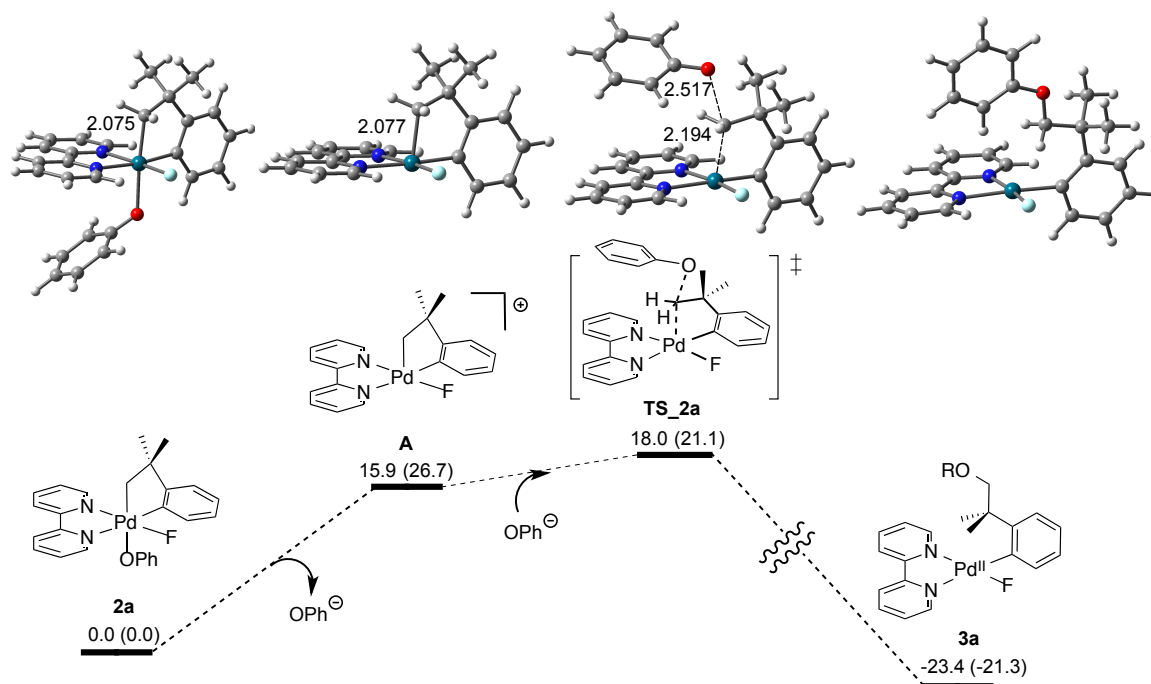
Figure 2.7. The Effect of the Counterion on the Rate of C–O Coupling from **2a**



Computational Studies

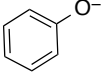
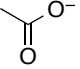
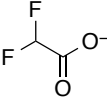
DFT calculations were conducted by Prof. Allan Canty at the University of Tasmania to further assess the viability of the mechanism proposed in Scheme 2.8 for OR = OPh, O₂CCF₂H, and OAc.^{1b,36,37} The calculated reaction profile is nearly identical for the three complexes, and a representative profile (for **2a**) is shown in Figure 2.8. In all cases, DFT scans for dissociation of the RO⁻ ligand from **2** show an essentially barrier-less process with steadily increasing energy to form **A**. For complexes **2a-c**, the formation of **A** is endergonic ($\Delta G = 7.1$ - 15.9 kcal/mol; Table 2.3, column 3). These data are consistent with the fact that **A** is not detected experimentally in these three systems and are also consistent with the experimental observation that anion exchange occurs at temperatures lower than those required for reductive elimination. Furthermore, the calculated ΔG values are in agreement with the experimental exchange results, with more electron rich ⁻OR requiring higher temperatures for dissociation (ΔG for PhO⁻ > AcO⁻ > CF₂HCO₂⁻; Table 2.3, column 3).

Figure 2.8. Energy Profile for Reductive Elimination from **2a**, Together with Gaussview Diagrams. Energies ΔG (ΔH) in kcal/mol and bond distances in Å.



The values of ΔG^\ddagger for S_N2 attack on intermediate **A** track well with the nucleophilicity of RO^- (ΔG^\ddagger for PhO^- = 2.1 kcal/mol; for AcO^- = 5.9 kcal/mol; for $CF_2HCO_2^-$ = 9.3 kcal/mol; Table 2.3, column 4). Because of the offsetting electronic requirements of the oxyanion dissociation and S_N2 reductive elimination steps, the overall ΔG^\ddagger values for moving from **2a-c** to **TS_2** are essentially identical within the error of DFT (ranging from 16.4 to 18.0 kcal/mol; Table 2.3, column 5). This is consistent with the experimental results showing very similar rates of reductive elimination from **2a-c** (Table 2.2).

Table 2.3. Summary of DFT Data for Reductive Elimination from **2a-c**

complex	OR	$\Delta G_{2 \rightarrow A}$ (kcal/mol)	$\Delta G_{A \rightarrow TS2}^\ddagger$ (kcal/mol)	$\Delta G_{2 \rightarrow TS2}^\ddagger$ (kcal/mol)
2a		15.9	2.1	18.0
2b		11.0	5.9	16.9
2c		7.1	9.3	16.4

Kinetic studies of the nitrate system were not feasible experimentally, therefore computational studies were carried out to gain more insight into this reductive elimination process. The formation of nitrate complex **2d** from **1** computes as exergonic by just 0.9 kcal/mol (Scheme 2.9). This computation is consistent with experimental NMR data showing the presence of an equilibrium between **2d** and **1d** (Figure 2.9) and is in contrast to the more nucleophilic oxygen donors in which the ligated phenoxide, acetate, and difluoroacetate complexes (**2a**, **2a**, and **2c**) are the sole species detected (*vide infra*). Despite the weak nucleophilicity of the nitrate coupling partner, DFT calculations show a low barrier for nucleophilic attack at the Pd^{IV}-alkyl carbon in intermediate **A**. Overall, the combined experimental and computational mechanistic investigations support an S_N2-type reductive elimination pathway proceeding via a cationic, five-coordinate intermediate for all nucleophiles examined.

Scheme 2.9. Equilibria and Reaction Pathway for Reductive Elimination from **2d**. Energies ΔG (ΔH) are in kcal/mol.

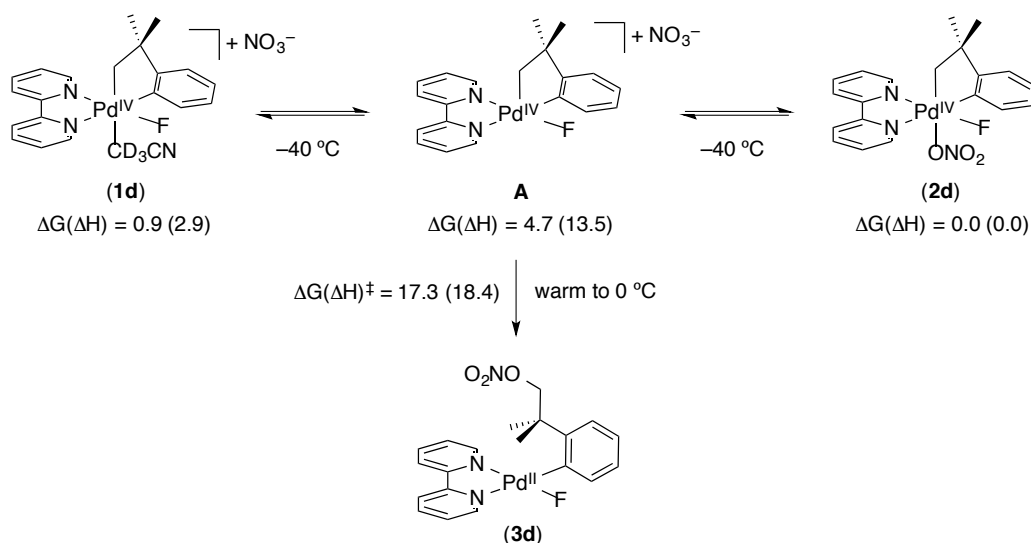
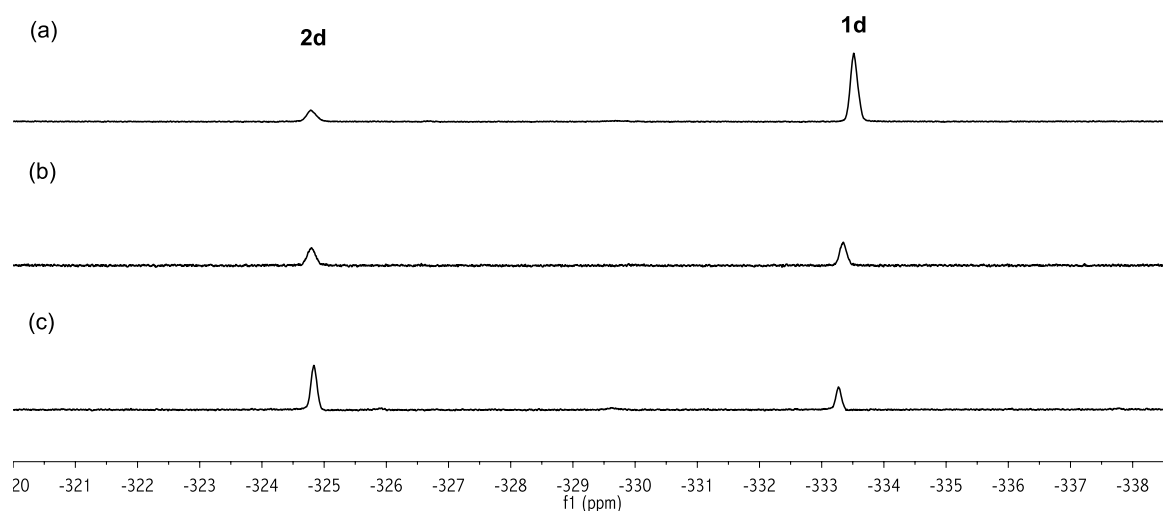


Figure 2.9. Identification of an equilibrium between **1d** and **2d** in the presence of (a) 1 equiv of NBu_4NO_3 (b) 20 equiv of NBu_4NO_3 and (c) 50 equiv of NBu_4NO_3 at -40°C



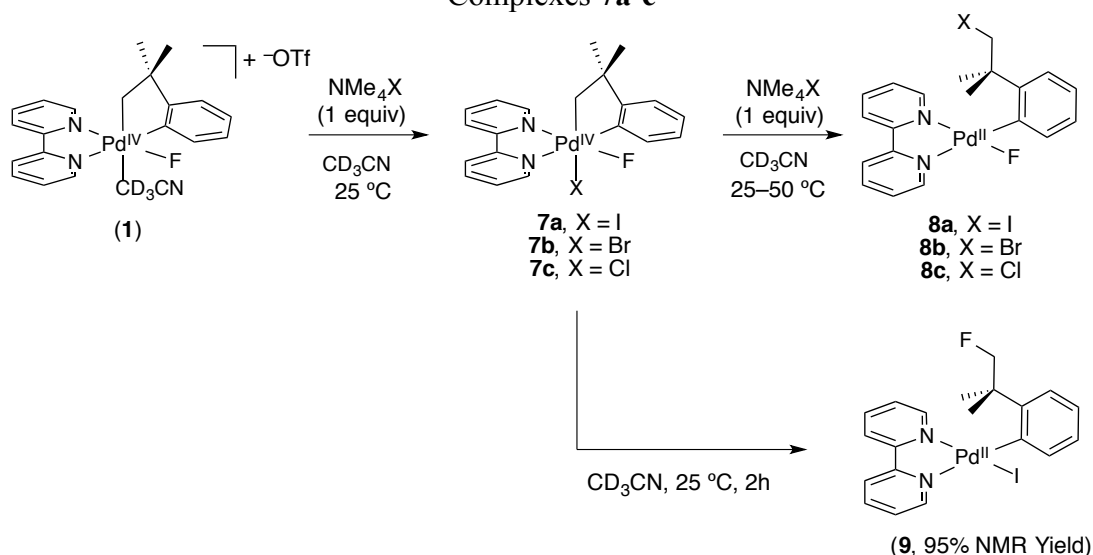
2.2.2. Carbon–Halogen Bond-Forming Reductive Elimination from Pd^{IV} : Evidence for Re-Oxidative Addition Pathways with Non-Traditional Nucleophiles

We reasoned that replacement of the labile triflate ligand in **1** with other X-type ligands (i.e., Cl, Br, I) would allow the reactivity, selectivity, and mechanism of C–halogen bond-forming reductive elimination from Pd^{IV} to be more generally explored.^{2,38,39} preliminary studies of Pd^{IV} –halide species **7a-c** provide insight into their relative reactivity

towards C–X (X = Cl, Br, I) vs. C–F bond-forming reductive elimination.^{18a} The treatment of model complex **1** with NMe₄X (Cl, Br, I) led to the *in situ* formation of Pd^{IV} complexes **7a-c** (Scheme 2.10). In comparison to the phenoxide-ligated complex **2a** in section 2.2.1, the halide adducts **7a-c** were unstable and could not be isolated. *In situ* characterization of these complexes were therefore carried out at or below room temperature.

In the presence of 1 equiv of exogenous halide, complexes **7a** and **7b** underwent selective C(sp³)–Br and C(sp³)–I coupling, respectively, after 2–4 h at room temperature. Thermolysis of the chloride adduct **7a** led to clean C(sp³)–Cl bond formation after 2 h at 50 °C. The relative rates of C(sp³)–X coupling track well with the leaving group ability of the halides and suggest the following trend: I > Br > Cl > F. These results mirror catalytic development in the area of Pd^{II/IV} catalysis in which methods for C–F bond formation remain less prevalent in the literature.⁴⁰

Scheme 2.10. Competitive C–Halogen Reductive Elimination from *in situ* Generated Complexes **7a-c**



Interestingly, we observed a dramatic difference in the reactivity/selectivity for C–halogen reductive elimination from **7a** in the absence of exogenous iodide. As shown in Scheme 2.10, exclusive C–F reductive elimination from iodide adduct **7a** was observed after 2 h at room temperature. Notably, these mild conditions contrast the high temperatures

typically required for C–F reductive elimination in this model system.¹⁸ One possible explanation for this observation is depicted in Scheme 2.11: (i) Facile C(sp³)–I reductive elimination initially occurs, generating the kinetic product **8a**. (ii) In the absence of added iodide, this reductive elimination event is reversible and the alkyl iodide undergoes an intramolecular oxidative addition to form an unstable Pd^{IV} isomer. (iii) C(sp³)–F reductive elimination readily occurs from this intermediate, providing mild access to the alkyl fluoride product **9**. Previous work by Campora⁴¹ has demonstrated the feasibility of alkyl-iodide oxidative addition in a related Pd^{II/IV} system.⁴²

Scheme 2.11. Proposed Mechanism for the Observed Reactivity Depicted in Scheme 2.10

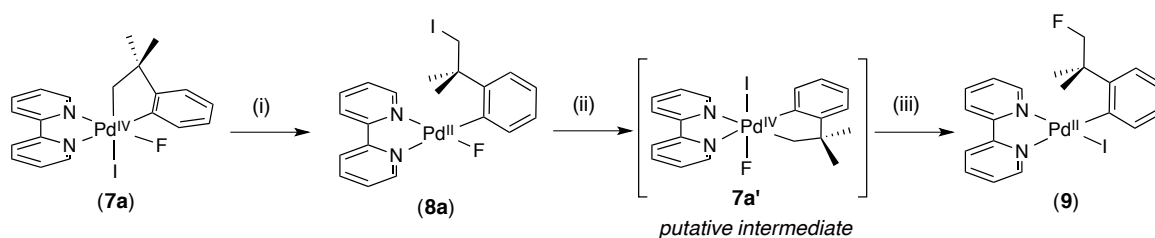
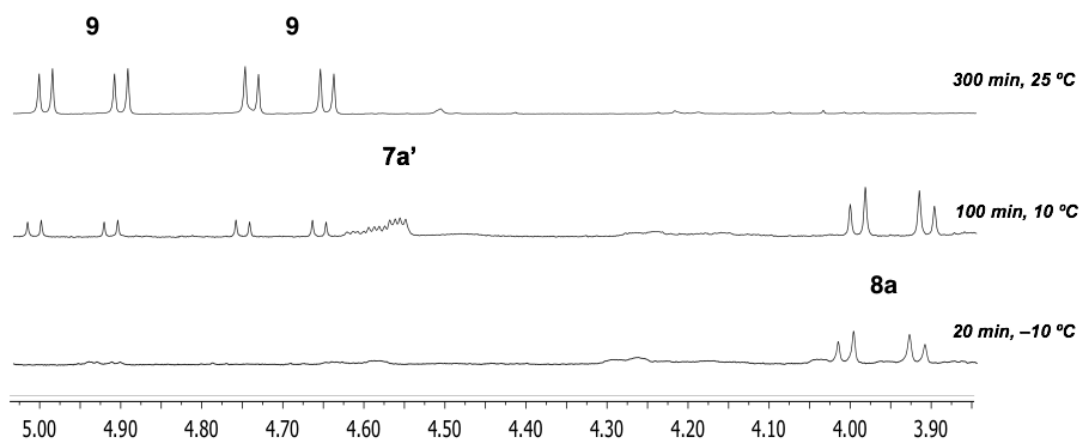


Figure 2.10. Monitoring the Reactivity of Complex **7a** by ¹H NMR spectroscopy. The methylene proton resonances are shown.



To gain evidence in support of the proposed reversible reductive elimination event, complex **1** was treated with 1 equiv of NBu₄I, and the reaction was monitored by ¹H NMR spectroscopy (Figure 2.10). Consistent with our hypothesis, alkyl iodide **8a** was detected after 20 min at -10 °C (Figure 2.10, bottom spectra). However, over time, new ¹H NMR

resonances consistent with a new Pd^{IV} intermediate appeared (proposed species **7a'** and/or other isomers) with concomitant decay of **8a** and growth of the C–F coupled product **9**. Finally, warming the reaction mixture to room temperature led to complete consumption of the reactive intermediates and >95% conversion to the C–F reductive elimination product (Figure 2.10, top spectra). Overall, these preliminary results support the feasibility of the pathway outlined in Scheme 2.11.

As a final set of studies, we sought to explore the generality of the transformation proposed in Scheme 2.11. We reasoned that if oxidative addition of the pendant alkyl iodide was occurring, then complexes containing even better leaving groups should also participate in this intramolecular reaction. The reactivity of Pd^{II} complexes **5d** and **5f** containing alkyl-nitrate and tosylate functionalities was therefore monitored by ¹H NMR spectroscopy.

As depicted in Figure 2.11, the treatment of alkyl nitrate **5d** with 1 equiv of NMe₄Cl led to formation of the previously characterized C–Cl reductive elimination product **8c** after 36 h at 50 °C. The tosylate analogue was even more reactive, consistent with its greater leaving group ability, as subjecting **5f** to 1 equiv of NMe₄Cl led to C–Cl coupling after 2 h at 10 °C (eq. 2). Importantly, studies carried out in the absence of Pd suggest that this reactivity is likely not the result of direct nucleophilic attack of Cl[−] at the alkyl carbon (eq. 3).

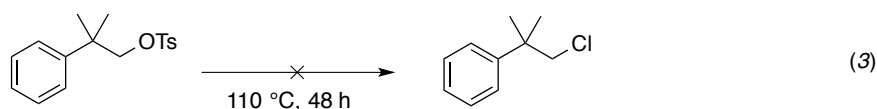
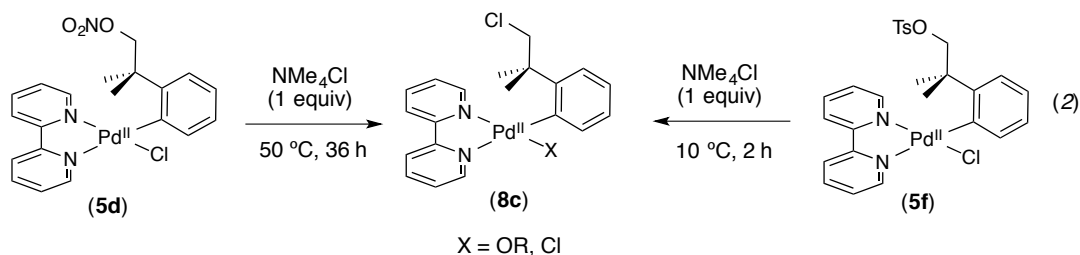
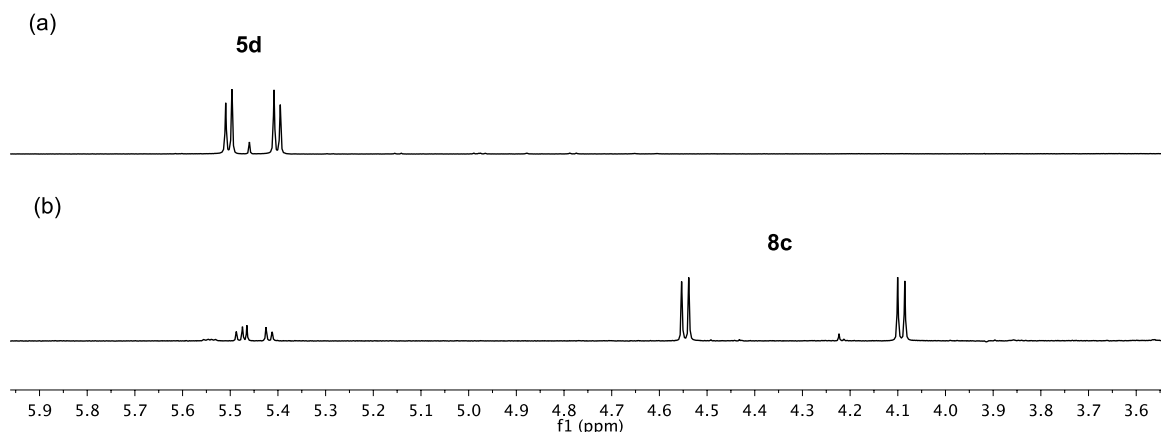


Figure 2.11. ^1H NMR spectra of (a) complex **5d** at 25 °C (b) treatment of **5d** with 1 equiv of NMe_4Cl at 50 °C for 36 h to form complex **8c**. The methylene proton resonances are shown.



2.2.3. Exploring the Synthesis and Reactivity of a Model Pd^{IV} (biphenyl) System

In parallel with studies centered on alkyl- Pd^{IV} derivatives, we also examined the synthesis and reactivity of Pd^{IV} complexes containing sp^2 -hybridized carbons. Initial studies targeted Pd^{IV} complexes of general structure **12** for several reasons. First, reductive elimination is favored at sp^3 over sp^2 carbon centers for all of the nucleophiles examined in our initial model system, which precludes study of the latter transformation. In addition, model complex **12** would allow us to assess the viability of direct $\text{C}(\text{sp}^2)\text{-O}$ vs. $\text{C}(\text{sp}^2)\text{-F}$ reductive elimination from an octahedral Pd^{IV} center with electronic deficient OR^- ligands.⁷

As shown in Scheme 2.12, Pd^{IV} complexes **12a** and **12b** were prepared via a multi-step synthetic sequence starting from Pd^{II} precursor $[(\text{COD})\text{PdCl}_2]$ (COD = 1,5-cyclooctadiene). Lithiation of 1,2-dibromobiphenyl at low temperature and subsequent treatment with $[(\text{COD})\text{PdCl}_2]$ gave the corresponding $[(\text{COD})\text{Pd}(\text{biphenyl})]$ complex **10** in 44% yield. Ligand exchange with bipyridine afforded the penultimate product **11**, which was isolated as a bright orange solid in 95% yield. The treatment of $[(\text{bpy})\text{Pd}(\text{biphenyl})]$ (**11**) with the F^+ oxidant NFTPT (*N*-Fluoro-trimethylpyridinium triflate) and the corresponding NBu_4OR salt afforded the desired Pd^{IV} complexes **12a** and **12b** in 54 and 62% isolated yields, respectively. X-ray quality crystals of **12b** were obtained from a concentrated

dichloromethane solution at 40 °C, and an ORTEP representation of the structure is shown in Figure 2.12.

Scheme 2.12. Synthesis of Pd^{IV} Model System **12**

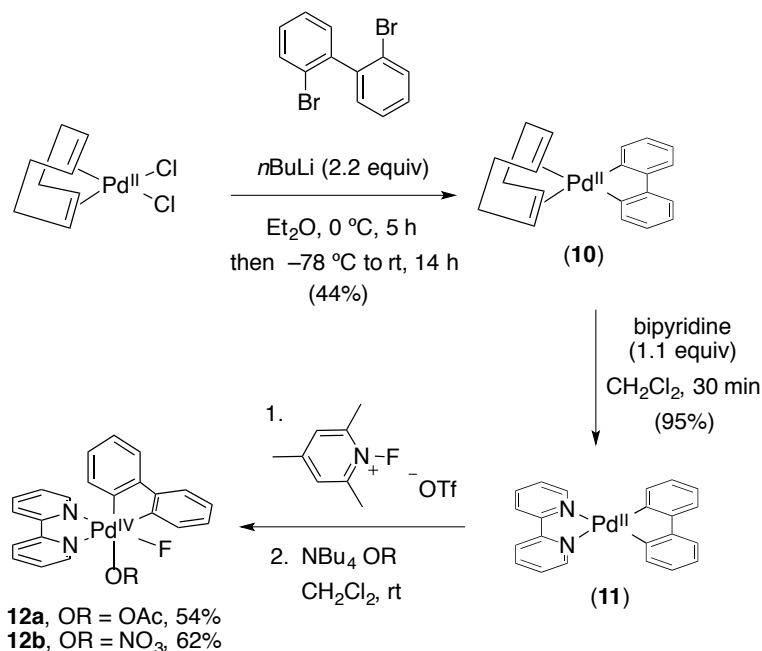
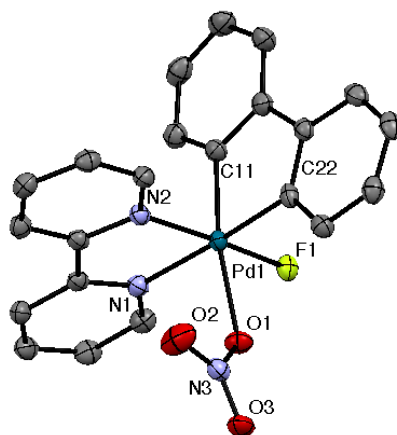


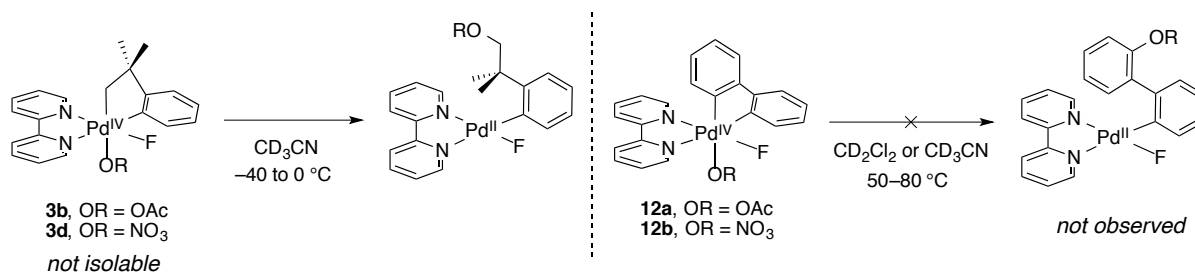
Figure 2.12. ORTEP Representation of Pd^{IV} Complex **12b**. Thermal ellipsoids are drawn at 50% probability. Hydrogen atoms are omitted for clarity.



In contrast to acetate and nitrate bound complexes **3b** and **3d**, complexes **12a** and **12b** were remarkably stable and did not undergo C(sp²)-O or C(sp²)-F reductive elimination after heating between 50-80 °C overnight (Scheme 2.13). The difference in reactivity between **3** and **12** can be attributed, in part, to the requirement for reductive elimination to occur from a

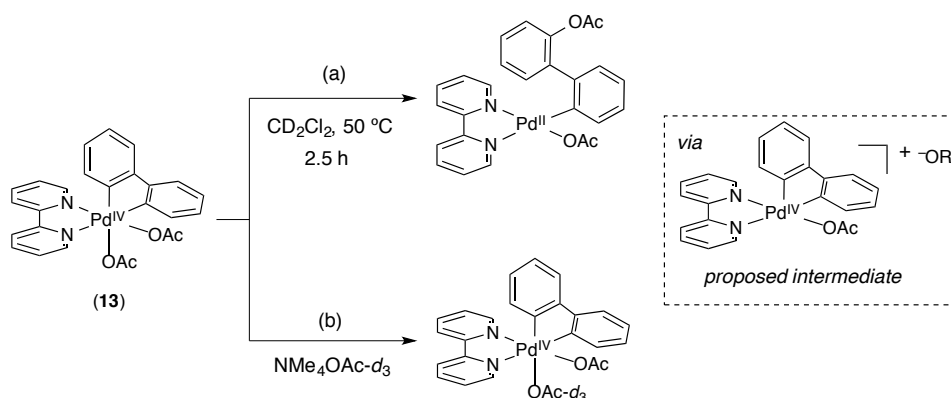
pentacoordinate intermediate in these model systems. Previous work has shown that carbon–heteroatom reductive elimination reactions from Pd^{IV} and Pt^{IV} centers often proceed from five-coordinate species following ligand dissociation.^{2,7,13,15,18} However, in the biphenyl system, dissociation of the electron-deficient nitrate and acetate anions from **12** would lead to a cationic intermediate that prevents the direct, *cis* reductive elimination needed for C(sp²)–O coupling. The lack of products attributed to C(sp²)–F reductive elimination can be rationalized by the strength of the Pd^{IV}–F bond and the challenging nature of the C(sp²)–F reductive elimination event.⁴⁰

Scheme 2.13. Difference in Stability/Reactivity of Model Complexes **3** and **12** Towards C–O Coupling with Acetate and Nitrate as Coupling Partners



To provide further evidence for this hypothesis, the reactivity of complex **13** bearing two labile acetate ligands was studied. Diacetate **13** was synthesized via oxidation of precursor **11** with MesI(OAc)₂. In contrast to **12**, complex **13** underwent C(sp²)–O bond-forming reductive elimination upon heating at 50 °C for 2.5 h (Scheme 2.14a). Facile ligand exchange of the [–]OAc *trans* to the sp²–C in complex **12** with NMe₄OAc-*d*₃ suggests that a five-coordinate intermediate is accessible (Scheme 2.14b). These preliminary results provide evidence for C(sp²)–O reductive elimination proceeding from a five-coordinate complex, which is consistent with the vast majority of reductive elimination reactions from Pd^{IV} centers.^{2,7,13,15,18}

Scheme 2.14. Reactivity of Diacetate Complex 13



2.3. Conclusions

In summary, this chapter describes experimental and computational studies of carbon–heteroatom bond-forming reductive elimination from Pd^{IV} complexes. In section 2.2.1 we demonstrate that oxyanions ranging from strongly nucleophilic phenoxide to weakly nucleophilic tosylate and nitrate participate as coupling partners in $\text{C}(\text{sp}^3)\text{--O}$ bond-forming reactions. In all cases, $\text{C}(\text{sp}^3)\text{--O}$ bond formation occurs with high selectivity over $\text{C}(\text{sp}^2)\text{--O}$ coupling, which is in contrast to the selectivity that typically occurs from low-valent Pd centers. Additives have a profound impact on the chemoselectivity of these reductive elimination reactions. Specifically, the addition of excess RO^- limits competing $\text{C}(\text{sp}^3)\text{--C}(\text{sp}^2)$ bond-forming reductive elimination, while the presence of Lewis acidic cations suppresses competing $\text{C}(\text{sp}^3)\text{--F}$ coupling. Both experimental and computational mechanistic investigations are consistent with an $\text{S}_{\text{N}}2$ -type reductive elimination pathway proceeding via a cationic, five-coordinate intermediate.

Studies in section 2.2.2 provide evidence for the reversibility of this reductive elimination process when good leaving groups (i.e., iodide, nitrate, and tosylate) serve as coupling partners. Finally, section 2.2.3 explores the synthesis and reactivity of an analogous sp^2 -hybridized model system. These complexes exhibit remarkable stability and do not undergo $\text{C}(\text{sp}^2)\text{--O}$ coupling reactions with weakly nucleophilic anions such as nitrate.

We anticipate that the detailed studies described herein will ultimately prove valuable in the development, optimization, and mechanistic understanding of high-valent Pd-catalyzed C(sp³)-heteroatom coupling reactions.

2.4. Experimental Procedures and Characterization of Compounds

2.4.1. General Procedures and Materials and Methods

General Procedures

All experiments were conducted under ambient atmosphere unless otherwise stated. NMR spectra were obtained on a Varian VNMR 700 (699.76 MHz for ¹H; 175.95 MHz for ¹³C) or a Varian VNMR 500 (500.09 MHz for ¹H; 470.56 MHz for ¹⁹F; 125.75 MHz for ¹³C; 202.43 MHz for ³¹P) spectrometer. ¹H and ¹³C chemical shifts are reported in parts per million (ppm) relative to TMS, with the residual solvent peak as an internal reference. ¹⁹F chemical shifts were reported in ppm relative to CCl₃F. NMR signals were assigned based on the following 2D experiments: ¹H/¹H COSY, ¹H/¹H TOCSY, ¹H/¹H NOESY, ¹H/¹H ROESY, ¹H/¹³C HSQC, ¹H/¹⁹F HOESY. Abbreviations used in the NMR data: s, singlet; d, doublet; t, triplet; q, quartet; m, multiplet; dd, doublet of doublets; td, triplet of doublets; ddd, doublet of doublets of doublets; br, broad signal. Mass spectral data were obtained on a Micromass magnetic sector mass spectrometer in electrospray ionization mode. X-ray crystallographic data were collected on a Bruker SMART APEX-I CCD-based X-ray diffractometer.

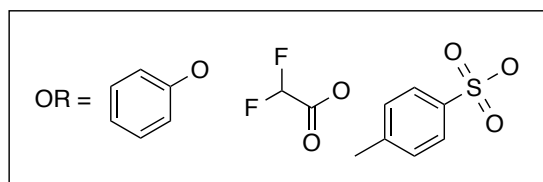
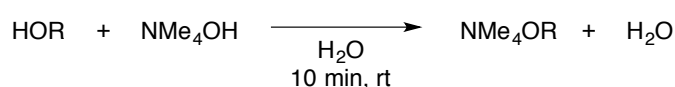
Materials and Methods

The following compounds were prepared via literature procedures: Pd^{II}(CH₂CMe₂-*o*-C₆H₄)(COD),⁴³ [(bpy)Pd^{IV}(CH₂CMe₂-*o*-C₆H₄)(F)(OTf)] (1),^{18a} lithium *p*-toluenesulfonate, cesium trifluoromethanesulfonate,⁴⁴ and sodium dimethyl phosphate.⁴⁵ All syntheses were conducted under ambient atmosphere. The cyclobutane by-product (4) was characterized by comparison of its ¹H NMR spectrum with that reported in the literature.⁴⁶ Sodium trifluoromethanesulfonate, potassium trifluoromethanesulfonate, sodium *p*-toluenesulfonate, potassium nitrate, tetramethylammonium acetate, and tetramethylammonium hydroxide solution (1 M in H₂O) were obtained from Sigma Aldrich. Phenol, sodium acetate, sodium nitrate, *p*-toluenesulfonic acid monohydrate, and tetramethylammonium chloride were obtained from Acros. Sodium phenoxide, tetramethylammonium nitrate, lithium nitrate, and 15-crown-5 were obtained from Alfa Aesar. 1-Fluoro-2,4,6-trimethylpyridinium triflate

(NFTPT) and iodomesitylene diacetate were obtained from TCI America. Cesium nitrate was obtained from Fisher. Difluoroacetic acid was obtained from Oakwood. Acetonitrile (Aldrich), dichloromethane (Fisher), pentane (Fisher), petroleum ether (Fisher), and diethyl ether (EMD) were used without further purification. CD₃CN, CD₂Cl₂, and CD₃OD were obtained from Cambridge Isotopes Laboratories and used without further purification.

2.4.2. Synthesis and Characterization of Compounds

General Procedure for the Synthesis of NMe₄OR [OR = phenoxide (OPh), difluoroacetate (O₂CCF₂H), tosylate (OTs)]

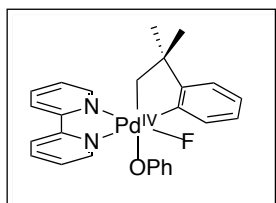


A 20 mL vial was charged with HOR (2.5 mmol). NMe₄OH (2.5 mL of a 0.1 M solution in H₂O) was then added, and the mixture was stirred for 10 min at room temperature. H₂O was removed under reduced pressure (heating at 80 °C). The product was further dried by heating at 70 °C under vacuum for 15 h.

NMe₄OPh was obtained according to the procedure above as a light brown powder (401 mg, 96% yield). ¹H NMR (700 MHz, CD₃OD, 25 °C): δ 6.99 (t, *J*_{HH} = 7.7 Hz, 2H), 6.62 (d, *J*_{HH} = 7.7 Hz, 2H), 6.44 (t, *J*_{HH} = 7.7 Hz, 1H), 3.13 (s, NMe₄, 12H). ¹³C NMR (176 MHz, CD₃OD, 25 °C): δ 164.55, 128.57, 117.76, 114.65, 54.41 (t, *J*_{14N-13C} = 4.0 Hz, N(CH₃)₄).

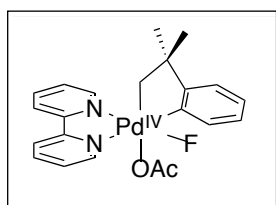
NMe₄O₂CCF₂H was obtained according to the procedure above as a white powder (410 mg, 97% yield). ¹H NMR (700 MHz, CD₃CN, 25 °C): δ 5.57 (t, *J*_{HF} = 57.0 Hz, 1H), 3.16 (s, NMe₄, 12 H). ¹³C NMR (176 MHz, CD₃CN): δ 165.38 (t, *J*_{CF} = 22.4 Hz), 111.05 (t, *J*_{CF} = 250 Hz), 54.92 (t, *J*_{14N-13C} = 4.0 Hz, N(CH₃)₄). ¹⁹F NMR (471 MHz, CD₃CN): δ -122.25 (d, *J*_{HF} = 57.0 Hz).

NMe₄OTs was obtained according to the procedure above as a white powder (556 mg, 91% yield). ¹H NMR (700 MHz, CD₃CN, 25 °C) δ 7.61 (d, *J*_{HH} = 7.8 Hz, 2H), 7.16 (d, *J*_{HH} = 7.8 Hz, 2H), 3.11 (s, NMe₄, 12H), 2.34 (s, 3H). ¹³C NMR (176 MHz, CD₃CN): δ 146.03, 138.38, 128.24, 125.65, 55.09 (t, *J*_{14N-13C} = 5.3 Hz, N(CH₃)₄), 20.24.



Synthesis of [(bpy)Pd^{IV}(CH₂CMe₂-*o*-C₆H₄)(F)(OPh)] (2a). A 20 mL vial was charged with [(bpy)Pd^{IV}(CH₂CMe₂-*o*-C₆H₄)(F)(OTf)] (1) (30 mg, 0.053 mmol, 1.0 equiv), and CH₃CN (5 mL) was added. NaOPh (6.8 mg, 0.059 mmol, 1.1 equiv) was added, and the

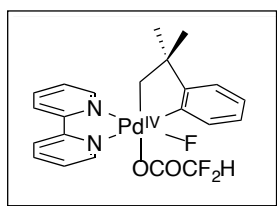
resulting red solution was stirred for 5 min at room temperature. The reaction mixture was then filtered through celite, and the filtrate was collected and concentrated by rotary evaporation. The precipitate was washed with diethyl ether (3 x 5 mL) and then redissolved in CH₂Cl₂ (2 mL). Pentane (5 mL) was added to precipitate the product, which was isolated as a red solid (19 mg, 73% yield). ¹H NMR (500 MHz, CD₃CN, 20 °C): δ 8.91 (d, *J*_{HH} = 5.1 Hz, 1H), 8.36 (d, *J*_{HH} = 7.9 Hz, 1H), 8.19 (m, 1H), 8.11 (d, *J*_{HH} = 8.1 Hz, 1H), 8.04-7.92 (multiple peaks, 2H), 7.83 (d, *J*_{HH} = 5.9 Hz, 1H), 7.77 (m, 1H), 7.38 (m, 1H), 7.31 (t, *J*_{HH} = 7.6 Hz, 1H), 7.23 (dd, *J*_{HH} = 7.9 Hz, *J*_{HH} = 1.7 Hz, 1H), 7.10 (dd, *J*_{HH} = 7.6 Hz, *J*_{HH} = 1.7 Hz, 1H), 6.38 (t, *J*_{HH} = 7.7 Hz, 2H), 6.13 (t, *J*_{HH} = 7.7 Hz, 1H), 5.61 (d, *J*_{HH} = 7.7 Hz, 2H), 4.33 (dd, *J*_{HF} = 15.9 Hz, *J*_{HH} = 6.3 Hz, 1H), 3.72 (dd, *J*_{HH} = 6.3, *J*_{HF} = 2.5 Hz, 1H), 1.41 (s, 3H), 1.06 (s, 3H). ¹³C NMR (176 MHz, CD₃CN, 20 °C): δ 166.10, 159.46, 156.35, 155.02, 151.48, 151.12, 147.17, 141.00, 140.64, 130.24, 128.07, 127.81, 127.71, 127.56, 127.13, 125.53, 124.72, 123.02, 120.33, 114.19, 64.56, 45.98, 31.31, 30.44. ¹⁹F NMR (470 MHz, CD₃CN, 20 °C): δ -340.8 (d, *J*_{FH} = 15.9 Hz) HRMS-electrospray (m/z): [M - OPh]⁺ calcd. for C₂₀H₂₀FN₂Pd, 413.0645; Found, 413.0651.



***in situ* Generation of [(bpy)Pd^{IV}(CH₂CMe₂-*o*-C₆H₄)(F)(OAc)] (2b).** A screw cap NMR tube was charged with [(bpy)Pd^{IV}(CH₂CMe₂-*o*-C₆H₄)(F)(OTf)] (1) (5.0 mg, 0.0088 mmol, 1.0 equiv). A solution of NMe₄OAc (1.2 mg, 0.0088 mmol, 1.0

equiv) in CD₃CN (0.5 mL) was added, and the NMR tube was placed in an NMR spectrometer where the probe had been pre-cooled to -10 °C. The sample was allowed to equilibrate in the spectrometer for 5 min before acquiring the spectra. ¹H NMR (500 MHz, CD₃CN, -10 °C): δ 8.88 (d, *J*_{HH} = 5.1 Hz, 1H), 8.47-8.39 (multiple peaks, 2H), 8.26 (t, *J*_{HH} =

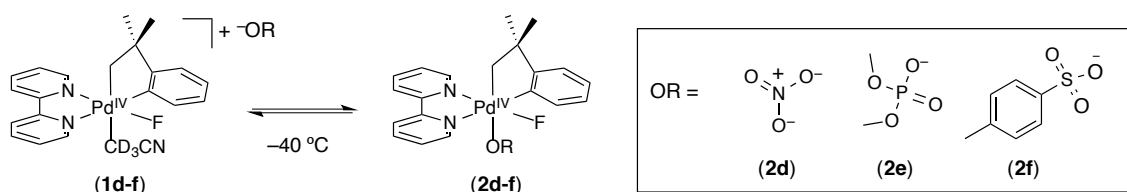
7.8 Hz, 1H), 8.13 (t, $J_{\text{HH}} = 7.9$ Hz, 1H), 8.01-7.92 (multiple peaks: 2H), 7.83 (dd, $J_{\text{HH}} = 7.8$ Hz, $J_{\text{HH}} = 5.1$ Hz, 1H), 7.38 (t, $J_{\text{HH}} = 7.9$ Hz, 1H), 7.25 (m, 1H), 7.18 (m, 1H), 7.02 (d, $J_{\text{HH}} = 7.4$ Hz, 1H), 4.28 (dd, $J_{\text{HF}} = 15.3$ Hz, $J_{\text{HH}} = 6.3$ Hz, 1H), 3.35 (dd, $J_{\text{HH}} = 6.3$ Hz, $J_{\text{HF}} = 2.9$ Hz, 1H), 1.61 (s, 3H), 1.34 (s, 3H), 0.98 (s, 3H). ^{13}C NMR (176 MHz, CD_3CN , -10 °C): δ 175.12, 159.14, 156.75, 152.81, 151.71, 147.01, 140.88, 140.53, 130.25, 127.62, 127.22, 126.91, 126.70, 125.05, 124.29, 122.90, 67.23, 46.01, 31.16, 30.65, 24.75. ^{19}F NMR (470 MHz, CD_3CN , -10 °C): δ -327.5 (d, $J_{\text{FH}} = 15.3$ Hz).



in situ Generation of $[(\text{bpy})\text{Pd}^{\text{IV}}(\text{CH}_2\text{CMe}_2\text{-}o\text{-C}_6\text{H}_4)(\text{F})(\text{O}_2\text{C}_2\text{F}_2\text{H})]$ (**2c**). A screw cap NMR tube was charged with $[(\text{bpy})\text{Pd}^{\text{IV}}(\text{CH}_2\text{CMe}_2\text{-}o\text{-C}_6\text{H}_4)(\text{F})(\text{OTf})]$ (**1**) (5.0 mg, 0.0088 mmol, 1.0 equiv). A solution of $\text{NMe}_4\text{OCOCF}_2\text{H}$ (1.5 mg, 0.0089 mmol, 1.0

equiv) in CD_3CN (0.5 mL) was added, and the NMR tube was placed in an NMR spectrometer where the probe had been pre-cooled to -10 °C. The sample was allowed to equilibrate in the spectrometer for 5 min before acquiring spectra. ^1H NMR (500 MHz, CD_3CN , -10 °C): δ 8.89 (d, $J_{\text{HH}} = 5.1$ Hz, 1H), 8.47-8.41 (multiple peaks: 2H), 8.29 (dd, $J_{\text{HH}} = 7.9$ Hz, $J_{\text{HH}} = 1.9$ Hz, 1H), 8.18 (t, $J_{\text{HH}} = 7.8$ Hz, 1H), 7.96 (d, $J_{\text{HH}} = 5.8$ Hz, 1H), 7.91-7.83 (multiple peaks, 2H), 7.43 (dd, $J_{\text{HH}} = 7.8$ Hz, $J_{\text{HH}} = 5.8$ Hz, 1H), 7.26 (t, $J_{\text{HH}} = 7.4$ Hz, 1H), 7.20 (td, $J_{\text{HH}} = 7.4$ Hz, $J_{\text{HH}} = 1.8$ Hz, 1H), 7.05 (dd, $J_{\text{HH}} = 7.4$ Hz, $J_{\text{HH}} = 1.8$ Hz, 1H), 5.47 (t, $J_{\text{HF}} = 56$ Hz, 1H), 4.49 (dd, $J_{\text{HH}} = 15.3$ Hz, $J_{\text{HF}} = 6.1$ Hz, 1H), 3.65 (dd, $J_{\text{HH}} = 6.1$ Hz, $J_{\text{HF}} = 2.8$ Hz, 1H), 1.37 (s, 3H), 1.01 (s, 3H). ^{13}C NMR (176 MHz, CD_3CN , -10 °C): δ 166.27 (t, $J_{\text{CF}} = 23.9$ Hz, CCF_2H), 159.06, 156.76, 156.31, 152.70, 151.79, 147.17, 141.32, 140.86, 129.75, 127.87, 127.45, 127.31, 126.95, 125.19, 124.60, 123.09, 109.90 (t, $J_{\text{CF}} = 248.7$ Hz, CF_2H), 69.49, 46.45, 30.97, 30.33. ^{19}F NMR (470 MHz, CD_3CN , -10 °C): δ -327.6 (d, $J_{\text{FH}} = 15.3$ Hz, Pd-F), -123.9 (d, $J_{\text{FH}} = 56$ Hz, CH-F_2)

General Procedure for the *in situ* Generation of Pd^{IV} Derivatives **2d-f**

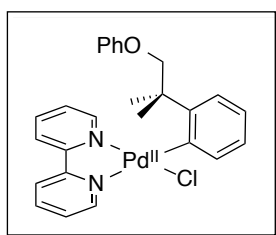


A screw cap NMR tube was charged with [(bpy)Pd^{IV}(CH₂CMe₂-*o*-C₆H₄)(F)(OTf)] (**1**) (5.0 mg, 0.0088 mmol, 1.0 equiv). A solution of the corresponding NR₄OR salt (0.0089 mmol, 1.0 equiv) in CD₃CN (0.5 mL) was added, and an NMR tube was placed in the NMR spectrometer where the probe had been pre-cooled to -40 °C. The sample was allowed to equilibrate in the spectrometer for 5 min before acquiring spectra. The Pd^{IV}-OR products **2d-f** are formed as equilibrium mixtures with the cationic solvento complex **1d-f**. Complexes **1d-f** have identical spectra data to complex **1** from the literature. We believe that **1**, which contains a very weakly coordinating triflate anion, also exists as a cationic acetonitrile solvate in CD₃CN. Low temperature ¹H and ¹⁹F NMR characterization for complexes **2d-f** are reported below. ¹³C NMR data could not be obtained for these complexes due to their instability over the time period required for the experiment.

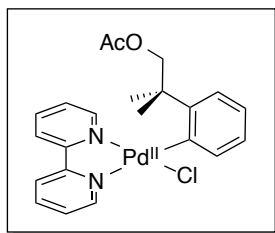
[(bpy)Pd^{IV}(CH₂CMe₂-*o*-C₆H₄)(F)(ONO₂)] **2d** was generated *in situ* according to the procedure above and characterized at low temperature (-40 °C in CD₃CN). The Pd^{IV} nitrate product formed as an equilibrium mixture with the cationic solvento complex **1d** (**1d** : **2d** = 4 : 1 as determined by ¹⁹F NMR spectroscopy). A ¹H-¹H ROESY spectrum confirms that the two species are undergoing exchange on the NMR timescale at -40 °C. ¹H NMR (500 MHz, CD₃CN, -40 °C): δ 8.87 (m, 1H), 8.58 (m, 1H), 8.49 (t, *J*_{HH} = 7.5 Hz, 1H), 8.30 (m, 1H), 8.23 (t, *J*_{HH} = 7.5 Hz, 1H), 7.89 (br, 1H), 7.76 (d, *J*_{HH} = 8.0 Hz, 1H), 7.48 (br, 1H), 7.23 (m, 1H), 7.08 (m, 1H), 4.76-4.67 (multiple peaks, 2H), 4.04 (br, 1H) 1.35 (s, 3H), 0.99 (s, 3H). ¹⁹F NMR (470 MHz, CD₃CN, -40 °C): δ -324.80 (br, Pd-*F*_{2d}), -333.55 (br, Pd-*F*_{1d}).

[(bpy)Pd^{IV}(CH₂CMe₂-*o*-C₆H₄)(F)(OPO(OMe)₂)] **2e** was generated *in situ* according to a modified version of the procedure above and characterized at low temperature (20 °C in DMSO). The Pd^{IV} phosphate adduct formed as an equilibrium mixture of the cationic solvento complex **1e** and the phosphate-bound complex **2e** (**1e** : **2e** = 1.5 : 1.0 as determined by ¹⁹F-NMR spectroscopy). A ¹H-¹H ROESY spectrum confirms that the two species are undergoing exchange on the NMR timescale at 20 °C. ¹H NMR (500 MHz, DMSO, 20 °C): δ 8.90 (d, *J*_{HH} = 7.6 Hz, 1H), 8.78-8.72 (multiple peaks, 2H), 8.42-8.39 (m, 1H), 8.32 (t, *J*_{HH} = 7.8 Hz, 1H), 8.04 (m, 1H), 7.93 (t, *J*_{HH} = 7.6 Hz, 1H), 7.80 (m, 1H), 7.67 (m, 1H), 7.30-7.15 (multiple peaks, 2H), 6.99 (d, *J*_{HH} = 7.3 Hz, 1H), 4.36 (dd, *J*_{HF} = 14.9, *J*_{HH} = 5.9 Hz, 1H), 3.62 (d, *J*_{HH} = 5.9 Hz, 1H), 2.91 (d, *J*_{HP} = 10.6 Hz, 3H), 1.31 (s, 3H), 1.06 (s, 3H). ³¹P NMR (202 MHz, DMSO) δ 2.82 (q, *J*_{HP} = 10.6 Hz, **P**_{2e}), 1.38 (br, **P**_{1e}). ¹⁹F NMR (470 MHz, DMSO) δ -328.46 (d, *J*_{HF} = 14.9 Hz, Pd-*F*_{2e}), -329.07 (d, *J*_{HF} = 13.8 Hz, Pd-*F*_{1e}).

[(bpy)Pd^{IV}(CH₂CMe₂-*o*-C₆H₄)(F)(OTs)] (2f) was generated *in situ* according to the procedure above and characterized at low temperature (−30 °C in CD₃CN). The Pd^{IV} tosylate product formed as an equilibrium mixture with the cationic solvento complex **1f** (**1f** : **2f** = 1.0 : 1.4 as determined by ¹⁹F NMR spectroscopy). A ¹H-¹H ROESY spectrum confirms that the two species are undergoing exchange on the NMR timescale at −30 °C. ¹H NMR (500 MHz, CD₃CN, −30 °C): δ 8.72 (d, *J*_{HH} = 5.0 Hz, 1H), 8.61-8.52 (m, 1H), 8.39, 8.30 (t, *J*_{HH} = 7.0 Hz, 1H), 8.26-8.12 (multiple peaks: 3H), 8.08 (d, *J*_{HH} = 7.7 Hz, 1H), 8.05-7.92 (m, 1H), 7.75 (m, 1H), 7.43 (t, *J*_{HH} = 7.0 Hz, 1H), 7.28-7.20 (multiple peaks, 2H), 7.03 (dd, *J*_{HH} = 7.2, 2.0 Hz, 1H), 6.93 (m, 2H), 6.85 (m, 2H), 4.62 (dd, *J*_{HF} = 15.1, *J*_{H-H} 5.6 Hz, 1H), 3.87 (d, *J*_{HH} = 5.6 Hz, 1H), 2.33 (s, 3H), 1.34 (s, 3H), 0.96 (s, 3H). ¹⁹F NMR (470 MHz, CD₃CN, −40 °C): δ −323.73 (br, Pd-*F*_{2f}), −334.13 (br, Pd-*F*_{1f}).

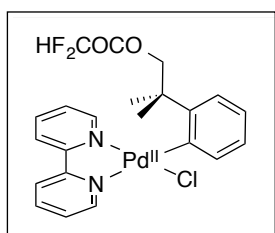


Synthesis of [(bpy)Pd^{II}(C₆H₄-*o*-CMe₂CH₂OPh)(Cl)] (5a). A 20 mL vial was charged with [(bpy)Pd^{IV}(CH₂CMe₂-*o*-C₆H₄)(F)(OTf)] (**1**) (50 mg, 0.089 mmol, 1.0 equiv) and sodium phenoxide (52 mg, 0.44 mmol, 5.0 equiv). CH₃CN (4 mL) was added, and the resulting solution was stirred for 2 h at 50 °C. The reaction mixture was cooled to room temperature, filtered through a Celite plug, and concentrated via rotary evaporation. The crude oil was redissolved in CH₂Cl₂ (4 mL), and a saturated solution of NaCl (5 mL) was added. The mixture was stirred at room temperature for 30 min. The organic layer was then separated, dried over MgSO₄, and filtered through Celite. The filtrate was concentrated to 1 mL, and petroleum ether was added until the product precipitated. The precipitate was collected and dried under vacuum to afford **5a** as a yellow solid (33 mg, 72% yield). ¹H NMR (700 MHz, CD₂Cl₂, 25 °C) δ 9.25 (d, *J*_{HH} = 5.7 Hz, 1H), 8.03 (td, *J*_{HH} = 7.6 Hz, 1.2 Hz, 1H), 7.92 (d, *J*_{HH} = 7.6 Hz, 1H), 7.83-7.74 (multiple peaks, 2H), 7.67 (td, *J*_{HH} = 7.8 Hz, *J*_{HH} = 1.6 Hz, 1H), 7.62 (ddd, *J*_{HH} = 7.6 Hz, *J*_{HH} = 5.7 Hz, *J*_{HH} = 1.2 Hz, 1H), 7.46 (m, 1H), 7.30 (dd, *J*_{HH} = 8.0 Hz, *J*_{HH} = 1.6 Hz, 1H), 7.10-6.98 (multiple peaks, 2H), 6.88-6.92 (multiple peaks, 3H), 6.67 (t, *J*_{HH} = 7.2 Hz, 1H), 6.49 (m, 2H) 6.30 (d, *J*_{HH} = 8.7 Hz, 1H), 3.85 (d, *J*_{HH} = 8.7 Hz, 1H), 1.66 (s, 3H), 1.66 (s, 3H). ¹³C NMR (176 MHz, CD₂Cl₂, 25 °C): δ 158.94, 155.36, 153.53, 151.23, 150.23, 149.18, 147.85, 138.84, 138.09, 134.63, 128.72, 127.28, 126.24, 126.18, 124.20, 123.39, 121.34, 121.23, 119.43, 113.77, 77.52, 40.24, 28.46, 27.56. HRMS-electrospray (m/z): [M − Cl]⁺ calcd. for C₂₆H₂₅N₂OPd, 487.0996; Found, 487.1010.



Synthesis of [(bpy)Pd^{II}(C₆H₄-*o*-CMe₂CH₂OAc)(Cl)] (5b). A 20 mL vial was charged with [(bpy)Pd^{IV}(CH₂CMe₂-*o*-C₆H₄)(F)(OTf)] (1) (50 mg, 0.089 mmol, 1.0 equiv) and sodium acetate (37 mg, 0.45 mmol, 5.0 equiv). CH₃CN (4 mL) was added, and the resulting solution was stirred for 5 h at room temperature. The reaction

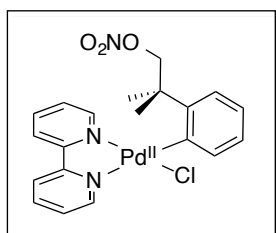
mixture was filtered through a Celite plug, and solvent was removed by rotary evaporation. The crude oil was redissolved in CH₂Cl₂ (4 mL), and a saturated solution of NaCl (5 mL) was added. The mixture was stirred at room temperature for 30 min. The organic layer was then separated, dried over MgSO₄, and filtered through Celite. The filtrate was concentrated to 1 mL, and petroleum ether was added until the product precipitated. The precipitate was collected and dried under vacuum to afford **5b** as a yellow solid (33 mg, 76% yield). ¹H NMR (700 MHz, CD₂Cl₂, 25 °C) δ 9.26 (d, *J*_{HH} = 5.7 Hz, 1H), 8.12-8.05 (multiple peaks: 3H), 7.99 (td, *J*_{HH} = 8.1 Hz, *J*_{HH} = 1.8 Hz, 1H), 7.77 (dd, *J*_{HH} = 7.3 Hz, *J*_{HH} = 1.5 Hz, 1H), 7.65 (ddd, *J*_{HH} = 7.1 Hz, *J*_{HH} = 5.7 Hz, *J*_{HH} = 1.6 Hz, 1H), 7.58 (dd, *J*_{HH} = 5.5 Hz, *J*_{HH} = 1.8 Hz, 1H), 7.26 (ddd, *J*_{HH} = 8.1 Hz, *J*_{HH} = 5.5 Hz, *J*_{HH} = 1.8 Hz, 1H), 7.21 (dt, *J*_{HH} = 8.0 Hz, *J*_{HH} = 1.5 Hz, 1H), 6.98 (ddd, *J*_{HH} = 8.0 Hz, *J*_{HH} = 7.3, *J*_{HH} = 1.5 Hz, 1H), 6.90 (td, *J*_{HH} = 7.3 Hz, *J*_{HH} = 1.5 Hz, 1H), 4.99 (d, *J*_{HH} = 10.7 Hz, 1H), 4.55 (d, *J*_{HH} = 10.7 Hz, 1H), 1.80 (s, 3H), 1.68 (s, 3H), 1.62 (s, 3H). ¹³C NMR (176 MHz, CD₂Cl₂, 25 °C): δ 170.69, 155.91, 153.42, 151.45, 149.38, 149.29, 147.91, 139.03, 138.61, 134.82, 127.25, 126.52, 126.36, 124.27, 123.33, 121.99, 121.44, 73.90, 39.46, 28.06, 27.69, 20.69. HRMS-electrospray (*m/z*): [M – Cl]⁺ calcd. for C₂₂H₂₃N₂O₂Pd, 453.0789; Found, 453.0793.



Synthesis of [(bpy)Pd^{II}(C₆H₄-*o*-CMe₂CH₂OCOCF₂H)(Cl)] (5c). [(bpy)Pd^{IV}(CH₂CMe₂-*o*-C₆H₄)(F)(OTf)] (1) (100 mg, 0.178 mmol, 1.0 equiv) and tetramethylammonium difluoroacetate (150 mg, 0.88 mmol, 5.0 equiv) were combined in CH₃CN (5 mL), and the resulting solution was stirred for 1 h at 40 °C. The reaction mixture

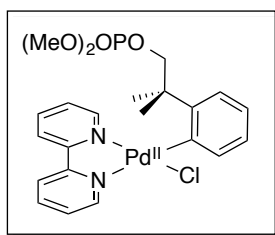
was then filtered through a Celite plug, and solvent was removed by rotary evaporation. The crude oil was redissolved in CH₂Cl₂ (5 mL), an excess of NMe₄Cl was added, and the resulting solution was stirred for 5 min. The solution was then washed 5 times with water, dried over MgSO₄, and filtered through Celite. The filtrate was concentrated to 1 mL, and petroleum ether was added to precipitate the product. The precipitate was collected and dried

under vacuum to afford **5c** as a yellow solid (65 mg, 70% yield). ^1H NMR (500 MHz, CD_2Cl_2 , 25 °C) δ 9.26 (d, $J_{\text{HH}} = 5.3$ Hz, 1H), 8.18-8.07 (multiple peaks: 3H), 8.01 (td, $J_{\text{HH}} = 7.8$ Hz, $J_{\text{HH}} = 1.6$ Hz, 1H), 7.80 (dd, $J_{\text{HH}} = 7.3$ Hz, $J_{\text{HH}} = 1.4$ Hz, 1H), 7.66 (ddd, $J_{\text{HH}} = 7.1$ Hz, $J_{\text{HH}} = 5.3$ Hz, $J_{\text{HH}} = 1.9$ Hz, 1H), 7.59 (dd, $J_{\text{HH}} = 5.6$ Hz, $J_{\text{HH}} = 1.6$ Hz, 1H), 7.28 (ddd, $J_{\text{HH}} = 7.2$ Hz, $J_{\text{HH}} = 5.6$ Hz, $J_{\text{HH}} = 1.3$ Hz, 1H), 7.24 (dd, $J_{\text{HH}} = 7.5$ Hz, $J_{\text{HH}} = 1.6$ Hz, 1H), 7.01 (td, $J_{\text{HH}} = 7.5$ Hz, $J_{\text{HH}} = 1.4$ Hz, 1H), 6.93 (td, $J_{\text{HH}} = 7.3$ Hz, $J_{\text{HH}} = 1.6$ Hz, 1H), 5.81 (t, $J_{\text{HF}} = 53$ Hz, 1H), 5.11 (d, $J_{\text{HH}} = 10.6$ Hz, 1H), 5.01 (d, $J_{\text{HH}} = 10.6$ Hz, 1H), 1.69 (s, 3H), 1.68 (s, 3H). ^{13}C NMR (176 MHz, CD_2Cl_2 , 25 °C): δ 162.39 (t, $J_{\text{CF}} = 28.2$ Hz, CCF_2H), 155.94, 153.44, 151.33, 149.36, 148.26, 147.85, 139.13, 138.79, 134.95, 127.23, 126.56, 126.54, 124.58, 123.51, 122.10, 121.50, 106.86 (t, $J_{\text{CF}} = 248.2$ Hz, CF_2H), 75.92, 39.53, 27.61, 27.49. ^{19}F NMR (470 MHz, CD_2Cl_2 , 25 °C): δ -127.16 (d, $J_{\text{FH}} = 53$ Hz, CH-F_2). HRMS-electrospray (m/z): $[\text{M} + \text{NH}_4]^+$ calcd. for $\text{C}_{22}\text{H}_{25}\text{ClF}_2\text{N}_3\text{O}_2\text{Pd}$, 542.0633; Found, 542.0635.



Synthesis of $[(\text{bpy})\text{Pd}^{\text{II}}(\text{C}_6\text{H}_4\text{-}o\text{-CMe}_2\text{CH}_2\text{ONO}_2)(\text{Cl})]$ (5d**).** A 20 mL vial was charged with $[(\text{bpy})\text{Pd}^{\text{IV}}(\text{CH}_2\text{CMe}_2\text{-}o\text{-C}_6\text{H}_4)(\text{F})(\text{OTf})]$ (**1**) (50 mg, 0.089 mmol, 1.0 equiv) and sodium nitrate (38 mg, 0.45 mmol, 5.0 equiv). CH_3CN (4 mL) was added, and the resulting solution was stirred for 5 h at room temperature. The reaction

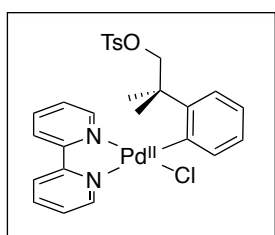
mixture was filtered through a Celite plug, and solvent was removed by rotary evaporation. The crude oil was redissolved in CH_2Cl_2 (4 mL), and a saturated solution of NaCl (5 mL) was added. The mixture was stirred at room temperature for 30 min. The organic layer was then separated, dried over MgSO_4 , and filtered through Celite. The filtrate was concentrated to 1 mL, and petroleum ether was added until the product precipitated. The precipitate was collected and dried under vacuum to afford **5d** as a pale yellow solid (39 mg, 88% yield). ^1H NMR (500 MHz, CD_2Cl_2 , 25 °C) δ 9.26 (d, $J_{\text{HH}} = 5.6$ Hz, 1H), 8.16-8.06 (multiple peaks, 3H), 8.01 (t, $J_{\text{HH}} = 6.6$ Hz, 1H), 7.82 (d, $J_{\text{HH}} = 7.5$ Hz, 1H), 7.66 (td, $J_{\text{HH}} = 5.6$ Hz, $J_{\text{HH}} = 2.6$ Hz, 1H), 7.58 (d, $J_{\text{HH}} = 6.6$ Hz, 1H), 7.28 (t, $J_{\text{HH}} = 6.6$ Hz, 1H), 7.23 (d, $J_{\text{HH}} = 7.5$ Hz, 1H), 7.03 (t, $J_{\text{HH}} = 7.5$ Hz, 1H), 6.94 (t, $J_{\text{HH}} = 7.5$ Hz, 1H), 5.86 (d, $J_{\text{HH}} = 9.6$ Hz, 1H), 4.99 (d, $J_{\text{HH}} = 9.6$ Hz, 1H), 1.69 (s, 3H), 1.68 (s, 3H). ^{13}C NMR (176 MHz, CD_2Cl_2 , 25 °C): δ 155.86, 153.43, 151.36, 149.35, 147.84, 147.70, 139.16, 138.82, 134.95, 127.09, 126.67, 126.54, 124.76, 123.62, 122.04, 121.49, 82.56, 39.05, 27.90, 27.74. HRMS-electrospray (m/z): $[\text{M} + \text{NH}_4]^+$ calcd. for $\text{C}_{20}\text{H}_{24}\text{ClN}_4\text{O}_3\text{Pd}$, 509.0566; Found, 509.0566.



Synthesis of [(bpy)Pd^{II}(C₆H₄-*o*-CMe₂CH₂OPO(OMe)₂)(Cl)] (**5e**).

A 20 mL vial was charged with [(bpy)Pd^{IV}(CH₂CMe₂-*o*-C₆H₄)(F)(OTf)] (**1**) (100 mg, 0.176 mmol, 1.0 equiv) and sodium dimethyl phosphate (130 mg, 0.88 mmol, 5.0 equiv). DMSO (5 mL) was added, and the resulting solution was stirred at 50 °C for 1 h.

Following conversion to the reductive elimination product, NMe₄Cl (~3 equiv) was added, and the reaction mixture was stirred for an additional 10 min. Water (20 mL) was then added to the DMSO solution, which was extracted with CH₂Cl₂ (20 mL). The organic layer was then washed thoroughly with water (5 x 20 mL) to remove residual DMSO, dried over MgSO₄, and filtered through Celite. The filtrate was concentrated to 1 mL, and petroleum ether (4 mL) was added to precipitate the product. The precipitate was collected and dried under vacuum to afford **5e** as a yellow solid (78 mg, 80% yield). ¹H NMR (700 MHz, CD₂Cl₂, 25 °C) δ 9.25 (d, *J*_{HH} = 5.3 Hz, 1H), 8.12-8.05 (multiple peaks, 2H), 8.07 (dd, *J*_{HH} = 8.0 Hz, *J*_{HH} = 1.6 Hz, 1H), 7.99 (t, *J*_{HH} = 7.8 Hz, 1H), 7.78 (dd, *J*_{HH} = 7.4 Hz, *J*_{HH} = 1.6 Hz, 1H), 7.64 (ddd, *J*_{HH} = 7.1 Hz, *J*_{HH} = 5.3 Hz, *J*_{HH} = 1.6 Hz, 1H), 7.59 (d, *J*_{HH} = 5.6 Hz, 1H), 7.28 (ddd, *J*_{HH} = 7.8 Hz, *J*_{HH} = 5.6 Hz, *J*_{HH} = 1.6 Hz, 1H), 7.23 (d, *J*_{HH} = 8.0 Hz, 1H), 7.00 (m, 1H), 6.89 (t, *J*_{HH} = 7.4 Hz, 1H), 4.86 (dd, *J*_{HH} = 9.5 Hz, *J*_{HP} = 4.9 Hz, 1H), 4.36 (dd, *J*_{HH} = 9.5 Hz, *J*_{HP} = 4.9 Hz, 1H), 3.60-3.53 (multiple peaks, 6H), 1.74 (s, 3H), 1.73 (s, 3H). ¹³C NMR (176 MHz, CD₂Cl₂, 25 °C): δ 155.76, 153.55, 151.55, 149.30, 148.45, 148.04, 139.09, 138.61, 134.92, 127.40, 126.71, 126.45, 124.40, 123.37, 121.95, 121.44, 76.87, 76.83, 40.47, 40.42, 27.48, 27.33. ³¹P NMR (202 MHz, CD₂Cl₂, 25 °C): δ 0.89. HRMS-electrospray (*m/z*): [M – Cl]⁺ calcd. for C₂₂H₂₆N₂O₄PPd, 519.0660; Found, 519.0678.



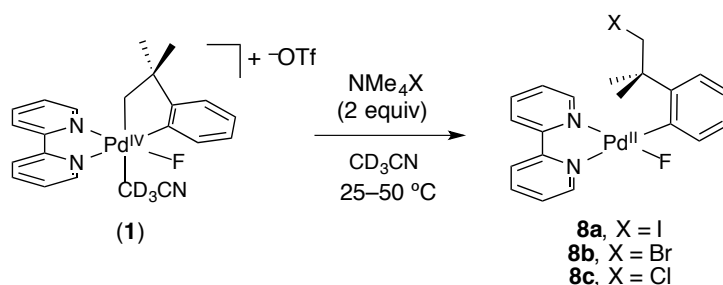
in situ Synthesis of [(bpy)Pd^{II}(C₆H₄-*o*-CMe₂CH₂OTs)(Cl)] (**5f**).

A 4 mL vial was charged with [(bpy)Pd^{IV}(CH₂CMe₂-*o*-C₆H₄)(F)(OTf)] (**1**) (10 mg, 0.018 mmol, 1.0 equiv) and a solution of NaOTs (8.6 mg, 0.044 mmol, 2.5 equiv)/ NMe₄OTs (10.6 mg, 0.044 mmol, 2.5 equiv) in CD₃CN (1 mL) was added. After stirring at 25 °C for 12 h

NMe₄Cl (~3 equiv) was added to the crude reaction mixture. The resulting solution was transferred into an NMR tube and placed in an NMR spectrometer where the probe had been set to 10 °C. Complex **5f** formed in 68% crude yield as determined by ¹H NMR analysis, and the respective signals are reported. Complex **5f** was not stable at room temperature and therefore could not be isolated. ¹H NMR (700 MHz, CD₃CN, 10 °C) δ 9.07 (d, *J*_{HH} = 5.2 Hz,

1H), 8.37-8.27 (multiple peaks, 2H), 8.22-8.18 (multiple peaks, 1H), 8.08 (t, $J_{\text{HH}} = 7.8$ Hz, 1H), 7.74-7.67 (multiple peaks, 2H), 7.51 (d, $J_{\text{HH}} = 8.3$ Hz, 2H), 7.43 (dd, $J_{\text{HH}} = 5.6, 1.6$ Hz, 1H), 7.30 (d, $J_{\text{HH}} = 7.3$ Hz, 1H), 7.18 (d, $J_{\text{HH}} = 8.3$ Hz, 2H), 6.95 (d, $J_{\text{HH}} = 7.3$ Hz, 1H), 6.87 (t, $J_{\text{HH}} = 7.3$ Hz, 1H), 5.18 (d, $J_{\text{HH}} = 9.3$ Hz, 1H), 4.65 (d, $J_{\text{HH}} = 9.3$ Hz, 1H), 2.32 (s, 3H), 1.57 (s, 3H), 1.56 (s, 3H). ^{13}C NMR (176 MHz, CD_3CN , 10 °C): δ 155.77, 153.72, 151.04, 148.39, 147.83, 145.15, 144.83, 139.93, 139.59, 138.82, 135.00, 129.71, 127.61, 127.24, 127.06, 126.87, 124.57, 123.54, 123.01, 122.52, 79.89, 39.71, 26.78, 26.53, 20.36.

General Procedure for the Formation of Reductive Elimination Products **8a-c**



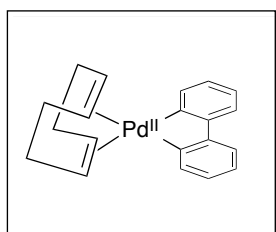
A 4 mL vial was charged with $[(\text{bpy})\text{Pd}^{\text{IV}}(\text{CH}_2\text{CMe}_2\text{-}o\text{-C}_6\text{H}_4)(\text{F})(\text{OTf})]$ (**1**) (10 mg, 0.018 mmol, 1.0 equiv) and a solution of the corresponding tetrabutylammonium halide (0.036 mmol, 2.0 equiv) in CD_3CN (1 mL) was added. After stirring at the indicated time and temperature, analysis by ^1H NMR spectroscopy showed formation of the Pd^{II} reductive elimination products **8a-c**. Complexes **8a-c** were formed in >95% conversion and characterized *in situ* by ^1H NMR spectroscopy. Characterization of the Pd^{IV} intermediates **7a-c** were not carried out.

$[(\text{bpy})\text{Pd}^{\text{II}}(\text{C}_6\text{H}_4\text{-}o\text{-CMe}_2\text{CH}_2\text{I})(\text{F})]$ (**8a**) was formed in >95% yield and characterized *in situ* according to the procedure above. ^1H NMR (400 MHz, CD_3CN , 25 °C) δ 9.54 (d, $J_{\text{HH}} = 5.6$ Hz, 1H), 8.31 (multiple peaks, 2H), 8.20 (m, 1H), 8.15 (m, 1H), 8.08 (m, 1H), 7.77 (d, $J_{\text{HH}} = 7.6$ Hz, 2H), 7.65 (d, $J_{\text{HH}} = 7.6$ Hz, 1H), 7.36 (m, 1H), 7.26 (d, $J_{\text{HH}} = 7.9$ Hz, 1H), 6.94 (t, $J_{\text{HH}} = 7.3$ Hz, 1H), 6.84 (t, $J_{\text{HH}} = 7.3$ Hz, 1H), 4.01 (d, $J_{\text{HH}} = 9.5$ Hz, 1H), 3.91 (d, $J_{\text{HH}} = 9.5$ Hz, 1H), 1.88 (s, 3H), 1.78 (s, 3H).

$[(\text{bpy})\text{Pd}^{\text{II}}(\text{C}_6\text{H}_4\text{-}o\text{-CMe}_2\text{CH}_2\text{Br})(\text{F})]$ (**8b**) was formed in >95% yield and characterized *in situ* according to the procedure above. ^1H NMR (500 MHz, CD_3Cl , 25 °C) δ 9.49 (d, $J_{\text{HH}} = 5.3$ Hz, 1H), 8.09 (d, $J_{\text{HH}} = 7.9$ Hz, 2H), 8.03 (t, $J_{\text{HH}} = 7.9$ Hz, 1H), 7.98 (t, $J_{\text{HH}} = 7.9$ Hz, 1H), 7.83 (d, $J_{\text{HH}} = 7.5$ Hz, 1H), 7.60 (multiple peaks, 2H), 7.29 (t, $J_{\text{HH}} = 5.3$ Hz, 1H), 7.22

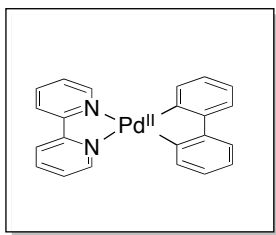
(d, $J_{\text{HH}} = 7.9$ Hz, 1H), 6.97 (t, $J_{\text{HH}} = 7.5$ Hz, 1H), 6.90 (t, $J_{\text{HH}} = 7.5$ Hz, 1H), 4.44 (d, $J_{\text{HH}} = 9.7$ Hz, 1H), 3.91 (d, $J_{\text{HH}} = 9.7$ Hz, 1H), 2.00 (s, 3H), 1.89 (s, 3H).

[(bpy)Pd^{II}(C₆H₄-*o*-CMe₂CH₂Cl)(F)] (8c) was formed in >95% NMR yield and characterized *in situ* according to the procedure above. ¹H NMR (700 MHz, CD₃CN, 25 °C) δ 9.12 (m, 1H), 8.32 (multiple peaks, 2H), 8.18 (t, $J_{\text{HH}} = 7.9$ Hz, 1H), 8.09 (t, $J_{\text{HH}} = 7.8$ Hz, 1H), 7.77 (d, $J_{\text{HH}} = 7.5$ Hz, 1H), 7.71 (t, $J_{\text{HH}} = 7.8$ Hz, 1H), 7.53 (d, $J_{\text{HH}} = 7.5$ Hz, 1H), 7.34 (t, $J_{\text{HH}} = 5.6$ Hz, 1H), 7.24 (d, $J_{\text{HH}} = 7.9$ Hz, 1H), 6.98 (t, $J_{\text{HH}} = 7.5$ Hz, 1H), 6.90 (t, $J_{\text{HH}} = 7.5$ Hz, 1H), 4.55 (d, $J_{\text{HH}} = 10.4$ Hz, 1H), 4.09 (d, $J_{\text{HH}} = 10.4$ Hz, 1H), 1.84 (s, 3H), 1.70 (s, 3H).

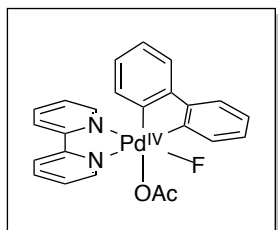


Synthesis of [(COD)Pd^{II}(C₆H₄-*o*-C₆H₆)] (10).

2,2'-dibromobiphenyl (2.0 g, 6.4 mmol, 1.0 equiv) was weighed into a N₂ flushed round bottom flask and dissolved in 50 mL of dried diethyl ether. The resulting solution was allowed to cool to 0 °C under a constant flow of N₂. At this temperature, *n*-BuLi (5.9 mL, 14.1 mmol, 2.2 equiv) was added dropwise and the colorless solution turned yellow. After stirring for 5 hr at 0 °C, the reaction mixture was then cooled to -78 °C and PdCl₂(COD) (1.8 g, 6.4 mmol, 1.0 equiv) was added in small increments over a 5 min period. The resulting suspension was allowed to stir for 14 hours and gradually warm to room temperature. Solvent was then removed by rotary evaporation and the dark grey residue was re-dissolved in dichloromethane and allowed to stir with activated carbon (20 mg) for 30 min. The suspension was then filtered through a celite plug and the resulting orange solution was concentrated to about 15 mL. Hexanes (40 mL) was added to precipitate the product. The contents of the flask were then cooled to -30 °C for 5 h and filtered to afford the title complex as a pale yellow solid (1.03 g, 44%). ¹H NMR (700 MHz, CD₂Cl₂, 25 °C): δ 7.24 (dd, $J_{\text{HH}} = 7.5$ Hz, $J_{\text{HH}} = 1.5$ Hz, 2H), 7.02 (d, $J_{\text{HH}} = 7.5$ Hz, 2H), 6.98 (t, $J_{\text{HH}} = 7.5$ Hz, 2H), 6.83 (td, $J_{\text{HH}} = 7.5$ Hz, 1.5 Hz, 2H), 6.04 (dd, $J_{\text{HH}} = 4.6$ Hz, $J_{\text{HH}} = 2.4$ Hz, 4H), 2.72-2.75 (multiple peaks, 4H), 2.64-2.52 (multiple peaks, 4H). ¹³C NMR (176 MHz, CD₂Cl₂, 25 °C): δ 164.80, 156.58, 133.98, 125.66, 119.93, 116.09, 28.95.

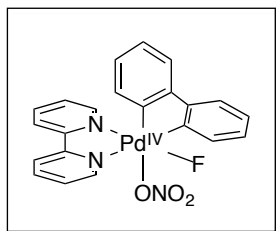


Synthesis of [(bpy)Pd^{II}(C₆H₄-*o*-C₆H₄)] (11). Complex **10** (890 mg, 2.42 mmol, 1.0 equiv) was weighed into a round bottom flask and dissolved in 100 mL of CH₂Cl₂. 2,2-bipyridine (402 mg, 2.57 mmol, 1.1 equiv) was added and the resulting solution was allowed to stir at room temperature for 30 min. The solution was then concentrated to about 10 mL and hexanes was added until the product precipitated. The contents in the flask were cooled to -30 °C for 2 hr and then filtered to afford the title compound as a bright orange solid (935 mg, 95%). ¹H NMR (700 MHz, CD₂Cl₂, 25 °C): δ 9.24 (dd, *J*_{HH} = 7.8 Hz, *J*_{HH} = 1.6 Hz, 2H), 8.11 (d, *J*_{HH} = 7.8 Hz, 2H), 8.04 (dd, *J*_{HH} = 7.8 Hz, *J*_{HH} = 1.6 Hz, 2H), 7.61 (dd, *J*_{HH} = 7.8 Hz, *J*_{HH} = 1.6 Hz, 2H), 7.46 (d, *J*_{HH} = 7.3 Hz, 2H), 7.31 (dd, *J*_{HH} = 7.3 Hz, *J*_{HH} = 1.5 Hz, 2H), 7.01 (t, *J*_{HH} = 7.3 Hz, 2H), 6.95-6.86 (multiple peaks, 2H). ¹³C NMR (176 MHz, CD₂Cl₂, 25°C): δ 163.82, 157.29, 155.38, 151.23, 138.32, 133.99, 125.97, 124.80, 123.92, 122.35, 119.31. HRMS-electrospray (*m/z*): [M + H]⁺ calcd. for C₂₂H₁₇N₂Pd, 415.0421; Found, 415.0425.



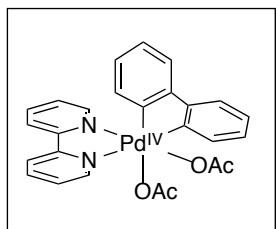
Synthesis of [(bpy)Pd^{IV}(C₆H₄-*o*-C₆H₄)(OAc)(F)] (12a). [(bpy)Pd^{II}(C₆H₄-*o*-C₆H₄)] (**11**) (30 mg, 0.072 mmol, 1.0 equiv) and 1-Fluoro-2,4,6-trimethylpyridinium triflate (NFTPT) (21 mg, 0.072 mmol, 1.0 equiv) were combined in a 4 mL vial and dissolved in CD₂Cl₂ (0.5 mL). NMe₄OAc (10.5 mg, 0.079 mmol, 1.1 equiv) was then added in slight excess. The reaction mixture was allowed to stir for 5 min and then filtered through Celite. The filtrate was collected and solvent was removed by rotary evacuation. The yellow residue was washed with diethyl ether (3 x 10 mL) and redissolved in CH₂Cl₂ (2 mL). The solution was then washed 5 times with water, dried with MgSO₄, and filtered through Celite. The filtrate was concentrated to 1 mL and petroleum ether (5 mL) was added to precipitate the product. The precipitate was filtered and dried under vacuum to afford the title complex as a yellow solid (19 mg, 54 %). ¹H NMR (500 MHz, CD₃OD, 25 °C) δ 9.13 (d, *J*_{HH} = 5.1 Hz, 1H), 8.73 (d, *J*_{HH} = 8.2 Hz, 1H), 8.58 (d, *J*_{HH} = 7.8 Hz, 1H), 8.49 (t, *J*_{HH} = 8.2 Hz, 1H), 8.17 (t, *J*_{HH} = 7.8 Hz, 1H), 8.10-8.03 (m, 1H), 7.97 (d, *J*_{HH} = 7.6 Hz, 1H), 7.90 (d, *J*_{HH} = 6.0 Hz, 1H), 7.72 (d, *J*_{HH} = 7.6 Hz, 1H), 7.58 (d, *J*_{HH} = 7.4 Hz, 1H), 7.46-7.32 (multiple peaks, 2H), 7.24 (t, *J*_{HH} = 7.6 Hz, 1H), 7.09 (t, *J*_{HH} = 7.4 Hz, 1H), 6.73 (t, *J*_{HH} = 7.4 Hz, 1H), 6.17 (d, *J*_{HH} = 7.4 Hz, 1H), 1.80 (s, 3H). ¹³C NMR (176 MHz, CD₃OD, 25 °C): δ 178.19, 169.29, 156.92, 156.29, 152.38, 150.77, 147.18, 146.42, 144.29, 141.71, 141.58,

129.43, 128.79, 128.58, 128.42, 128.09, 127.79, 127.67, 127.24, 124.72, 123.68, 123.49, 123.19, 23.37. ^{19}F NMR (470 MHz, CD_3OD , 25 °C): δ -344.46 (s, Pd-F). HRMS-electrospray (m/z): $[\text{M} - \text{F}]^+$ calcd. For $\text{C}_{24}\text{H}_{19}\text{N}_2\text{O}_2\text{Pd}$, 473.0476; Found, 473.0484.



Synthesis of $[(\text{bpy})\text{Pd}^{\text{IV}}(\text{C}_6\text{H}_4\text{-}o\text{-}\text{C}_6\text{H}_4)(\text{ONO}_2)(\text{F})]$ (12b).

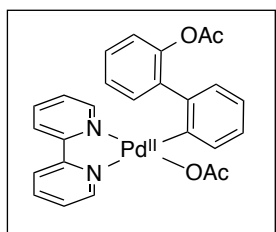
$[(\text{bpy})\text{Pd}^{\text{II}}(\text{C}_6\text{H}_4\text{-}o\text{-}\text{C}_6\text{H}_4)]$ (**11**) (30 mg, 0.072 mmol, 1.0 equiv) and 1-Fluoro-2,4,6-trimethylpyridinium triflate (NFTPT) (21 mg, 0.072 mmol, 1.0 equiv) were combined in a 20 mL vial and dissolved in CH_2Cl_2 (4 mL). NBu_4NO_3 (33 mg, 0.11 mmol, 1.5 equiv) was then added in slight excess. The reaction mixture was allowed to stir for 5 min and then filtered through Celite. The filtrate was collected and solvent was removed by rotary evacuation. The yellow residue was washed with diethyl ether (3 x 10 mL) and redissolved in CH_2Cl_2 (2 mL). The solution was then washed 5 times with water, dried with MgSO_4 , and filtered through Celite. The filtrate was concentrated to 1 mL and petroleum ether (5 mL) was added to precipitate the product. The precipitate was filtered and dried under vacuum to afford the title complex as a yellow solid (22 mg, 62 %). ^1H NMR (500 MHz, CD_3OD , 25 °C) δ 9.20 (d, $J_{\text{HH}} = 5.1$ Hz, 1H), 8.85 (d, $J_{\text{HH}} = 8.2$ Hz, 1H), 8.75 (d, $J_{\text{HH}} = 8.2$ Hz, 1H), 8.61 (t, $J_{\text{HH}} = 8.2$ Hz, 1H), 8.33 (t, $J_{\text{HH}} = 8.2$ Hz, 1H), 8.20 (m, 1H), 7.95 (d, $J_{\text{HH}} = 6.8$ Hz, 1H), 7.88 (d, $J_{\text{HH}} = 7.4$ Hz, 1H), 7.79 (d, $J_{\text{HH}} = 7.4$ Hz, 1H), 7.64 (d, $J_{\text{HH}} = 7.4$ Hz, 1H), 7.56 (t, $J_{\text{HH}} = 6.8$ Hz, 1H), 7.49 (t, $J_{\text{HH}} = 7.4$ Hz, 1H), 7.32 (t, $J_{\text{HH}} = 7.4$ Hz, 1H), 7.17 (t, $J_{\text{HH}} = 7.4$ Hz, 1H), 6.78 (t, $J_{\text{HH}} = 7.4$ Hz, 1H), 6.28 (d, $J_{\text{HH}} = 7.4$ Hz, 1H). ^{13}C NMR (176 MHz, CD_3OD , 25 °C): δ 169.54, 156.43, 155.75, 151.42, 147.22, 146.42, 143.37, 143.04, 142.51, 129.22, 128.99, 128.42, 128.00, 125.99, 124.75, 124.16. ^{19}F NMR (470 MHz, CD_3OD , 25 °C): δ -338.19 (s, Pd-F). HRMS-electrospray (m/z): $[\text{M} - \text{NO}_3]^+$ calcd. for $\text{C}_{22}\text{H}_{16}\text{FN}_2\text{Pd}$, 433.0327; Found, 433.0337.



Synthesis of $[(\text{bpy})\text{Pd}^{\text{IV}}(\text{C}_6\text{H}_4\text{-}o\text{-}\text{C}_6\text{H}_4)(\text{OAc})_2]$ (13).

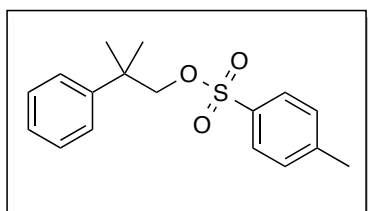
$[(\text{bpy})\text{Pd}^{\text{II}}(\text{C}_6\text{H}_4\text{-}o\text{-}\text{C}_6\text{H}_4)]$ (**11**) (30 mg, 0.072 mmol, 1.0 equiv) and iodomesitylene diacetate (29 mg, 0.080 mmol, 1.1 equiv) were charged in a 20 mL vial and dissolved in CH_2Cl_2 (3 mL). The reaction mixture was allowed to stir for 5 min and then filtered through Celite. The filtrate was collected and solvent was removed by rotary evacuation. The yellow residue was washed with diethyl ether (5 x 10 mL), redissolved in CH_2Cl_2 (1 mL), and precipitated with pentane (4 mL). The precipitate was filtered and dried under vacuum to

afford the title complex as an orange-yellow solid (29 mg, 76%). ^1H NMR (700 MHz, CD_2Cl_2 , 25 °C): δ 9.36 (d, $J_{\text{HH}} = 5.1$ Hz, 1H), 8.26–8.20 (multiple peaks, 2H), 8.10 (d, $J_{\text{HH}} = 8.0$ Hz, 1H), 8.07 (d, $J_{\text{HH}} = 8.0$ Hz, 1H), 7.93 (m, 1H), 7.86 (td, $J_{\text{HH}} = 5.1$ Hz, $J_{\text{HH}} = 3.1$ Hz, 1H), 7.75 (d, $J_{\text{HH}} = 5.9$ Hz, 1H), 7.57 (dd, $J_{\text{HH}} = 7.4$ Hz, $J_{\text{HH}} = 1.7$ Hz, 1H), 7.41 (dd, $J_{\text{HH}} = 7.3$ Hz, $J_{\text{HH}} = 1.6$ Hz, 1H), 7.34 (t, $J_{\text{HH}} = 7.4$ Hz, 1H), 7.25–7.10 (multiple peaks: 2H), 6.98 (t, $J_{\text{HH}} = 7.3$ Hz, 1H), 6.65 (m, 1H), 6.33 (d, $J_{\text{HH}} = 7.3$ Hz, 1H), 1.87 (s, 3H), 1.73 (s, 3H). ^{13}C NMR (176 MHz, CD_2Cl_2 , 25 °C): δ 173.46, 169.92, 157.32, 156.05, 152.89, 149.45, 147.40, 145.91, 140.15, 140.05, 130.52, 130.41, 127.97, 127.12, 127.09, 126.76, 126.65, 125.86, 122.89, 122.69, 122.20, 122.01, 25.07, 23.46. HRMS-electrospray (m/z): $[\text{M} - \text{OAc}]^+$ calcd. For $\text{C}_{24}\text{H}_{19}\text{N}_2\text{O}_2\text{Pd}$, 473.0476; Found, 473.0493.



Synthesis of $[(\text{bpy})\text{Pd}^{\text{II}}(\text{C}_6\text{H}_4\text{-}o\text{-}\text{C}_6\text{H}_4\text{-OAc})(\text{OAc})]$

$[(\text{bpy})\text{Pd}^{\text{IV}}(\text{C}_6\text{H}_4\text{-}o\text{-}\text{C}_6\text{H}_4)(\text{OAc})_2]$ (**13**) (25 mg, 0.047 mmol, 1.0 equiv) was charged into a 20 mL vial and dissolved in CH_2Cl_2 (4 mL). The solution was sealed with a Teflon lined cap and allowed to stir at 50 °C for 2.5 h. The solution was then filtered through Celite and solvent was removed by rotary evaporation. The residue was washed several times with diethyl ether (5 x 10 mL), redissolved in CH_2Cl_2 (1 mL), and precipitated with pentane (5 mL). The precipitate was filtered and dried under vacuum to afford the title complex as a yellow solid (17 mg, 68%). ^1H NMR (500 MHz, CD_2Cl_2 , 25 °C) δ 8.51 (d, $J_{\text{HH}} = 7.7$ Hz, 1H), 8.45 (d, $J_{\text{HH}} = 5.2$ Hz, 1H), 8.00–7.93 (multiple peaks, 2H), 7.91–7.86 (multiple peaks, 2H), 7.84 (m, 1H), 7.81–7.75 (m, 1H), 7.54 (ddd, $J_{\text{HH}} = 7.1$, $J_{\text{HH}} = 5.2$, $J_{\text{HH}} = 1.9$ Hz, 1H), 7.22–7.15 (multiple peaks, 2H), 7.14–7.08 (multiple peaks, 2H), 7.07–7.01 (multiple peaks, 2H), 6.88 (dd, $J_{\text{HH}} = 7.9$, $J_{\text{HH}} = 1.5$ Hz, 1H), 2.18 (s, 3H), 2.04 (s, 3H). ^{13}C NMR (176 MHz, CD_2Cl_2 , 25 °C): δ 176.76, 169.85, 155.66, 153.52, 153.06, 152.83, 148.81, 147.64, 140.92, 138.96, 138.17, 137.83, 136.23, 133.86, 128.88, 127.08, 126.32, 126.12, 125.08, 124.96, 123.04, 122.15, 121.60, 121.34, 23.62, 20.93. HRMS-electrospray (m/z): $[\text{M} - \text{OAc}]^+$ calcd. For $\text{C}_{24}\text{H}_{19}\text{N}_2\text{O}_2\text{Pd}$, 473.0485; Found, 473.0476.



Synthesis of 2-methyl-2-phenylpropyl tosylate. 2-methyl-2-phenyl-propanol (900 mg, 6 mmol, 1.0 equiv) was dissolved in THF and cooled to 0 °C. nBuLi (2.5 ml, 6.2 mmol of a 2.5 M solution in hexanes) was added dropwise and the reaction

mixture was allowed to stir at 0 °C for 30 min. A solution of *p*-toluenesulfonyl chloride (1.3 g, 6.6 mmol, 1.1 equiv) in THF (5 mL) was added at this temperature. The resulting colorless solution was stirred at 0 °C for 30 min, allowed to warm to room temperature and stirred at this temperature for another 2 h. The solution was slowly quenched with isopropanol (10 mL). The solvent was removed on a rotatory evaporator to afford a slightly yellow oil. Purification by flash column chromatography (mobile phase: 9:1 hexane: ethyl acetate) afforded the title product as a white solid (1.5 g 42% yield). ¹H NMR (700 MHz, CD₃Cl, 25 °C) δ 7.63 (d, *J*_{HH} = 8.3 Hz, 2H), 7.27–7.21 (multiple peaks, 6H), 7.18 (m, 1H), 3.96 (s, 2H), 2.42 (s, 4H), 1.32 (s, 6H). ¹³C NMR (176 MHz, CD₃Cl, 25 °C) δ 144.67, 144.51, 132.74, 129.70, 128.31, 127.83, 126.50, 125.84, 78.40, 38.42, 25.24, 21.63.

2.4.3. General Procedures for Mechanistic Experiments

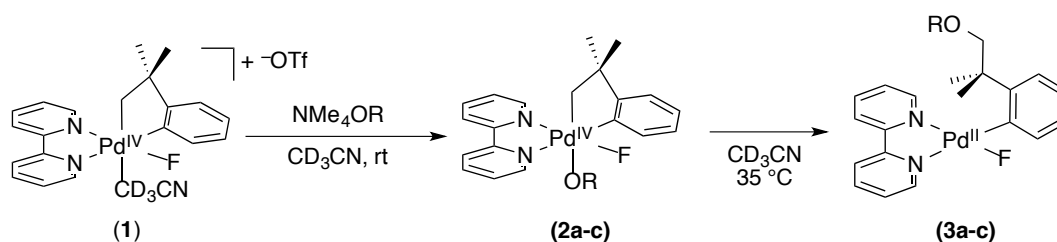
Procedure for the Method of Continuous Variation

A Job plot for the complexation of Na⁺ with [(bpy)Pd^{IV}(CH₂CMe₂-C₆H₄)(F)(OTf)] (**1**) was constructed using the method described by Newcomb and co-workers.⁴⁷ A series of ¹⁹F NMR spectra were collected with different relative ratios of NaOTf and **1** while maintaining a constant total concentration ([NaOTf] + [**1**]) of 35.5 mM in CD₃CN). At each ratio, the chemical shift (δ) of the Pd^{IV}-F resonance was determined, and Δδ values represent the difference between δ_F in the presence of NaOTf versus in free **1**. Samples were prepared from standard solutions of **1** (0.5 M in CD₃CN) and NaOTf (0.5 M in CD₃CN). Additional CD₃CN was added to maintain a constant total volume of 0.4 mL. Each data point in Figure 2.2 is the average of three trials shown in Table 2.4, and the error represents the standard deviation of the Δδ values. The maximum shift was observed when the mol fraction of **1** was 0.5, indicative of 1:1 binding.

Table 2.4. Chemical Shift Data for Job Plot at 25 °C

[1] (M)	[NaOTf] (M)	Trial 1 (δ ppm)	Trial 2 (δ ppm)	Trial 3 (δ ppm)
0.031	0.0044	-335.99	-335.94	-335.93
0.027	0.0089	-336.07	-336.01	-336.02
0.022	0.013	-336.19	-366.13	-336.16
0.018	0.018	-336.30	-336.29	-336.29
0.013	0.022	-336.43	-336.37	-336.35
0.0089	0.027	-336.58	-336.5	-336.54
0.0044	0.031	-336.87	-336.63	-336.60

Procedure for Determining the Order in Reagents



Determining the Order in Pd. Complex **1** (4.0 mg, 0.0071 mmol, 1.0 equiv) was added to an NMR tube equipped with a Teflon lined screw cap. Various amounts of NMe_4OR (0.018 mmol-0.071 mmol) were weighed into 4 mL vials, and the solids were dissolved in CD_3CN (0.5 mL). The resulting solution was added to the NMR tube to generate **2a-c** *in situ*. The tube was immediately placed in an NMR spectrometer that had been pre-heated to 35 °C. The rate of reductive elimination from **2** to **3** was monitored by ^1H NMR spectroscopy at this temperature. A plot of $(\ln[2])$ vs. time showed that the rate of reductive elimination is first-order in Pd^{IV} . A representative plot for **2a** is shown in Figure 2.13.

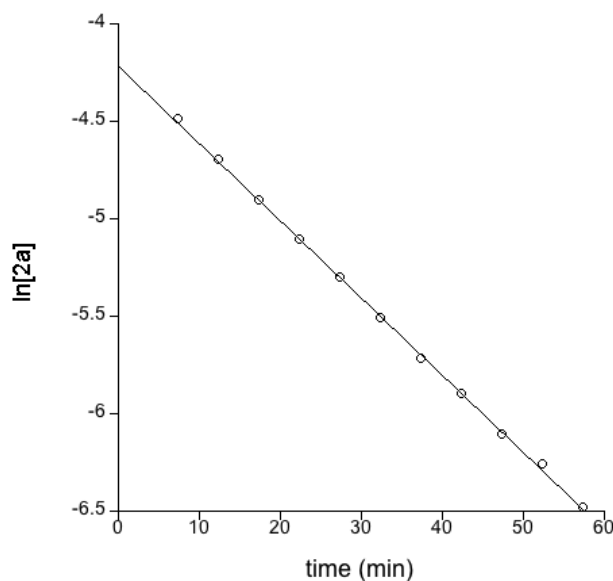


Figure 2.13. $(\ln[2a])$ vs time plot. $y = -4.21 - 0.0396x$. $R^2 = 0.9995$. Starting conditions: $T = 35\text{ }^\circ\text{C}$; $[2a]_0 = 0.014\text{ M}$, $[\text{OPh}]_0 = 0.070\text{ M}$.

Determining the Order in OR . Complex **1** (4.0 mg, 0.0071 mmol, 1.0 equiv) was added to an NMR tube equipped with a Teflon lined screw cap. Various amounts of NMe_4OR (0.018 mmol-0.071 mmol) were weighed into 4 mL vials, and the solids were dissolved in CD_3CN (0.5 mL). The resulting solution was added to the NMR tube to generate **2a-c** *in situ*. The tube was immediately placed in an NMR spectrometer that had been pre-heated to 35 °C. The rate of reductive elimination from **2** to form **3** was monitored by ^1H NMR spectroscopy at

this temperature. A plot of k_{obs} vs. $[\text{OR}^-]$ showed that the rate of reductive elimination is zero-order in OR^- . A representative plot for complex **2a** is shown in Figure 2.14.

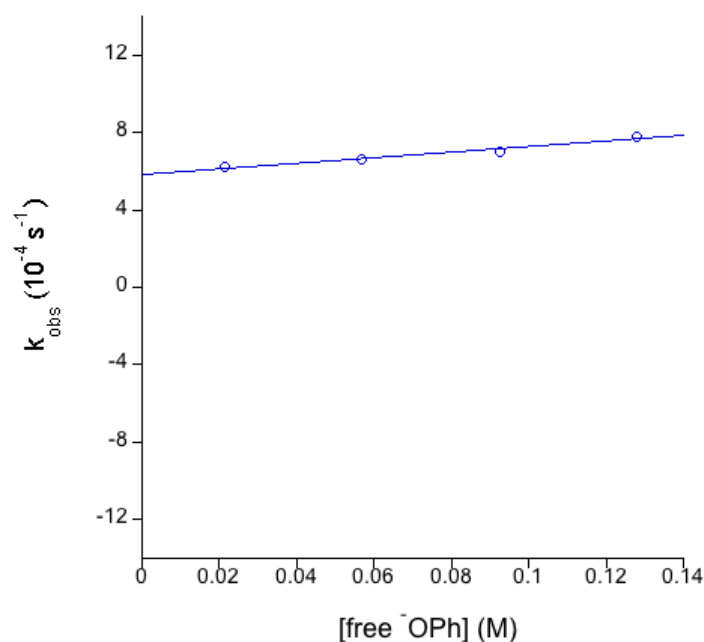


Figure 2.14. Plot of k_{obs} vs. $[\text{free } \text{OPh}^-]$. $y = 0.00059 + 0.0014x$, $R^2 = 0.9712$. The slope of the line is approximately zero.

Procedure for Determining Rate Constants Under Anhydrous Conditions

Purification of reagents and solvents: NMe_4OR salts were dried under vacuum over P_2O_5 at 80°C for 2 days and then stored under an inert atmosphere. CD_3CN was dried over CaH_2 and then stored under activated 3 \AA molecular sieves for 2 days in the glove box. All reagents and solvents were weighed out in the glove box.

Experimental Procedure: NMe_4OR (0.036 mmol, 5.0 equiv) was weighed into a 4 mL vial and then dried CD_3CN was added to dissolve the solid (0.5 mL). The resulting solution was added to a Teflon lined screw cap NMR tube charged with complex **1** (4.0 mg, 0.0071 mmol, 1.0 equiv) at room temperature to generate **2a-c** *in situ*. The tube was immediately placed in an NMR spectrometer that had been pre-heated to 35°C . The rate of reductive elimination from **2** to form **3** was monitored by ^1H NMR spectroscopy at this temperature. Concentration versus time data were acquired by integration of the ^1H NMR signals of **2** and **3**. The rate constants were obtained by fitting the decay of **2** to single exponentials. In all cases, the reported k_{obs} is the average rate constant associated with the decay of **2** over three reaction runs. A representative reaction profile for complex **2a** is shown in Figure 2.15.

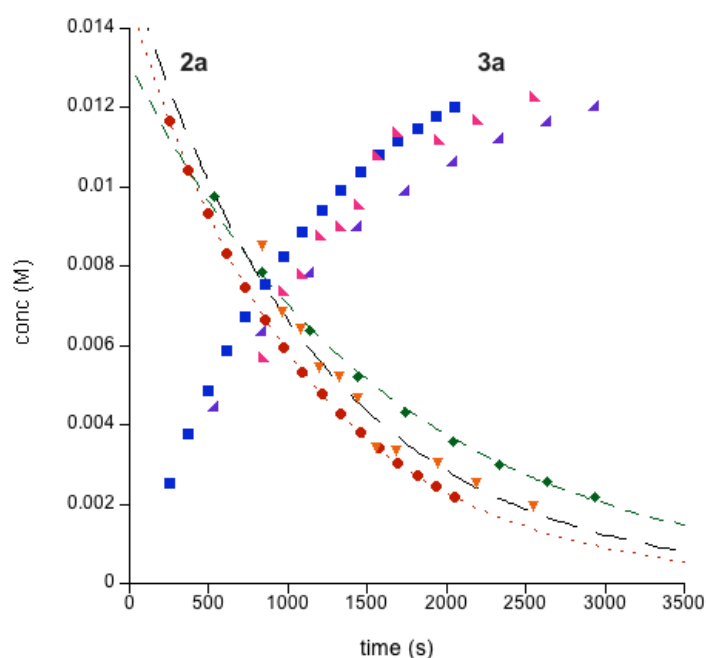
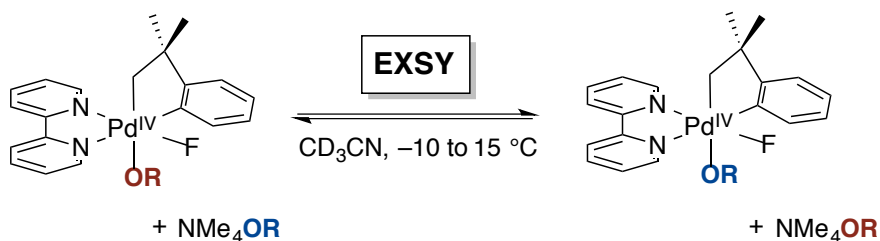


Figure 2.15. Plot of concentration vs. time for reductive elimination from **2a** (generated *in situ*) to form **3a** under anhydrous conditions.

EXSY Studies

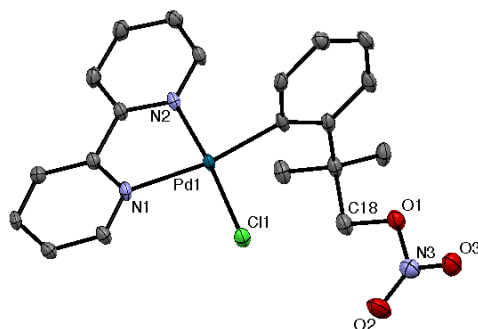


The lability of OR^- in Pd^{IV} complexes **2a-c** was investigated. A 2D EXSY (EXchange SpectroscopY) experiment was carried out to obtain information about exchange between free and bound $[\text{OR}^-]$ on the EXSY timescale. Complex **1** (4.0 mg, 0.007 mmol, 1.0 equiv) and a solution of the corresponding NMe_4OR (0.035 mmol, 5.0 equiv) in CD_3CN (0.5 mL) were combined in an NMR tube at room temperature and immediately placed in an NMR spectrometer pre-cooled to the respective temperature ($-10\text{ }^\circ\text{C}$ to $15\text{ }^\circ\text{C}$). ROESY spectra showed cross peaks between free and bound OR^- , suggesting that exchange is occurring on the EXSY timescale.

2.4.4. X-ray Structural Determination

All X-ray data were collected and solved by Dr. Jeff Kampf at the University of Michigan. The experimental details are described below.

X-Ray Crystallography Experimental Data of **3d**



Pale yellow (near colorless) plates of **3d** were grown from a petroleum ether / dichloromethane solution of the compound at $-30\text{ }^{\circ}\text{C}$. A crystal of dimensions $0.16 \times 0.02 \times 0.02\text{ mm}$ was mounted on a Rigaku AFC10K Saturn 944+ CCD-based X-ray diffractometer equipped with a low temperature device and Micromax-007HF Cu-target micro-focus rotating anode ($\lambda = 1.54187\text{ \AA}$) operated at 1.2 kW power (40 kV, 30 mA). The X-ray intensities were measured at 85(1) K with the detector placed at a distance 42.00 mm from the crystal. A total of 3481 images were collected with an oscillation width of 1.0° in ω . The exposure time was 2 sec. for the low angle images, 10 sec. for high angle. The integration of the data yielded a total of 27038 reflections to a maximum 2θ value of 136.42° of which 4059 were independent and 3855 were greater than $2\sigma(I)$. The final cell constants were based on the xyz centroids 18791 reflections above $10\sigma(I)$. Analysis of the data showed negligible decay during data collection; the data were processed with CrystalClear 2.0 and corrected for absorption. The structure was solved and refined with the Bruker SHELXTL (version 2008/4) software package, using the space group P1bar with $Z = 2$ for the formula $\text{C}_{21}\text{H}_{22}\text{ClN}_3\text{O}_3\text{Pd}$. Full matrix least-squares refinement based on F^2 converged at $R1 = 0.0369$ and $wR2 = 0.0970$ [based on $I > 2\sigma(I)$], $R1 = 0.0385$ and $wR2 = 0.0993$ for all data. Acknowledgement is made for funding from NSF grant CHE-0840456 for X-ray instrumentation.

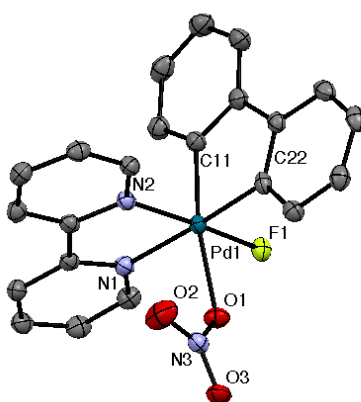
Sheldrick, G.M. SHELXTL, v. 2008/4; Bruker Analytical X-ray, Madison, WI, 2008.

CrystalClear Expert 2.0 r12, Rigaku Americas and Rigaku Corporation (2011), Rigaku Americas, 9009, TX, USA 77381-5209, Rigaku Tokyo, 196-8666, Japan.

Table 2.5. Selected Bond Lengths (Å) and Angles (°) for **3d**

Pd(1)-C(11)	2.009(3)	C(11)-Pd(1)-N(2)	92.60(13)
Pd(1)-N(2)	2.059(3)	C(11)-Pd(1)-N(1)	169.99(13)
Pd(1)-N(1)	2.125(3)	N(2)-Pd(1)-Cl(1)	173.93(8)
Pd(1)-Cl(1)	2.3060(9)	C(11)-Pd(1)-Cl(1)	92.78(10)

X-Ray Crystallography Experimental Data of **12b**



Yellow blocks of **12b** were grown from a dichloromethane solution at 40 °C. A crystal of dimensions 0.22 x 0.20 x 0.16 mm was mounted on a Bruker SMART APEX-I CCD-based X-ray diffractometer equipped with a low temperature device and fine focus Mo-target X-ray tube ($\lambda = 0.71073$ Å) operated at 1500 W power (50 kV, 30 mA). The X-ray intensities were measured at 85(1) K; the detector was placed at a distance 5.081 cm from the crystal. A total of 2067 frames were collected with a scan width of 0.5° in ω and 0.45° in ϕ with an exposure time of 30 s/frame. The integration of the data yielded a total of 28480 reflections to a maximum 2θ value of 54.30° of which 4203 were independent and 3533 were greater than $2\sigma(I)$. The final cell constants were based on the xyz centroids of 9961 reflections above $10\sigma(I)$. Analysis of the data showed negligible decay during data collection; the data were processed with SADABS and corrected for absorption. The structure was solved and refined with the Bruker SHELXTL (version 2008/4) software package, using the space group P2(1)/n with $Z = 4$ for the formula $C_{22}H_{16}FN_3O_3Pd$. All non-hydrogen atoms were refined anisotropically with the hydrogen atoms placed in idealized positions. Full matrix least-squares refinement based on F^2 converged at $R1 = 0.0287$ and $wR2 = 0.0681$ [based on $I >$

2sigma(I)], R1 = 0.0370 and wR2 = 0.0734 for all data.

Sheldrick, G.M. SHELXTL, v. 2008/4; Bruker Analytical X-ray, Madison, WI, 2008.

CrystalClear Expert 2.0 r12, Rigaku Americas and Rigaku Corporation (2011), Rigaku Americas, 9009, TX, USA 77381-5209, Rigaku Tokyo, 196-8666, Japan.

Table 2.6. Selected Bond Lengths (Å) and Angles (°) for **12b**

Pd(1)-F(1)	1.9517(14)	F(1)-Pd(1)-C(11)	88.26(8)
Pd(1)-O(1)	2.1849(17)	C(11)-Pd(1)-C(22)	82.13(10)
Pd(1)-N(1)	2.125(2)	C(22)-Pd(1)-O(1)	95.27(9)
Pd(1)-N(2)	2.002(2)	N(2)-Pd(1)-N(1)	79.92(8)
Pd(1)-C(11)	2.002(2)	F(1)-Pd(1)-N(2)	173.56(7)
Pd(1)-C(22)	2.009(2)	C(22)-Pd(1)-N(1)	176.00(9)

2.4.5. Computational Details

All computations were carried out by Prof. Allan Canty and collaborators at the University of Tasmania. The experimental details for these calculations are described below.

Gaussian 09⁴⁸ was used for DFT calculations at the B3LYP level for optimization, using the Stuttgart/Dresden ECP (SDD) basis set for Pd⁴⁸ and the 6-31G(d) basis set for other atoms (referred to as BS1). Single point calculations were performed at the B3LYP-D3 level;⁴⁸ these calculations utilized the quadruple- ξ valence polarized def2-QZVP⁴⁸ basis set on Pd along with the corresponding ECP and the 6-311+G(2d,p) basis set on other atoms (referred to as BS2). All calculations were carried out with acetonitrile as solvent using the IEFPCM (SCRF) model. All thermodynamic data were calculated at the standard state (298.15 K and 1 atm). Energy differences calculated by DFT methods are rendered less rigorous when dissociation, ion separation, and changes in the number of species are involved. To partly account for this, entropy calculations were adjusted by the method proposed by Okuno.⁴⁸ All transition structures contained one imaginary frequency, exhibiting atom displacements

consistent with the anticipated reaction pathway. The nature of transition structures was confirmed by Intrinsic Reaction Coordinate (IRC) searches, vibrational frequency calculations, and potential energy surface scans.

2.5. References

-
- (1) Adapted with permission from (a) Camasso, N. M.; Pérez-Temprano, M. H.; Sanford, M. S. *J. Am. Chem. Soc.* **2014**, *136*, 12771. © American Chemical Society (b) Canty, A. J.; Ariafard, A.; Camasso, N. M.; Higgs, A. T.; Yates, B. F.; Sanford, M. S. *Dalton Trans.* **2017**, *46*, 3742. © Royal Society of Chemistry
 - (2) (a) Canty, A. J. *Dalton Trans.* **2009**, 10409. (b) Vedernikov, A. N. *Top. Organomet. Chem.* **2010**, *31*, 101. (c) Racowski, J. M.; Sanford, M. S. *Top. Organomet. Chem.* **2011**, *35*, 61. (d) Desnoyer, A.; Love, J. A. *Chem. Soc. Rev.* **2017**, *46*, 197.
 - (3) For select reviews on ligand-directed C–H functionalization, see: (a) Lyons, T. W.; Sanford, M. S. *Chem. Rev.* **2010**, *110*, 1147. (b) Neufeldt, S. R.; Sanford, M. S. *Acc. Chem. Res.* **2012**, *45*, 936. (c) Engle, K. M.; Mei, T.-S.; Wasa, M.; Yu, J.-Q. *Acc. Chem. Res.* **2012**, *45*, 788.
 - (4) For select examples of Pd^{II} catalyzed C(sp³)–H oxygenation, see: (a) Desai, L. V.; Hull, K. L.; Sanford, M. S. *J. Am. Chem. Soc.* **2004**, *126*, 9542. (b) Zhang, J.; Khaskin, E.; Anderson, N. P.; Zavalij, P. Y.; Vedernikov, A. N. *Chem. Commun.* **2008**, 3625. (c) Zhang, S.-Y.; He, G.; Zhao, Y.; Wright, K.; Nack, W. A.; Chen, G. *J. Am. Chem. Soc.* **2012**, *134*, 7313. (d) Zhou, L.; Lu, W. *Org. Lett.* **2014**, *16*, 508. (e) Xu, Y.; Yan, G.; Ren, Z.; Dong, G. *Nature Chem.* **2015**, *7*, 829. (f) Thompson, S.; Thach, D. Q.; Dong, G. *J. Am. Chem. Soc.* **2015**, *137*, 11586. (g) Huang, Z.; Wang, C.; Dong, G. *Angew. Chem. Int. Ed.* **2016**, *128*, 5385.
 - (5) (a) Pilarski, L. T.; Selander, N.; Böse, D.; Szabó, K. *J. Org. Lett.* **2009**, *11*, 5518. (b) Pilarski, L. T.; Janson, P. G.; Szabó, K. *J. Org. Chem.* **2011**, *76*, 1503. (c) Check, C. T.; Henderson, W. H.; Wray, B. C.; Vanden Eynden, M. J.; Stambuli, J. P. *J. Am. Chem. Soc.* **2011**, *133*, 18503. (d) Alam, R.; Pilarski, L. T.; Pershagen, E.; Szabó, K. *J. Am. Chem. Soc.* **2012**, *134*, 8778. (e) Zhu, H.; Chen, P.; Liu, G. *J. Am. Chem. Soc.* **2014**, *136*, 1766. (f) Chen, C.; Chen, P.; Liu, G. *J. Am. Chem. Soc.* **2015**, *137*, 15648. (g) Yin, G.; Mu, X.; Liu, G. *Acc. Chem. Res.* **2016**, *49*, 2413.
 - (6) (a) Alexanian, E. J.; Lee, C.; Sorensen, E. J. *J. Am. Chem. Soc.* **2005**, *127*, 7690. (b) Liu, G. S.; Stahl, S. S. *J. Am. Chem. Soc.* **2006**, *128*, 7179. (c) Desai, L. V.; Sanford, M. S. *Angew. Chem. Int. Ed.* **2007**, *46*, 5737. (d) Muñiz, K.; Hovelman, C. H.; Streuff, J. *J. Am. Chem. Soc.* **2008**, *130*, 763. (e) Zhu, M.-K.; Zhao, J.-F.; Loh, T.-P. *J. Am. Chem. Soc.* **2010**, *132*, 6284. (f) Neufeldt, S. R.; Sanford, M. S. *Org. Lett.* **2012**, *15*, 46. (g) Martinez, C.; Wu, Y.; Weinstein, A. B.; Stahl, S. S.; Liu, G.; Muñiz, K. *J. Org. Chem.* **2013**, *78*, 6309.
 - (7) C(sp²)–O reductive elimination from Pd^{IV}: (a) Racowski, J. M.; Dick, A. R.; Sanford, M. S. *J. Am. Chem. Soc.* **2009**, *131*, 10974. (b) Dick, A. R.; Kampf, J. W.; Sanford, M. S. *J. Am. Chem. Soc.* **2005**, *127*, 12790.
 - (8) Gary, J. B.; Sanford, M. S. *Organometallics* **2011**, *30*, 6143.
 - (9) Yamamoto, Y.; Kuwabara, S.; Matsuo, S.; Ohno, T.; Nishiyama, H.; Itoh, K. *Organometallics* **2004**, *23*, 3898.

-
- (10) (a) Oloo, W. N.; Zavalij, P. Y.; Zhang, J.; Khaskin, E.; Vedernikov, A. N. *J. Am. Chem. Soc.* **2010**, *132*, 14400. (b) Oloo, W. N.; Zavalij, P. Y.; Vedernikov, A. N. *Organometallics* **2013**, *32*, 5601.
- (11) Qu, F.; Khusnutdinova, J. R.; Rath, N. P.; Mirica, L. M. *Chem. Commun.* **2014**, *50*, 3036.
- (12) C(sp²)-O reductive elimination from Pd^{III}: Powers, D. C.; Geibel, M. A. L.; Klein, J. E. M. N.; Ritter, T. *J. Am. Chem. Soc.* **2009**, *131*, 17050.
- (13) For studies of C(sp³)-O reductive elimination at Pt see: (a) Luinstra, G. A.; Labinger, J. A.; Bercaw, J. E. *J. Am. Chem. Soc.* **1993**, *115*, 3004. (b) Williams, B. S.; Holland, A. W.; Goldberg, K. I. *J. Am. Chem. Soc.* **1999**, *121*, 252. (c) Williams, B. S.; Goldberg, K. I. *J. Am. Chem. Soc.* **2001**, *123*, 2576. (d) Canty, A. J.; Denney, M. C.; van Koten, G.; Skelton, B. W.; White, A. H. *Organometallics* **2004**, *23*, 5432. (e) Vedernikov, A. N.; Binfield, S. A.; Zavalij, P. Y.; Khusnutdinova, J. R. *J. Am. Chem. Soc.* **2006**, *128*, 82. (f) Khusnutdinova, J. R.; Zavalij, P. Y.; Vedernikov, A. N. *Organometallics* **2007**, *26*, 3466. (g) Smythe, N. A.; Grice, K. A.; Williams, B. S.; Goldberg, K. I. *Organometallics* **2009**, *28*, 277. (h) Khusnutdinova, J. R.; Newman, L. L.; Zavalij, P. Y.; Lam Y.-F.; Vedernikov, A. N. *J. Am. Chem. Soc.* **2008**, *130*, 2174. (i) Vedernikov, A. N. *Chem. Commun.* **2009**, *32*, 4781. (j) Vedernikov, A. N. *Acc. Chem. Res.* **2012**, *45*, 803.
- (14) C(sp³)-O reductive elimination at Pd^{II}, see: Marquard, S. L.; Hartwig, J. F. *Angew. Chem. Int. Ed.* **2011**, *50*, 7119.
- (15) (a) Canty, A. J.; Done, M. C.; Skelton, B. W.; White, A. H. *Inorg. Chem. Commun.* **2001**, *4*, 648. (b) Canty, A. J.; Denney, M. C.; Skelton, B. W.; White, A. H. *Organometallics* **2004**, *23*, 1122. (c) Canty, A. J.; Denney, M. C.; van Koten, G.; Skelton, B. W.; White, A. H. *Organometallics* **2004**, *23*, 5432. (d) Sbergaeva, A. V.; Zavalij, P. Y.; Vedernikov, A. N. *J. Am. Chem. Soc.* **2016**, *138*, 1446.
- (16) For reviews on low-valent Pd-catalyzed cross-coupling reactions, see: (a) Littke, A. F.; Fu, G. C. *Angew. Chem. Int. Ed.* **2002**, *41*, 4176. (b) Nicolaou, K. C.; Bulger, P. G.; Sarlah, D. *Angew. Chem. Int. Ed.* **2005**, *44*, 4442. (c) Sather, A. C.; Buchwald, S. L. *Acc. Chem. Res.* **2016**, *49*, 2146.
- (17) McMurtrey, K. B.; Racowski, J. M.; Sanford, M. S. *Org. Lett.* **2012**, *14*, 4094.
- (18) (a) Racowski, J. M.; Gary, J. B.; Sanford, M. S. *Angew. Chem. Int. Ed.* **2012**, *51*, 3414. (b) Pérez-Temprano, M. H.; Racowski, J. M.; Kampf, J. W.; Sanford, M. S. *J. Am. Chem. Soc.* **2014**, *136*, 4097. (c) Pendleton, I. M.; Pérez-Temprano, M. H.; Sanford, M. S.; Zimmerman, P. M. *J. Am. Chem. Soc.* **2016**, *138*, 6049.
- (19) Mann, G.; Shelby, Q.; Roy, A. H.; Hartwig, J. F. *Organometallics* **2003**, *22*, 2775.
- (20) Unless otherwise noted, all Pd^{IV} complexes were formed as a >20:1 ratio of stereoisomers.
- (21) In our system, treatment of **1** with NaOH or NMe₄OH led to the formation of a complex mixture of products.
- (22) (a) Richmond, T. G. *Coord. Chem. Rev.* **1990**, *105*, 221. (b) Grushin, V. V. *Chem. Eur. J.* **2002**, *8*, 1006. (c) Campbell, M. G.; Ritter, T. *Chem. Rev.* **2015**, *115*, 612.
- (23) (a) Fraser, S. L.; Antipin, M. Y.; Khroustalyov, V. N.; Grushin, V. V. *J. Am. Chem. Soc.* **1997**, *119*, 4769. (b) Pilon, M. C.; Grushin, V. V. *Organometallics* **1998**, *17*, 1774. (c) Roe, D. C.; Marshall, W. J.; Davidson, F.; Soper, P. D.; Grushin, V. V. *Organometallics* **2000**, *19*, 4575. (d) Grushin, V. V.; Marshall, W. J. *Angew. Chem., Int. Ed.* **2002**, *41*, 4476.
- (24) Tetramethyl- and tetrabutylammonium salts were used for low temperature NMR characterization, except for complex **2e**, which was generated with sodium dimethyl phosphate in DMSO.

-
- (25) Complexes **2d-f** are formed as an equilibrium mixture with the corresponding cationic species (likely the acetonitrile adduct, [(bpy)Pd(CH₂CMe₂-*o*-C₆H₄)(F)(CH₃CN)]⁺X⁻). This is likely due to the poor nucleophilicity of the oxyanions.
- (26) The tosylate reductive elimination product could not be isolated cleanly and was therefore characterized by crude NMR.
- (27) Reductive elimination from complex **2e** only proceeded cleanly in DMSO.
- (28) Engle, K. M.; Mei, T.-S.; Wang, X.; Yu, J.-Q. *Angew. Chem., Int. Ed.* **2011**, *50*, 1478.
- (29) For an example of H-bonding between HF and a Pd^{IV}-fluoride, see: Ball, N. D.; Sanford, M. S. *J. Am. Chem. Soc.* **2009**, *131*, 3796.
- (30) For a review of Job Plots in organometallic chemistry, see: Renny, J. S.; Tomasevich, L. L.; Tallmadge, E. H.; Collum, D. B. *Angew. Chem., Int. Ed.* **2013**, *52*, 11998
- (31) Pearson, R. G. *J. Am. Chem. Soc.* **1963**, *85*, 3533.
- (32) For select examples of lewis acid activated reductive eliminations, see: (a) Huang, J.; Haar, C. M.; Nolan, S. P.; Marcone, J. E.; Moloy, K. G. *Organometallics* **1999**, *18*, 297. (b) Nakao, Y.; Yada, A.; Ebata, S.; Hiyama, T. *J. Am. Chem. Soc.* **2007**, *129*, 2428. (c) Liberman-Martin, A. L.; Levine, D. S.; Liu, W.; Bergman, R. G.; Tilley, T. D. *Organometallics* **2016**, *35*, 1064.
- (33) The values of k_{obs} for reductive elimination from complexes **2a-c** under rigorously anhydrous conditions (ie, in an inert atmosphere glovebox with dried solvent and reagents) were nearly identical to those obtained under ambient conditions (i.e., on the benchtop with commercial solvents and reagents) where trace amounts of water are expected. Only the addition of exogenous water (10-500 equiv) impacted the reductive elimination kinetics.
- (34) Pawlikowski, A. V.; Getty, A. D.; Goldberg, K. I. *J. Am. Chem. Soc.* **2007**, *129*, 10382.
- (35) In order to ensure that the increase in the observed rate constant can be attributed to a cation effect rather than being the result of a change in reaction medium, we monitored the rate of reductive elimination from **2a** to form **3a** in the presence of 5 equivalents of NMe₄OPh and 200 equiv of 15-crown-5. The observed rate constants were indistinguishable from each other.
- (36) Gaussian 09 was used at the B3LYP level for geometry optimization with acetonitrile as solvent utilizing the SDD basis set on Pd and the 6-31G(d) basis set for other atoms. Single point energy calculations for all structures at the M06 level employed the quadrupole- ξ valence def2-QZVP basis set on Pd along with the corresponding ECP and the 6-311+G(2d,p) basis set on other atoms.
- (37) An alternative pathway that would also be consistent with the experimental data is direct reductive elimination following isomerization to a different Pd^{IV} isomer. However, DFT calculations suggest that this pathway is much higher in energy.
- (38) For select examples of C-H halogenation, see: (a) Giri R.; Chen X.; Yu, J.-Q. *Angew. Chem. Int. Ed.* **2005**, *44*, 2112. (b) Dick, A. R.; Kampf, J. W.; Sanford, M. S. *J. Am. Chem. Soc.* **2005**, *127*, 12790. (c) Whitfield, S. R.; Sanford, M. S. *J. Am. Chem. Soc.* **2007**, *129*, 15142. (d) Xiong, H.-Y.; Cahard, D.; Pannecoucke, X. Besset, T. *Eur. J. Org. Chem.* **2016**, 3625. (e) Yang, X.; Sun, Y.; Sunb, T.; Rao Y. *Chem. Commun.* **2016**, *52*, 6423.
- (39) (a) van Asselt R.; Rijnberg E.; Elsevier C. *J. Organometallics* **1994**, *13*, 706. (b) Canty A. J., Hoare J.L.; Davies N.W.; Traill P. R. *Organometallics* **1998**, *17*, 2046. (c) Viagloek, A. *Acc. Chem. Res.* **2015**, *48*, 238.
- (40) (a) Grushin, V. V.; *Acc. Chem. Res.* **2010**, *43*, 160. (b) Engle, K. M.; Mei, T. S.; Wang, X.; Yu, J. Q.; *Angew. Chem. Int. Ed.* **2011**, *50*, 1478-1491. (c) Furuya, T.; Kamlet, A. S.;

-
- Ritter, T.; *Nature* **2011**, *473*, 470-477. (d) Sather, A. C.; Buchwald, S. L. *Acc. Chem. Res.* **2016**, *49*, 2146.
- (41) Campora, J.; Palma, P.; del Rio, D.; Lopez, J. A.; Valerga, P. *Chem. Commun.* **2004**, *13*, 1490.
- (42) For an example of oxidative addition of an iodoarene to Pd^{II}, see: Vicente-Hernández, I.; Chicote, M.-T.; Vicente, J.; Bautista, D. *Chem. Commun.* **2016**, *52*, 594.
- (43) Campora, J.; Lopez, J. A.; Palma, P.; Rio, D.; Carmona, E.; Valerga, P.; Graiff, C.; Tiripicchio, A. *Inorg. Chem.* **2001**, *40*, 4116.
- (44) Russel, D. G.; Senior, J. B. *Can. J. Chem.* **1980**, *58*, 22.
- (45) Bunton, C.; Mhala, M. M.; Oldham, K. G.; Vernon, C. A. *J. Chem. Soc.* **1960**, 3293.
- (46) Chaumontet, M.; Piccardi, R.; Audic, N.; Hitce, J.; Peglion, J.-L.; Clot, E.; Baudoin, O. *J. Am. Chem. Soc.* **2008**, *130*, 15157.
- (47) Blanda, M. T.; Horner, J. H.; Newcomb, M. *J. Org. Chem.* **1989**, *54*, 4626.
- (48) (a) Frisch, M. J.; et al. *Gaussian 09*, revision A.02; Gaussian, Inc.: Wallingford, CT, 2009. (b) Andrae, H.; Haussermann, U.; Dolg, M.; Stoll, H.; Preuss, H. *Theor. Chim. Acta* **1990**, *77*, 123. (c) Weigend, F.; Furche, F.; Aldrichs, R. *J. Chem. Phys.* **2003**, *119*, 12753. (d) Okuno, Y. *Chem. Eur. J.* **1997**, *3*, 212. (e) Ehrlich, S.; Moellmann, J.; Grimme, S. *Acc. Chem. Res.* **2013**, *46*, 916. (f) Antony, J.; Sure, R.; Grimme, S. *Chem. Commun.* **2015**, *51*, 1764.

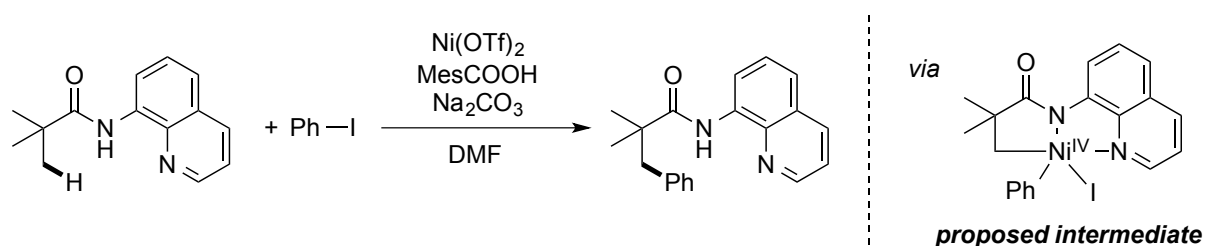
CHAPTER 3

Design, Synthesis, and Reactivity of Organometallic Ni^{IV} Complexes¹

3.1. Introduction

In recent years, nickel-catalyzed cross-coupling reactions have emerged as valuable synthetic methods for the construction of carbon–carbon and carbon–heteroatom bonds.² The mechanisms of these transformations are generally proposed to involve sequences of 1 and 2e⁻ redox events that interconvert Ni⁰, Ni^I, Ni^{II} and/or Ni^{III} intermediates.^{2,3} In contrast, organometallic Ni^{IV} intermediates are rarely invoked in cross-coupling reactions.⁴ While a few recent reports have proposed the intermediacy of Ni^{IV} (for example, in Ni-catalyzed C–H bond functionalization reactions), the transient nature of these intermediates has hindered definitive characterization and confirmation of their mechanistic roles (Scheme 3.1).⁵ Overall, examples of well-defined Ni^{IV} complexes are exceedingly rare,^{1,6} and the reactivity of these species in carbon–carbon and carbon–heteroatom bond-forming reactions has not been thoroughly investigated.^{1,6}

Scheme 3.1. Ni-Catalyzed C(sp³)–H Functionalization via Proposed Ni^{IV} Intermediate



This chapter describes the design, synthesis, and characterization of a series of organometallic Ni^{IV} complexes accessed by the reaction of Ni^{II} precursors with different 2e⁻

oxidants. We demonstrate the importance of the trifluoromethyl (CF₃) ligand and tris(pyrazolyl)borate (Tp) scaffold in stabilizing these traditionally transient species. Furthermore, reactivity studies show that these Ni^{IV} complexes participate in highly selective carbon–carbon and carbon–heteroatom bond-forming reactions that remain extremely challenging to achieve at lower oxidation states of Ni.⁷

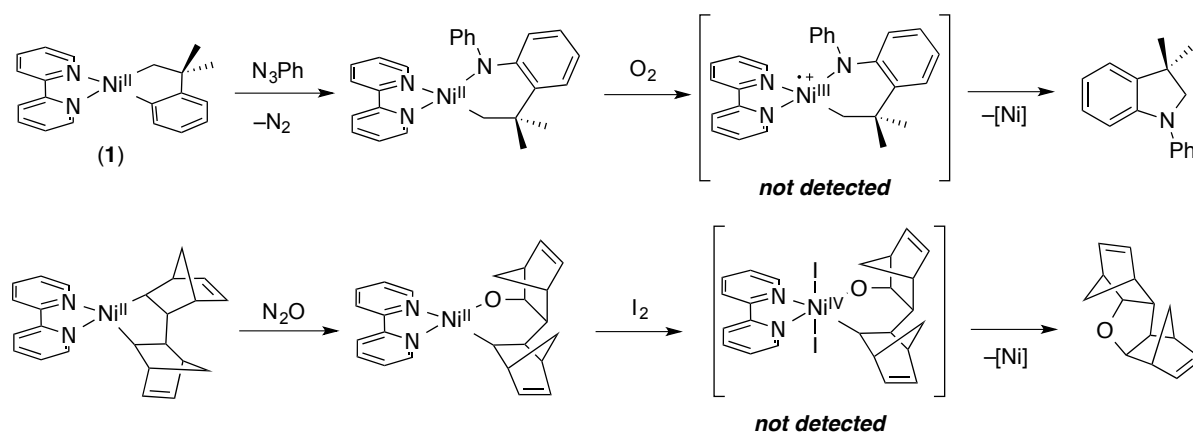
3.2. Results and Discussion

3.2.1. Design, Synthesis, and Carbon–Heteroatom Coupling Reactions of Organometallic Ni^{IV} Complexes

Initial Studies with Bipyridine-Supported Ni^{II} Complex

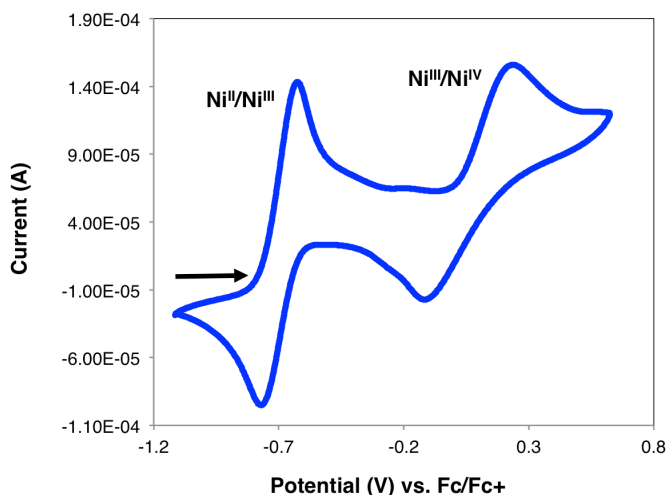
We first sought to access a model Ni^{IV} complex via the 2e⁻ oxidation of the Ni^{II} starting material [(bpy)Ni^{II}(CH₂CMe₂-*o*-C₆H₄)] (**1**). Seminal work by Hillhouse first demonstrated that cyclometalated Ni complexes such as **1** undergo oxidatively-induced carbon–carbon and carbon–heteroatom bond-forming reactions in the presence of stoichiometric oxidants.⁸ Although the authors proposed Ni^{III} and/or Ni^{IV} intermediates in these reactions, no high-valent species were detected (Scheme 3.2). These studies suggested that high-valent Ni intermediates can promote challenging bond-forming reactions and that modification of the ligand environment could enable a direct study of their reactivity.

Scheme 3.2. Previous Studies by Hillhouse Demonstrating C–X Coupling via Proposed Ni^{III} and Ni^{IV} intermediates



Electrochemical analyses of [(bpy)Ni^{II}(CH₂CMe₂-*o*-C₆H₄)] (**1**) were carried out in our lab to further assess the accessibility and stability of high-valent Ni. As shown in Figure 3.1, the cyclic voltammogram of **1** in CH₃CN shows two oxidative waves at approximately -0.61 V and +0.27 V versus Fc/Fc⁺ (Fc = ferrocene). We assign these features to the Ni^{II}/Ni^{III} and the Ni^{III}/Ni^{IV} couples, respectively. These waves are both quasi-reversible and at relatively low potentials, suggesting that Ni^{IV} could be accessible and potentially isolable with this ligand system.

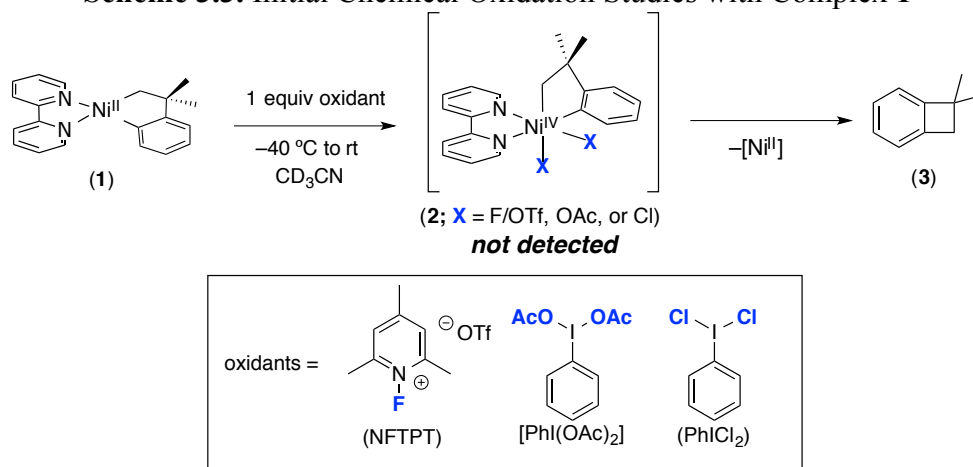
Figure 3.1. Cyclic Voltammogram of (bpy)Ni^{II}(CH₂CMe₂-*o*-C₆H₄). [Ni] = 0.01 M in CH₃CN; [NBu₄BF₄] = 0.1 M; Scan Rate = 100 mV/s



The chemical oxidation of **1** was first examined using three different inner-sphere oxidants that are known to promote the $2e^-$ oxidation of other group 10 metal complexes: *N*-fluoro-2,4,6-trimethylpyridinium triflate (NFTPT), iodobenzene diacetate [PhI(OAc)₂], and iodobenzene dichloride (PhICl₂) (Scheme 3.3).⁹ We anticipated that these oxidants would react with **1** to generate coordinatively saturated, diamagnetic Ni^{IV} intermediates of general structure **2** (X = F/OTf, OAc, or Cl). If intermediate **2** were sufficiently long-lived, it should be detectable by NMR spectroscopy. The treatment of **1** with each of these oxidants in CD₃CN resulted in near quantitative formation of benzocyclobutane **3** within minutes at room temperature (Scheme 3.3). Organic product **3** is likely generated via C(sp²)-C(sp³) bond-forming reductive elimination from Ni^{IV} intermediate **2**. However, **2** could not be detected by

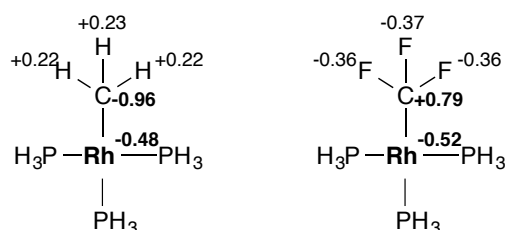
^1H NMR spectroscopy at room temperature or at $-40\text{ }^\circ\text{C}$ with any of these oxidants, suggesting that this putative intermediate is highly unstable.

Scheme 3.3. Initial Chemical Oxidation Studies with Complex **1**



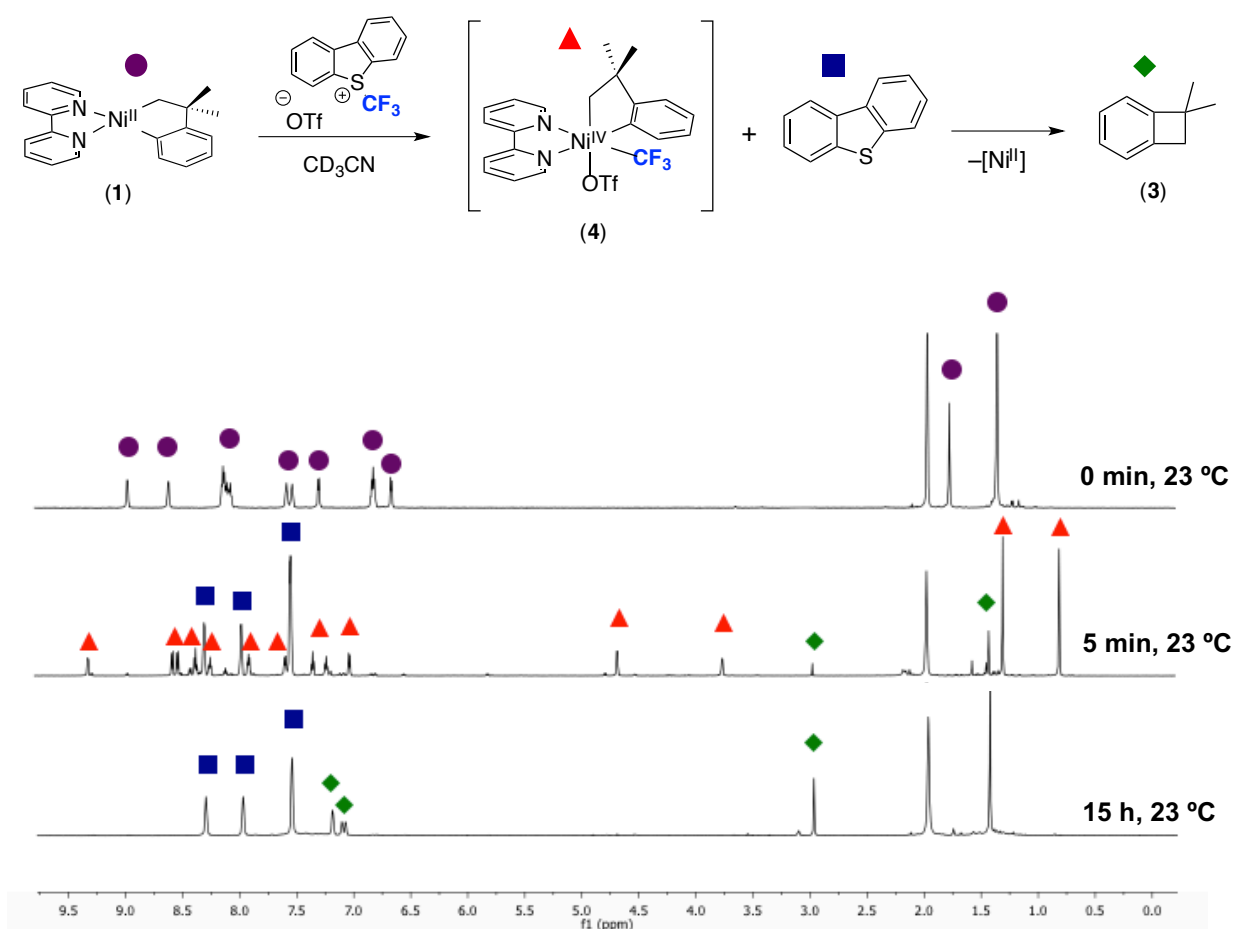
We reasoned that this type of Ni^{IV} intermediate might be stabilized by replacing one of the X-type ligands with a trifluoromethyl group (CF_3).^{7c,d,10,11} The trifluoromethyl ligand uniquely exhibits both electron-accepting¹² and electron-donating¹³ character, thereby disfavoring reductive elimination processes, while also providing stabilization to high-valent metal centers.^{7c,14,15} This apparent contradiction can be rationalized by competing inductive effects. The strongly electronegative fluorine atoms sequester electrons from the neighboring metal center, disfavoring reductive elimination processes. At the same time, the strong *trans* influence of a CF_3 group has been well documented. Experimental studies have shown that it serves as an excellent σ -donor to the adjacent metal center, and, as such, $\text{M}-\text{CF}_3$ bonds are typically very strong (Figure 3.2).^{10,13}

Figure 3.2. Computed Natural Atomic Charges for $\text{Rh}-\text{CH}_3$ and $\text{Rh}-\text{CF}_3$ Complexes Illustrating the Unique Electronic Effects of a Trifluoromethyl Group on a Metal System



In an effort to install a CF₃ ligand onto the putative Ni^{IV} center, we tested the reactivity of the Ni^{II} precursor **1** with strong electrophilic trifluoromethylating reagents. In the event, the reaction of **1** with the “CF₃⁺” oxidant *S*-(trifluoromethyl)dibenzothiophenium triflate (Umemoto’s Reagent) in CD₃CN at room temperature resulted in transfer of a CF₃ ligand to Ni to form a detectable, diamagnetic Ni–CF₃ complex (Scheme 3.4). This intermediate persists in solution for several hours, and *in situ* ¹H and ¹⁹F NMR spectroscopic studies implicate the formation of Ni^{IV} complex **4**. Complex **4** undergoes C(sp²)–C(sp³) coupling to form benzocyclobutane **3** over the course of 15 h at 25 °C. The detection of **4** in this reaction provided the first evidence that Ni^{IV} can be formed under these conditions and suggested that further modification of the ligand scaffold could yield an isolable Ni^{IV} complex.

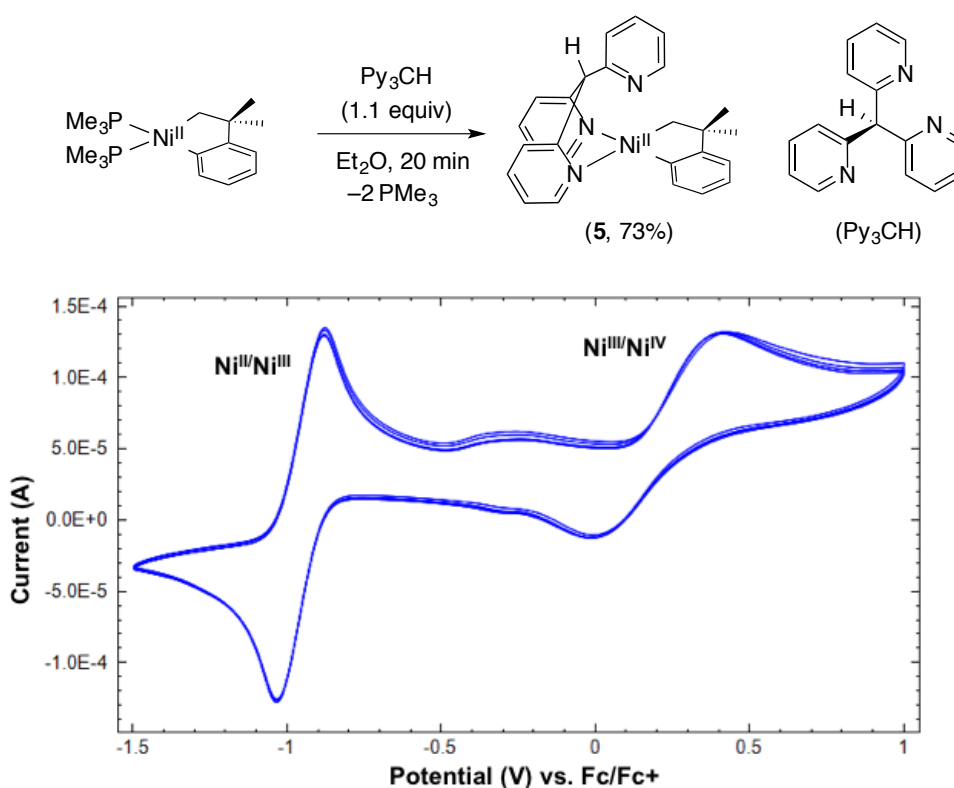
Scheme 3.4. Formation of a Detectable Ni^{IV} Intermediate by the Oxidation of Complex **1** with Umemoto’s Reagent



Installation of a Stabilizing Tripodal Ligand

Previous work from our lab and others have demonstrated that facially coordinated tridentate ligands can have a dramatic stabilizing effect on octahedral Pd^{IV} and Pt^{IV} complexes.^{16,17} Based on these precedents, we replaced the bidentate bipyridine ligand in **1** with a facial tridentate ligand, tris(2-pyridyl)methane (Py₃CH), to further enhance the stability of the proposed Ni^{IV} intermediate. Complex **5** was prepared in 73% isolated yield via the treatment of [(PMe₃)Ni^{II}(CH₂CMe₂-*o*-C₆H₄)] with 1.1 equiv of Py₃CH in diethyl ether (Figure 3.3). Cyclic voltammety studies of Ni^{II} complex **5** reveal two distinct oxidation peaks (−0.85 V and 0.35 V) that are comparable potentials to those observed for bpy derivative **1**. These data suggest that high-valent Ni intermediates with this ligand system should be accessible with a similar set of oxidants.

Figure 3.3. Synthesis and Cyclic Voltammogram of Ni^{II} Complex **5**. [Ni] = 0.01 M in CH₃CN; [NBu₄BF₄] = 0.1 M; Scan Rate = 100 mV/s



Consistent with the electrochemical analysis, the chemical oxidation of [(Py₃CH)Ni^{II}(CH₂CMe₂-*o*-C₆H₄)] (**5**) with Umemoto's Reagent in CH₃CN at 25 °C led to an

immediate color change from dark red to yellow with concomitant formation of the diamagnetic Ni^{IV}-CF₃ complex **6** as determined by NMR spectroscopy (Scheme 3.5). Complex **6** was isolated in 92% yield by recrystallization from benzene, and X-ray quality crystals were obtained via slow evaporation of a concentrated acetone solution (Figure 3.4). The solid-state structure of this Ni^{IV} complex displays the expected octahedral geometry, with tridentate facial coordination of the Py₃CH ligand. Notably, Umemoto's Reagent is frequently used as an oxidant in transition-metal catalysis¹⁸; as such, the isolation and characterization of **6** suggests the potential feasibility of Ni^{II/IV} catalysis manifolds employing this reagent.

Scheme 3.5. Synthesis of the Stable Ni^{IV} Complex **6**

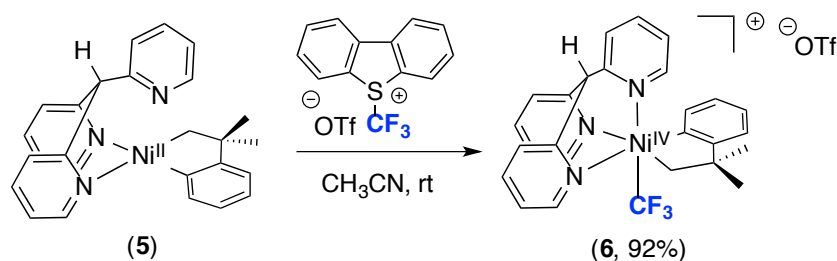
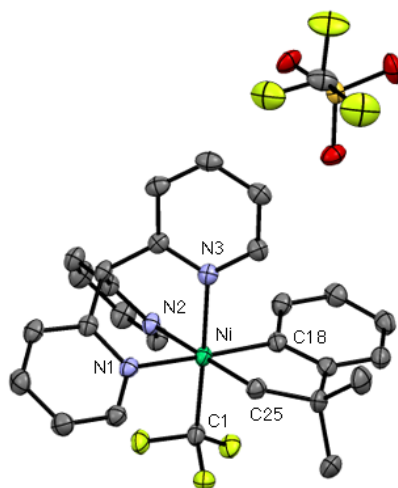


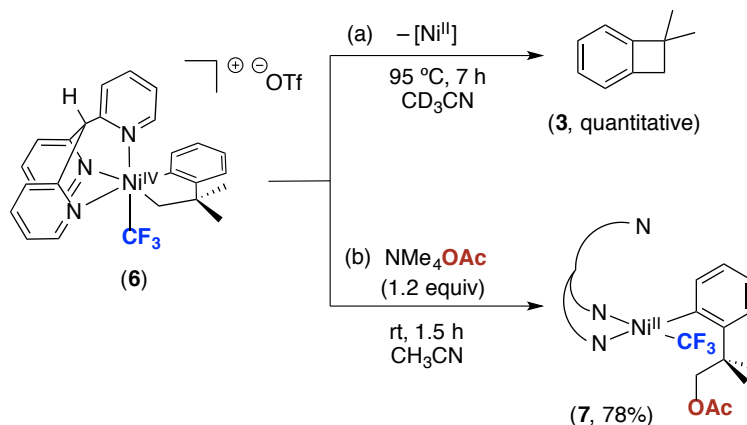
Figure 3.4. ORTEP Diagram of Cationic Complex **6**. Thermal ellipsoids are drawn at 50% probability. Hydrogen atoms and disorder in the triflate are omitted for clarity



We next investigated the reactivity of this isolated Ni^{IV} complex towards both carbon-carbon and carbon-heteroatom coupling reactions. Upon heating at 95 °C for 7 h, complex **6** underwent C(sp²)-C(sp³) bond-forming reductive elimination to produce benzocyclobutane **3**

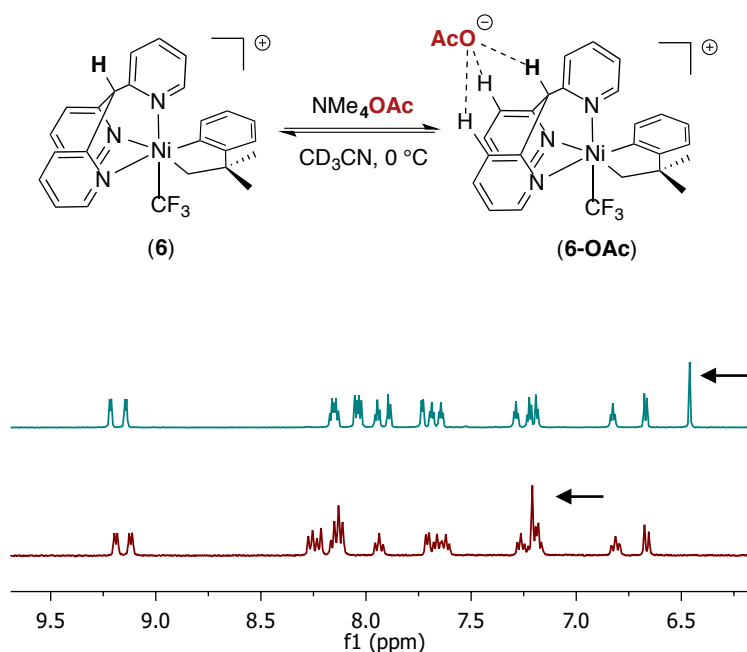
in quantitative yield (Scheme 3.6a). Furthermore, the treatment of **6** with exogenous acetate (1.2 equiv of NMe_4OAc) in CH_3CN at room temperature resulted in selective $\text{C}(\text{sp}^3)\text{-O}$ coupling to afford Ni^{II} product **7** in >98% yield, as determined by ^{19}F NMR spectroscopy. Complex **7** was isolated as a yellow powder in 78% yield (Scheme 3.6b).

Scheme 3.6. Reactivity of Complex **6** Towards: (a) $\text{C}(\text{sp}^2)\text{-C}(\text{sp}^3)$ Reductive Elimination and (b) $\text{C}(\text{sp}^3)\text{-O}$ Coupling



While complex **6** reacted cleanly with NMe_4OAc , several other nucleophiles (for example, NMe_4X with $\text{X} = \text{OPh}$, SPh , F) afforded complicated mixtures of products. We hypothesized that this might be due, at least in part, to the overall +1 charge on **6**, which would render the complex highly electrophilic and thus susceptible to side reactions involving electron transfer.¹⁹ In addition, solid-state binding interactions between anions and the tris(pyridyl) methane backbone at other metal centers have been well documented.^{16f,19} Consistent with these findings, the treatment of **6** with NMe_4OAc at $0\text{ }^\circ\text{C}$ revealed a 0.8 ppm downfield shift of the methine proton resonance in the ^1H NMR spectrum, likely corresponding to formation of the acetate adduct **6-OAc** in Figure 3.5. In the presence of stronger bases, this interaction could potentially lead to equilibrium deprotonation of the acidic proton and subsequent decomposition of the complex.¹⁹ Thus, for our next studies we targeted a tridentate supporting ligand that would stabilize Ni^{IV} without participating in these undesirable side reactions.

Figure 3.5. Evidence for Ligand-Anion Interactions in Complex **6**



Scope of Carbon–Heteroatom Coupling from TpNi^{IV}

The anionic tripodal ligand tris(pyrazolyl)borate (Tp) has served as an effective scaffold for stabilizing related Pd^{IV} and Pt^{IV} complexes.¹⁷ In addition, we reasoned that the borohydride moiety would likely be compatible with strong nucleophiles and would minimize the decomposition pathways observed with complex **6**. We thus next targeted the neutral TpNi^{IV} complex **9**.

Anionic TpNi^{II} complex **8** was prepared in 90% yield via ligand exchange between $[(\text{PMe}_3)\text{Ni}^{\text{II}}(\text{CH}_2\text{CMe}_2\text{-}o\text{-C}_6\text{H}_4)]$ and KTp (Scheme 3.7). $[(\text{Tp})\text{Ni}^{\text{IV}}(\text{CH}_2\text{CMe}_2\text{-}o\text{-C}_6\text{H}_4)(\text{CF}_3)]$ (**9**) was then prepared by the treatment of **8** with Umemoto's reagent in CH_3CN at room temperature and was isolated in 92% after purification by flash chromatography. Yellow crystals of **9** were obtained via slow evaporation of a methanol solution, and an ORETP diagram of the structure is shown in Figure 3.6. The $\text{Ni}^{\text{IV}}\text{-CF}_3$ bond distances in both **5** (1.956 Å) and **9** (1.941 Å) are considerably longer than typical $\text{Ni}^{\text{II}}\text{-CF}_3$ bond lengths reported in the literature (1.853-1.921 Å).¹⁵ While complexes of higher oxidation states may be expected to

have shorter bond distances due to enhanced electrophilicity, this discrepancy may be due to increased steric crowding at the octahedral centers.

Scheme 3.7. Synthesis of $[(\text{Tp})\text{Ni}^{\text{IV}}(\text{CH}_2\text{CMe}_2\text{-}o\text{-C}_6\text{H}_4)(\text{CF}_3)]$ (**9**)

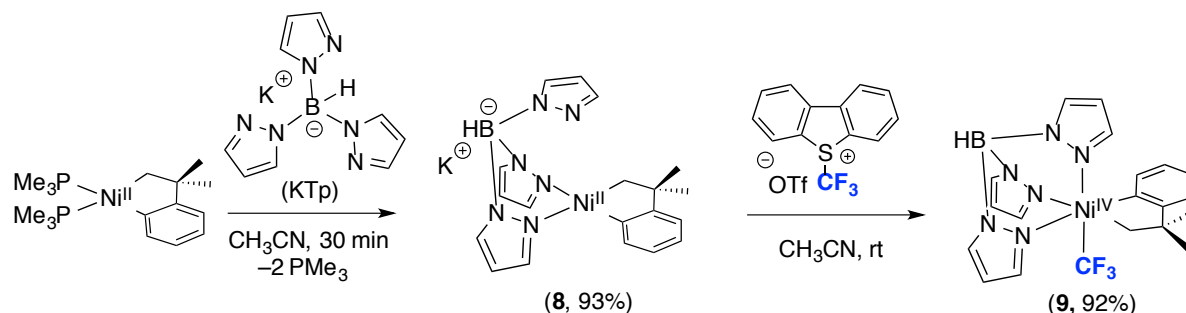
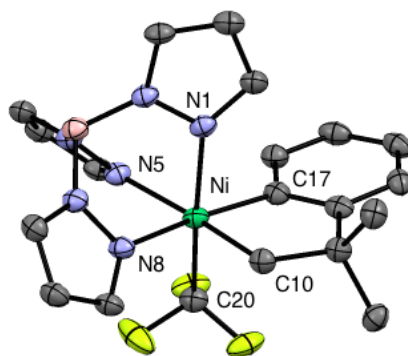


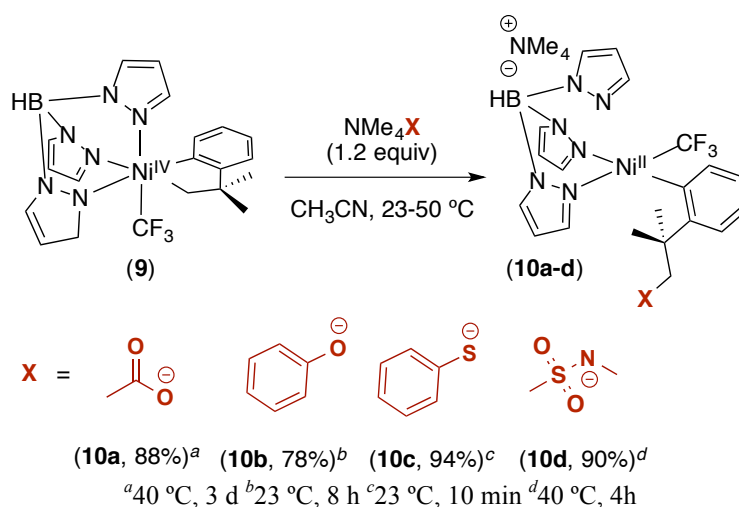
Figure 3.6. ORTEP Diagram of Complex **9**. Thermal ellipsoids are drawn at 50% probability. Hydrogen atoms are omitted for clarity.



TpNi^{IV} complex **9** was found to react with a diverse set of nucleophiles $[\text{NMe}_4\text{X}; \text{X} = \text{OAc}, \text{OPh}, \text{SPh}, \text{and } \text{N}(\text{Me})(\text{Ms}), \text{where } \text{Ms} = \text{MeSO}_2^-]$ to yield the products of $\text{C}(\text{sp}^3)\text{-oxygen}$, $\text{C}(\text{sp}^3)\text{-sulfur}$, and $\text{C}(\text{sp}^3)\text{-nitrogen}$ coupling (Scheme 3.8; products **10a-d**). The $\text{C}(\text{sp}^3)\text{-heteroatom}$ coupling reactions to form **10a-d** were extremely selective and high-yielding (>98% conversion as determined by ^{19}F NMR spectroscopy; 78-94% isolated yields). Products derived from competing $\text{C}(\text{sp}^2)\text{-C}(\text{sp}^3)$ coupling or $\text{C}(\text{sp}^2)\text{-heteroatom}$ coupling were not detected in the ^1H NMR spectra of the crude reaction mixtures. Notably, $\text{C}(\text{sp}^3)\text{-heteroatom}$ coupling reactions of this type are rare in organometallic chemistry,²⁰ and most previously reported examples involve second or third row metal centers. In addition, the observation of selective $\text{C}(\text{sp}^3)\text{-heteroatom}$ coupling is complementary to the reactivity of other oxidation

states of Ni, where C(sp²)-heteroatom bond formation has significant precedent.^{4j,l,m,21} Other nucleophiles including halides (i.e., Cl⁻, Br⁻, I⁻), trifluoroacetate, and more electron-deficient sulfonamides were also examined; however, these anions were unreactive after heating at 90 °C for several days. We rationalize these results based on the comparatively weaker nucleophilicities of these coupling partners.²²

Scheme 3.8. Selective C(sp³)-O, C(sp³)-S, and C(sp³)-N Bond Formation from **9**



Whereas Ni^{II} products **10a-d** were stable towards isolation, the treatment of Ni^{IV} complex **9** with 1 equiv of NBU₄N₃ led to intermediate **10e**, which was observed *in situ* but was unstable in solution (Scheme 3.9). Azide intermediate **10e** slowly converted to 3,3'-dimethylindoline (quantitative conversion) over 15 h at room temperature. This transformation likely proceeds via the pathway shown in Scheme 3.9. Here, the pendant alkyl azide that results from C-N coupling inserts into the C(sp²)-Ni bond to generate Ni^{II} intermediate **11**. Related intermolecular azide insertions into Ni^{II}-C bonds have been reported by Hillhouse.^{4f,g} Protonation of the Ni-N bond by adventitious water then releases the indoline product.

Scheme 3.9. Distinct Reactivity of Ni^{IV} Complex **9** with Azide as the Nucleophile

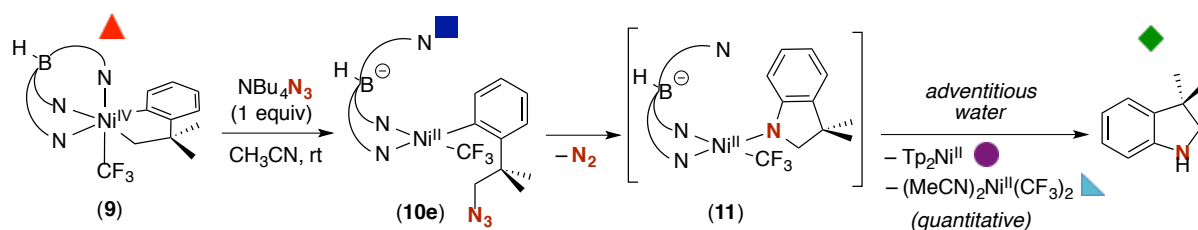


Figure 3.7. ¹H NMR Spectra Showing the Reaction Progress for the Formation of 3,3-dimethylindoline from Complex **9** and Azide Intermediate **10e** after (a) 2 h, 23 °C and (b) 15 h, 23 °C

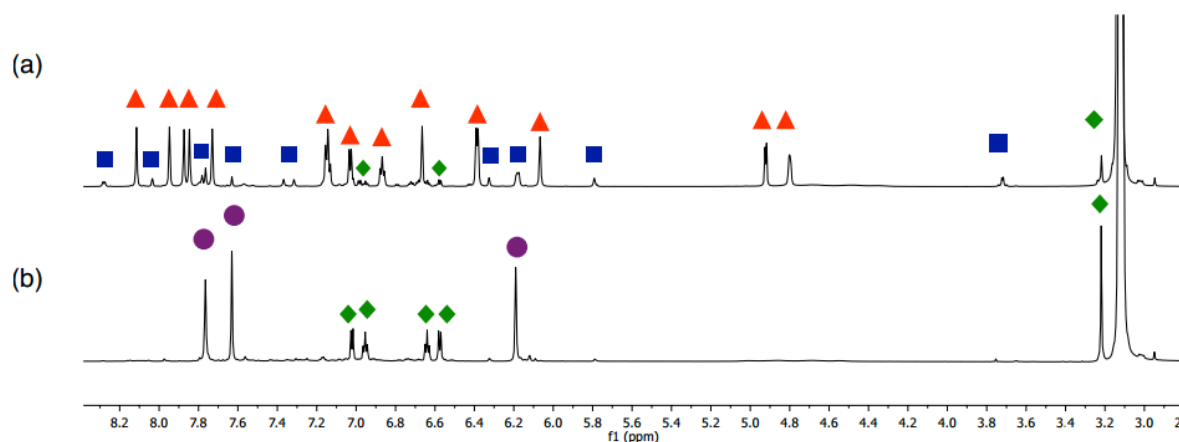
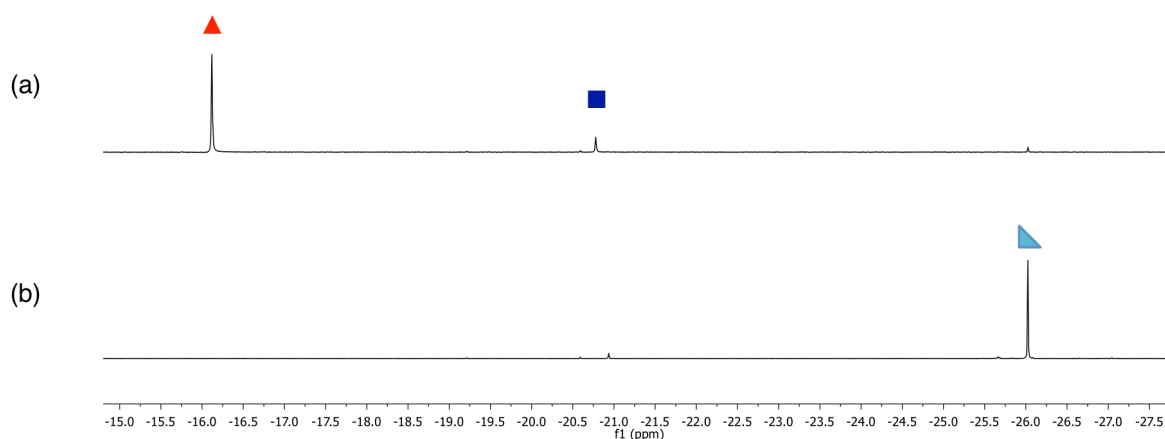


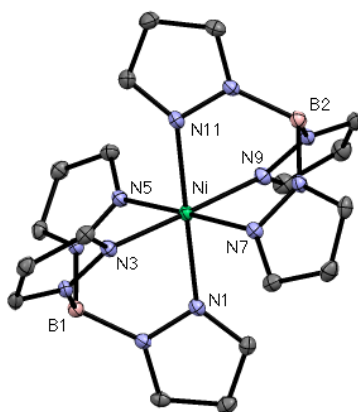
Figure 3.8. ¹⁹F NMR Spectra Showing the Reaction Progress for the Formation of Ni^{II}(MeCN)₂(CF₃)₂ from Complex **9** and Azide Intermediate **10e** after (a) 2 h, 23 °C and (b) 15 h, 23 °C



The Ni^{II} byproducts of the reaction shown in Scheme 3.9 are Tp_2Ni and $(\text{CD}_3\text{CN})_2\text{Ni}(\text{CF}_3)_2$ (Figures 3.7 and 3.8). These are presumably generated via ligand disproportionation from the initial reductive elimination product, $\text{TpNi}^{\text{II}}\text{CF}_3$. X-ray quality

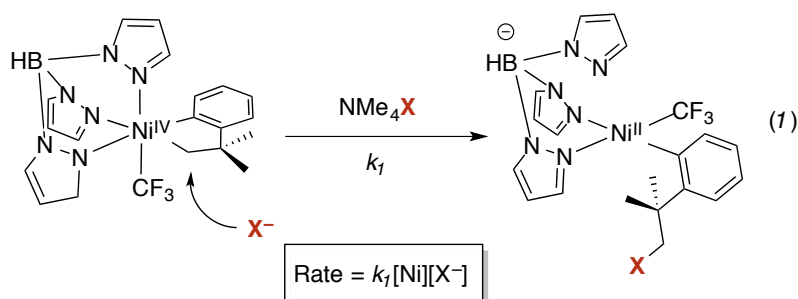
crystals of Tp_2Ni were obtained from the crude acetonitrile reaction mixture and an ORTEP diagram is shown in Figure 3.9.

Figure 3.9. ORTEP diagram of Tp_2Ni . Thermal ellipsoids are drawn at 50% probability. Hydrogen atoms are omitted for clarity.



Mechanistic Insights

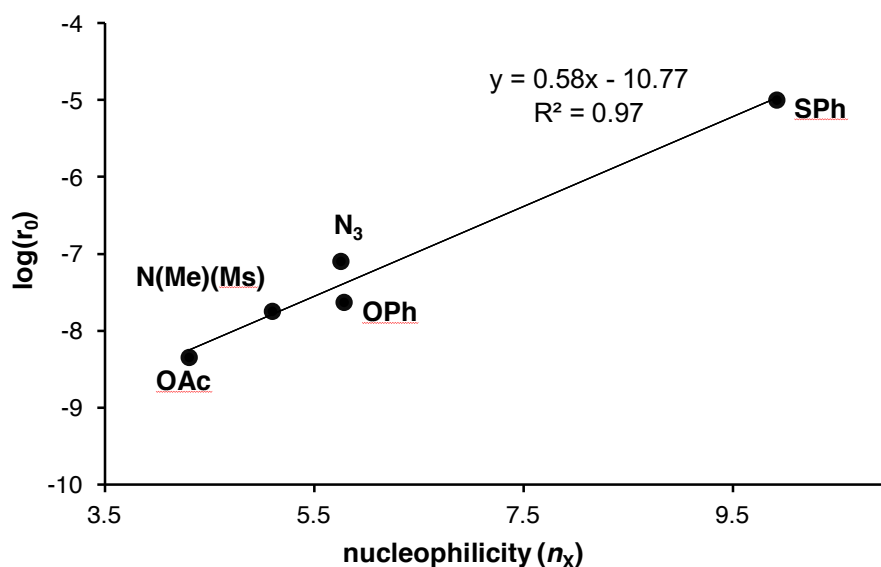
Finally, we sought to gain insights into the mechanism of these $\text{C}(\text{sp}^3)$ –heteroatom coupling reactions. Related transformations at octahedral Pd^{IV} and Pt^{IV} centers are believed to proceed via $\text{S}_{\text{N}}2$ -type attack on the metal–C bond by the nucleophile^{20a,b,c,f,g,h}. In the current system, an $\text{S}_{\text{N}}2$ mechanism would be expected to show a first-order kinetic dependence on both $[\text{Ni}]$ and NMe_4X . Indeed, rate studies of the reaction between **9** and NMe_4OAc showed that this transformation is first-order in $[\text{Ni}]$ and first-order in NMe_4OAc , consistent with an $\text{S}_{\text{N}}2$ pathway (eq. 1).



Another common feature of $\text{S}_{\text{N}}2$ reactions is that the reaction rates show a correlation with the Swain-Scott nucleophilicity parameters.^{22a} These nucleophilicity parameters (n_{X} ,

where X = a series of different nucleophiles) are derived from a prototypical S_N2 reaction (that of a given nucleophile with CH₃I).^{22b} The initial rate (r₀) of C–heteroatom coupling at **9** with AcO[−], PhO[−], PhS[−], [−]N(Me)(Ms), and N₃[−] was determined at 23 °C in CD₃CN. A plot of log(r₀) versus n_X is shown in Figure 3.10. The excellent linear correlation (R² = 0.97) provides further support for an S_N2 type C–X coupling pathway in this system.

Figure 3.10. Correlation Between Experimental Initial Rates (r₀) of Reductive Elimination from Complex **9** and Swain-Scott Nucleophilicity Values (n_X)

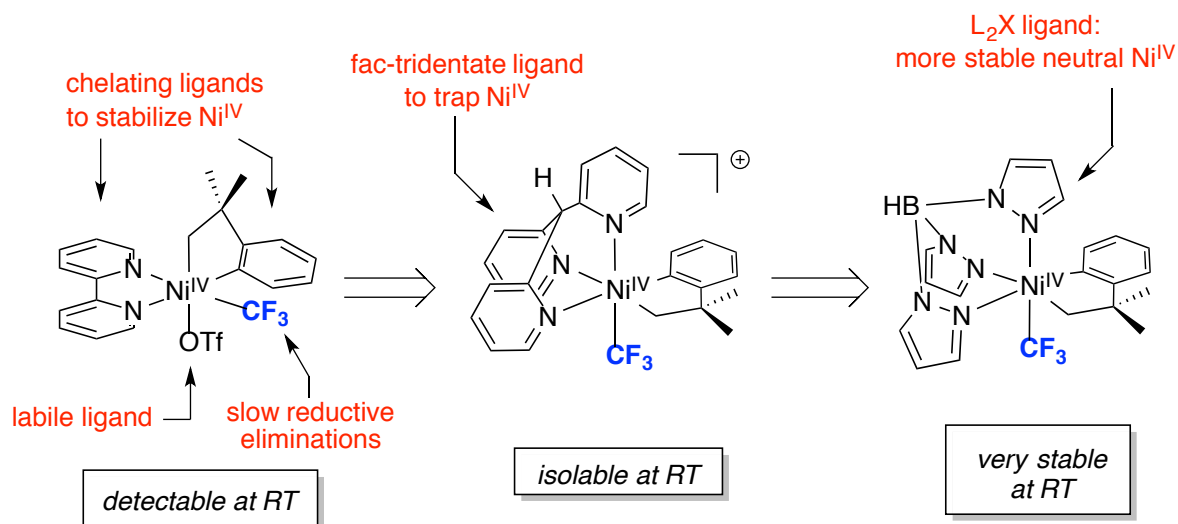


Outlook

The studies described herein demonstrate the feasibility of generating Ni complexes in the +4 oxidation state that can undergo important and challenging bond-forming reactions. Moreover, the systematic development of a series of Ni^{IV} complexes has revealed important design principles that lay the foundation for our continued studies of high-valent Ni chemistry. In particular, the use of Umemoto's reagent as an inner sphere CF₃⁺ transfer reagent to forge a Ni^{IV}–CF₃ bond demonstrates that CF₃ ligands can stabilize a Ni^{IV} center and limit/slow down reductive elimination processes. Replacement of the bidentate bipyridine ligand for facially-coordinated tridentate ligand scaffolds also proved critical for stabilizing this rare oxidation state. The anionic nitrogen-donor ligand, tris(pyrazolyl) borate, was found to be the most

effective, providing coordinative saturation and electron density to the Ni center. These design features allowed us to directly study this unusual oxidation state and have been implemented in our ongoing studies of high-valent Ni model systems.

Figure 3.11. Design Features of Model Ni^{IV} System



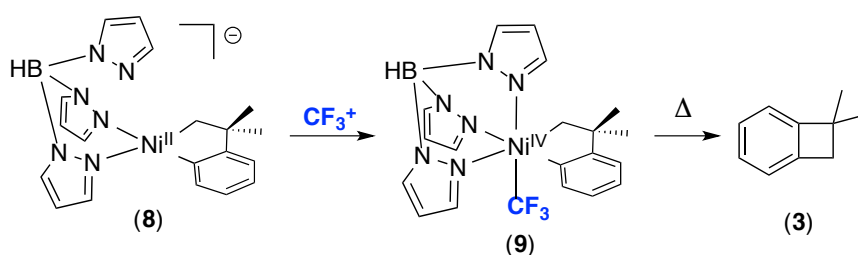
3.2.2. Aryl–CF₃ Bond-Forming Reductive Elimination from Ni^{IV}¹

Section 3.2.1 described the formation of a stable TpNi^{IV} complex accessed by the 2e⁻ oxidation of a cyclometalated Ni^{II} precursor with the “CF₃⁺” oxidant *S*-(trifluoromethyl) dibenzothiophenium triflate (Figure 3.11). This complex was found to undergo highly selective C(sp²)-C(sp³) and C(sp³)-heteroatom coupling upon heating; however, no products derived from C–CF₃ bond formation were observed under any of the reaction conditions. The preferential coupling of the C(sp²)-C(sp³) ligands suggested that other CF₃-ligated Ni^{IV} complexes could be stable for isolation due to the sluggish reactivity of CF₃ towards reductive elimination reactions.

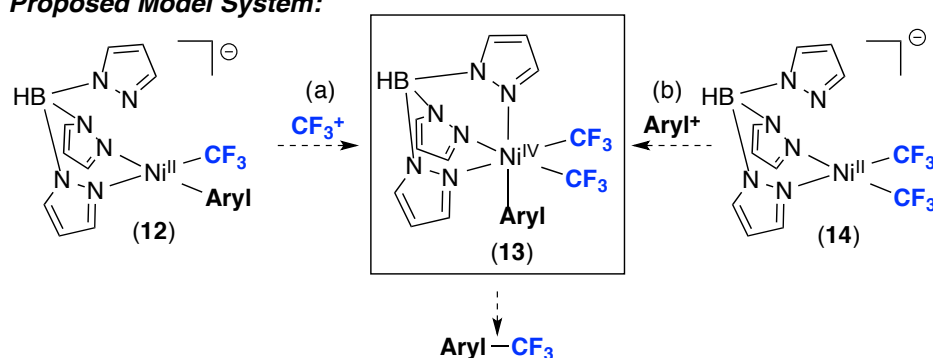
¹ Work in this section was collaborative with James Bour. His contributions involved the synthesis of complexes related to the aryl-based oxidation pathway as well as complete characterization of complex **13** (X-ray, elemental analysis, NMR spectroscopy). My work focused on the synthesis and scope of complexes related to the trifluoromethyl-based oxidation pathway as well as mechanistic studies of the system.

Scheme 3.10. Targeted Model System for Studying Ar–CF₃ Coupling from Ni^{IV}

Previous System:



Proposed Model System:



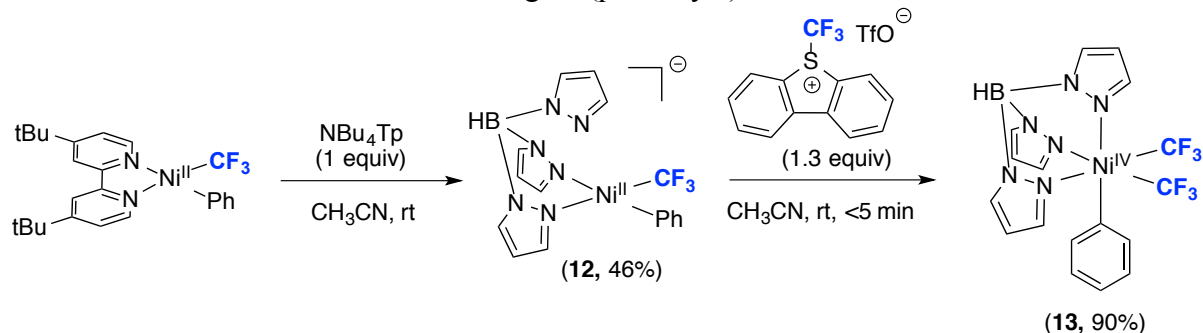
We envisioned that an appropriately designed nickel complex bearing trifluoromethyl ligands could allow the reactivity of Ni^{IV} towards catalytically relevant aryl–CF₃ bond formation to be directly investigated. We hypothesized that a Ni^{IV} model system of general structure **13** could be accessed by two complementary pathways: (a) via the oxidation of **12** with CF_3^+ reagents (by analogy to our previous system) or (b) via the reaction of **14** with aryl electrophiles (Aryl^+) (Scheme 3.10). This strategy would allow the accessibility of Ni^{IV} with both types of oxidants to be assessed. Furthermore, the viability of aryl–CF₃ coupling from high-valent nickel could be directly investigated.

Synthesis and Reactivity of Targeted Ni^{IV}(Aryl)(CF₃) Complex

We first sought to access **13** by the $2e^-$ oxidation of $\text{NBu}_4[\text{TpNi}^{\text{II}}(\text{Ph})(\text{CF}_3)]$ (**12**) with *S*-(trifluoromethyl)-dibenzothiophenium triflate (Umemoto's Reagent). The Ni^{II} starting material $[\text{TpNi}^{\text{II}}(\text{Ph})(\text{CF}_3)]\text{NBu}_4$ (**12**) was prepared via treatment of a 0.085 M solution of $(\text{dtbpy})\text{Ni}^{\text{II}}(\text{Ph})(\text{CF}_3)$ (dtbpy = 4,4'-di-*tert*-butylbipyridine) in acetonitrile with 1 equiv of NBu_4Tp . The reaction changed color from dark orange to yellow-brown along with

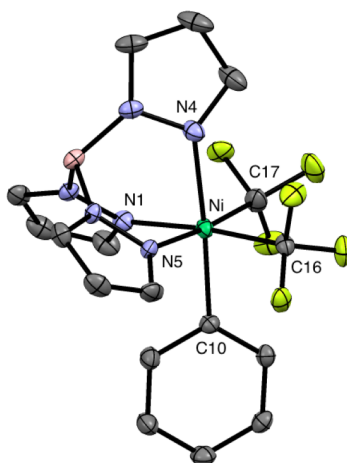
concomitant precipitation of dtbpy. Product **12** was isolated in 46% yield after recrystallization from an ether/pentane solution (Scheme 3.11)

Scheme 3.11. Synthesis of $[\text{TpNi}^{\text{IV}}(\text{Ph})(\text{CF}_3)_2]$ (**13**) via the Oxidation of **12** with Umemoto's Reagent (pathway a)



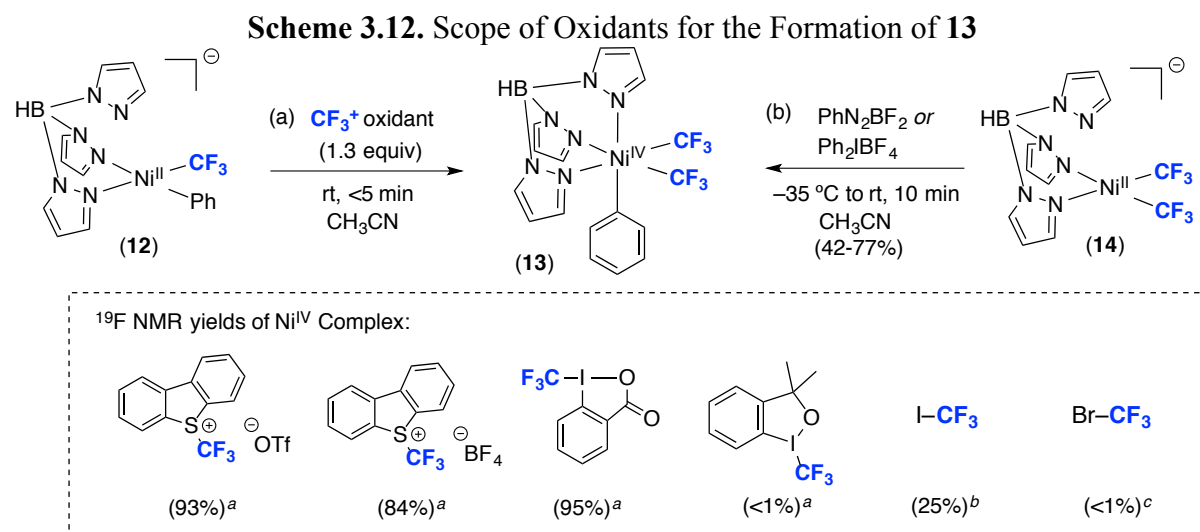
The treatment of **12** with 1.3 equiv of Umemoto's reagent afforded the diamagnetic Ni^{IV} product $\text{TpNi}^{\text{IV}}(\text{Ph})(\text{CF}_3)_2$ (**13**) in 93% NMR yield and 90% isolated yield following purification from flash chromatography. Complex **13** was characterized by ^1H , ^{13}C , ^{11}B , and ^{19}F NMR spectroscopy, elemental analysis, and X-ray crystallography (Figure 3.12).

Figure 3.12. ORTEP Diagram of Complex **13**. Thermal ellipsoids are drawn at 50% probability. Hydrogen atoms and disorder in the trifluoromethyl ligands have been omitted for clarity



The rapid formation of **13** prompted the investigation of additional trifluoromethyl-based oxidants. The oxidation of **12** with 1-trifluoromethyl-1,2-benziodoxolone (Togni Reagent II) afforded **13** in 95% yield as determined by ^{19}F NMR spectroscopy. Given the strongly oxidizing character of Umemoto- and Togni-type reagents, the accessibility of Ni^{IV}

with milder trifluoromethyl sources was also examined. While the use of trifluoromethyl bromide as an oxidant did not lead to product formation, the treatment of **12** with excess trifluoromethyl iodide afforded **13** in a modest 25% ^{19}F NMR yield.²³ A mixture of paramagnetic and diamagnetic resonances were observed in the ^1H and ^{19}F NMR spectra, suggesting alternate or competing radical mechanisms may be occurring with this oxidant.



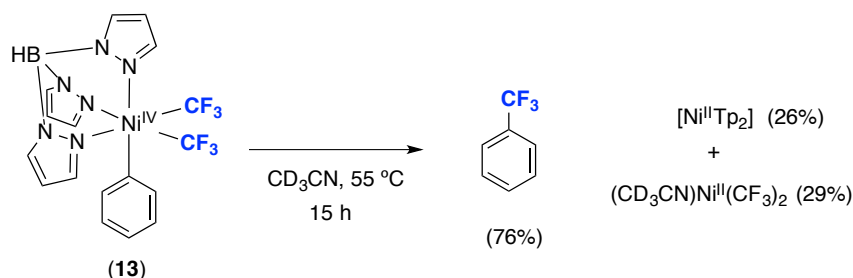
^a1.3 equiv oxidant, r.t., 5 min, ^b10 equiv oxidant (2.5 M solution in MeCN), r.t., 6 h, ^c10 equiv oxidant (0.25 M solution in CH_3CN), rt, 24 h

Seminal studies by Vicic^{15b} and Mirica^{15c} have shown that $\text{Ni}^{\text{II}}(\text{CF}_3)_2$ complexes react with outer-sphere $1e^-$ oxidants to yield Ni^{III} products. However, the analogous $2e^-$ oxidation of such complexes had not been disclosed at the time of our work. The treatment of Tp-ligated $\text{Ni}^{\text{II}}(\text{CF}_3)_2$ (**14**) with electrophilic arylating reagents (diphenyliodonium tetrafluoroborate (Ph_2IBF_4) and phenyl diazonium tetrafluoroborate (PhN_2BF_4) afforded Ni^{IV} complex **13** in 77% and 42% yield, respectively. (Scheme 3.12, pathway b). These results demonstrate that $\text{Ni}^{\text{II/IV}}$ manifolds are accessible under mild reaction conditions with aryl diazonium and diaryliodonium reagents.

We next investigated the reactivity of the Ni^{IV} product **13**. Upon heating at $55\text{ }^\circ\text{C}$ for 15 h in CD_3CN , **13** underwent clean $\text{C}(\text{sp}^2)-\text{CF}_3$ bond-forming reductive elimination to afford benzotrifluoride in 76% yield as determined by ^{19}F NMR spectroscopy (Scheme 3.13). The Ni^{II} byproducts of the reaction²⁴ were characterized as $\text{Ni}^{\text{II}}\text{Tp}_2$ (26% yield, maximum yield

50%) and $(\text{CD}_3\text{CN})_2\text{Ni}^{\text{II}}(\text{CF}_3)_2$ (29% yield, maximum yield 50%),^{1a,25} which are presumably generated via ligand disproportionation from the initial reductive elimination product, $\text{TpNi}^{\text{II}}\text{CF}_3$. This reaction represents the first reported example of high yielding aryl- CF_3 reductive elimination from a discrete Ni complex.²⁶

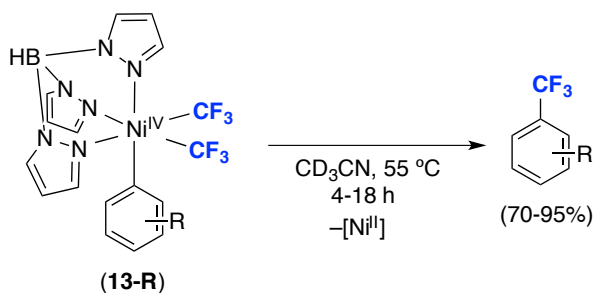
Scheme 3.13. Reductive Elimination from Complex **13** to Form Benzotrifluoride



Mechanistic Investigations

A series of Ni^{IV} complexes bearing substituted aryl ligands were prepared to investigate electronic effects on this aryl- CF_3 coupling reaction. The complexes **13-OMe**, **13-Me**, **13-Br**, and **13-CO₂Me** were synthesized via the treatment of $\text{NBu}_4[(\text{Tp})\text{Ni}^{\text{II}}(\text{CF}_3)_2]$ (**14**) with the respective Ar_2IBF_4 reagents. Heating the substituted Ni^{IV} complexes at $55\text{ }^\circ\text{C}$ in CD_3CN for 4-18 h afforded the corresponding benzotrifluorides in 70-95% yield as determined by ^{19}F NMR spectroscopy (Table 3.1). Reductive elimination from each complex was monitored by ^{19}F NMR spectroscopy at $55\text{ }^\circ\text{C}$, and a representative reaction profile for complex **13** ($\text{R} = \text{H}$) is shown in Figure 3.13. In all cases, first-order kinetic behavior was observed.

Table 3.1. Reductive Elimination from Ni^{IV} Complexes **13-R** at $55\text{ }^\circ\text{C}$. Yields of $\text{Ar}-\text{CF}_3$ are determined by ^{19}F NMR integration against the fluorine standard 4,4'-difluorobiphenyl



Complex	Time (h)	Ar-CF ₃ ¹⁹ F NMR Yield (%)
13-H	15	76
13-OMe	4	95
13-Me	15	71
13-Br	16	81
13-CO ₂ Me	18	70

Figure 3.13. Plot of concentration vs. time data for reductive elimination from **13-H** to form benzotrifluoride (Ar-CF₃) at 55 °C. $y_{13-H} = 0.023e^{-0.00026x}$ $R^2 = 0.99$; $y_{Ar-CF_3} = 0.017(1 - e^{-0.00020x})$, $R^2 = 0.99$

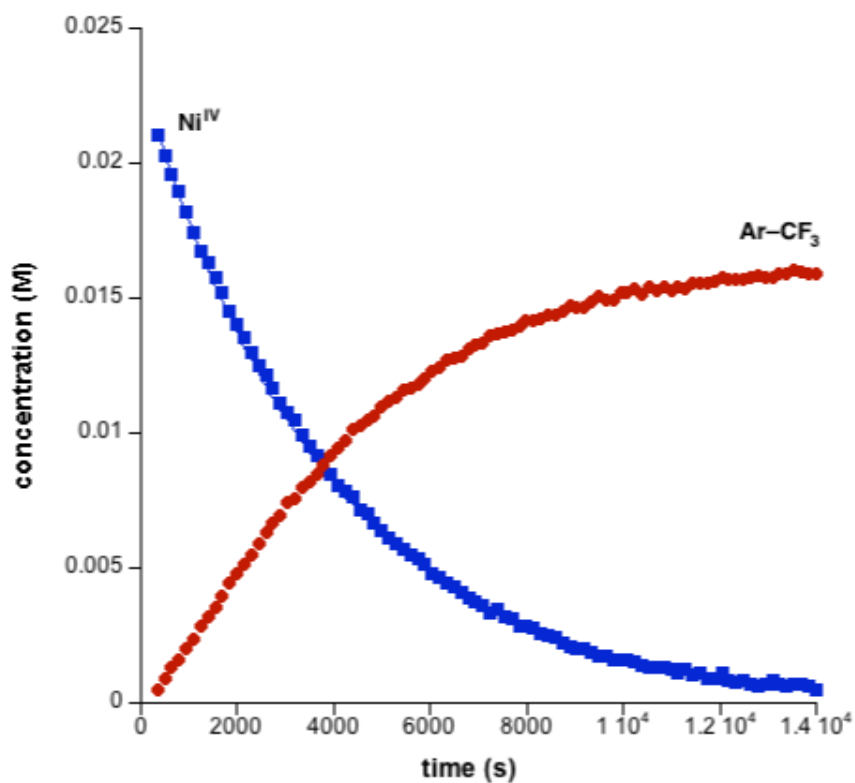
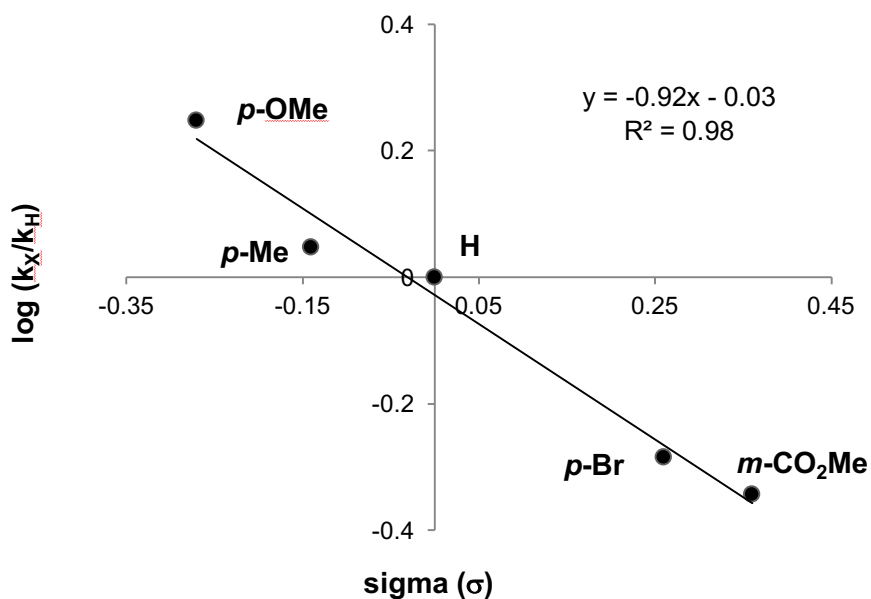
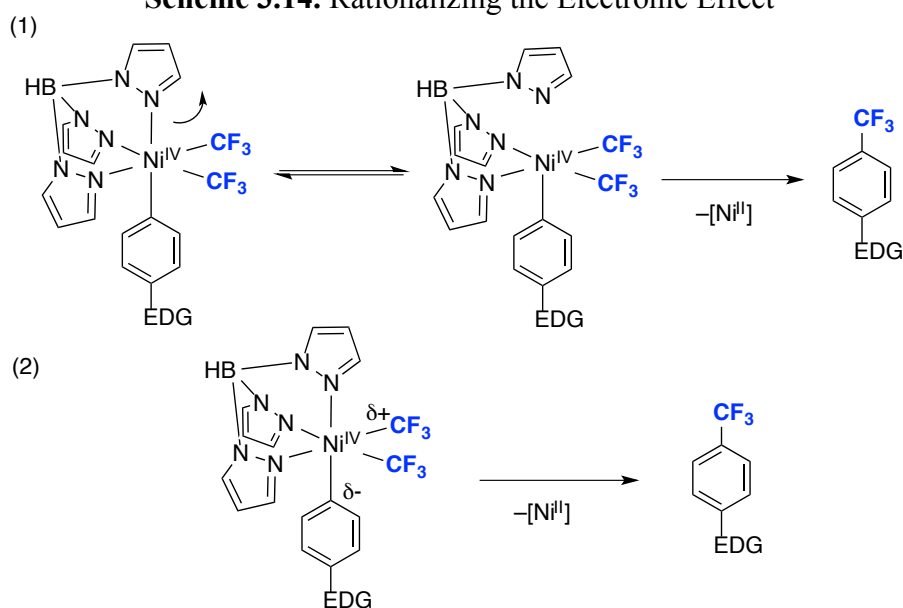


Figure 3.14. Hammett Plot for Reductive Elimination from **13-R**



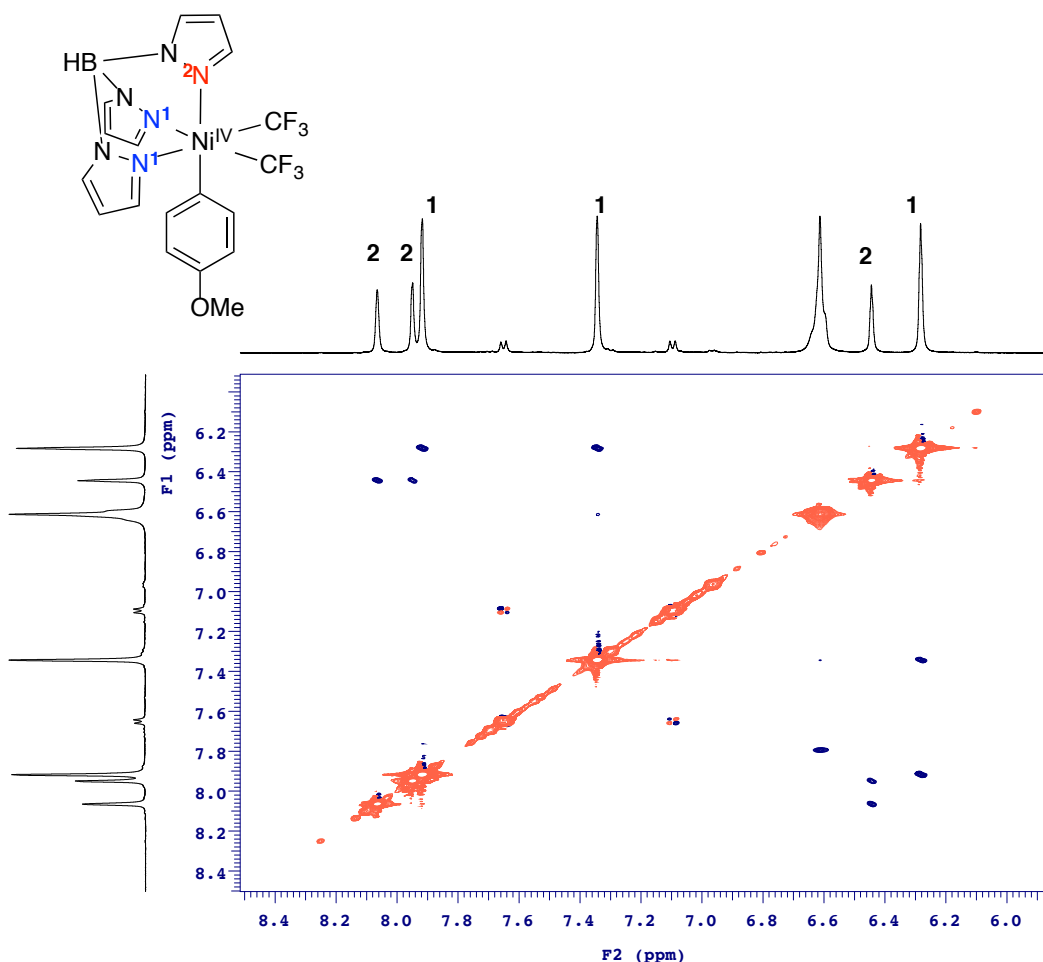
The rate constants (k_{obs}) for each reaction were obtained by fitting the decay of **13-R** to single exponentials, and a Hammett plot of the resulting data is shown in Figure 3.14. The plot shows a ρ value of -0.91 , indicating that reductive elimination is accelerated by electron-donor substituents on the aromatic ring. This effect mirrors the trend reported for aryl-CF₃ bond-forming reductive elimination from related Pd^{IV}(aryl)(CF₃) complexes.²⁷ The observed electronic effect can be rationalized in two ways: (1) the larger *trans* effect of electron-rich σ -aryl groups facilitates ligand dissociation to generate a reactive five-coordinate Ni^{IV} intermediate from which reductive elimination occurs and/or (2) the electron donor substituents accelerate a nucleophilic attack by the σ -aryl ligand onto the electrophilic CF₃ group in the transition state (Scheme 3.14).^{28,29}

Scheme 3.14. Rationalizing the Electronic Effect



Various mechanistic studies were carried out to probe the lability of the pyrazole ligands in **13**. The *p*-methoxy ligated Ni^{IV} complex **13-OMe** was used as the substrate for these studies as it is expected to exhibit the greatest *trans* effect. EXSY experiments were first performed to determine whether exchange of the axial and equatorial pyrazole ligands could be observed.³⁰ As shown in Figure 3.15, the ¹H/¹H ROESY spectrum showed no chemical exchange cross peaks between pyrazole rings 1 or 2 from -10 °C to 40 °C on the NMR time scale. We also conducted line broadening studies of **13-OMe** between -25 °C and 25 °C. However, no differences in peak width between the equatorial and axial ligands were observed at these temperatures.

Figure 3.15. $^1\text{H}/^1\text{H}$ ROESY Spectrum of **13-OMe** at 40 °C Showing No Chemical Exchange Between the Pyrazole Rings on the NMR Time Scale



We next examined ligand substitution reactions with nucleophilic anions to gain further insights into possible exchange processes at the Ni^{IV} center. The treatment of **13** with NMe_4SPh led to consumption of the $\text{Ni}^{\text{IV}}\text{-CF}_3$ starting material (-19.3 ppm) and formation of a new ^{19}F NMR resonance at -22.3 ppm (Scheme 3.15).³¹ This ^{19}F NMR shift is within the range of $\text{Ni}^{\text{IV}}\text{-CF}_3$ peaks reported in the literature.^{1,6h} We therefore tentatively assign this as the thiophenolate adduct **15**. Complex **15** was stable in solution for several hours. Upon heating at 50 °C for 12 h, the consumption of **15** was accompanied by the growth of two quartets in the ^{19}F NMR spectrum that we attribute to stereoisomer **15'**. The two ^{19}F quartets couple one another ($J_{\text{FF}} = 4.2$ Hz) which is indicative of two inequivalent CF_3 groups on the Ni center (Figure 3.16). The proposed structure **15'** bears two distinct CF_3 ligands, and is therefore consistent with the ^{19}F

NMR data. Additional heating of the crude reaction mixture (3 h at 50 °C) led to C(sp²)-SPh coupling to form the diphenyl sulfide, which was determined to be the major product by GC/MS analysis. These results provide preliminary evidence for pyrazole lability in our model system.

Scheme 3.15. The Reactivity of **13** with NMe₄SPh, Demonstrating Pyrazole Lability at Ni^{IV}

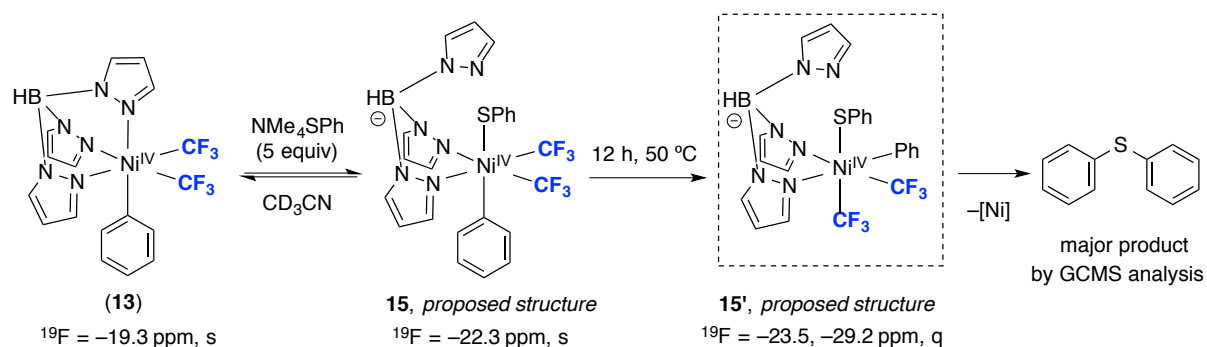
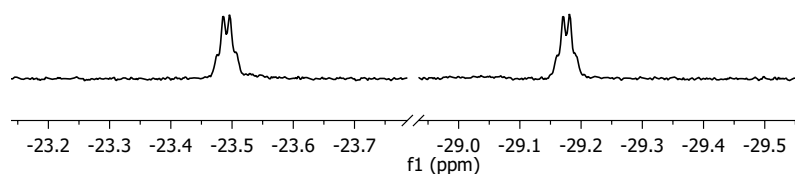


Figure 3.16. ¹⁹F NMR Resonances of Proposed Complex **15'**



Low Temperature Studies with Bipyridine-Ligated Derivatives

While facially coordinated tridentate ligands provide stabilization for the isolation of discrete high-valent complexes, bidentate-nitrogen donor ligands such as bipyridines are commonly used in Ni-catalyzed C–C and C–heteroatom coupling reactions, making them much more catalytically relevant.³² Moreover, if aryl–CF₃ reductive elimination is preceded by ligand dissociation to generate a five coordinate intermediate, replacement of the tridentate Tp scaffold with the bidentate 4,4'-di-*tert*-butylbipyridine (dtbpy) would enable even milder conditions for aryl-trifluoromethyl coupling.

The treatment of dtbpy-supported Ni^{II} complexes **16** and **17** with 1.5 equiv of Umemoto's Reagent or PhN₂BF₄, respectively, afforded benzotrifluoride in 57% and 67%

yield as determined by ^{19}F NMR spectroscopy (Scheme 3.16). Notably, these transformations proceeded to completion within 10 min at room temperature. As such, they are among the fastest reported examples of aryl– CF_3 coupling at a group 10 metal center.^{10,33} Monitoring these reactions by ^{19}F NMR spectroscopy at $-25\text{ }^\circ\text{C}$ showed the presence of the same transient diamagnetic intermediate in both cases.³⁴ The ^{19}F NMR resonances associated with this intermediate (a pair of quartets at -19.8 and -23.8 ppm, $J_{\text{FF}} = 7.9$ Hz; Figure 3.17) are consistent with an unsymmetrical Ni^{IV} bis-trifluoromethyl complex of general structure **18**. The decay of intermediate **18** was accompanied by growth of the resonance associated with benzotrifluoride. Overall, these results strongly suggest that organometallic Ni^{IV} complexes are accessible under mild conditions using catalytically relevant bidentate-nitrogen donor ligands.

Scheme 3.16. Oxidation and Subsequent Aryl- CF_3 Coupling from $(\text{dtbpy})\text{Ni}^{\text{II}}$ Complexes **16** and **17**

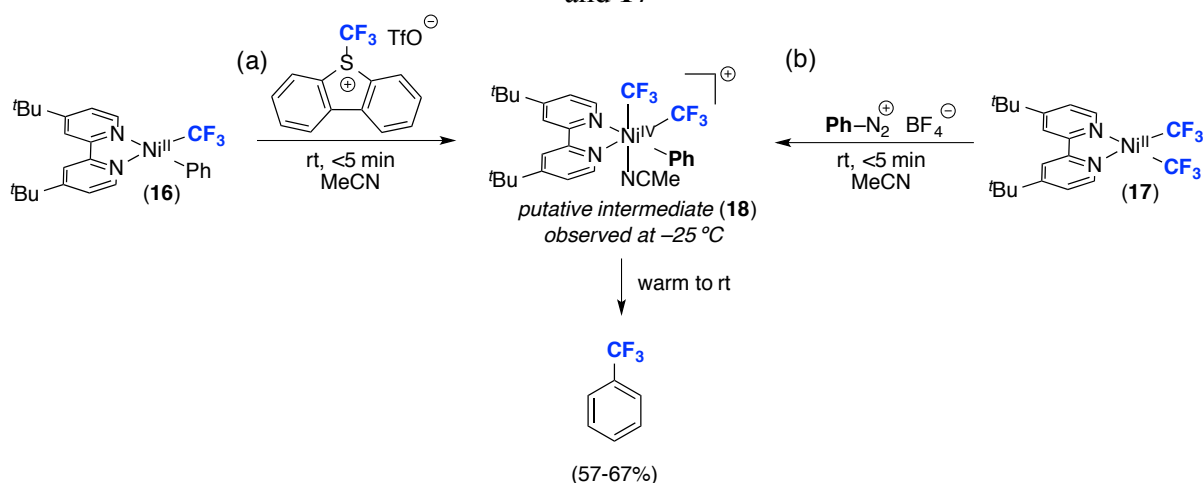
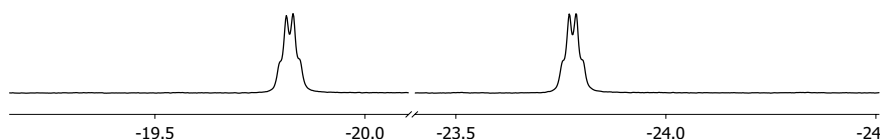


Figure 3.17. ^{19}F NMR Spectrum at $-25\text{ }^\circ\text{C}$ Showing the Two Signals Assigned to the CF_3 Resonances of Ni^{IV} Intermediate **18**



3.3. Conclusions

The combined fundamental studies described in this chapter demonstrate the mild accessibility of organometallic Ni^{IV} complexes as well as their reactivity in challenging bond-forming reactions. The replacement of bidentate ligands with facially coordinating tridentate scaffolds proved critical for the isolation and characterization of these traditionally reactive species. Moreover, the implementation of chelating carbon ligands and trifluoromethyl groups served to both stabilize the Ni center and facilitate catalytically-relevant reactivity.

In section 3.2.1 we demonstrated that a CF₃⁺ oxidant (Umemoto's reagent) can be used to access a series of isolable Ni^{IV}-CF₃ complexes. In these studies, the CF₃ group served as a stabilizing bystander ligand, as these Ni^{IV} complexes underwent selective C(sp³)-C(sp²) coupling as well as C(sp³)-heteroatom bond-forming reactions in the presence of exogenous nucleophiles. Finally, the incorporation of CF₃ and Ar ligands in section 3.2.2 provided a platform for assessing the accessibility of Ni^{IV} with aryl-based oxidants. These complexes underwent high-yielding C(sp²)-CF₃ reductive elimination under mild conditions, demonstrating the first examples of trifluoromethylation from a Ni^{IV} center.

We anticipate that the ability of Ni^{IV} complexes to engage in selective carbon-carbon and carbon-heteroatom coupling reactions can ultimately be exploited in catalysis. A key challenge for achieving this objective will be to delineate the classes of oxidants and supporting ligands that enable selective access to Ni^{IV} (rather than more common Ni^{III}) intermediates. This should allow for the design of catalytic sequences in which a Ni-carbon bond-forming step (e.g., transmetalation, C-H activation) is coupled with oxidation and reductive elimination via Ni^{II/IV} catalysis.

3.4. Experimental Procedures and Characterization of Compounds

3.4.1. General Procedures and Materials and Methods

General Procedures

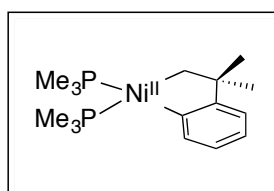
All experiments and manipulations were carried out under an inert nitrogen atmosphere using standard glovebox or Schlenk techniques unless otherwise indicated. NMR spectra were obtained on a Varian VNMR 700 (699.76 MHz for ^1H ; 175.95 MHz for ^{13}C), a Varian VNMR 500 (500.09 MHz for ^1H ; 470.56 MHz for ^{19}F) or a Varian VNMR 400 spectrometer (399.54 MHz for ^1H ; 128.187 for ^{11}B). ^1H and ^{13}C chemical shifts are reported in parts per million (ppm) relative to TMS, with the residual solvent peak as an internal reference. ^{19}F chemical shifts and ^{11}B chemical shifts are reported in ppm and are referenced on a unified scale, where the single primary reference is the frequency of the residual solvent peak in the ^1H NMR spectrum. Abbreviations used in the NMR data: s, singlet; d, doublet; dd, doublet of doublets; t, triplet; td, triplet of duplets; m, multiplet; br, broad signal. Elemental analyses were conducted by Midwest Microlabs. Cyclic voltammetry was performed using a CHI600C potentiostat from CH instruments. The electrodes were obtained from BASi. Mass spectral data were obtained on a Micromass magnetic sector mass spectrometer in electrospray ionization mode. X-ray crystallographic data were collected on a Bruker SMART APEX-I CCD-based X-ray diffractometer. Flash chromatography was conducted using a Biotage Isolera One system with cartridges containing high performance silica gel.

Materials and Methods

The following compounds were prepared via literature procedures: [(bpy)Ni^{II}(CH₂CMe₂-*o*-C₆H₄)] (**1**),³⁵ (PPh₃)₂Ni(CF₃)(OTFA),³⁶ Ph₂IBF₄,³⁷ (4-MeOC₆H₄)₂IBF₄,³⁸ (4-Br-C₆H₄)(Mes)IBF₄,³⁹ (3-CO₂MeC₆H₄)(Mes)IBF₄,⁴ (dtbpy)₂Ni(CF₃)₂,^{15b} tris(2-pyridyl)methane,^{16f} NMe₄OPh,^{21g} and NMe₄N(Me)(Ms)^{21f}. 1,1-dimethylbenzocyclobutane (**4**)⁴⁰ and 3,3'-dimethylindoline⁴¹ were characterized by comparison of their ^1H NMR spectra with those reported in the literature. 2-methyl-2-phenylpropyl magnesium chloride (0.5 M solution in diethyl ether), (PMe₃)₂NiCl₂, *S*-(trifluoromethyl) dibenzothiophenium triflate, 4,4'-di-*tert*-butylbipyridine, NMe₄OAc, and NBu₄N₃ were obtained from Aldrich. The tetramethylammonium salts were dried over P₂O₅ at 70 °C under vacuum for 15 h and stored in the glovebox prior to use. Electrochemical studies of complexes **1** and **5** were performed

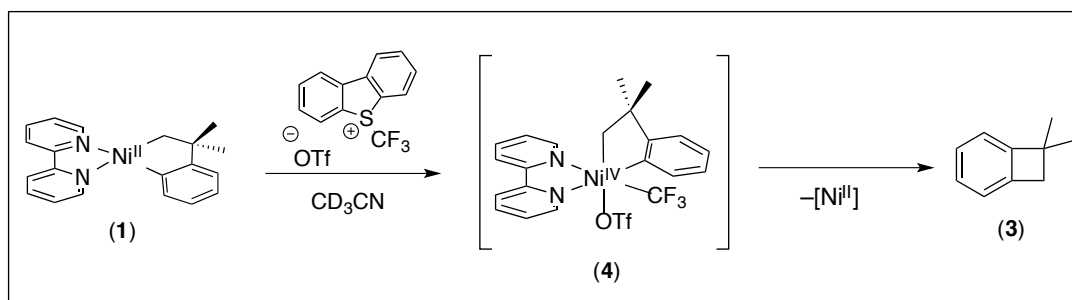
with electrochemical grade NBu_4BF_4 , which was purchased from Aldrich and used without further purification. *N*-fluoro-2,4,6-trimethylpyridinium triflate was obtained from TCI America. Iodobenzene diacetate was obtained from Oakwood. 3-(Trifluoromethyl)anisole was obtained from Matrix Scientific. Potassium tris(pyrazolyl)borate (KTp) was purchased from Strem. CD_3CN (Cambridge Isotopes) was dried over 4 Å molecular sieves prior to use. Diethyl ether (EMD), tetrahydrofuran (Fisher), and pentane (Fisher) were deaerated via an N_2 sparge and dried using a solvent purification system. Acetonitrile (Alfa Aesar, anhydrous >99.8%), acetone (Sigma-Aldrich), and benzene (EMD) were used without further purification. Celite was dried under vacuum for 12 h at 50 °C prior to use.

3.4.2. Synthesis and Characterization of Compounds



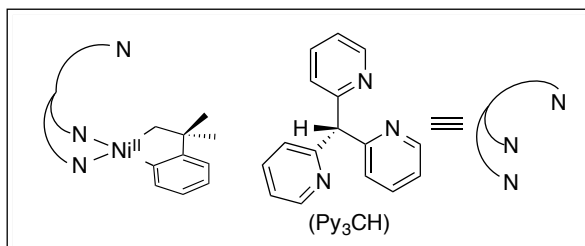
Synthesis of $[(\text{PMe}_3)_2\text{Ni}^{\text{II}}(\text{CH}_2\text{CMe}_2\text{-}o\text{-C}_6\text{H}_4)]$.

$[(\text{PMe}_3)_2\text{Ni}^{\text{II}}(\text{CH}_2\text{CMe}_2\text{-}o\text{-C}_6\text{H}_4)]$ was synthesized from the following modification of a literature procedure.³⁵ In the glovebox, $(\text{PMe}_3)_2\text{NiCl}_2$ (1.0 g, 3.54 mmol, 1.0 equiv) was weighed in a 150 mL round bottom Schlenk flask. The solid was dissolved in 60 mL of anhydrous diethyl ether. A sub-stoichiometric amount of MgI_2 pellets (approximately 50 mg) were dissolved in 5 mL of diethyl ether and added to the reaction flask. The Schlenk flask was capped with a septum and taken out of the glovebox. The flask was put under a constant flow of nitrogen and cooled to –78 °C (dry ice/acetone bath). At this temperature, 2-methyl-2-propyl phenyl magnesium chloride (16 mL of a 0.5 M solution in diethyl ether) was added dropwise. The resulting solution was allowed to gradually warm to room temperature overnight during which time the reaction turned from purple-red to green. Solvent was removed on the Schlenk line to afford a brown residue and the flask was brought back into the glovebox. Pentane was added (75 mL) and the solution was filtered through a Celite plug. Solvent was concentrated to approximately 10 mL at which point orange crystals began to form. The crystals were collected and dried under vacuum (720 mg, 60 % yield). The spectra for the title complex matched that reported in the literature.³⁵ It should be noted that this complex is highly air and moisture sensitive.



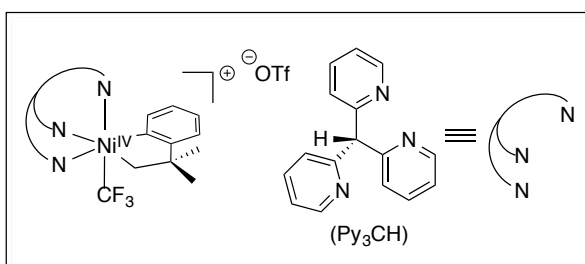
***in situ* Characterization of [(bpy)Ni^{II}(CH₂CMe₂-*o*-C₆H₄)(CF₃)(OTf)] (4).** A screw cap NMR tube was charged with [(bpy)Ni^{II}(CH₂CMe₂-*o*-C₆H₄)] (1) (8.0 mg, 0.023 mmol, 1.0 equiv) and CD₃CN (0.6 mL) was added. *S*-(Trifluoromethyl)dibenzothiophenium triflate (9.3 mg, 0.023 mmol, 1.0 equiv) was subsequently added at room temperature, and the dark blue solution immediately turned light yellow. The NMR tube was then removed from the glovebox and transferred to a liquid nitrogen/ethyl acetate bath (−84 °C). The sample was then placed in the NMR spectrometer where the probe had been pre-cooled to −25 °C. The sample was allowed to equilibrate in the spectrometer for 5 min before acquiring spectra. The starting material and oxidant were fully consumed to generate the Ni^{IV} complex as a mixture of two isomers. Major isomer 4 was formed in a 10:1 isomeric ratio as determined by integration of the methylene protons in the crude ¹H NMR spectrum. Only the signals of the major isomer are reported. Because of very low intensity, the carbon resonances of the CF₃ groups could not be observed directly in the ¹³C NMR spectrum. The values were extracted from a ¹⁹F–¹³C HMBC NMR experiment.

At the time of acquisition, approximately 10% of cyclobutane product 3 had already formed. Over the course of 15 h, the consumption of 4 to form 3 was monitored by ¹H NMR spectroscopy at room temperature. ¹H NMR (700 MHz, CD₃CN, −25 °C) δ 9.30 (d, *J*_{HH} = 5.4 Hz, 1H), 8.57 (d, *J*_{HH} = 8.1 Hz, 1H), 8.52 (d, *J*_{HH} = 8.1 Hz, 1H), 8.41–8.31 (multiple peaks, 2H), 8.24 (m, 1H), 7.95–7.85 (multiple peaks, 2H), 7.58 (d, *J*_{HH} = 8.1 Hz, 1H), 7.34 (t, *J*_{HH} = 7.4 Hz, 1H), 7.22 (t, *J*_{HH} = 7.7 Hz, 1H), 7.01 (dd, *J*_{HH} = 7.6, 1.8 Hz, 1H), 4.67 (d, *J*_{HH} = 5.6 Hz, 1H), 3.75 (d, *J*_{HH} = 5.6 Hz, 1H), 1.29 (s, 3H), 0.80 (s, 3H). ¹³C NMR (176 MHz, CD₃CN, −25 °C) δ 159.27, 153.94, 152.90, 149.05, 141.28, 140.97, 139.04, 135.28, 132.60, 128.08, 127.81, 127.33, 127.22, 126.63, 124.28, 124.16, 123.36 (Ni–CF₃, shift for CF₃ group extracted from ¹⁹F–¹³C HMBC NMR spectrum), 122.56 (−OSO₂CF₃, shift for CF₃ group extracted from ¹⁹F–¹³C HMBC NMR spectrum), 80.73, 47.20, 30.29, 29.63. ¹⁹F NMR (471 MHz, CD₃CN, −25 °C) δ −20.42 (s, Ni–CF₃), −79.52 (s, −OSO₂CF₃).



Synthesis of $[(\text{Py}_3\text{CH})\text{Ni}^{\text{II}}(\text{CH}_2\text{CMe}_2\text{-}o\text{-C}_6\text{H}_4)]$ (5**).** A 20 mL vial was charged with $[(\text{PMe}_3)_2\text{Ni}^{\text{II}}(\text{CH}_2\text{CMe}_2\text{-}o\text{-C}_6\text{H}_4)]$ (300 mg, 0.88 mmol, 1.0 equiv). The solid was dissolved in diethyl ether (10 mL). Tris(2-

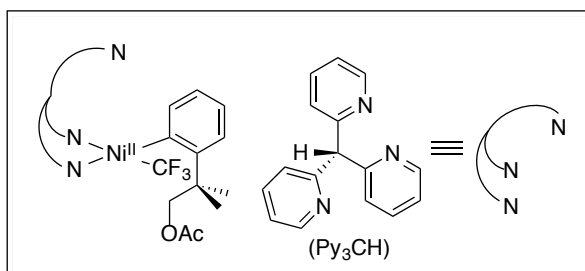
pyridyl)methane (238 mg, 0.96 mmol, 1.1 equiv) was added, and the light orange solution immediately turned red. The reaction mixture was allowed to stir for 30 min. The solution was then concentrated to approximately 3 mL, during which time the product precipitated from solution. The precipitate was collected by filtration. The resulting solid was dried under vacuum to afford complex **5** as a bright red solid (281 mg, 73% yield). Ni^{II} complex **5** exists as a mixture of equilibrating isomers due to the fluxional pyridyl arm. As a result, the ^1H and ^{13}C NMR spectra of complex **5** are extremely broad, even at $-25\text{ }^\circ\text{C}$. Because of extensive overlap between the isomers, not all of the individual resonances in the ^{13}C NMR spectrum could be extracted. ^1H NMR (700 MHz, CD_3CN , $-25\text{ }^\circ\text{C}$) δ 9.04 (br, 1H), 8.46 (br, 2H), 7.85 (br, 4H), 7.40 (br, 2H), 7.19 (br, 3H), 6.63 (td, $J_{\text{HH}} = 7.2, 1.3$ Hz, 1H), 6.49 (dd, $J_{\text{HH}} = 7.2, 1.3$ Hz, 1H), 6.46 (td, $J_{\text{HH}} = 7.2, 1.2$ Hz, 1H), 6.17 (dd, $J_{\text{HH}} = 7.2, 1.2$ Hz, 1H), 6.00 (s, 1H), 1.28 (s, 6H), 0.72 (s, 2H). ^{13}C NMR (176 MHz, CD_3CN , $-25\text{ }^\circ\text{C}$) δ 169.22, 164.63, 159.20, 150.95, 149.17, 137.33, 136.55, 124.93, 124.11, 122.44, 121.41, 119.74, 61.28, 47.39, 46.11, 33.32, 22.28, 13.56. HRMS-electrospray (m/z): $[\text{M}]^+$ calcd. for $\text{C}_{26}\text{H}_{25}\text{N}_3\text{Ni}$, 437.1396; found, 437.1404.



Synthesis of $[(\text{Py}_3\text{CH})\text{Ni}^{\text{IV}}(\text{CH}_2\text{CMe}_2\text{-}o\text{-C}_6\text{H}_4)(\text{CF}_3)(\text{OTf})]$ (6**).** A 20 mL vial was charged with $[(\text{Py}_3\text{CH})\text{Ni}^{\text{II}}(\text{CH}_2\text{CMe}_2\text{-}o\text{-C}_6\text{H}_4)]$ (**5**) (200 mg, 0.46 mmol, 1.0 equiv). The solid was dissolved in acetonitrile (5

mL). *S*-(Trifluoromethyl) dibenzothiophenium triflate (202 mg, 0.50 mmol, 1.1 equiv) was added at rt, and the red solution immediately turned yellow. The reaction mixture was then removed from the glovebox and concentrated in vacuo. Benzene (5 mL) was added to the residue, and yellow crystals precipitated from solution over the course of 10 min. The solids were filtered, collected, and dried under vacuum to afford complex **6** as a yellow solid (278 mg, 92% yield). ^1H NMR (700 MHz, CD_3CN , $23\text{ }^\circ\text{C}$) δ 9.21 (d, $J_{\text{HH}} = 5.6$ Hz, 1H), 9.14 (d, J_{HH}

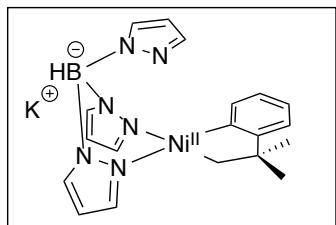
= 5.6 Hz, 1H), 8.20-8.09 (multiple peaks, 2H), 8.08-8.00 (multiple peaks, 2H), 7.95 (td, $J_{\text{HH}} = 7.6, 1.5$ Hz, 1H), 7.87 (m, 1H), 7.73 (d, $J_{\text{HH}} = 5.9$ Hz, 1H), 7.69 (dd, $J_{\text{HH}} = 7.5, 5.9$ Hz, 1H), 7.64 (m, 1H), 7.29 (m, 1H), 7.22 (t, $J_{\text{HH}} = 7.2$ Hz, 1H), 7.19 (d, $J_{\text{HH}} = 7.6$ Hz, 1H), 6.83 (d, $J_{\text{HH}} = 8.7$ Hz, 1H), 6.67 (d, $J_{\text{HH}} = 8.7$ Hz, 1H), 6.46 (s, 1H), 5.15 (dd, $J_{\text{HH}} = 5.7$ Hz, $J_{\text{HF}} = 2.5$ Hz, 1H), 4.92 (d, $J_{\text{HH}} = 5.7$ Hz, 1H), 1.68 (s, 3H), 1.56 (s, 3H). ^{13}C NMR (176 MHz, CD_3CN , 23 °C) δ 160.08, 159.51, 153.34, 153.25, 153.15, 152.62, 150.98, 150.89, 141.54, 141.35, 141.18, 132.35, 127.64, 127.09, 126.98, 126.64, 125.87, 125.75, 125.25, 125.12, 124.93, 122.56 ($^-$ OSO₂CF₃, shift for CF₃ group extracted from ^{19}F - ^{13}C HMBC NMR spectrum), 199.47 (Ni-CF₃, shift for CF₃ group extracted from ^{19}F - ^{13}C HMBC NMR spectrum), 81.62, 58.98, 47.43, 30.87, 30.26. ^{19}F NMR (471 MHz, CD_3CN , 23 °C) δ -13.12 (s, Ni-CF₃), -79.32 (s, $^-$ OSO₂CF₃). HRMS-electrospray (m/z): [M - OTf]⁺ calcd. for C₂₇H₂₅F₃N₃Ni, 506.1349; found, 506.1351. Elemental Analysis calcd. for C₂₇H₂₅F₃N₃Ni: C, 51.25; H, 3.84; N, 6.40. Found: C, 51.46; H, 3.95; N, 6.24.



Synthesis of [(Py₃CH)Ni^{II}(C₆H₄-o-CMe₂CH₂OAc)(CF₃)] (7). A 20 mL vial was charged with [(Py₃CH)Ni^{IV}(CH₂CMe₂-o-C₆H₄)(CF₃)(OTf)] (6) (50 mg, 0.076 mmol, 1.0 equiv). The solid was dissolved in acetonitrile (5 mL). NMe₄OAc (12 mg, 0.091

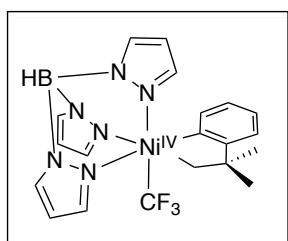
mmol, 1.2 equiv) was added at rt, and the resulting solution was stirred at room temperature for 1.5 h. Solvent was then removed *in vacuo*. The yellow residue was re-dissolved in benzene, and the solution was concentrated. This process was repeated two times to remove NMe₄OTf and excess NMe₄OAc. The residue was then washed with diethyl ether (2 x 10 mL) and dried under vacuum to afford complex 7 as a yellow solid (33 mg, 78% yield). ^1H NMR (500 MHz, CD_3CN , 23 °C) δ 9.15 (d, $J_{\text{HH}} = 5.5$ Hz, 1H), 8.75 (m, 1H), 7.95 (m, 1H), 7.90 (m, 1H), 7.82 (d, $J_{\text{HH}} = 5.5$ Hz, 1H), 7.78 (td, $J_{\text{HH}} = 7.6, 1.7$ Hz, 1H), 7.74 (d, $J_{\text{HH}} = 7.7$ Hz, 1H), 7.70 (d, $J_{\text{HH}} = 7.6$ Hz, 1H), 7.46 (t, $J_{\text{HH}} = 7.7$ Hz, 1H), 7.41 (d, $J_{\text{HH}} = 7.1$ Hz, 1H), 7.24 (d, $J_{\text{HH}} = 7.9$ Hz, 1H), 7.08 (d, $J_{\text{HH}} = 7.9$ Hz, 1H), 6.98-6.91 (multiple peaks, 2H), 6.68 (t, $J_{\text{HH}} = 7.4$ Hz, 1H), 6.43 (t, $J_{\text{HH}} = 7.4$ Hz, 1H), 6.09 (s, 1H), 4.77 (d, $J_{\text{HH}} = 10.7$ Hz, 1H), 4.65 (d, $J_{\text{HH}} = 10.7$ Hz, 1H), 2.45 (s, 3H), 2.12 (s, 3H) 1.98 (s, 3H). ^{13}C NMR (176 MHz, CD_3CN , 23 °C) δ 171.06, 160.13, 158.33, 158.03, 156.57, 153.33, 152.49, 150.14, 149.42, 138.88, 138.20, 137.35, 136.77, 134.44 (Ni-CF₃, shift for CF₃ group extracted from ^{19}F - ^{13}C HMBC NMR spectrum),

127.23, 126.42, 125.90, 124.02, 123.07, 122.94, 122.58, 121.77, 121.64, 74.33, 60.85, 39.39, 27.76, 27.24, 20.47. ^{19}F NMR (471 MHz, CD_3CN , 23 °C) δ -22.45, (s, Ni- CF_3). HRMS-electrospray (m/z): $[\text{M}]^+$ calcd. for $\text{C}_{29}\text{H}_{28}\text{F}_3\text{N}_3\text{NiO}_2$, 565.1482; found, 565.1486



Synthesis of $[\text{K}(\text{Tp})\text{Ni}^{\text{II}}(\text{CH}_2\text{CMe}_2\text{-}o\text{-C}_6\text{H}_4)]$ (8**).** A 20 mL vial was charged with $[(\text{PMe}_3)_2\text{Ni}^{\text{II}}(\text{CH}_2\text{CMe}_2\text{-}o\text{-C}_6\text{H}_4)]$ (250 mg, 0.73 mmol, 1.0 equiv). The solid was dissolved in acetonitrile (8 mL). Potassium trispyrazolylborate (202 mg, 0.80 mmol, 1.1 equiv) was added at rt, and the dark orange solution was stirred at

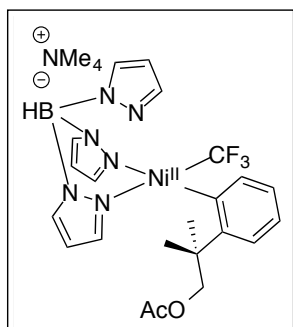
rt for 30 min. Solvent and free PMe_3 were removed *in vacuo*. Diethyl ether (10 mL) was added to the brown residue, and the insoluble material was collected. Complex **8** was dried under vacuum and isolated as a yellow solid (301 mg, 93% yield). ^1H NMR (700 MHz, CD_3CN , 23 °C) δ 8.13 (br, 3H), 7.57 (br, 3H), 6.74 (d, $J_{\text{HH}} = 7.3$ Hz, 1H), 6.69 (t, $J_{\text{HH}} = 7.3$ Hz, 1H), 6.56 (d, $J_{\text{HH}} = 7.3$ Hz, 1H), 6.52 (t, $J_{\text{HH}} = 7.3$ Hz, 1H), 6.13 (br, 3H), 4.71 (br, B-**H**), 1.31 (s, 6 H), 1.14 (s, 2H). ^{13}C NMR (128 MHz, CD_3CN , 23 °C) δ 170.14, 164.49, 140.79, 138.19, 134.75, 121.85, 120.77, 119.73, 103.60, 47.16, 40.62, 33.61. ^{11}B NMR (128 MHz, CD_3CN , 23 °C) δ -2.40 (d, $J_{\text{BH}} = 112.0$ Hz).



Synthesis of $[(\text{Tp})\text{Ni}^{\text{IV}}(\text{CH}_2\text{CMe}_2\text{-}o\text{-C}_6\text{H}_4)(\text{CF}_3)]$ (9**).** a 20 mL vial was charged with $\text{K}[(\text{Tp})\text{Ni}^{\text{II}}(\text{CH}_2\text{CMe}_2\text{-}o\text{-C}_6\text{H}_4)]$ (**8**) (210 mg, 0.47 mmol, 1.0 equiv) in the glovebox. The solid was dissolved in acetonitrile (15 mL). *S*-(Trifluoromethyl) dibenzothiophenium triflate (247 mg, 0.61 mmol, 1.3 equiv) was added at room

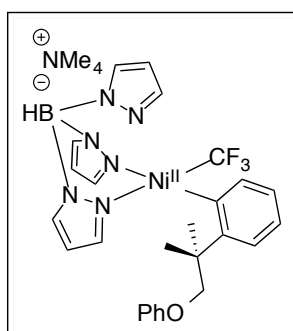
temperature and the yellow-orange solution immediately turned yellow-brown. The reaction mixture was taken out of the glovebox and the solvent was removed by rotary evaporation. The crude yellow-brown solid was purified by flash chromatography on silica gel (mobile phase: ethyl acetate/hexanes with a gradient from 90:10 to 80:20). Compound **9** was isolated as a yellow solid (204 mg, 92% yield). ^1H NMR (700 MHz, CD_3CN , 23 °C) δ 8.13 (d, $J_{\text{HH}} = 1.9$ Hz, 1H), 7.96 (d, $J_{\text{HH}} = 1.9$ Hz, 1H), 7.88 (d, $J_{\text{HH}} = 2.3$ Hz, 1H), 7.85 (d, $J_{\text{HH}} = 2.3$ Hz, 1H), 7.74 (d, $J_{\text{HH}} = 2.2$ Hz, 1H), 7.15 (multiple peaks, 2H), 7.04 (d, $J_{\text{HH}} = 7.5$ Hz, 1H), 6.88 (t, $J_{\text{HH}} = 7.5$ Hz, 1H), 6.68 (d, $J_{\text{HH}} = 2.1$ Hz, 1H), 6.40 (multiple peaks, 2H), 6.08 (t, $J_{\text{HH}} = 2.1$ Hz, 1H), 4.93 (d, $J_{\text{HH}} = 5.5$ Hz, 1H), 4.81 (dd, $J_{\text{HH}} = 5.5$ Hz, $J_{\text{HF}} = 2.4$ Hz, 1H), 4.52 (br, B-**H**), 1.53 (s, 3H), 1.44 (s, 3H). ^{13}C NMR (128 MHz, CD_3CN , 23 °C) δ 160.51, 156.03, 142.68, 141.64,

141.51, 135.56, 135.48, 135.17, 132.68, 126.65, 125.96, 125.59, 120.55 (Ni-CF₃, shift for CF₃ group extracted from ¹⁹F-¹³C HMBC NMR spectrum), 105.94, 105.88, 105.64, 77.67, 46.98, 31.01, 30.25. ¹⁹F NMR (471 MHz, CD₃CN, 23 °C) δ -16.11 (s, Ni-CF₃). ¹¹B NMR (128 MHz, CD₃CN, 23 °C) δ -4.37 (d, *J*_{BH} = 115.9 Hz).



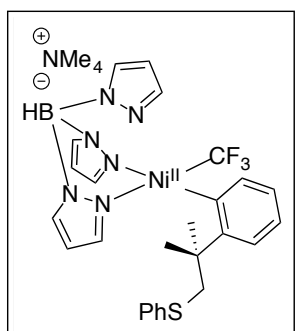
[NMe₄(Tp)Ni^{II}(C₆H₄-*o*-CMe₂CH₂OAc)(CF₃)] (10a). A 20 mL vial was charged with [(Tp)Ni^{IV}(CH₂CMe₂-*o*-C₆H₄)(CF₃)] (**9**) (30 mg, 0.063 mmol, 1.0 equiv). The solid was dissolved in acetonitrile (5 mL). NMe₄OAc (10 mg, 0.075 mmol, 1.2 equiv) was added, and the resulting solution was stirred at 40 °C for 3 days. The reaction mixture was then cooled to room temperature, and solvent was removed *in vacuo*. The resulting yellow residue was washed several

times with diethyl ether (3 x 10 mL). The solids were further dried under vacuum to afford complex **10a** as a yellow solid (33 mg, 88% yield). ¹H NMR (700 MHz, CD₃CN, 23 °C) δ 8.12 (d, *J*_{HH} = 2.3 Hz, 1H), 8.07 (d, *J*_{HH} = 7.4 Hz, 1H), 7.81 (d, *J*_{HH} = 1.8 Hz, 1H), 7.72 (d, *J*_{HH} = 1.8 Hz, 1H), 7.49 (d, *J*_{HH} = 2.3 Hz, 1H), 7.38 (d, *J*_{HH} = 2.3 Hz, 1H), 7.00 (d, *J*_{HH} = 7.4 Hz, 1H), 6.73 (m, 1H), 6.61 (t, *J*_{HH} = 7.4 Hz, 1H), 6.28 (d, *J*_{HH} = 2.0 Hz, 1H), 6.25 (d, *J*_{HH} = 2.0 Hz, 1H), 6.20 (d, *J*_{HH} = 2.2 Hz, 1H), 5.80 (d, *J*_{HH} = 2.2 Hz, 1H), 4.83 (br, B-H), 4.48 (d, *J*_{HH} = 10.7 Hz, 1H), 4.35 (d, *J*_{HH} = 10.7 Hz, 1H), 3.12 (s, 12H), 2.15 (s, 3H), 1.94 (s, 3H), 1.86 (s, 3H). ¹³C NMR (176 MHz, CD₃CN, 23 °C) δ 170.79, 159.57, 150.58, 142.40, 142.18, 140.75, 138.14 (Ni-CF₃, shift for CF₃ group extracted from ¹⁹F-¹³C HMBC NMR spectrum), 136.35, 135.49, 134.76, 134.19, 124.95, 121.24, 120.81, 104.05, 103.84, 103.46, 73.96, 56.23, 39.38, 27.25, 27.02, 20.17. ¹⁹F NMR (471 MHz, CD₃CN, 23 °C) δ -20.62 (s, Ni-CF₃). ¹¹B NMR (128 MHz, CD₃CN, 23 °C) δ -2.54 (d, *J*_{BH} = 116.9 Hz). HRMS-electrospray (*m/z*): [M - NMe₄]⁻ calcd. for C₂₂H₂₅BF₃N₆NiO₂, 531.1438; found, 531.1442.



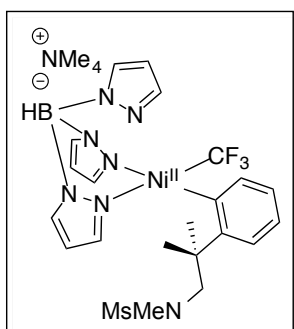
Synthesis of [(NMe₄(Tp)Ni^{II}(C₆H₄-*o*-CMe₂CH₂OPh)(CF₃)] (10b). A 20 mL vial was charged with [(Tp)Ni^{IV}(CH₂CMe₂-*o*-C₆H₄)(CF₃)] (**9**) (30 mg, 0.063 mmol, 1.0 equiv). The solid was dissolved in acetonitrile (5 mL). NMe₄OPh (13 mg, 0.075 mmol, 1.2 equiv) was added, and the resulting solution was stirred at room temperature for 8 h. The solvent was removed *in vacuo*, and the resulting yellow residue was washed several times with diethyl ether

(3 x 10 mL). The solids were further dried under vacuum to afford complex **10b** as a yellow solid (31 mg, 78% yield). ^1H NMR (700 MHz, CD_3CN , 23 °C) δ 8.13 (d, $J_{\text{HH}} = 7.9$ Hz, 1H), 8.02 (d, $J_{\text{HH}} = 2.3$ Hz, 1H), 7.80 (d, $J_{\text{HH}} = 1.8$ Hz, 1H), 7.72 (d, $J_{\text{HH}} = 1.8$ Hz, 1H), 7.48 (d, $J_{\text{HH}} = 2.3$ Hz, 1H), 7.34 (d, $J_{\text{HH}} = 2.3$ Hz, 1H), 7.21 (t, $J_{\text{HH}} = 7.9$ Hz, 2H), 7.08 (d, $J_{\text{HH}} = 7.9$ Hz, 1H), 6.87 (multiple peaks, 3H), 6.71 (t, $J_{\text{HH}} = 7.9$, 1H), 6.63 (t, $J_{\text{HH}} = 7.2$ Hz, 1H), 6.40 (d, $J_{\text{HH}} = 2.0$ Hz, 1H), 6.31 (d, $J_{\text{HH}} = 2.0$ Hz, 1H), 6.18 (s, 1H), 5.80 (t, $J_{\text{HH}} = 2.2$ Hz, 1H), 4.81 (br, B-*H*), 4.39 (d, $J_{\text{HH}} = 8.7$ Hz, 1H), 4.36 (d, $J_{\text{HH}} = 8.7$ Hz, 1H), 3.07 (s, 12H), 2.30 (s, 3H), 1.85 (s, 3H). ^{13}C NMR (176 MHz, CD_3CN , 23 °C) δ 159.84, 159.54, 151.22, 142.50, 142.18, 140.77, 138.57 (Ni- CF_3 , shift for CF_3 group extracted from ^{19}F - ^{13}C HMBC NMR spectrum), 136.13, 135.39, 134.67, 134.37, 129.22, 125.05, 121.22, 120.80, 119.89, 114.50, 104.03, 103.81, 103.44, 77.96, 55.72, 40.00, 27.19, 27.15. ^{19}F NMR (471 MHz, CD_3CN , 23 °C) δ -20.52 (s, Ni- CF_3). ^{11}B NMR (128 MHz, CD_3CN , 23 °C) δ -2.57 (d, $J_{\text{BH}} = 115.7$ Hz). HRMS-electrospray (m/z): $[\text{M} - \text{NMe}_4]^-$ calcd. for $\text{C}_{26}\text{H}_{27}\text{BF}_3\text{N}_6\text{NiO}$, 565.1645; Found, 565.1640.



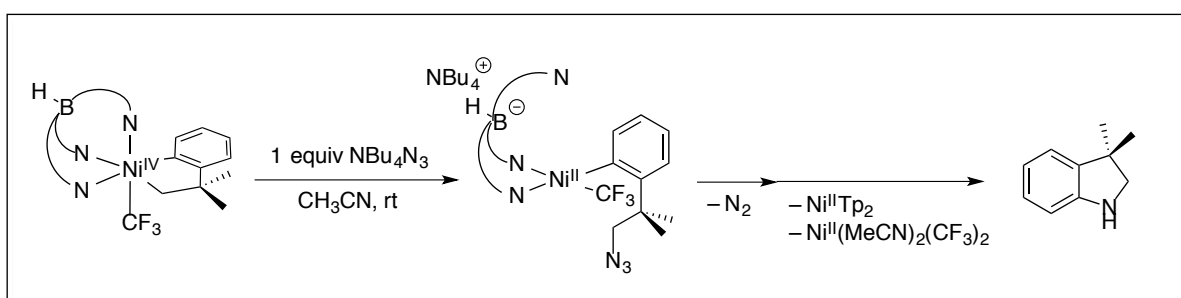
Synthesis of $[(\text{NMe}_4)(\text{Tp})\text{Ni}^{\text{II}}(\text{C}_6\text{H}_4\text{-}o\text{-CMe}_2\text{CH}_2\text{SPh})(\text{CF}_3)]$ (**10c**).

A 20 mL vial was charged with $[(\text{Tp})\text{Ni}^{\text{IV}}(\text{CH}_2\text{CMe}_2\text{-}o\text{-C}_6\text{H}_4)(\text{CF}_3)]$ (**9**) (50 mg, 0.11 mmol, 1.0 equiv). The solid was dissolved in acetonitrile (5 mL). NMe_4SPh (23 mg, 0.13 mmol, 1.2 equiv) was added, and the resulting solution was stirred at room temperature for 10 min. The solvent was removed *in vacuo*, and the resulting yellow residue was washed several times with diethyl ether (3 x 10 mL). The solids were further dried under vacuum to afford complex **10c** as a yellow solid (68 mg, 94% yield). ^1H NMR (700 MHz, CD_3CN , 23 °C) δ 8.20 (d, $J_{\text{HH}} = 7.4$ Hz, 1H), 8.04 (d, $J_{\text{HH}} = 2.2$ Hz, 1H), 7.77 (d, $J_{\text{HH}} = 1.9$ Hz, 1H), 7.73 (d, $J_{\text{HH}} = 1.9$ Hz, 1H), 7.40 (d, $J_{\text{HH}} = 2.2$ Hz, 1H), 7.31-7.24 (multiple peaks, 3H), 7.18 (t, $J_{\text{HH}} = 7.6$ Hz, 2H), 7.09 (t, $J_{\text{HH}} = 7.8$ Hz, 1H), 7.04 (d, $J_{\text{HH}} = 7.8$ Hz, 1H), 6.72 (t, $J_{\text{HH}} = 7.2$ Hz, 1H), 6.66 (t, $J_{\text{HH}} = 7.2$ Hz, 1H), 6.32 (br, 1H), 6.28 (br, 1H), 6.17 (br, 1H), 5.77 (br, 1H), 4.83 (br, B-*H*), 3.68 (d, $J_{\text{HH}} = 12.9$ Hz, 1H), 3.67 (d, $J_{\text{HH}} = 12.9$ Hz, 1H), 3.08 (s, 12H), 2.19 (s, 3H), 1.95 (s, 3H). ^{13}C NMR (176 MHz, CD_3CN , 23 °C) δ 159.24, 152.73, 142.37, 142.06, 140.90, 139.31, 138.99 (Ni- CF_3 , shift for CF_3 group extracted from ^{19}F - ^{13}C HMBC NMR spectrum), 136.03, 135.34, 134.70, 134.38, 128.60, 127.85, 124.95, 124.68, 121.26, 120.87, 103.99, 103.89, 103.43, 55.16, 47.94, 40.21, 29.29, 29.28. ^{19}F NMR (471 MHz, CD_3CN , 23 °C) δ -20.50 (s, Ni- CF_3). ^{11}B NMR (128 MHz, CD_3CN , 23 °C) δ -2.57 (d, $J_{\text{BH}} = 113.4$ Hz). HRMS-electrospray (m/z): $[\text{M} - \text{NMe}_4]^-$ calcd. for $\text{C}_{26}\text{H}_{27}\text{BF}_3\text{N}_6\text{NiS}$, 581.1417; found, 581.1430.



Synthesis of [(NMe₄)(Tp)Ni^{II}(C₆H₄-*o*-CMe₂CH₂NMeSO₂Me)(CF₃)] (10d). A 20 mL vial was charged with [(Tp)Ni^{IV}(CH₂CMe₂-*o*-C₆H₄)(CF₃)] (9) (50 mg, 0.11 mmol, 1.0 equiv). The solid was dissolved in acetonitrile (5 mL). NMe₄N(Me)(Ms) (23 mg, 0.13 mmol, 1.2 equiv) was added, and the resulting solution was stirred at 40 °C for 4 h. The reaction mixture was cooled to room temperature, and the solvent was removed *in vacuo*. The yellow residue was washed several times with diethyl ether (3 x 10 mL). The solids were further dried under vacuum to afford complex **10d** as a yellow solid (65 mg, 90% yield).

¹H NMR (700 MHz, CD₃CN, 23 °C) δ 8.26 (d, *J*_{HH} = 7.3 Hz, 1H), 8.05 (d, *J*_{HH} = 2.2 Hz, 1H), 7.80 (br, 1H), 7.75 (s, 1H), 7.43-7.38 (m, 1H), 7.33 (br, 1H), 7.02 (d, *J*_{HH} = 7.8 Hz, 1H), 6.72 (t, *J*_{HH} = 7.4 Hz, 1H), 6.68 (t, *J*_{HH} = 7.2 Hz, 1H), 6.33 (br, 1H), 6.22 (d, *J*_{HH} = 2.0 Hz, 1H), 6.19 (d, *J*_{HH} = 2.5 Hz, 1H), 5.81 (br, 1H), 4.87 (br, B-*H*), 3.30 (d, *J*_{HH} = 13.9 Hz, 1H), 3.22 (d, *J*_{HH} = 13.9 Hz, 1H), 3.08 (s, 12H), 2.61 (s, 3H), 2.52 (s, 3H), 2.09 (s, 3H), 1.98 (s, 3H). ¹³C NMR (176 MHz, CD₃CN, 23 °C) δ 159.53, 151.85, 142.15, 141.95, 141.10, 138.51 (Ni-CF₃, shift for CF₃ group extracted from ¹⁹F-¹³C HMBC NMR spectrum), 136.01, 135.45, 134.88, 134.27, 125.41, 121.32, 120.81, 104.00 (two overlapping peaks), 103.57, 61.64, 55.74, 40.30, 37.98, 32.90, 28.80, 28.11. ¹⁹F NMR (471 MHz, CD₃CN, 23 °C) δ -20.48 (s, Ni-CF₃). ¹¹B NMR (128 MHz, CD₃CN, 23 °C) δ -2.57 (d, *J*_{BH} = 114.4 Hz). HRMS-electrospray (*m/z*): [M-NMe₄]⁻ calcd. for C₂₂H₂₈BF₃N₇NiO₂S, 580.1424; found, 580.1398.



***in situ* Observation and Decomposition of [(NBu₄)(Tp)Ni^{II}(C₆H₄-*o*-CMe₂CH₂N₃)(CF₃)] (10e).** A J. Young valve NMR tube equipped with an O-ring seal was charged with [(Tp)Ni^{IV}(CH₂CMe₂-*o*-C₆H₄)(CF₃)] (9) (10 mg, 0.021 mmol, 1.0 equiv). This solid was dissolved in acetonitrile (0.5 mL). NBu₄N₃ (6.0 mg, 0.021 mmol, 1.0 equiv) was added, and the resulting solution was monitored at room temperature by ¹H and ¹⁹F NMR spectroscopy.

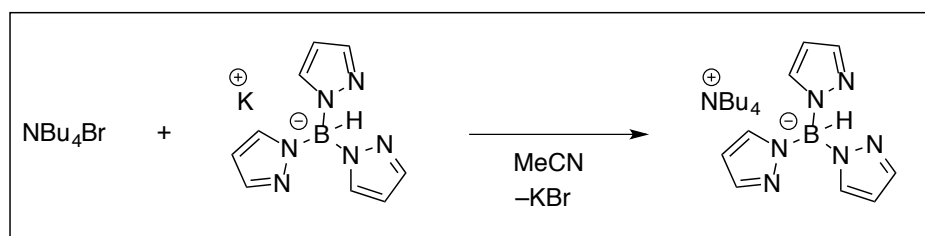
Over the course of 1 h, the reaction mixture changed color from yellow to purple. Over an additional 15 h, the color changed again to orange.

Intermediate **10e** was observed *in situ* and characterized at approximately 20% conversion (see p. S16, Fig. S2a). ^1H NMR (700 MHz, CD_3CN , 23 °C) δ 8.28 (d, $J_{\text{HH}} = 7.2$ Hz, 1H), 8.03 (d, $J_{\text{HH}} = 2.0$ Hz, 1H), 7.79 (m, 1H), 7.63 (br, 1H), 7.37 (br, 1H), 7.32 (br, 1H), 7.10 (m, 1H), 6.72 (t, $J_{\text{HH}} = 7.4$ Hz, 1H), 6.64 (t, $J_{\text{HH}} = 7.4$ Hz, 1H), 6.43 (d, $J_{\text{HH}} = 6.9$ Hz, 1H), 6.33 (br, 1H), 6.19 (overlapping peaks, 1H), 5.79 (br, 1H), 3.72 (d, $J_{\text{HH}} = 11.9$ Hz, 1H), 3.71 (d, $J_{\text{HH}} = 11.9$ Hz, 1H), 2.02 (s, 3H), 1.76 (s, 3H). ^{19}F NMR (471 MHz, CD_3CN , 23 °C) δ -20.59 (s, Ni- CF_3).

After 15 h at room temperature, complex **9** and intermediate **10e** were fully consumed to generate 3,3'-dimethylindoline in quantitative conversion. Reaction conversion was determined by integration of the methylene protons of 3,3'-dimethylindoline vs an internal standard, 3-(trifluoromethyl)anisole via ^1H NMR spectroscopy. 3,3'-dimethylindoline was characterized by comparison of its ^1H NMR spectrum with that reported in the literature⁴¹ and by mass spectrometry.

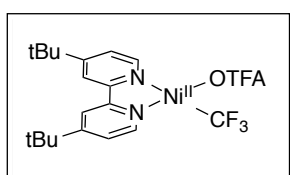
The $[\text{Ni}^{\text{II}}]$ byproducts of the reaction were $\text{Ni}^{\text{II}}(\text{MeCN})_2(\text{CF}_3)_2$ (identified by comparison of its ^{19}F NMR spectrum with that reported in the literature^{20c} and $\text{Ni}^{\text{II}}\text{Tp}_2$, which was characterized by X-ray crystallography. These complexes are likely formed through a ligand disproportionation reaction following the protonation of the indoline.

Synthesis of NBu_4Tp

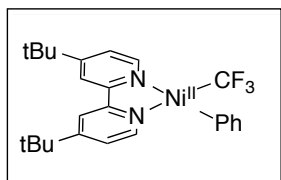


A 20 mL vial was charged with potassium trispyrazolylborate (KTP) (300 mg, 1.19 mmol, 1.0 equiv), and the white solid was dissolved in acetonitrile (3 mL). A solution of tetrabutylammonium bromide (NBu_4Br) (383 mg, 1.19 mmol, 1.0 equiv) in acetonitrile (3 mL) was added to the KTP solution, and a white solid immediately precipitated. The reaction

mixture was filtered, and the filtrate was collected and concentrated under vacuum to afford tetrabutylammonium trispyrazolylborate (NBu₄Tp) as a white solid (520 mg, 96% yield). ¹H NMR (700 MHz, CD₃CN, 23 °C): δ 7.66-7.12 (multiple peaks, 6H), 6.06 (dd, *J*_{HH} = 1.8 Hz, 3H), 4.76 (q, *J*_{HB} = 112 Hz, 1H), 3.22-2.85 (m, 8H), 1.60 (m, 8H), 1.36 (m, 8H), 0.98 (t, *J*_{HH} = 7.4 Hz, 12H). ¹¹B NMR (225 MHz, CD₃CN, 23 °C): δ -1.13 (d, *J*_{BH} = 112 Hz). ¹³C NMR (176 MHz, CD₃CN, 23 °C): δ 138.55, 132.93, 102.65, 58.29, 23.30, 19.32, 12.79. HRMS-electrospray (*m/z*): [M - NBu₄]⁻ calcd. for C₉H₁₀BN₆, 213.1065; found, 213.1066.

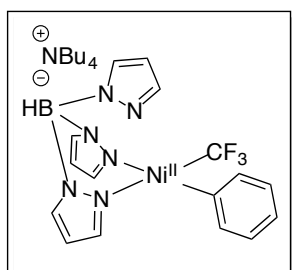


Synthesis of [(dtbpy)Ni^{II}(CF₃)(OTFA)]: Under ambient conditions, a 200 mL round bottomed flask was charged with (PPh₃)₂Ni(CF₃)(OTFA)³⁶ (1.0 g, 1.3 mmol, 1.0 equiv) and 4,4'-di-*tert*-butylbipyridine (385 mg, 1.4 mmol, 1.1 equiv). Dry dichloromethane (50 mL) was added, and the resulting dark orange solution stirred for 5 min at room temperature. The volatiles were removed under reduced pressure, and pentane (20 mL) was added to triturate the residue. The resulting solids were collected, washed with a 10:1 solution of pentane: diethyl ether (3 x 30 mL), and dried under reduced pressure to afford (dtbpy)Ni(CF₃)(OTFA) as a yellow solid (603 mg, 91% yield). The ¹H and ¹³C NMR spectra of this complex were recorded at -30 °C to slow the fluxional processes associated with this complex. ¹H NMR (700 MHz, CD₂Cl₂, -30 °C): δ 8.21 (br, 1H), 7.82 (br, 2H), 7.74 (br, 1H), 7.46 (br, 1H), 7.39 (br, 1H), 1.36 (br, 18H). ¹³C NMR (176 MHz, CD₂Cl₂, -30 °C): δ 165.83, 165.42, 161.98, 155.35, 153.10, 152.84, 147.40, 124.26, 124.06, 118.36, 117.81, 115.08, 35.66, 35.62, 29.91, 29.85. ¹⁹F NMR (471 MHz, CD₂Cl₂, 23 °C): δ -34.40 (br, 3F, CF₃), -75.35 (br, 3F, OCOCF₃). IR (ATR, cm⁻¹): 1695 (s), 1617 (m), 1415 (m), 1195 (s).



Synthesis of [(dtbpy)Ni^{II}(CF₃)(Ph)] (16): In the glovebox, a 150 mL round bottomed flask was charged with (dtbpy)Ni^{II}(CF₃)(OTFA) (590 mg, 1.16 mmol, 1.0 equiv), and this yellow solid was dissolved in THF (60 mL). The resulting solution was cooled to -35 °C, and then ZnPh₂ (140 mg, 0.63 mmol, 0.55 equiv) in THF (5 mL) was added. The reaction mixture was allowed to warm to room temperature over approximately 5 min, during which time the solution changed color from dark orange to dark red. The solution was then filtered through a 3 cm pad of basic alumina, and the pad was washed with THF (5 mL). The washes were combined, and the volatiles were removed under reduced pressure. The resulting dark red

residue was triturated with pentane (10 mL), and the solids were collected by filtration. The solids were washed with additional pentane (40 mL) and then dried under reduced pressure to yield complex **16** as an orange solid (334 mg, 61% yield) ^1H NMR (700 MHz, CD_2Cl_2 , 23 °C): δ 8.78 (d, $J_{\text{HH}} = 6.0$ Hz, 1H), 7.90 (d, $J_{\text{HH}} = 2.0$ Hz, 1H), 7.84 (d, $J_{\text{HH}} = 2.0$ Hz, 1H), 7.65-7.61 (multiple peaks, 2H), 7.50 (dd, $J_{\text{HH}} = 6.0, 2.0$ Hz, 1H), 7.14 (dd, $J_{\text{HH}} = 6.1, 2.0$ Hz, 1H), 7.11 (d, $J_{\text{HH}} = 6.0$ Hz, 1H), 7.00 (multiple peaks, 2H), 6.89 (t, $J_{\text{HH}} = 7.3$ Hz, 1H), 1.40 (s, 9H), 1.31 (s, 9H). ^{13}C NMR (176 MHz, CD_2Cl_2 , 23 °C): δ 163.32, 163.20, 155.20, 154.05, 151.51, 151.48, 150.63, 139.31 (q, $J_{\text{CF}} = 359$ Hz), 135.45, 125.96, 123.73, 123.23, 122.01, 117.51, 117.22, 35.36, 35.29, 29.96, 29.88. ^{19}F NMR (377 MHz, CD_3CN , 23 °C): δ -21.95 (s, 3 F). HRMS-electrospray (m/z): $[\text{M} - \text{F}]^+$ calcd. for $\text{C}_{25}\text{H}_{29}\text{F}_2\text{N}_2\text{Ni}$, 453.1652; found, 453.1644. Elemental Analysis calcd. for $\text{C}_{25}\text{H}_{29}\text{F}_2\text{N}_2\text{Ni}$, C: 63.45, H: 6.18, N: 5.92; found, C: 63.30, H: 6.26, N: 5.82

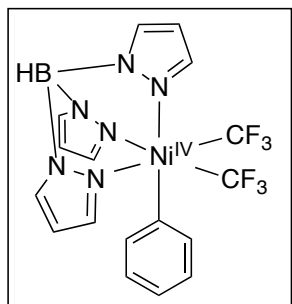


Synthesis of $[\text{NBu}_4(\text{Tp})\text{Ni}^{\text{II}}(\text{CF}_3)(\text{Ph})]$ (12**):** In the glovebox, a 20 mL vial was charged with $(\text{dtbpy})\text{Ni}^{\text{II}}(\text{CF}_3)(\text{Ph})$ (200 mg, 0.43 mmol, 1.0 equiv), and the orange solid was dissolved in a minimal amount of acetonitrile (3 mL). A solution of NBu_4Tp (194 mg, 0.43 mmol, 1.0 equiv) in acetonitrile (2 mL) was added, and the resulting dark orange solution immediately changed color to yellow-brown. Over

the course of approximately 5 min, 4,4'-di-*tert*-butylbipyridine (dtbpy) precipitated from solution in the form of a white crystalline solid. The solution was concentrated to approximately 3 mL, which led to further precipitation of dtbpy. The precipitate was collected on a fritted filter and washed with acetonitrile (5 mL). The filtrates were collected and concentrated under reduced pressure. The resulting brown residue was washed with ether (3 x 10 mL) and pentane (3 x 10 mL) and the remaining solid was collected to afford complex **12** as a light tan powder (130 mg, 46% yield).

The ^1H and ^{13}C NMR spectra of **12** were recorded at -10 °C in order to resolve the fluxional pyrazolyl signals. ^1H NMR (700 MHz, CD_3CN , -10 °C): δ 7.89 (br, 3H), 7.43 (d, $J_{\text{HH}} = 7.3$ Hz, 2H), 7.30 (br signal, 3H), 6.76 (m, 2H), 6.66 (t, $J_{\text{HH}} = 7.3$ Hz, 1H), 6.14 (br, 3H), 5.00-4.36 (br, B-H), 3.15-3.04 (m, 8H), 1.61 (m, 8H), 1.36 (m, 8H), 0.98 (t, $J_{\text{HH}} = 7.4$ Hz, 12H). ^{13}C NMR (176 MHz, CD_2Cl_2 , -10 °C): δ 164.98, 141.70, 139.25 (q, $J_{\text{CF}} = 361$ Hz), 136.51, 134.81, 124.48, 120.44, 103.78, 58.51, 23.65, 19.64, 13.48. ^{11}B NMR (225 MHz, CD_3CN , 23 °C): δ -2.62 (d, $J_{\text{BH}} = 114$ Hz) ^{19}F NMR (471 MHz, CD_3CN , 23 °C): δ -21.32 (s, 3F). Elemental

Analysis calcd. for C₃₂H₅₁BF₃N₇Ni, C: 58.21, H: 7.79, N: 14.85; found, C: 58.27, H: 7.91, N: 14.83.



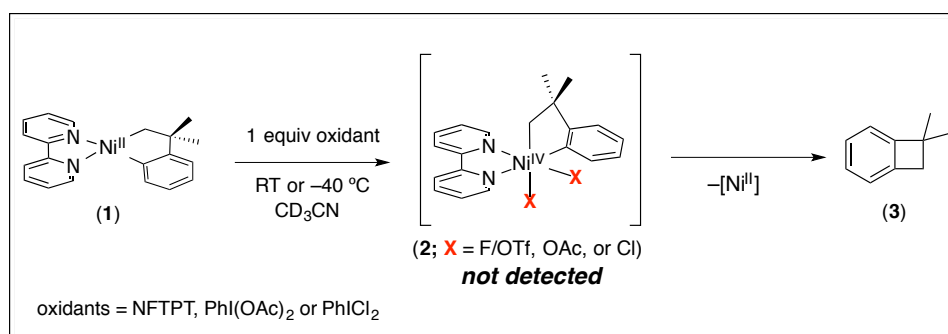
Synthesis of [(Tp)Ni^{IV}(CF₃)₂(Ph)] (13). Procedure A:

[NBu₄(Tp)Ni^{II}(CF₃)(Ph)] (12) (120 mg, 0.18 mmol, 1.0 equiv) and *S*-(trifluoromethyl) dibenzothiophenium triflate (95 mg, 0.24 mmol, 1.3 equiv) were combined in a 20 mL vial under an inert atmosphere. Acetonitrile (8 mL) was added, and the resulting yellow solution was allowed to stand for 1 min at room temperature. The vial was then removed from the glovebox and concentrated under reduced pressure. The resulting yellow-brown residue was purified by silica gel chromatography (mobile phase: hexanes/ethyl acetate with a gradient from 100:1 to 60:40). Complex 13 was isolated as a yellow solid (79 mg, 90% yield). ¹H NMR (700 MHz, CD₃CN, 23 °C): δ 8.05 (s, 1H), 7.94 (d, *J*_{HH} = 2.3 Hz, 1H), 7.91 (d, *J*_{HH} = 2.3 Hz, 2H), 7.31 (d, *J*_{HH} = 2.3 Hz, 2H), 7.14 (t, *J*_{HH} = 7.0 Hz, 1H), 6.97 (t, *J*_{HH} = 7.7 Hz, 2H), 6.72 (s, 2H), 6.43 (t, *J*_{HH} = 2.2 Hz, 1H), 6.27 (t, *J*_{HH} = 2.2 Hz, 2H), 4.69 (br, B-*H*). ¹³C NMR (176 MHz, CD₃CN, 23 °C): δ 158.54, 143.53, 143.18, 136.60, 135.98, 135.15, 127.46, 126.69, 112.44 (q, *J*_{CF} = 383 Hz), 106.28, 105.97. ¹¹B NMR (225 MHz, CD₃CN, 23 °C): δ -4.22 (d, *J*_{BH} = 117.7 Hz). ¹⁹F NMR (379 MHz, CD₃CN, 23 °C): δ -19.38 (s, 6F). Elemental Analysis calcd. for C₁₇H₁₈BF₆N₆Ni, C: 41.94, H: 3.11, N: 17.26; found, C: 41.59, H: 2.95, N: 17.37

General Procedure B: Under an inert atmosphere, a 20 mL vial was charged with [NBu₄(Tp)Ni^{II}(CF₃)₂] (14) (230 mg, 0.35 mmol, 1.0 equiv) and acetonitrile (17 mL). The resulting yellow-orange solution was then cooled to -35 °C. After equilibrating for 10 min at this temperature, the corresponding diaryl iodonium or aryldiazonium salt was added to the solution of 14. The vial was shaken vigorously for 10 s, at which point the reaction mixture immediately turned brown. After 3 min at -35 °C the solution was warmed to room temperature. The reaction was removed from the glovebox and filtered through a 2 cm thick pad of silica on the benchtop. The pad was washed with THF (5 mL), and the combined filtrates were concentrated to dryness under reduced pressure. The crude solid was further purified by flash chromatography (mobile phase: hexanes/ethyl acetate with a gradient from 100:1 to 90:10). The products 13-OMe, 13-Me, 13-Br, and 13-CO₂Me were isolated in 24-48% yield.

3.4.3. NMR Oxidation Studies

Initial Oxidant Screen with Ni^{II} Precursor 1

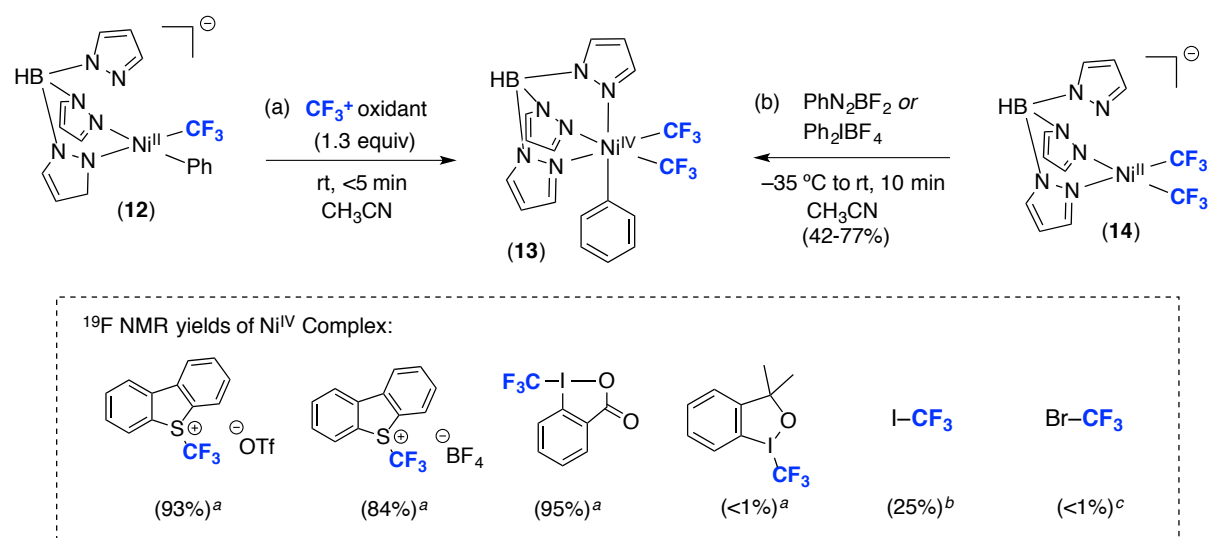


Experimental Procedure: A screw cap NMR tube was charged with [(bpy)Ni^{II}(CH₂CMe₂-*o*-C₆H₄)] (**1**) (8.0 mg, 0.023 mmol, 1.0 equiv) and CD₃CN (0.6 mL) was added. *N*-fluoro-2,4,6-trimethylpyridinium triflate (NFTPT) (6.7 mg, 0.023 mmol, 1.0 equiv) was subsequently added at room temperature, and the dark blue solution immediately turned light yellow. In two separate experiments, the hypervalent iodine reagents PhI(OAc)₂ (7.4 mg, 0.023 mmol, 1.0 equiv) or PhICl₂ (6.3 mg, 0.023 mmol, 1.0 equiv) were added to Ni^{II} precursor (**1**) in CD₃CN at room temperature. Under these conditions, the dark blue solutions immediately turned red-brown. ¹H NMR spectroscopic analyses of the crude reaction mixtures were consistent with formation of cyclobutane product **3** with any of the three oxidants.

The oxidant screens were repeated at low temperature in an attempt to observe proposed intermediates **2** by NMR spectroscopy. The solutions were prepared as previously described; however, the reagents were cooled prior to mixing in a glovebox cold well (at approximately -40 °C). Once the oxidants were added, the NMR tubes were removed from the glovebox and placed in a liquid nitrogen/ethyl acetate bath (-84 °C). The samples were then placed in the NMR spectrometer where the probe had been pre-cooled to -40 °C. The samples were allowed to equilibrate in the spectrometer for 5 min before acquiring spectra.

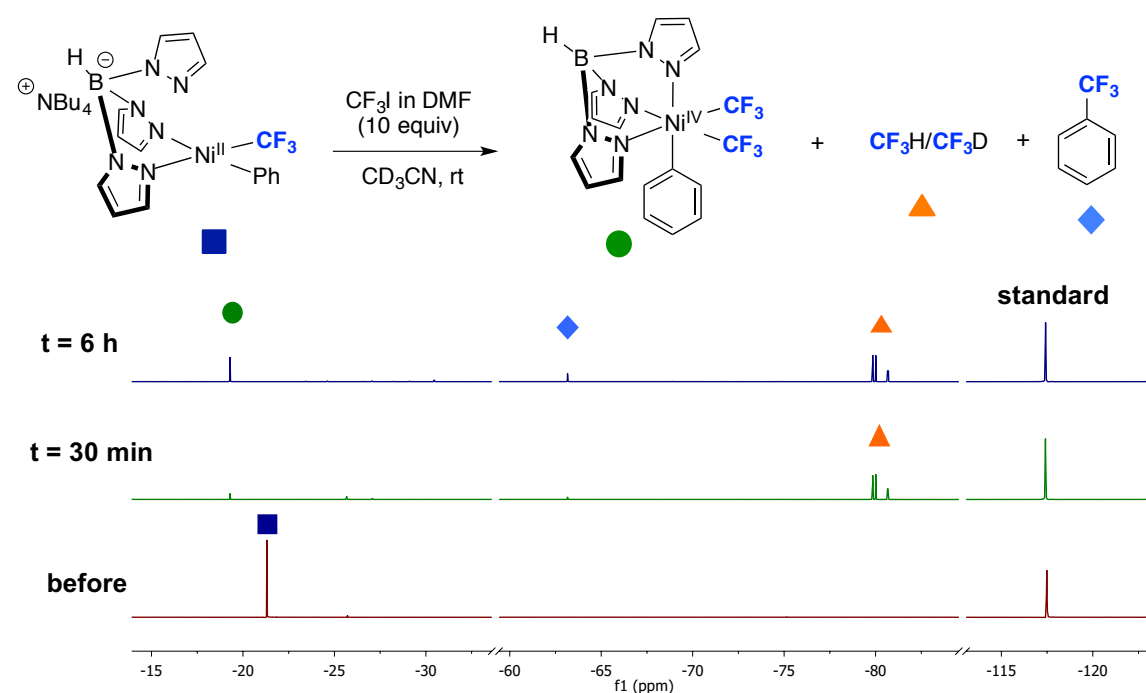
In all cases, attempts to detect proposed intermediates **2** at or below room temperature were unsuccessful. Instead, cyclobutane product **3** was observed as the major product.

Trifluoromethyl Oxidation Studies to Form Ni^{IV} Complex 13



General Procedure A: A screw cap NMR tube was charged with complex **12** (5.0 mg, 0.0076 mmol, 1.0 equiv), 4,4'-difluorobiphenyl, and 0.5 mL of CD_3CN . The ratio between the standard and **12** was determined by ^{19}F NMR integration. The NMR sample was taken back into the glovebox and the respective oxidant (0.0098 mmol, 1.3 equiv) was added. After 10 min, the sample was analyzed by ^{19}F NMR spectroscopy to determine the yield of Ni^{IV} complex **13** (84-93%).

Figure 3.18. ^{19}F NMR Spectra Monitoring the Reaction Progress of **12** in the Presence of CF_3I



General Procedure B: A screw cap NMR tube was charged with complex **12** (5.0 mg, 0.0076 mmol, 1.0 equiv), 4,4'-difluorobiphenyl, and 0.5 mL of acetonitrile- d_3 . The ratio between the standard and **12** was determined by ^{19}F NMR integration. The NMR sample was taken back into the glovebox and CF_3I was added from a 2.5 M solution in dimethylformamide (30 μL , 0.076 mmol, 10 equiv). After 30 min at room temperature, the sample was analyzed by ^{19}F NMR spectroscopy and only fluoroform was observed. However, after an additional 6 h at room temperature, Ni^{IV} complex **13** was formed in 25% yield. These data suggest that this process likely involves the formation of CF_3 radicals and paramagnetic Ni^{III} intermediates (Figure 3.18).

In situ Observation of $(\text{dtbpy})\text{Ni}^{\text{IV}}$ Intermediate

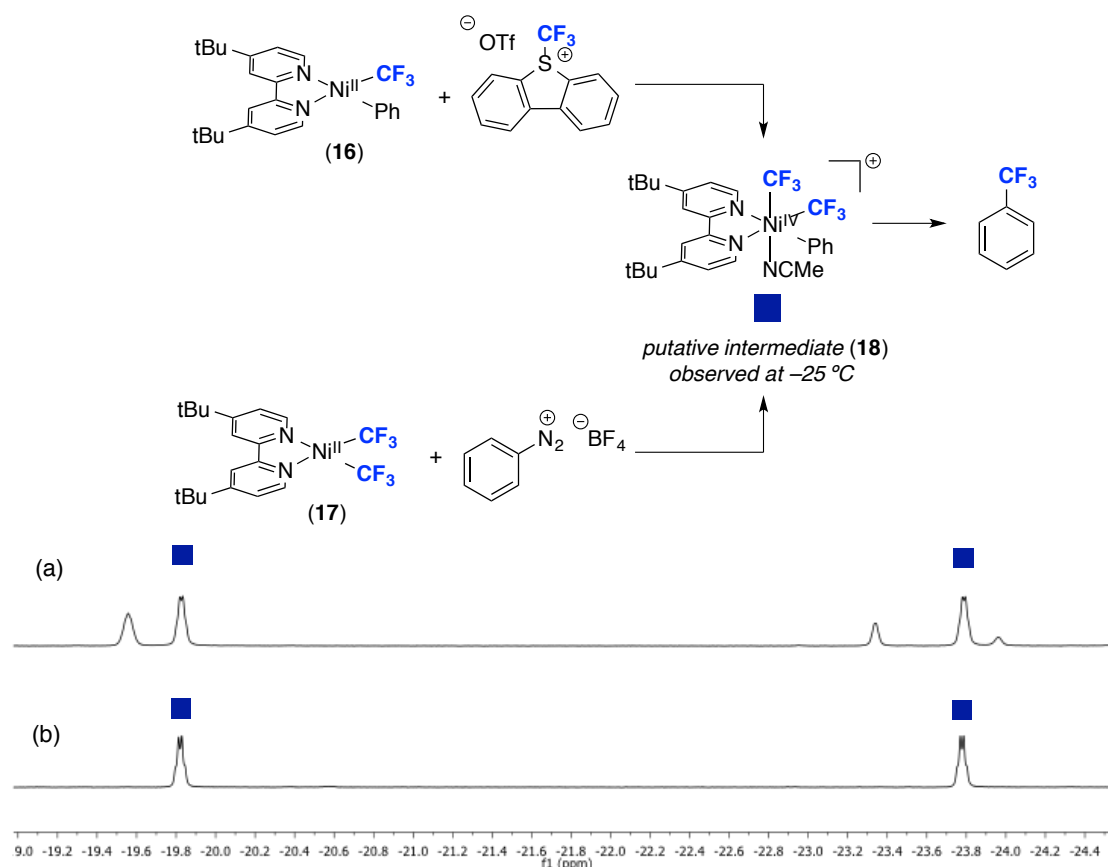


Figure 3.19. ^{19}F NMR Spectra at $-25\text{ }^\circ\text{C}$ Showing the Two Signals Assigned to the CF_3 Resonances of Ni^{IV} Intermediate **18** via (a) Pathway A; CF_3^+ Oxidant and (b) Pathway B; Aryl $^+$ Oxidant

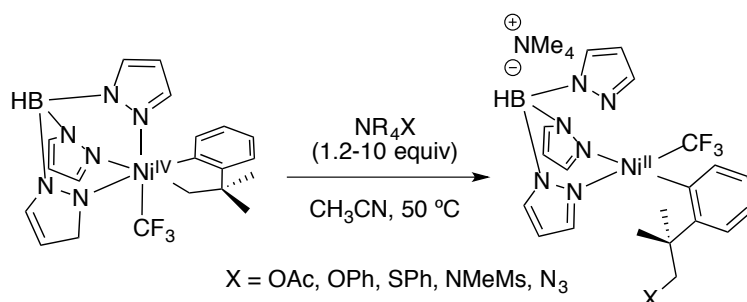
Procedure for Pathway A: A 4 mL vial was charged with complex **16** (8.0 mg, 0.017 mmol, 1.0 equiv), tetrabutylammonium triflate (19 mg, 0.051 mmol, 3.0 equiv), and 4,4'-difluorobiphenyl. CD_3CN (0.5 mL) was added, and the resulting solution was transferred to an

NMR tube. The sample was removed from the glovebox and placed in an NMR spectrometer pre-cooled to $-25\text{ }^{\circ}\text{C}$. The ratio between the standard and **16** was determined by ^{19}F NMR integration at this temperature. The sample was removed from the spectrometer, and a solution of *S*-(trifluoromethyl)dibenzothiophenium triflate (10 mg, 0.026 mmol, 1.5 equiv) in CD_3CN (0.2 mL) was added under a N_2 atmosphere. The NMR tube was shaken vigorously and then placed back into the NMR spectrometer at $-25\text{ }^{\circ}\text{C}$. After 1 min at this temperature, two new ^{19}F resonances (which we attribute to the formation of **18**) were observed in 21% yield along with 27% of the reductive elimination product (-19.8 ppm , $J_{\text{FF}} = 7.9\text{ Hz}$, -24.8 ppm , $J_{\text{FF}} = 7.9\text{ Hz}$). After 30 min at room temperature, the sample was analyzed by ^{19}F NMR spectroscopy and full consumption of putative intermediate **18** was observed along with 63% of benzo-trifluoride.

Procedure for Pathway B: A 4 mL vial was charged with complex **17** (4 mg, 0.0086 mmol, 1.0 equiv), tetrabutylammonium triflate (10 mg, 0.0025 mmol, 3.0 equiv), and the internal standard 4,4'-difluorobiphenyl. CD_3CN (0.5 mL) was added, and the resulting solution was transferred to an NMR tube. The sample was removed from the glovebox and placed in an NMR spectrometer pre-cooled to $-25\text{ }^{\circ}\text{C}$. The ratio between the standard and **17** was determined by ^{19}F NMR integration at this temperature. The sample was removed from the spectrometer and allowed to warm to room temperature, and a solution of PhN_2BF_4 (1.8 mg, 0.0095 mmol, 1.1 equiv) in CD_3CN (0.15 mL) was added under a N_2 atmosphere. The NMR tube was shaken vigorously for 15 s and then placed back into the NMR spectrometer at $-25\text{ }^{\circ}\text{C}$. After 1 min at this temperature, two new ^{19}F resonances (-19.8 ppm , $J_{\text{FF}} = 7.9\text{ Hz}$, -24.8 ppm , $J_{\text{FF}} = 7.9\text{ Hz}$) were observed in 28% yield along with 14% of the reductive elimination product, and 24% of unreacted **17** as determined by ^{19}F NMR integration against the standard. After 60 min at room temperature, the sample was analyzed by ^{19}F NMR spectroscopy and full consumption of intermediate **18** was observed along with 43% yield of benzo-trifluoride.

3.4.4. Reductive Elimination Studies

Determining Order in Reagents for C-X Bond Formation



Experimental Procedure: Complex **9** (4.0 mg, 0.0084 mmol, 1.0 equiv) was weighed into a J. Young valve NMR tube equipped with an O-ring seal. Various amounts of NMe_4OAc (0.010 mmol to 0.085 mmol) were weighed into 4 mL vials, and the solids were dissolved in CD_3CN (0.6 mL). The resulting solution was added to the NMR tube at room temperature. The tube was then placed into an NMR spectrometer that had been pre-heated to 50 °C. The rate of reductive elimination from **9** to form **10a** was monitored by ^{19}F NMR spectroscopy at 50 °C. Concentration versus time data were acquired by integration of the CF_3 signals of **9** and **10a** (Figure 3.20). Initial rates were obtained from the slope of a linear-fit line monitoring the first 10% of the reaction progress (Figure 3.21). A plot of $\ln(r_0)$ vs. $\ln([\text{OAc}^-])$ showed that the rate of reductive elimination is first-order in OAc^- (Figure 3.22).

Figure 3.20. Plot of Concentration versus Time for Reductive Elimination from **9** to form **10a** with 5 equiv of NMe_4OAc at 50 °C

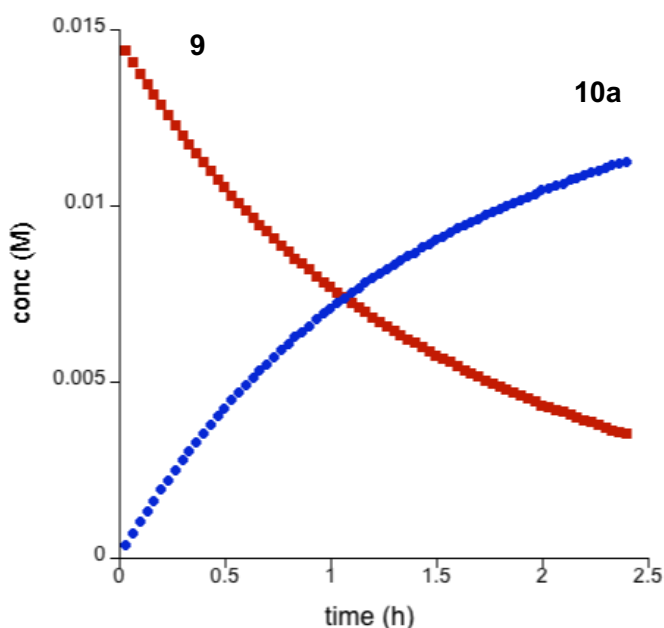


Figure 3.21. Initial Rates Plot of Concentration versus Time for Reductive Elimination from **9** to form **10a** at 50 °C. \blacktriangle = 10 equiv NMe₄OAc, $y_9 = 0.0148 - 5.07e^{-6}x$, $R^2 = 0.999$; $y_{10a} = -1.75e^{-5} + 5.06e^{-6}x$, $R^2 = 0.998$. \bullet = 5 equiv NMe₄OAc, $y_9 = 0.0143 - 2.04e^{-6}x$, $R^2 = 0.992$; $y_{10a} = 4.87e^{-4} + 2.04e^{-6}x$, $R^2 = 0.992$. \blacklozenge = 2.5 equiv NMe₄OAc, $y_9 = 0.0148 - 1.44e^{-6}x$, $R^2 = 0.999$; $y_{10a} = -4.01e^{-5} + 1.44e^{-6}x$, $R^2 = 0.998$. \blacksquare = 1.2 equiv NMe₄OAc, $y_9 = 0.0148 - 6.00e^{-7}x$, $R^2 = 0.998$; $y_{10a} = -1.08e^{-5} + 5.98e^{-7}x$, $R^2 = 0.998$.

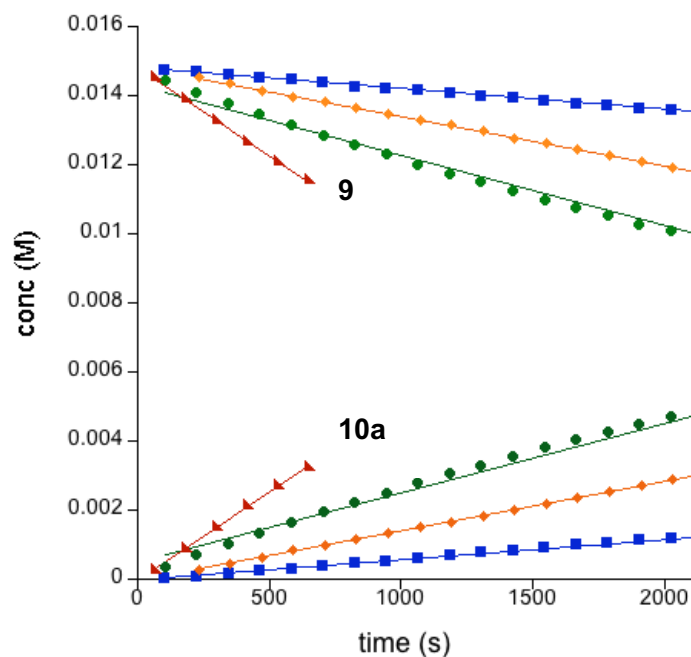
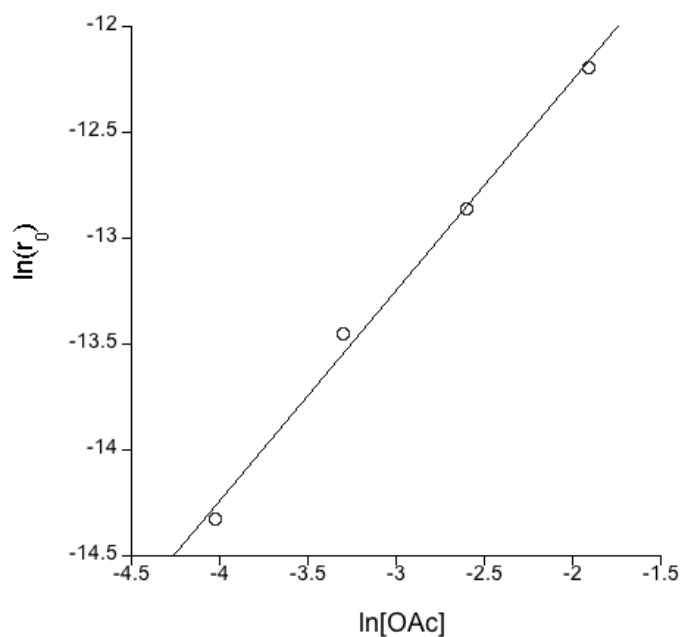
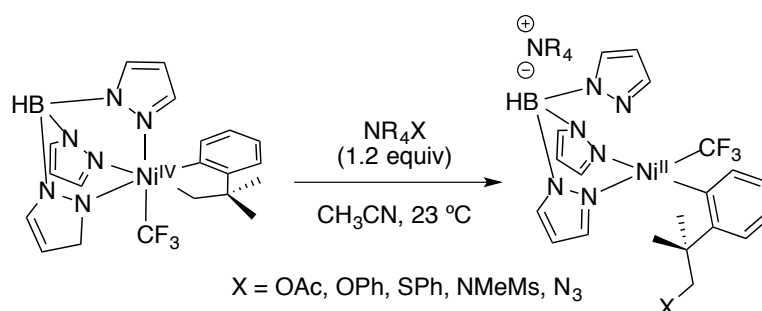


Figure 3.22. Plot of $\ln(r_0)$ versus $\ln([\text{OAc}])$. $y = 0.994x - 10.3$, $R^2 = 0.995$. The slope of the line is approximately 1



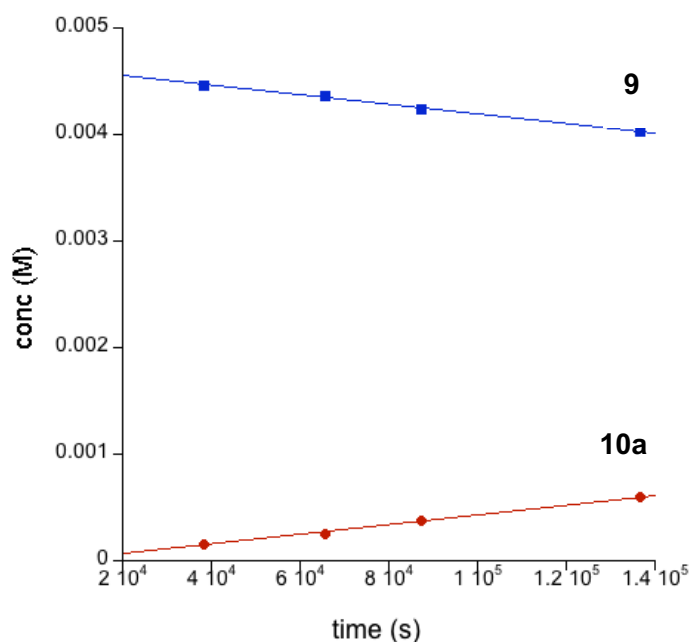
Determining Initial Rates for C–X Bond Formation at 23 °C



Experimental Procedure A: Complex **9** (3.5 mg, 0.0074 mmol, 1.0 equiv) was added to a J-Young valve NMR tube equipped with an O-ring seal. The respective nucleophile, NR_4X , where $X = \text{OAc}, \text{OPh}, \text{N}(\text{Me})(\text{Ms}), \text{N}_3$ (0.0089 mmol, 1.2 equiv), was weighed into a 4 mL vial and then dissolved in CD_3CN (1.6 mL). 3-(Trifluoromethyl)anisole (1.0 μL , 0.0074 mmol, 1.0 equiv) was added as an internal fluorine standard. The resulting solutions were added to the NMR tubes at 23 °C. The rates of reductive elimination were determined by monitoring the first 10% of the reaction progress by ^{19}F NMR spectroscopy at this temperature. Concentration versus time data were acquired from the integration of the CF_3 signals of **9** and **10** with respect to the internal standard. Initial rate values were obtained from the slope of a linear-fit line corresponding to the decay of **9**. A representative reaction profile is shown in Figure 3.23.

Experimental Procedure B: Complex **9** (3.5 mg, 0.0074 mmol, 1.0 equiv) was added to a J-Young valve NMR tube equipped with an O-ring seal. NMe_4SPh (0.0089 mmol, 1.2 equiv) was weighed into a 4 mL vial and dissolved in CD_3CN (1.6 mL). 3-(Trifluoromethyl)anisole (1.0 μL , 0.0074 mmol, 1.0 equiv) was added as an internal fluorine standard. The resulting solution was added to the NMR tube and immediately placed in a liquid nitrogen/ethyl acetate bath (-84 °C). The sample was then placed into an NMR spectrometer where the probe had been pre-set to 23 °C. The rate of reductive elimination was determined by monitoring approximately the first 10% of the reaction by ^{19}F NMR spectroscopy at this temperature. Concentration versus time data were acquired from the integration of the CF_3 signals of **9** and **10c** with respect to the internal standard. Initial rate values were obtained from the slope of a linear-fit line corresponding to the decay of **9**.

Figure 3.23. Initial Rates Plot of Concentration versus Time for Reductive Elimination from **9** to form **10a** at 23 °C. $y_9 = 0.00464 - 4.51e^{-9}x$, $R^2 = 0.996$; $y_{10a} = -2.23e^{-5} + 4.53e^{-9}x$, $R^2 = 0.994$



Nucleophilicity Values

The Swain-Scott nucleophilicity parameters for the various nucleophiles (acetate, phenoxide, thiophenolate, $\text{N}(\text{Me})(\text{Ms})$, and azide) were obtained from a report published by Pearson and co-workers.^{22b} These values are based on an $\text{S}_{\text{N}}2$ reaction between the nucleophiles and CH_3I in CH_3OH at 23 °C and are derived from the following equation:

$$\log \frac{k}{k_0} = ns$$

From this equation, k is the rate constant of a given $\text{S}_{\text{N}}2$ reaction using the nucleophile (X^-), n is the nucleophilicity, and s is the sensitivity. The reference rate constant, k_0 , corresponds to the reaction between CH_3OH and CH_3I . The nucleophilicity parameters for a given reaction are, therefore, defined as follows:

$$n = \log \frac{k_{\text{CH}_3\text{I} + \text{X}^-}}{k_{\text{CH}_3\text{I} + \text{CH}_3\text{OH}}}$$

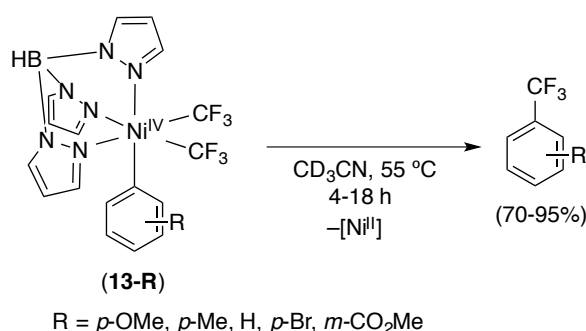
The reported nucleophilicity parameters were plotted vs. our experimental initial rates. The value for $\bar{\text{N}}(\text{Me})(\text{Ms})$ was not available and was, therefore, estimated based on the nucleophilicity value of a related sulfonamide, $\bar{\text{N}}\text{HSO}_2\text{Ph}$.

Table 3.2. Nucleophilicity Parameters and Initial Rate Values for C-X Bond-Formation Reactions from Complex **9** to form **10a-e**

Nucleophile (X^-)	Nucleophilicity (n_{X})	Initial Rate (r_0) (M/s)	$\log(r_0)$
$\bar{\text{OAc}}$	4.30	4.51e-9	-8.34
$\bar{\text{OPh}}$	5.75	8.07e-8	-7.09
$\bar{\text{SPh}}$	9.92	1.01e-5	-4.99
$\bar{\text{N}}(\text{Me})(\text{Ms})^*$	5.10	1.80e-8	-7.74
$\bar{\text{N}}_3$	5.78	2.34e-8	-7.63

*The nucleophilicity value for $\bar{\text{N}}(\text{Me})(\text{Ms})$ is an estimation based on the available n_{X} value for $\bar{\text{N}}\text{HSO}_2\text{Ph}$.

Hammet Plot



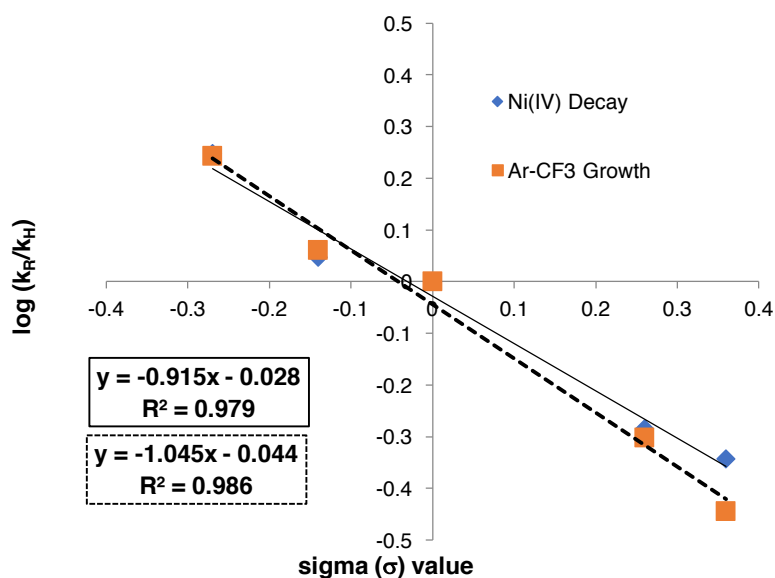
Experimental Procedure: A Teflon-lined screw cap NMR tube was charged with the respective Ni^{IV} complex **13-R** (R = *p*-OMe, *p*-Me, H, *p*-Br, *m*-CO₂Me) (0.010 mmol). 4,4'-Difluorobiphenyl (0.010 mmol, 1.0 equiv) was added as an internal standard. Dry CD₃CN (0.5 mL) was added, and the NMR sample was removed from the glovebox and placed in the NMR spectrometer pre-set to 55 °C. The rates of reductive elimination from complexes **13-R** to form the corresponding benzotrifluoride products were obtained by monitoring the reactions by ¹⁹F NMR spectroscopy at this temperature. Concentration versus time data were acquired from the integration of the ¹⁹F NMR signals of **13-R** and the substituted benzotrifluoride (**Ar-CF₃**) versus the internal standard. The rate constant for each experiment was determined by fitting the decay of **13-R** and the growth of the coupled product (**Ar-CF₃**) to single exponentials. A plot of the Hammett value,⁴² σ , versus $\log(k_{\text{R}}/k_{\text{H}})$ showed a linear correlation ($R^2 = 0.98$) with a negative slope, $\rho = -0.91$ (Figure 3.24, solid line). Rate constants obtained from the growth

of the Ar-CF₃ reductive elimination product gave a similar trend (Figure 3.24, dotted line; $\rho = -1.05$, $R^2 = 0.99$).

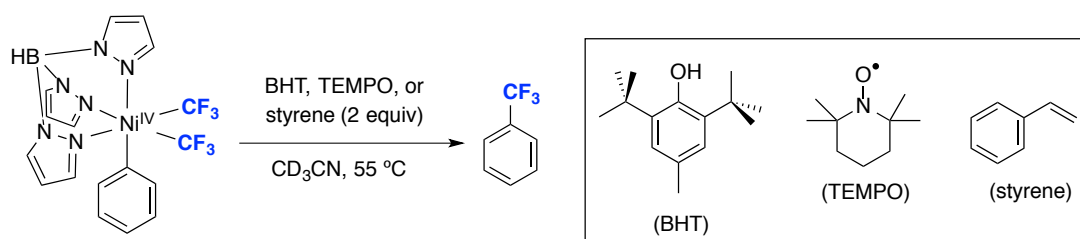
Table 3.3. Summary of Kinetic Data for Reductive Elimination from Complexes **13-R** at 55 °C

Substituent (R)	Hammett Value (σ)	Ni ^{IV} decay k_{obs} ($\times 10^{-4} \text{ s}^{-1}$)	Ar-CF ₃ growth k_{obs} ($\times 10^{-4} \text{ s}^{-1}$)
<i>p</i> -OMe	-0.27	4.6	3.5
<i>p</i> -Me	-0.14	2.9	2.2
H	0	2.6	2.0
<i>p</i> -Br	0.26	1.4	1.0
<i>m</i> -CO ₂ Me	0.36	1.1	0.74

Figure 3.24. Hammett Plot for Reductive Elimination from Ni^{IV} Complexes **13-R** to form the Corresponding Ar-CF₃ Coupled Product at 55 °C. The solid line represents kinetic data obtained from the decay in Ni^{IV} concentration over time, whereas the dotted line represents kinetic data obtained from the growth in Ar-CF₃ concentration over time.



Radical Trap Experiments

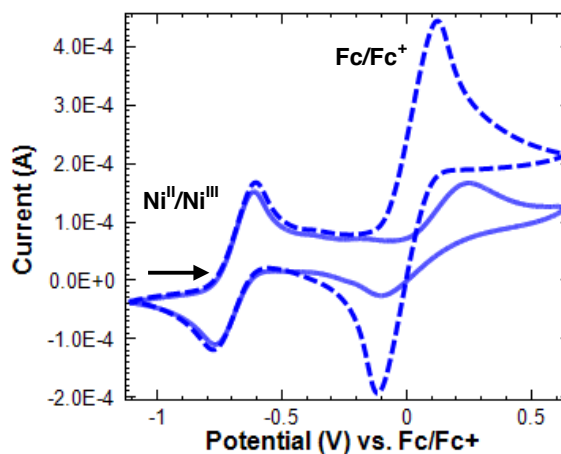
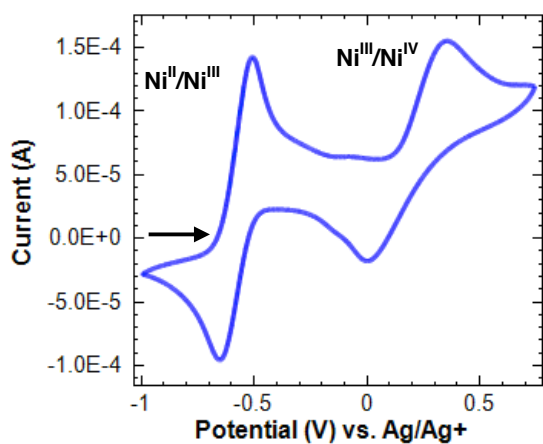


Experimental Procedure: A 4 mL vial was charged with Ni^{IV} complex **13** (4.0 mg, 0.0083 mmol, 1.0 equiv) and the respective radical trap (0.016 mmol, 2.0 equiv). 4,4'-Difluorobiphenyl was added as an internal standard. CD₃CN (0.5 mL) was added, and the resulting yellow solution was transferred to a Teflon-lined screw cap NMR tube and removed from the glovebox. The ratio between the standard and **13** was determined by ¹⁹F NMR integration at room temperature. The NMR tube was heated in an oil bath at 55 °C for 18 h. After the reaction reached completion, the solution was analyzed by ¹⁹F NMR spectroscopy to determine the yield of benzotrifluoride. In all cases, the yield of coupled product was not affected by the presence of radical traps, suggesting that the reductive elimination process does not proceed via radical homolysis.

Table 3.4. Comparison of Ar–CF₃ Yields from the Reductive Elimination of **13** in the Absence and Presence of Radical Traps

Radical Trap	¹⁹ F NMR Yield of Ar-CF ₃ (%)
None	76%
BHT	76%
TEMPO	79%
styrene	70%

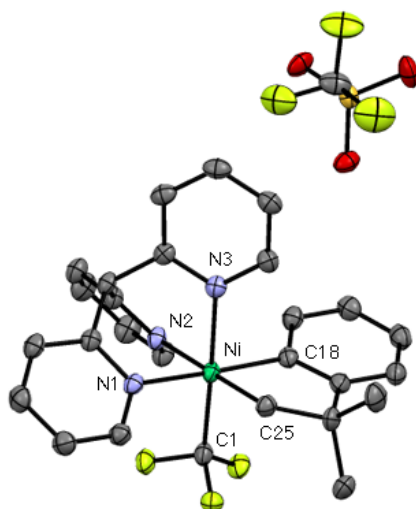
3.4.5. Cyclic Voltammetry Studies



General Procedure: Cyclic voltammetry was performed in a 3-electrode cell consisting of a 3 mm glassy carbon disc working electrode, a Ag/Ag⁺ reference electrode with a Ag wire in a fritted chamber containing a solution of AgBF₄ (0.01 M) and NBu₄BF₄ (0.1 M) in acetonitrile, and a Pt wire counter electrode. A 2 mL solution of the complex (0.01 M) and NBu₄BF₄ (0.1 M) in acetonitrile was added to the electrochemical cell. Cyclic voltammetry scans were taken at 100 mV/s. In order to determine the redox potentials of the complexes against Fc/Fc⁺, ferrocene (0.01 M) was added afterwards as an internal reference.

3.4.6. X-ray Structural Determination

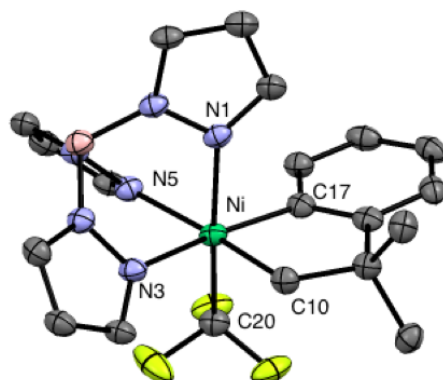
X-ray Crystallography Experimental Data of 6



Yellow block-like crystals of $[(\text{Py}_3\text{CH})\text{Ni}^{\text{IV}}(\text{CH}_2\text{CMe}_2\text{-}o\text{-C}_6\text{H}_4)(\text{CF}_3)(\text{OTf})]$ (**6**) were grown from an acetone solution of the compound at 25 °C. A crystal of dimensions 0.22 x 0.20 x 0.16 mm was mounted on a Rigaku AFC10K Saturn 944⁺ CCD-based X-ray diffractometer equipped with a low temperature device and Micromax-007HF Cu-target micro-focus rotating anode ($\lambda = 1.54187 \text{ \AA}$) operated at 1.2 kW power (40 kV, 30 mA). The X-ray intensities were measured at 85(1) K with the detector placed at a distance 42.00 mm from the crystal. A total of 3955 images were collected with an oscillation width of 1.0° in ω . The exposure time was 1 sec. for the low angle images, 8 sec. for high angle. The integration of the data yielded a total of 83621 reflections to a maximum 2θ value of 136.48° of which 5614 were independent and 5285 were greater than $2\sigma(I)$. The final cell constants were based on the xyz centroids 45119 reflections above $10\sigma(I)$. Analysis of the data showed negligible decay during data collection; the data were processed with CrystalClear 2.0 and corrected for absorption. The structure was solved and refined with the Bruker SHELXTL (version 2008/4) software package, using the space group P2(1)/n with $Z = 4$ for the formula $\text{C}_{31}\text{H}_{31}\text{F}_6\text{N}_3\text{NiO}_4\text{S}$. All non-hydrogen atoms were refined anisotropically with the hydrogen atoms placed in idealized positions. The triflate anion is disordered in two orientations. Full matrix least-squares refinement based on F^2 converged at $R1 = 0.0398$ and $wR2 = 0.1030$ [based on $I > 2\sigma(I)$], $R1 = 0.0418$ and $wR2 = 0.1045$ for all data.

Table 3.5. Selected Bond Lengths (Å) and Angles (°) for **6**

Ni(1)-N(1)	2.057(2)	N(1)-Ni(1)-N(2)	88.04(7)
Ni(1)-N(2)	2.073(2)	N(1)-Ni(1)-N(3)	88.09(7)
Ni(1)-N(3)	2.018(2)	N(1)-Ni(1)-C(18)	174.75(8)
Ni(1)-C(1)	1.956(2)	C(18)-Ni(1)-C(25)	82.27(9)
Ni(1)-C(18)	1.953(2)	C(1)-Ni(1)-C(25)	89.00(9)
Ni(1)-C(25)	2.006(2)	C(1)-Ni(1)-C(18)	92.63(9)

X-ray Crystallography Experimental Data of 9

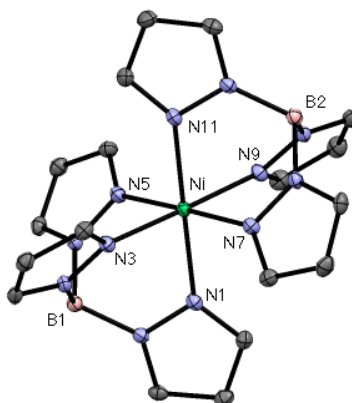
Yellow block-like crystals of **9** were grown from a methanol solution of the compound at 22 °C. A crystal of dimensions 0.19 x 0.06 x 0.02 mm was mounted on a Rigaku AFC10K Saturn 944+ CCD-based X-ray diffractometer equipped with a low temperature device and Micromax-007HF Cu-target micro-focus rotating anode ($\lambda = 1.54187 \text{ \AA}$) operated at 1.2 kW power (40 kV, 30 mA). The X-ray intensities were measured at 85(1) K with the detector placed at a distance 42.00 mm from the crystal. A total of 2028 images were collected with an oscillation width of 1.0° in ω . The exposure times were 1 sec. for the low angle images, 6 sec. for high angle. Rigaku d*trek images were exported to CrysAlisPro for processing and corrected for absorption. The integration of the data yielded a total of 15630 reflections to a maximum 2θ value of 138.58° of which 3185 were independent and 3178 were greater than $2\sigma(I)$. The final cell constants were based on the xyz centroids 13366 reflections above $10\sigma(I)$. Analysis of the data showed negligible decay during data collection. The structure was solved and refined with the Bruker SHELXTL (version 2014/6) software package, using the space group Cc with Z =

4 for the formula $C_{20}H_{22}BF_3N_6Ni$. All non-hydrogen atoms were refined anisotropically with the hydrogen atoms placed in both idealized and refined positions. Full matrix least-squares refinement based on F^2 converged at $R1 = 0.0357$ and $wR2 = 0.0947$ [based on $I > 2\sigma(I)$], $R1 = 0.0375$ and $wR2 = 0.0948$ for all data.

Table 3.6. Selected Bond Lengths (Å) and Angles (°) for **9**

Ni(1)-N(1)	2.019(3)	N(1)-Ni(1)-N(3)	90.99(10)
Ni(1)-N(3)	2.038(3)	C(17)-Ni(1)-N(5)	103.00(14)
Ni(1)-N(5)	2.093(4)	C(20)-Ni(1)-N(1)	172.14(14)
Ni(1)-C(17)	1.931(3)	C(17)-Ni(1)-C(20)	86.18(14)
Ni(1)-C(20)	1.941(3)	C(20)-Ni(1)-C(10)	91.21(14)
Ni(1)-C(10)	2.003(4)	C(10)-Ni(1)-N(1)	92.48(11)

X-ray Crystallography Experimental Data of Tp_2Ni^{II}



Purple polyhedra of $[NiTp_2]$ were grown from an acetonitrile solution of the compound at 25 °C. A crystal of dimensions 0.20 x 0.17 x 0.12 mm was mounted on a Rigaku AFC10K Saturn 944+ CCD-based X-ray diffractometer equipped with a low temperature device and Micromax-007HF Cu-target micro-focus rotating anode ($\lambda = 1.54187$ Å) operated at 1.2 kW power (40 kV, 30 mA). The X-ray intensities were measured at 85(1) K with the detector placed at a distance 42.00 mm from the crystal. A total of 3913 images were collected with an oscillation width of 1.0° in ω . The exposure time was 1 sec. for the low angle images, 6 sec. for high angle. The integration of the data yielded a total of 60418 reflections to a maximum 2θ value of 136.48° of which 3971 were independent and 3913 were greater than $2\sigma(I)$. The final cell

constants were based on the xyz centroids 47130 reflections above $10\sigma(I)$. Analysis of the data showed negligible decay during data collection; the data were processed with CrystalClear 2.0 and corrected for absorption. The structure was solved and refined with the Bruker SHELXTL (version 2008/4) software package, using the space group P2(1)/n with $Z = 4$ for the formula $C_{18}H_{20}B_2N_{12}Ni$. All non-hydrogen atoms were refined anisotropically with the hydrogen atoms placed in a combination of idealized and refined positions. Full matrix least-squares refinement based on F^2 converged at $R1 = 0.0287$ and $wR2 = 0.0815$ [based on $I > 2\sigma(I)$], $R1 = 0.0291$ and $wR2 = 0.0818$ for all data.

Table 3.7. Selected Bond Lengths (Å) and Angles (°) for Tp_2Ni

Ni(1)-N(3)	2.0806(12)	N(3)-Ni(1)-N(11)	92.93(5)
Ni(1)-N(11)	2.0814(12)	N(11)-Ni(1)-N(9)	86.17(5)
Ni(1)-N(9)	2.0855(13)	N(9)-Ni(1)-N(1)	94.22(5)
Ni(1)-N(1)	2.0863(12)	N(1)-Ni(1)-N(5)	86.97(5)
Ni(1)-N(5)	2.0909(12)	N(5)-Ni(1)-N(7)	177.81(5)
Ni(1)-N(7)	2.0982(12)	N(3)-Ni(1)-N(9)	178.81(5)

3.5. References

-
- (1) Adapted with permission from (a) Camasso, N. M.; Sanford, M. S. *Science* **2015**, *136*, 12771. © American Association for the Advancement of Science (b) Bour, J. R.; Camasso, N. M.; Sanford, M. S. *J. Am. Chem. Soc.* **2015**, *137*, 8034. © American Chemical Society
- (2) (a) Meijere, A. d.; Diederich, F. *Metal-Catalyzed Cross-Coupling Reactions*; Wiley-VCH: Weinheim, 2004. (b) Hu, X. *Chem. Sci.* **2011**, *2*, 1867. (c) Rosen, B. M.; Quasdorf, K. W.; Wilson, D. A.; Zhang, N.; Resmerita, A-M.; Garg, N. K.; Percec, V. *Chem Rev.* **2011**, *111*, 1346. (d) Montgomery, J. "Organonickel Chemistry" in *Organometallics in Synthesis: Fourth Manual* Lipshutz, B. H. (Ed.) Wiley, Hoboken, N.J., **2013**, pp. 319-428. (e) Tasker, S. Z.; Standley, E. A.; Jamison, T. F. *Nature* **2014**, *509*, 299. (f) Everson, D. A.; Weix, D. J. *J. Org. Chem.* **2014**, *79*, 4793. (g) Ananikov, V. *ACS Catal.* **2015**, *5*, 1964. (h) Cavalcanti, L. N.; Molander, G. A. *Top. Curr. Chem.* **2016**, *374*, 39. (i) Yamaguchi, J.; Muto, K.; Itami, K. *Top. Curr. Chem.* **2016**, *374*, 55.
- (3) For select examples of nickel catalyzed C–C and C–heteroatom coupling reactions invoking Ni^{III} intermediates, see: (a) Jones, G. D.; Martin, J. L.; McFarland, C.; Allen, O. R.; Hall, R. E.; Haley, A. D.; Brandon, R. J.; Konovalova, T.; Desrochers, P. J.; Pulay, P.; Vicic, D. A. *J. Am. Chem. Soc.* **2006**, *128*, 13175. (b) Zultanski, S.; Fu, G. C. *J. Am. Chem. Soc.* **2011**, *133*, 15362. (c) Hu, X. *Chem. Sci.* **2011**, *2*, 1867. (d) Joshi-Pangu, A.; Wang, C-Y.; Biscoe, M. R. *J. Am. Chem. Soc.* **2011**, *133*, 847. (e) Dudnik, A. S.; Fu, G. C. *J. Am. Chem. Soc.*

- 2012, 134, 10693. (f) Dai, Y. J.; Wu, F.; Zang, Z. H.; You, H. Z.; Gong, H. G. *Chem. Eur. J.* **2012**, 18, 808. (g) Schley, N. D.; Fu, G. C. *J. Am. Chem. Soc.* **2014**, 136, 16588. (h) Aihara, Y.; Tobisu, M.; Fukumoto, Y.; Chatani, N. *J. Am. Chem. Soc.* **2014**, 136, 15509. (i) Wu, X.; Zhao, Y.; Ge, H. *J. Am. Chem. Soc.* **2014**, 136, 1789. (j) Tellis, J. C.; Primer, D. N.; Molander, G. A. *Science* **2014**, 345, 433. (k) Zuo, Z.; Ahneman, D. T.; Chu, L.; Terrett, J. A.; Doyle, A. G.; MacMillan, D. W. C. *Science* **2014**, 345, 437. (l) Cornella, J.; Edwards, J. T.; Qin, T.; Kawamura, S.; Wang, J.; Pan, C-M.; Gianatassio, R.; Schmidt, M. A.; Eastgate, M. D.; Baran, P. S. *J. Am. Chem. Soc.* **2016**, 138, 2174. (m) Gui, Y.-Y.; Sun, L.; Lu, Z.-P.; Yu, D.-G. *Org. Chem. Front.* **2016**, 3, 522. (n) Shields, B. J.; Doyle, A. G. *J. Am. Chem. Soc.* **2016**, 138, 12719.
- (4) For select examples of stoichiometric C–C and C–heteroatom reductive elimination from Ni^{III}, see: (a) Burk, P.; Liu, M.; Miyashita, A.; Grubbs, R.H. *J. Am. Chem. Soc.* **1978**, 100, 2418. (b) Tsou, T. T.; Kochi, J. K. *J. Am. Chem. Soc.* **1978**, 100, 1634. (c) Tsou, T. T.; Kochi, J. K. *J. Am. Chem. Soc.* **1979**, 101, 7547. (d) Amatore, C.; Jutand, A. *Organometallics* **1988**, 7, 2203. (e) Matsunaga, P. T.; Hillhouse, G. L.; Rheingold, A. L. *J. Am. Chem. Soc.* **1993**, 115, 2075. (f) Koo, K.; Hillhouse, G. L. *Organometallics* **1995**, 14, 4421. (g) Koo, K.; Hillhouse, G. L. *Organometallics* **1996**, 15, 2669. (h) Jones, G. D.; McFarland, C.; Anderson, T. J.; Vicic, D. A. *Chem. Commun.* **2005**, 4211. (i) Lin, X. F.; Phillips, D. L. *J. Org. Chem.* **2008**, 73, 3680. (j) Higgs, A. T.; Zinn, P. J.; Sanford, M. S. *Organometallics* **2009**, 28, 6142. (k) Breitenfeld, J.; Woodrich, M.; Hu, X. *Organometallics* **2014**, 33, 5708. (l) Zheng, B.; Tang, F.; Luo, J.; Schultz, J. W.; Rath, N. P.; Mirica, L. M. *J. Am. Chem. Soc.* **2014**, 136, 6499. (m) Cloutier, J-P.; Vabre, B.; Mounang-Soumé, B.; Zargarian, D. *Organometallics* **2015**, 34, 133. (n) Xu, H.; Diccianni, J. B.; Katigbak, J.; Hu, C.; Zhang, Y.; Diao, T. *J. Am. Chem. Soc.* **2016**, 138, 4779.
- (5) For studies proposing the intermediacy of Ni^{IV}, see: (a) Terao, J.; Kambe, N. *Acc. Chem. Res.* **2008**, 41, 1545. (b) Aihara, Y.; Chatani, N. *J. Am. Chem. Soc.* **2013**, 135, 5308. (c) Aihara, Y.; Chatani, N. *J. Am. Chem. Soc.* **2014**, 136, 898. (d) Wu, X.; Zhao, Y.; Ge, H. *J. Am. Chem. Soc.* **2014**, 136, 1789. (e) Yan, S.-Y.; Liu, Y.-J.; Liu, B.; Liu Y.-H.; Zhang, Z.-Z.; Shi, B.-F. *Chem. Commun.* **2015**, 51, 7341.
- (6) For isolated organometallic Ni^{IV} complexes, see: (a) Klein, H.-F.; Bickelhaupt, A.; Jung, T.; Cordier, G. *Organometallics* **1994**, 13, 2557. (b) Klein, H. F.; Bickelhaupt, A.; Lemke, M.; Sun, H. J.; Brand, A.; Jung, T.; Rohr, C.; Florke, U.; Haupt, H. *J. Organometallics* **1997**, 16, 668. (c) Shimada, S.; Rao, M. L. N.; Tanaka, N. *Organometallics* **1999**, 18, 291. (d) Dimitrov, V.; Linden, A. *Angew. Chem., Int. Ed.* **2003**, 42, 2631. (e) Carnes, M.; Buccella, D.; Chen, J. Y. C.; Ramirez, A. P.; Turro, N. J.; Nuckolls, C.; Steigerwald, M. *Angew. Chem., Int. Ed.* **2009**, 48, 290. (f) Martinez, G. E.; Ocampo, C.; Park, Y. J.; Fout, A. R. *J. Am. Chem. Soc.* **2016**, 138, 4290. (g) Schultz, J. W.; Fuchigami, K.; Zheng, B.; Rath, N. P.; Mirica, L. M. *J. Am. Chem. Soc.* **2016**, 138, 12928. (h) Watson, M. B.; Rath, N. P.; Mirica, L. M. *J. Am. Chem. Soc.* **2017**, 139, 35. (i) Meucci, E. A.; Camasso, N. M.; Sanford, M. S. *Organometallics*, **2017**, 36, 247.
- (7) (a) Eisch, J. J.; Piotrowski, A. M.; Han, K. I.; Krüger, C.; Tsay, Y. H. *Organometallics* **1985**, 4, 224. (b) Carmona, E.; Gutiérrez-Puebla, E.; Marín, J. M.; Monge, A.; Paneque, M.; Poveda, M. L.; Ruíz, C. *J. Am. Chem. Soc.* **1989**, 111, 2883. (c) Dubinina, G. G.; Brennessel, W. W.; Miller, J. L.; Vicic, D. A. *Organometallics* **2008**, 27, 3933. (d) Jover, J.; Miloserdov, F. M.; Benet-Buchholz, J.; Grushin, V. V.; Maseras, F. *Organometallics* **2014**, 33, 6531.
- (8) See 4e-g, also: (a) Koo, K.; Hillhouse, G. L.; Rheingold, A. L. *Organometallics* **1995**, 14, 456. (b) Han, R.; Hillhouse, G. L. *J. Am. Chem. Soc.* **1997**, 119, 8135. (c) Koo, K.; Hillhouse, G. L. *Organometallics* **1998**, 17, 2924. (d) Lin, B. L.; Clough, C. R.; Hillhouse, G. L. *J. Am. Chem. Soc.* **2002**, 124, 2890.
- (9) (a) Lyons, T. W.; Sanford, M. S. *Chem. Rev.* **2010**, 110, 1147.

-
- (10) Tomashenko, O. A.; Grushin, V. V. *Chem. Rev.* **2011**, *111*, 4475.
- (11) (a) Menjon, B.; Martínez-Salvador, S.; Gomez-Saso, M. A.; Fornies, J.; Falvello, L. R.; Martín, A.; Tsipis, A. *Chem. Eur. J.* **2009**, *15*, 6371. (b) Ye Y.; Ball, N. D.; Kampf, J. W.; Sanford, M. S. *J. Am. Chem. Soc.* **2010**, *132*, 14682.
- (12) (a) Hansch, C.; Leo, A.; Taft, R. W. *Chem. Rev.* **1991**, *91*, 165. (b) Uneyama, K. *Organofluorine Chemistry*; Blackwell: Oxford, U.K., 2006.
- (13) (a) Appleton, T. G.; Chisholm, M. H.; Clark, H. C.; Manzer, L. E. *Inorg. Chem.* **1972**, *11*, 1786. (b) Appleton, T. G.; Clark, H. C.; Manzer, L. E. *Coord. Chem. Rev.* **1973**, *10*, 335 (c) Holmes, S. A.; Thomas, T. D. *J. Am. Chem. Soc.* **1975**, *97*, 2337.
- (14) Ball, N. D.; Gary, J. B.; Ye Y.; Sanford, M. S. *J. Am. Chem. Soc.*, **2011**, *133*, 7577.
- (15) (a) Yamaguchi, Y.; Ichioka, H.; Klein, A.; Brennessel W. W.; Vivic, D. A. *Organometallics*, **2012**, *31*, 1477. (b) Zhang, C.-P.; Wang, H.; Klein, A.; Biewer, C.; Stirnat, K.; Yamaguchi, Y.; Xu, L.; Gomez-Benitez, V.; Vivic, D. A. *J. Am. Chem. Soc.* **2013**, *135*, 8141. (c) Tang F.; Rath, N. P.; Mirica, L. M. *Chem. Commun.* **2015**, *51*, 3113.
- (16) Pd^{IV} and Pt^{IV} complexes of neutral tridentate ligands: (a) Brown, D. G.; Byers, P. K.; Canty, A. J. *Organometallics* **1990**, *9*, 1231. (b) Byers, P. K.; Canty, A. J.; Skelton, B. W.; White, A. H. *Organometallics* **1990**, *9*, 826. (c) Bennett, M. A.; Canty, A. J.; Felixberger, J. K.; Rendina, L. M.; Sutherland, C.; Willis, A. C. *Inorg. Chem.* **1993**, *32*, 1951. (d) Klaui, W.; Glaum, M.; Wagner, T.; Bennett, M. A. *J. Organomet. Chem.* **1994**, *472*, 355. (e) Bette, M.; Schmidt, J.; Steinborn, D. *Eur. J. Inorg. Chem.* **2013**, 2395. (f) Maleckis, A.; Kampf, J. W.; Sanford, M. S. *J. Am. Chem. Soc.* **2013**, *135*, 6618.
- (17) Pd^{IV} and Pt^{IV} tris(pyrazoyl)borate complexes: (a) O'Reilly, S. A.; White, P. S.; Templeton, J. L. *J. Am. Chem. Soc.* **1996**, *118*, 5684 (b) Canty, A. J.; Jin, H.; Roberts, A. S.; Skelton, B. W.; White, A. H. *Organometallics* **1996**, *15*, 5713. (c) Canty, A. J.; Jin, H.; Penny, J. D. *J. Organomet. Chem.* **1999**, *573*, 30. (d) Reinartz, S.; White, P. S.; Brookhart, M.; Templeton, J. L. *J. Am. Chem. Soc.* **2001**, *123*, 6425. (e) Campora, J.; Palma, P.; del Rio, D.; Carmona, E. *Organometallics* **2003**, *22*, 3345. (f) Campora, J.; Palma, P.; del Rio, D.; Lopez, J. A.; Valerga, P. *Chem. Commun.* **2004**, 1490. (g) Campora, J.; Palma, P.; del Rio, D.; Lopez, J. A.; Alvarez, E. *Organometallics* **2005**, *24*, 3624. (h) Maleckis, A.; Sanford, M. S. *Organometallics* **2011**, *30*, 6617.
- (18) (a) Ma, J.-A.; Cahard, D. *Journal of Fluorine Chemistry* **2007**, *128*, 975. (b) X. Wang, L. Truesdale, Yu, J.-Q. *J. Am. Chem. Soc.* **2010**, *132*, 3648. (c) Zhang, C. *Org. Biomol. Chem.* **2014**, *12*, 6580. (d) Merino, E.; Nevado, C. *Chem. Soc. Rev.* **2014**, *43*, 6598.
- (19) Martínez-García, H.; Morales, D.; Pérez, J.; Puerto, M.; del Río, I. *Chem. Eur. J.* **2014**, *20*, 5821.
- (20) (a) G. A. Luinstra, J. A. Labinger, J. E. Bercaw, *J. Am. Chem. Soc.* **1993**, *115*, 3004. (b) Pawlikowski, A. V.; Getty, A. D.; Goldberg, K. I. *J. Am. Chem. Soc.* **2007**, *129*, 10382. (c) Vedernikov, A. N. *Top. Organomet. Chem.* **2010**, *31*, 101. (d) Marquard, S. L.; Hartwig, J. F. *Angew. Chem. Int. Ed.* **2011**, *50*, 7119 (e) Feller, M.; Diskin-Posner, Y.; Leitun, G.; Shimon, L. J. W.; Milstein, D. *J. Am. Chem. Soc.* **2013**, *135*, 11040. (f) Pérez-Temprano, M. H.; Racowski, J. M.; Kampf, J. W.; Sanford, M. S. *J. Am. Chem. Soc.* **2014**, *136*, 4097. (g) Camasso, N. M.; Pérez-Temprano, M. H.; Sanford, M. S. *J. Am. Chem. Soc.* **2014**, *136*, 12771. (h) Pendleton, I. M.; Pérez-Temprano, M. H.; Sanford, M. S.; Zimmerman, P. M. *J. Am. Chem. Soc.* **2016**, *138*, 6049.
- (21) Higgs, A. T.; Zinn, P. J.; Sanford, M. S. *Organometallics* **2010**, *29*, 5446.
- (22) (a) Swain, C. G.; Scott, C. B. *J. Am. Chem. Soc.* **1953**, *75*, 141. (b) Pearson, R. G.; Sobel, H. R.; Songstad, J. *J. Am. Chem. Soc.* **1968**, *90*, 319.
- (23) In addition to complex **13**, 24% of Ph-CF₃ was also detected in the crude ¹⁹F spectrum. See the Experimental Section for more details.
- (24) A mixture of [Ni-CF₃] compounds is observed at the end of the reaction. After additional

-
- heating, these products converge to NiTp₂ and (MeCN)₂Ni(CF₃)₂.
- (25) The maximum yield of (CD₃CN)₂Ni(CF₃)₂ and NiTp₂ are both 50% respectively.
- (26) Vicic has reported the low yielding (11-22%) formation of aryl-CF₃ upon the treatment of (diphosphine)Ni^{II}(Ph)(CF₃) with Zn salts and/or water over extended reaction times. The nature of the reactive Ni species is unclear in this system. See ref. 7c.
- (27) Ball, N. D.; Gary, J. B.; Ye, Y.; Sanford M. S. *J. Am. Chem. Soc.* **2011**, *133*, 7577.
- (28) The presence of the radical traps styrene, TEMPO, or butylated hydroxytoluene (BHT) did not impact the yield of benzotrifluoride in reductive elimination from **2**. This suggests that reductive elimination does not proceed via a free radical mechanism.
- (29) Another possible pathway for aryl-CF₃ coupling from **13** would be the *in situ* formation of a Ni^{III} intermediate and subsequent reductive elimination from that species. In an attempt to probe for this possibility, we conducted the stoichiometric 1e⁻ chemical reduction of **13-Me** with Cp₂Co and then examined the resulting products. This reaction provided <5% yield of the aryl-CF₃ product along with organic products (CF₃H and toluene) consistent with the formation of free radical intermediates. This suggests strongly against aryl-CF₃ reductive elimination from Ni^{III}.
- (30) Perrin, C. L.; Dwyer, T. J. *Chem. Rev.* **1990**, *90*, 935.
- (31) The treatment of **13** with other nucleophiles such as ⁻F, ⁻SCN, PMe₃, and pyridine did not result in ligand substitution.
- (32) For select examples, see: (a) Wang, S.; Qian, Q. Gong, H. *Org. Lett.* **2012**, *14*, 3352. (b) Zultanski, S.; Fu, G. C. *J. Am. Chem. Soc.* **2013**, *135*, 624. (c) Biswas, S.; Weix, D. J. *J. Am. Chem. Soc.* **2013**, *135*, 16192. (d) Jensen, K. L.; Standley, E. A.; Jamison, T. F. *J. Am. Chem. Soc.* **2014**, *136*, 11145.
- (33) (a) Furuya, T.; Kamlet, A. S.; Ritter, T. *Nature* **2011**, *473*, 470. (b) Ye, Y.; Sanford, M. S. *Synlett* **2012**, *23*, 2005.
- (34) The reaction of complex **17** with PhN₂BF₄ was conducted at 23 °C and then rapidly cooled down to -25 °C to resolve J_{FF} coupling.
- (35) Campora, J.; Gutierrez, E.; Monge, Á.; Palma, P.; Poveda, M. L.; Ruiz, C.; Carmona, E. *Organometallics* **1994**, *13*, 1728.
- (36) Maleckis, A.; Sanford, M. S. *Organometallics* **2014**, *33*, 3831.
- (37) Chen, D.; Ochiai, M. *J. Org. Chem.* **1999**, *64*, 6804.
- (38) Bielawski, M.; Aili, D.; Olofsson, B. *J. Org. Chem.* **2008**, *73*, 4602.
- (39) Ichiishi, N.; Canty, A. J.; Yates, B. F.; Sanford, M. S. *Org. Lett.* **2013**, *15*, 5134.
- (40) Chaumontet, M.; Piccardi, R.; Audic, N.; Hitce, J.; Peglion, J.-L.; Clot, E.; Baudoin, O. *J. Am. Chem. Soc.* **2008**, *130*, 15157.
- (41) Erdelmeier, I.; Tailhan-Lomont, C.; Yadan, J.-C. *J. Org. Chem.* **2000**, *65*, 8152.
- (42) Ritchie, C. D., Sager, W. F. *Prog. Phys. Org. Chem.* **1964**, *2*, 323.

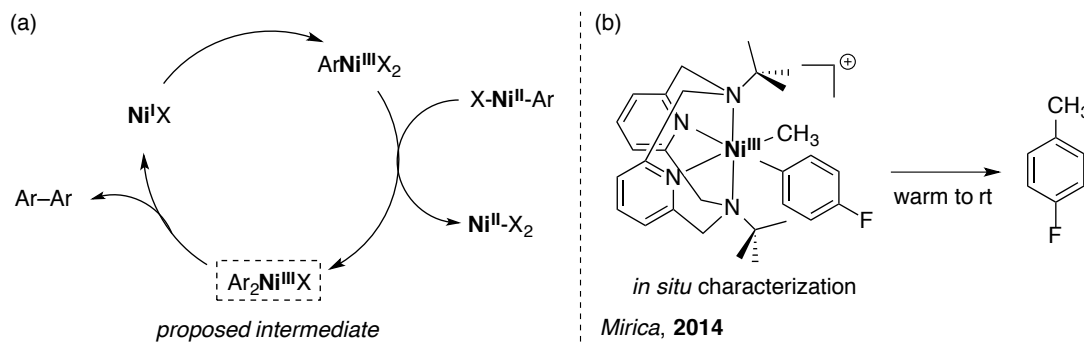
CHAPTER 4

Reactivity Studies of Organometallic Ni^{III} and Ni^{IV} Complexes¹

4.1. Introduction

Over the past several decades there have been numerous proposals that invoke Ni^{III} intermediates in nickel-catalyzed carbon–carbon and carbon–heteroatom bond-forming reactions.^{2,3} Seminal studies by Kochi first implicated transient diorgano-Ni^{III} species in Ni-mediated biaryl coupling (Figure 4.1).⁴ Twenty years later, Hillhouse demonstrated oxidative carbon–heteroatom bond-forming reactivity of cyclometallated Ni^{II} complexes, presumably via Ni^{III} intermediates.⁵ However, in all cases these intermediates were only inferred from reactivity and low temperature cyclic voltammetry studies, and were never directly observed or structurally characterized. The notorious instability of this oxidation state and the presence of paramagnetic species complicate the full understanding of Ni^{III}-mediated transformations. Indeed, examples of well-defined diorgano-Ni^{III} complexes remain rare, and the reactivity of these species towards important bond-forming reactions has largely eluded direct study (Figure 4.1b).^{6,7}

Figure 4.1. (a) Kochi Mechanism for Biaryl Coupling and (b) Stoichiometric Studies by Mirica Demonstrating C–C Coupling from *in situ*-generated Ni^{III}



In comparison to Ni^{III}, the involvement of Ni^{IV} intermediates in nickel-catalyzed transformations is less commonly accepted.⁸ Our lab⁹ and others¹⁰ have begun to investigate the synthesis and reactivity of organometallic Ni^{IV} complexes, providing evidence that these species are competent in carbon–carbon and carbon–heteroatom bond-forming reactions. Despite these contributions, very little work has been done to directly compare the properties of different oxidation states Ni (i.e., Ni^{III} vs. Ni^{IV}).^{7n,p} A fundamental understanding of the relative reactivity, selectivity, and mechanisms of transformations at high-valent nickel complexes would inform the rational development of new nickel-catalyzed reactions.

This chapter describes the synthesis and isolation of organometallic Ni^{III} and Ni^{IV} complexes and studies of their reactivity towards catalytically-relevant bond-forming reactions. We demonstrate that design strategies employed to isolate reactive Ni^{IV} centers (i.e., facially coordinated tridentate scaffolds, cycloneophyl groups, and electronically deactivating trifluoromethyl substituents) additionally serve to stabilize Ni^{III}. Electrochemical analyses and experimental studies provide insight into the relative reactivity of Ni^{III} and Ni^{IV} analogues in mediating carbon–carbon and carbon–heteroatom coupling reactions. In particular, the studies offer preliminary evidence that complementary selectivity can be achieved by accessing distinct oxidation states of nickel.

4.2. Results and Discussion

4.2.1. Carbon–Carbon Coupling Reactions from Diorgano-Ni^{III} Complexes¹

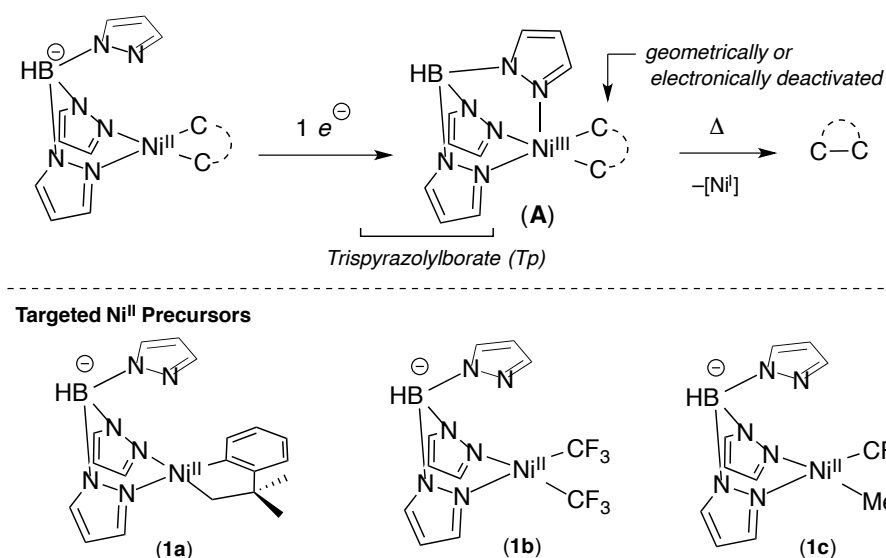
Design and Synthesis of Ni^{II} Precursors

In order to study the fundamental reactivity of traditionally unstable Ni^{III} species, we targeted a model system that implemented a number of key design principles borrowed from our earlier studies at high-valent Ni.⁹ A common design feature in known Ni^{III} and Ni^{IV}

¹Studies in this section were collaborative with James Bour. For the data presented here, James obtained the X-ray structure of complex **2b** and fit the EPR data of **1b** and **2b**.

complexes is that they contain multidentate nitrogen donor ligands that impart rigidity to the metal center.^{6,9} In addition, our lab and others have demonstrated that cyclometallated carbon donor ligands⁵ and perfluoroalkyl groups⁶ add additional stability, owing to their slow reductive eliminations.¹¹ Thus, for our model system we targeted diorgano-Ni^{III} complexes of general structure **A**, bearing a facially coordinated tris(pyrazolyl) borate (Tp) scaffold and traditionally inert carbon donor ligands (Figure 4.2).

Figure 4.2. Targeted Model System for Studying C–C Coupling from Isolable Ni^{III} Complexes

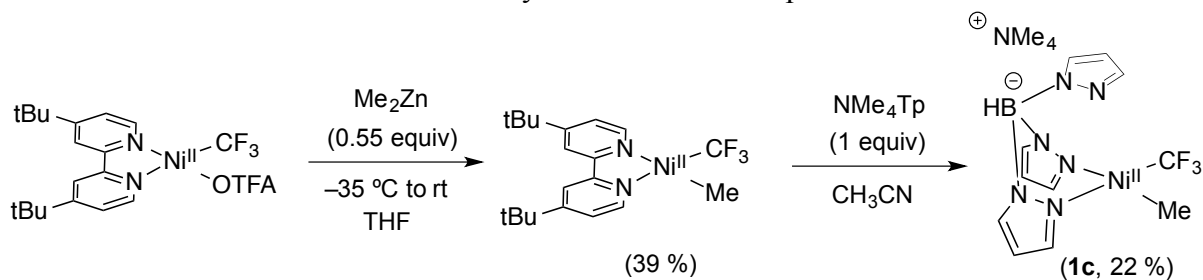


Ni^{II} precursors **1a** and **1b** were selected for our studies based on the aforementioned design criteria. Importantly, complex **1a** contains geometrically constrained ligands whereas **1b** features electronically deactivating trifluoromethyl groups, allowing their structures and reactivities to be compared. These complexes were synthesized from procedures described in Chapter 3. Ni^{II} precursor **1c** was also targeted for high-oxidation state studies as it bears both a trifluoromethyl ligand and a catalytically relevant methyl group.

Complex **1c** was prepared via a multi-step synthetic sequence commencing with the previously reported (dtbpy)Ni(CF₃)(OTFA) starting material (dtbpy = 4,4'-di-*tert*-butylbipyridine; OTFA = trifluoroacetate).^{9b} Transmetalation between (dtbpy)Ni(CF₃)(OTFA) and Me₂Zn at low temperature afforded the penultimate product

(dtbpy)Ni(CF₃)(Me), which was isolated as a bright red solid in 39% yield. The treatment of a 0.044 M solution of (dtbpy)Ni^{II}(CF₃)(Me) in acetonitrile with 1 equiv of NMe₄Tp led to a gradual change in color from dark red to yellow-brown along with concomitant precipitation of dtbpy. The Tp-ligated Ni^{II} precursor **1c** was isolated as a tan solid in 22% yield and was characterized by ¹H, ¹³C, ¹⁹F, and ¹¹B NMR spectroscopy as well as elemental analysis.

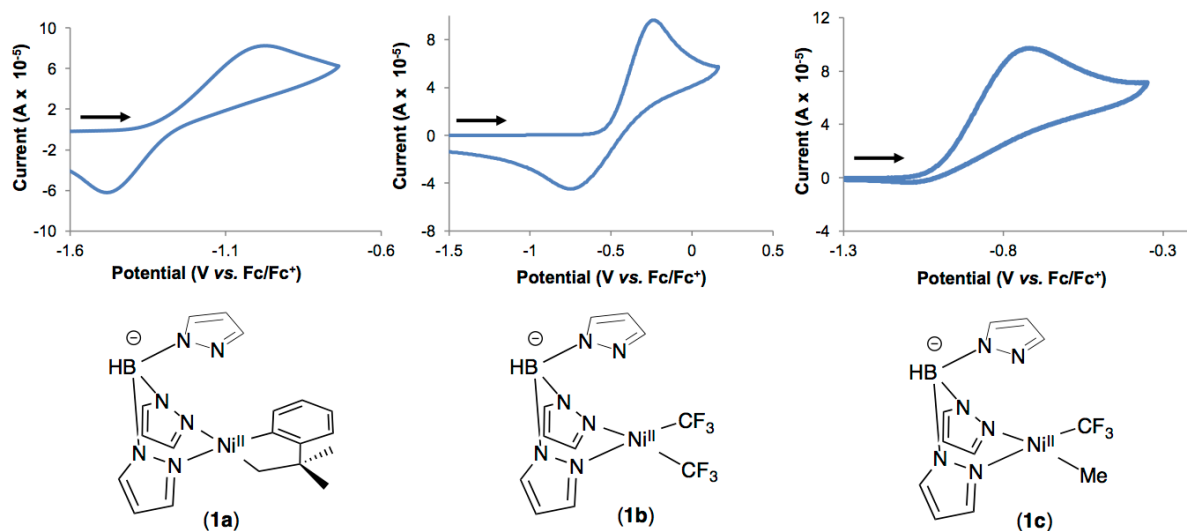
Scheme 4.1. Synthesis of Ni^{II} Complex **1c**



Electrochemical Analyses

The $1e^-$ oxidation of TpNi^{II} complexes **1a-f** was first evaluated using cyclic voltammetry (CV). We anticipated that complexes exhibiting reversible or quasi-reversible $1e^-$ oxidations by CV were most likely to form stable Ni^{III} complexes upon chemical oxidation. As shown in Figure 4.3, complexes **1a** and **1b** show quasi-reversible $1e^-$ oxidative waves, while **1c** exhibits a highly irreversible $1e^-$ oxidation, even at scan rates as high as 500 mV/s. The onset potentials of the Ni^{II/III} couples provide insight into the electronic character of the Ni^{II} complexes. As anticipated, complex **1a** bearing the strongly electron donating cyclometallated ligand has the lowest oxidation potential (-1.1 V vs. Fc/Fc⁺). The electron withdrawing trifluoromethyl ligands in **1b** and **1c** lead to more positive oxidation potentials (-0.5 V, -0.8 V vs. Fc/Fc⁺, respectively).

Figure 4.3. Cyclic Voltammograms of **1a-c** in MeCN. [Ni] = 0.01 M; [NBu₄PF₆] = 0.1 M; Scan Rate = 100 mV/s



One Electron Oxidation Studies

The chemical oxidation of complexes **1a-c** to generate Ni^{III} products **2a-c** was next investigated. Ferrocenium tetrafluoroborate (FcBF₄) was selected as the oxidant for *in situ* EPR and NMR studies due to its solubility in acetonitrile and suitable redox potential. The treatment of **1a** and **1b** with 1 equiv of FcBF₄ at -35 °C resulted in the immediate consumption of the Ni^{II} starting material and subsequent formation of paramagnetic species. These complexes exhibit diagnostic ¹¹B NMR shifts upon oxidation, and these provide a spectroscopic handle for paramagnetic NMR analyses (Scheme 4.2). Moreover, structures **2a** and **2b** were detectable by EPR spectroscopy, and a representative EPR spectrum showing the S = 1/2 Ni^{III} species **2a** is depicted in Figure 4.4.

Scheme 4.2. The *in situ* Generation of Ni^{III} Complexes **2a** and **2b**

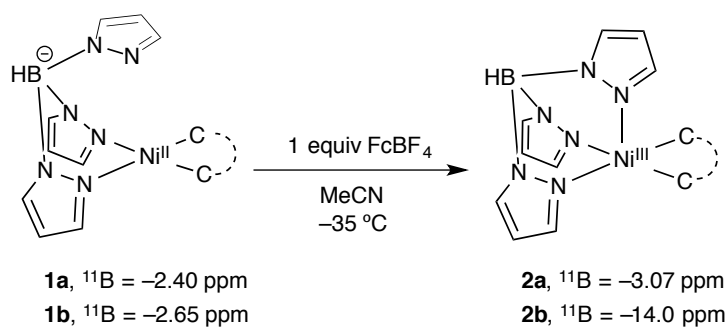
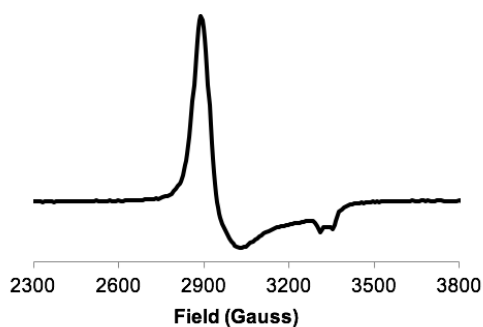


Figure 4.4. EPR Spectrum of **2a** at 98 K in PrCN:MeCN (3:1)



The synthesis and isolation of complexes **2a** and **2b** were carried out with AgBF_4 ($E^0 = -0.04$ vs. Fc/Fc^+) as the oxidant because of the ease at which the insoluble Ag^0 could be removed by filtration at low temperature.¹² Complex **2a** was isolated in 60% yield, and analytically pure samples were obtained via recrystallization from acetonitrile and trace amounts of dimethylformamide at -35 °C. Complex **2b** was purified by column chromatography and subsequently characterized by elemental analysis. The structures of the Ni^{III} complexes **2a** and **2b** were also confirmed by X-ray crystallography and ORTEP representations of both structures are shown in Figure 4.5. In both complexes, the tridentate ligand binds in a κ^3 -fashion, stabilizing the Ni^{III} centers. While **2a** exhibits a slightly disordered square planar geometry, complex **2b** is octahedral with an acetonitrile ligand occupying the sixth coordination site. The formation of the acetonitrile adduct is likely due to the electron-withdrawing trifluoromethyl ligands, which render this Ni^{III} complex more electrophilic than **2a**.

Figure 4.5. Synthesis and ORTEP Structure of Ni^{III} Complex **2a**. Thermal ellipsoids are drawn at 50% probability. Hydrogen atoms and disorder in the methyl groups have been omitted for clarity.

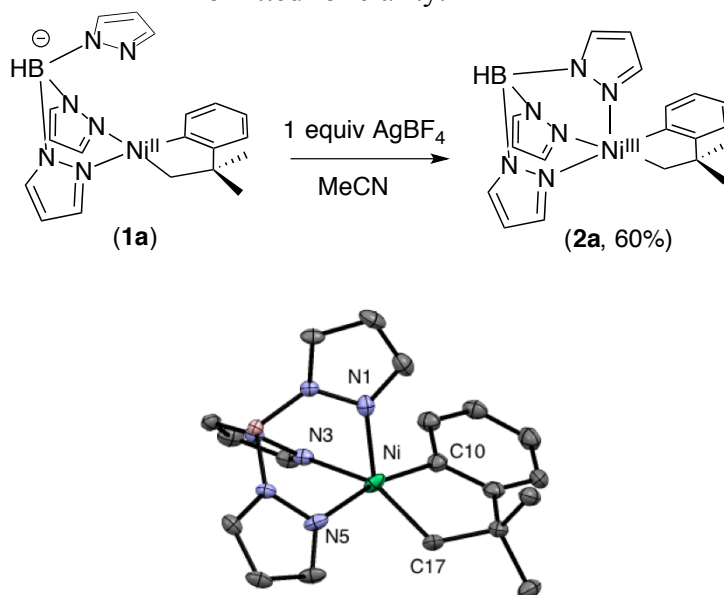
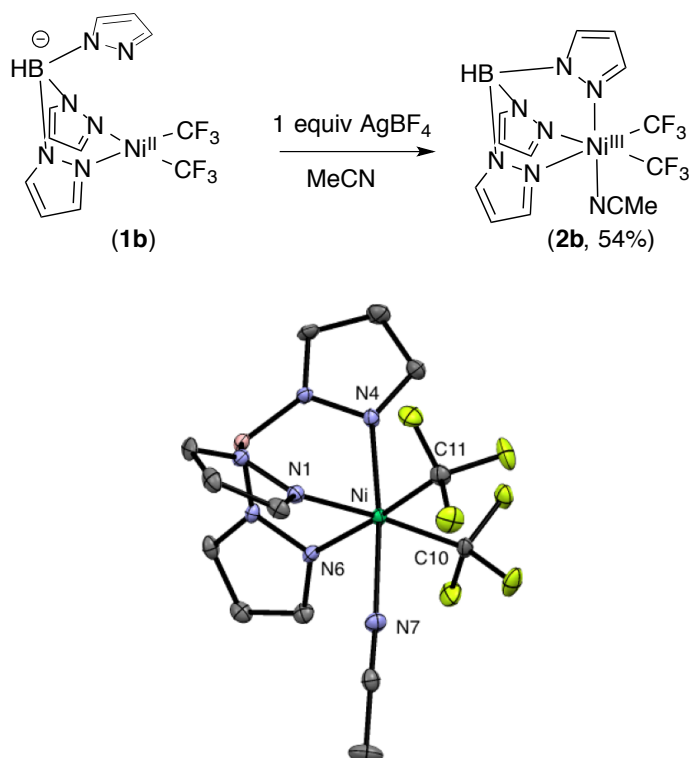


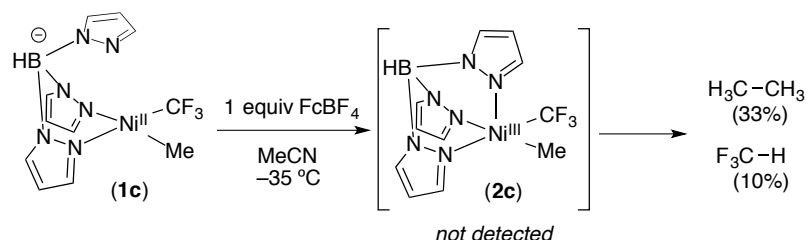
Figure 4.6. Synthesis and ORTEP Structure of Ni^{III} Complex **2b**. Thermal ellipsoids are drawn at 50% probability. Hydrogen atoms have been omitted for clarity.



The corresponding $1e^-$ oxidation of **1c** (conducted at $-35\text{ }^\circ\text{C}$ with FcBF₄ and then immediately frozen at $-196\text{ }^\circ\text{C}$) did not lead to a detectable Ni^{III} product, as determined by EPR

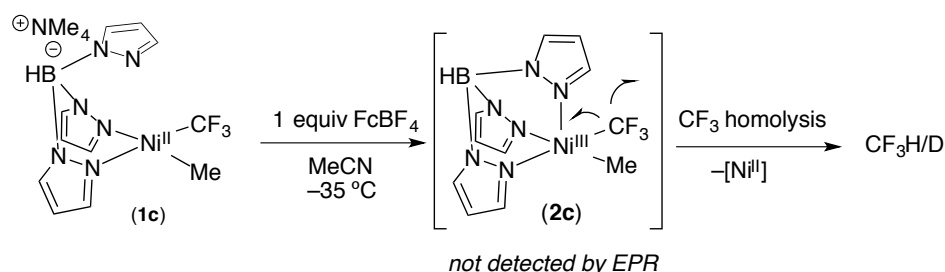
spectroscopy (Scheme 4.3). This observation is consistent with the CV of this complex which shows an irreversible Ni^{II/III} couple (Figure 4.3).

Scheme 4.3. One Electron Oxidation Studies of Complex **1c**



To further probe the instability of this putative Ni^{III} species, *in situ* NMR oxidations were carried out with **1c**. In a closed system, 1 equiv of FcBF₄ was added to a solution of complex **1c** in acetonitrile at -35°C . After 30 min at room temperature, ¹⁹F NMR spectroscopic analysis showed the presence of fluoroform (CF₃H/D) in 10% yield. This is presumably generated via Ni–CF₃ bond homolysis, which is a well-documented decomposition pathway of high-valent Ni complexes (Scheme 4.4).^{6g,h}

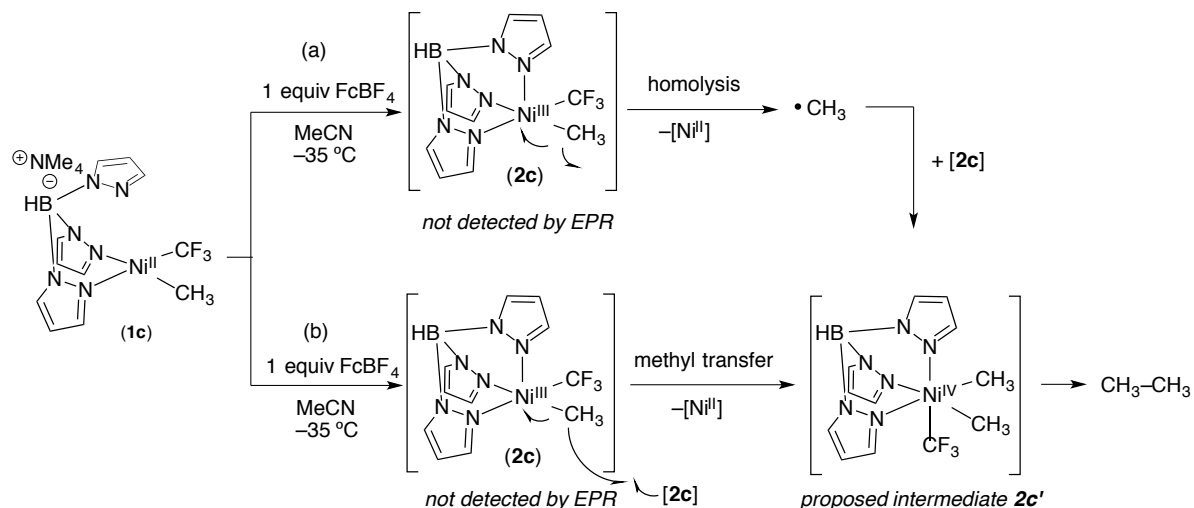
Scheme 4.4. Ni–CF₃ Bond Homolysis from Unstable Ni^{III} Intermediate **2c**



Analysis by ¹H NMR spectroscopy showed the formation of the C–C coupled product, ethane, in 33% yield. Diamagnetic proton resonances corresponding to an unstable Ni^{IV}–CH₃ complex were also observed by ¹H NMR spectroscopy. This complex could be formed via Ni–CH₃ bond homolysis to generate CH₃• which would then combine with another equivalent of **2c** to afford putative Ni^{IV} structure **2c'** (Scheme 4.5a). Alternatively, rapid methyl group transfer from TpNi^{III}(Me)(CF₃) (**2c**) to another molecule of **2c** is also a plausible pathway

(Scheme 4.5b). Related methyl group transfer pathways at Ni centers have been proposed in the literature.^{7m,13}

Scheme 4.5. Plausible Decomposition Pathways of Unstable Ni^{III} Intermediate **2c**



To provide evidence for the formation of a Ni^{IV}-CH₃ intermediate via either of the proposed pathways, an authentic sample of TpNi^{IV}(CH₃)₂(CF₃) (**2c'**) was prepared. The treatment of **1c** with excess MeI at room temperature led to the formation of a diamagnetic complex (proposed species **2c'**) that slowly underwent C-C coupling to form ethane (Scheme 4.6). This complex contains resonances associated with the Ni byproduct of the *in situ* 1 e⁻ oxidation studies of **1c** (Figure 4.7).^{7m} Overall, these results suggest that the instability of Ni^{III} complex **2c** could be attributed to both trifluoromethyl and methyl radical processes.

Scheme 4.6. The Oxidation of **1c** with CH₃I to Generate Proposed Ni^{IV} Complex **2c'**

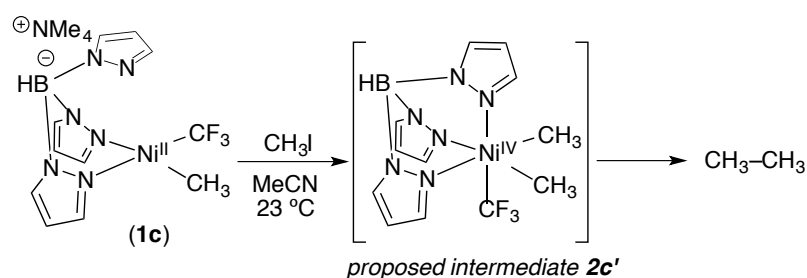
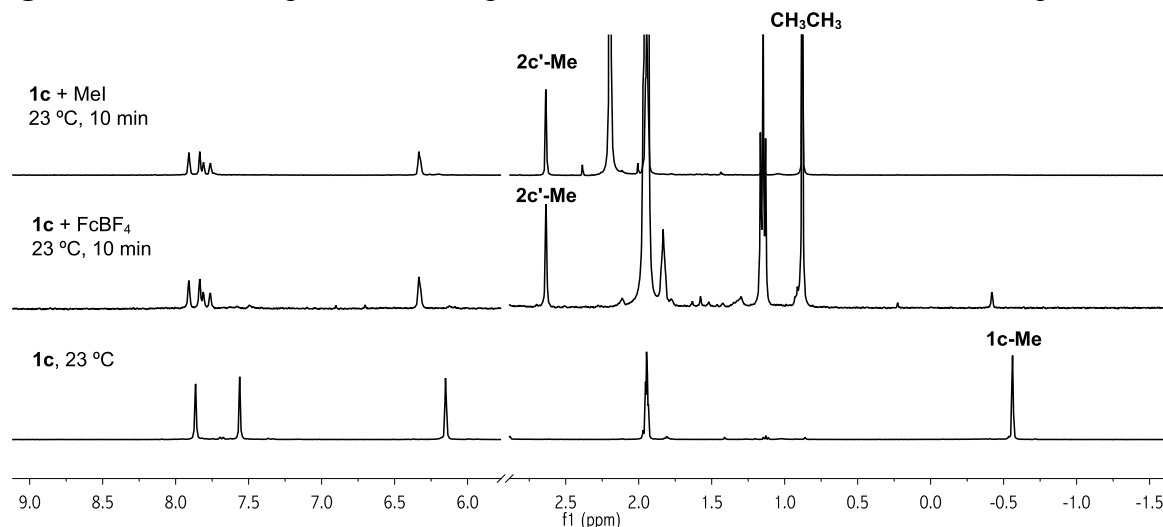


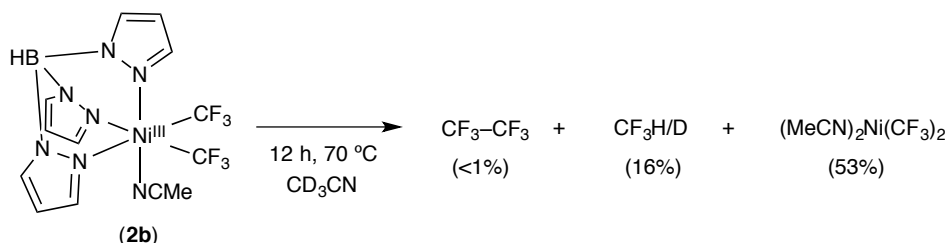
Figure 4.7. ^1H NMR Spectra Providing Evidence for the Formation of $\text{Ni}^{\text{IV}}\text{-Me}$ Species **2c'**



Reductive Elimination Studies

The isolation of Ni^{III} complexes **2a** and **2b** enabled a direct investigation of their reactivity towards C–C bond-forming reductive elimination. $\text{TpNi}(\text{CF}_3)_2(\text{MeCN})$ (**2b**) was inert to reductive elimination processes, as heating an acetonitrile solution of the complex at 70 °C for 12 h led to <1% of the expected coupled product, $\text{F}_3\text{C}-\text{CF}_3$ (Scheme 4.7).¹⁴ Instead, CF_3H (16%) and $[(\text{MeCN})_2\text{Ni}^{\text{III}}(\text{CF}_3)_2]$ (53%) were determined to be the major identifiable products by ^{19}F NMR spectroscopy. These data are consistent with $\text{Ni}^{\text{III}}\text{-CF}_3$ bond homolysis to generate CF_3 radicals, which has significant precedence at Ni^{III} centers.^{6g,h,15}

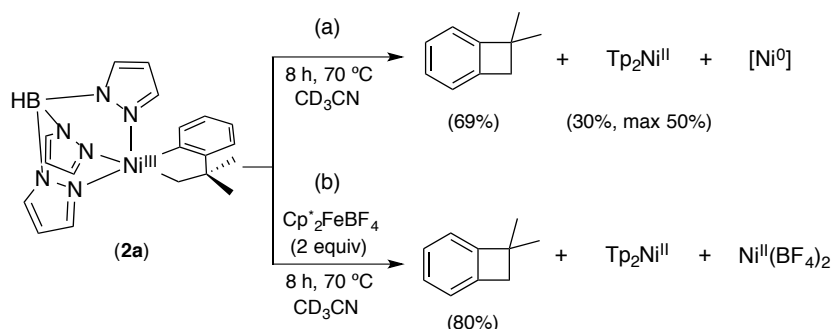
Scheme 4.7. Thermolysis of Ni^{III} Complex **2b**



The thermolysis of the metallacyclic Ni^{III} complex **2a** was next evaluated. Heating complex **2a** at 70 °C for 8 h led to $\text{C}(\text{sp}^3)\text{-C}(\text{sp}^2)$ bond-forming reductive elimination to generate 1,1-dimethyl benzocyclobutane in 69% yield as determined by ^1H NMR spectroscopy

(Scheme 4.8a). Analysis of the crude reaction mixture by paramagnetic ^{11}B NMR spectroscopy revealed the presence of $\text{Tp}_2\text{Ni}^{\text{II}}$ in 30% yield based on nickel (maximum theoretical yield = 50%). We propose that the TpNi^{I} reductive elimination product undergoes disproportionation and ligand exchange to yield $\text{Tp}_2\text{Ni}^{\text{II}}$ and Ni^0 . Notably, disproportionation of Ni^{I} to Ni^{II} and Ni^0 has been reported under similar conditions.^{5e,7i}

Scheme 4.8. Reactivity of Ni^{III} Complex **2a** Towards C–C Coupling in the (a) Absence and (b) Presence of the Weak Oxidant Additive, Cp^*FeBF_4



In a final set of studies, the reactivity of Ni^{III} complex **2a** was evaluated in the presence of a weak $1 e^-$ oxidant, Cp^*FeBF_4 (decamethylferrocenium tetrafluoroborate, = -0.59 mV vs. Fc/Fc^+).¹⁸ We hypothesize that the low yield of **2a** is due to unproductive side reactions between the Ni^{III} starting material and the Ni^{I} reductive elimination product. The addition of a weak oxidant should quench any Ni^{I} species and therefore potentially improve the yield of C–C coupling from Ni^{III} . Consistent with this hypothesis, the addition of 2 equiv of Cp^*FeBF_4 to thermolysis studies of **2a** led to an improved 80% yield of 1,1-dimethyl-benzocyclobutane (Scheme 4.8b).

4.2.2. Comparing the Stability, Reactivity, and Selectivity of Ni^{III} and Ni^{IV} Complexes in Coupling Reactions

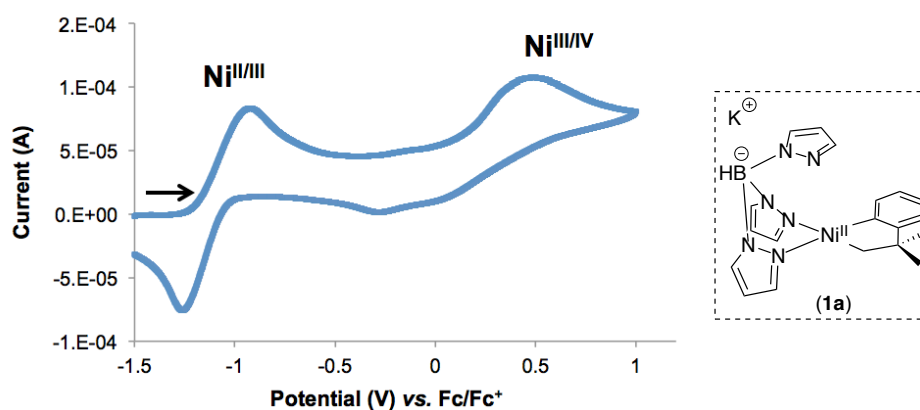
Initial Oxidation Studies

In parallel with studies centered on the isolation and reactivity of organometallic Ni^{III} , efforts were also focused on comparing the reactivity of these complexes to their Ni^{IV}

analogues. Complex **1a** was selected as the model Ni^{II} precursor for these studies due to our previous work with this system that demonstrated the combined stability and catalytically-relevant reactivity of Ni^{III} species **2a**.

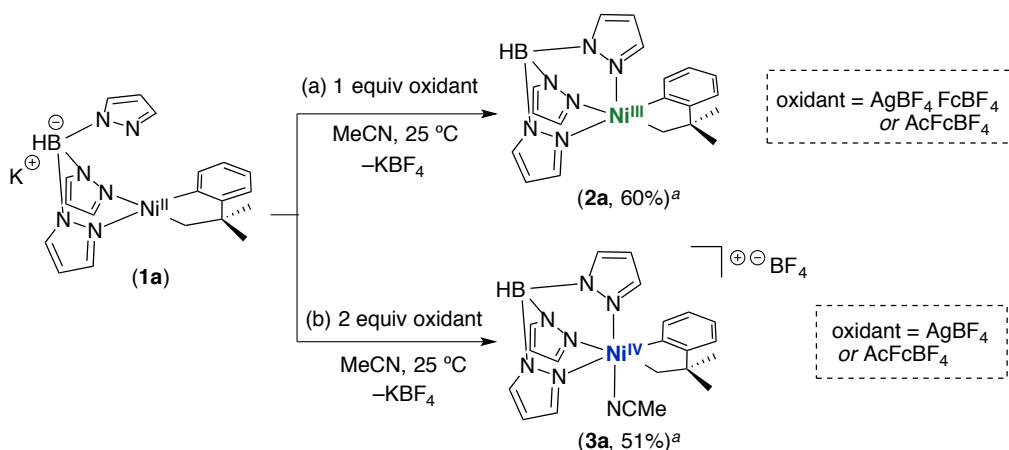
The accessibility and stability of the desired Ni^{IV} analogue was first evaluated by electrochemical analysis. Figure 4.8 displays the cyclic voltammogram (CV) of **1a** in acetonitrile using tetrabutylammonium tetrafluoroborate (NBu₄BF₄) as supporting electrolyte. The full CV of complex **1a** reveals a second oxidation wave (0.1 V vs. Fc/Fc⁺) that we attribute to the Ni^{III/IV} redox couple. The quasi-reversibility of this couple suggests that Ni^{IV} intermediates should be observable and potentially isolable with this ligand system.

Figure 4.8. Cyclic Voltammogram of **1a** in MeCN. [Ni] = 0.01 M, [NBu₄BF₄] = 0.1 M, scan rate = 100 mV/s



The chemical oxidation of **1a** with outer-sphere $1e^-$ oxidants was next investigated. The treatment of an acetonitrile solution of **1a** with 1 equiv of common $1e^-$ oxidants (AgBF₄, FcBF₄, or AcFcBF₄; acetylferrocenium tetrafluoroborate) afforded the previously synthesized Ni^{III} complex **2a** (Scheme 4.9a). Subjecting **1a** to 2 equiv of AgBF₄ or AcFcBF₄ led to the generation of a diamagnetic species consistent with cationic Ni^{IV} complex **3a** (Scheme 4.9b). Complex **3a** was isolated in 51% yield following low temperature filtration of Ag⁰ and was characterized by ¹H, ¹³C, and ¹¹B NMR spectroscopy. Notably, 2 equiv of FcBF₄ did not generate any detectable Ni^{IV} products after 30 min at room temperature.^{12,16} Overall, these results demonstrate the viability of sequential $1e^-$ oxidations at Ni^{II} with outer-sphere oxidants.

Scheme 4.9. Synthesis and Isolation of Ni^{III} Complex **2a** and Ni^{IV} Complex **3a**



^aIsolated yields obtained with AgBF₄ as the oxidant

The X-ray structure of the five-coordinate Ni^{III} complex **2a** shows a slightly distorted square pyramidal geometry, as seen with related Ni^{III} compounds in the literature (see Figure 4.5).^{1,7p} In contrast, Ni^{IV} complex **3a** is found to be octahedral with an acetonitrile group occupying the sixth coordination site, as detected by ¹H NMR spectroscopy (*vide infra*). The difference in coordination between the two complexes is likely related to the enhanced electrophilicity of the cationic Ni^{IV} center. The isolation of these complexes allowed their study towards challenging bond-forming reactions to be directly compared.

Reactivity and Selectivity Studies at Ni^{III} and Ni^{IV}

The impact of the oxidation state on the rates and selectivities of reductive elimination processes at Ni^{III} complex **2a** versus Ni^{IV} complex **3a** was next investigated. Upon heating to 55 °C, complexes **2** and **3** both undergo C(sp³)–C(sp²) bond-forming reductive elimination to form 1,1-dimethyl benzocyclobutane (**4**) in 68% and 93% yield, respectively (Scheme 4.10). The initial rate of this C–C bond-forming reaction at each complex was determined by monitoring the product formation by ¹H NMR spectroscopy at room temperature. As shown in Figure 4.9, the initial rate at cationic Ni^{IV} complex **3a** was approximately one order of magnitude faster than at the Ni^{III} analogue **2a** (3.10e⁻⁷ M/s vs. 3.26e⁻⁸ M/s, respectively, at 25 °C). This dramatic difference in reactivity demonstrates that Ni intermediates in the +4

oxidation state have the potential to promote more facile reductive elimination events than their lower valent counterparts.

Scheme 4.10. C(sp³)-C(sp²) Coupling to form 1,1-dimethyl benzocyclobutane Product **4** from (a) Ni^{III} Complex **2a** and (b) Ni^{IV} Complex **3a** Conducted at 55 °C

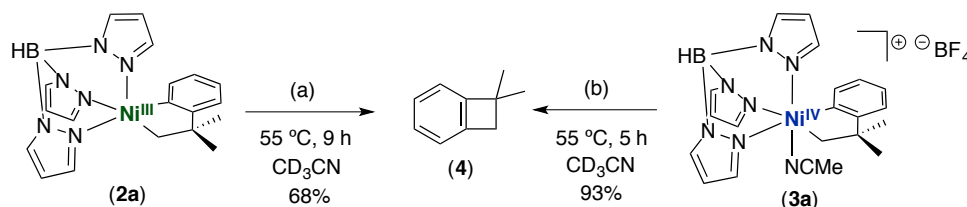
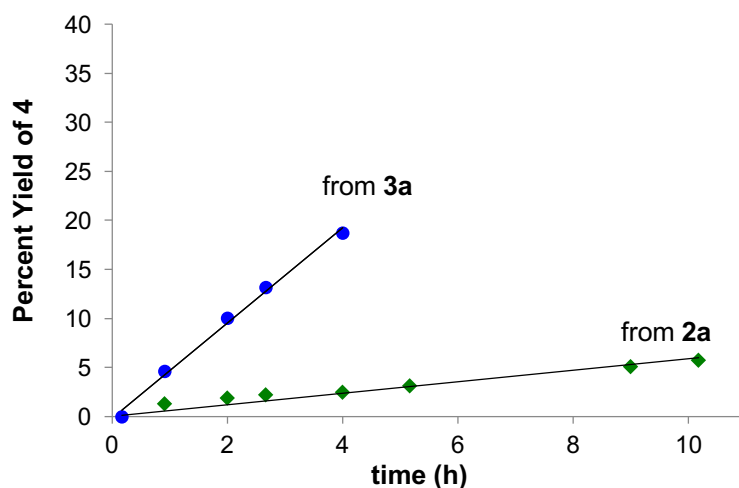


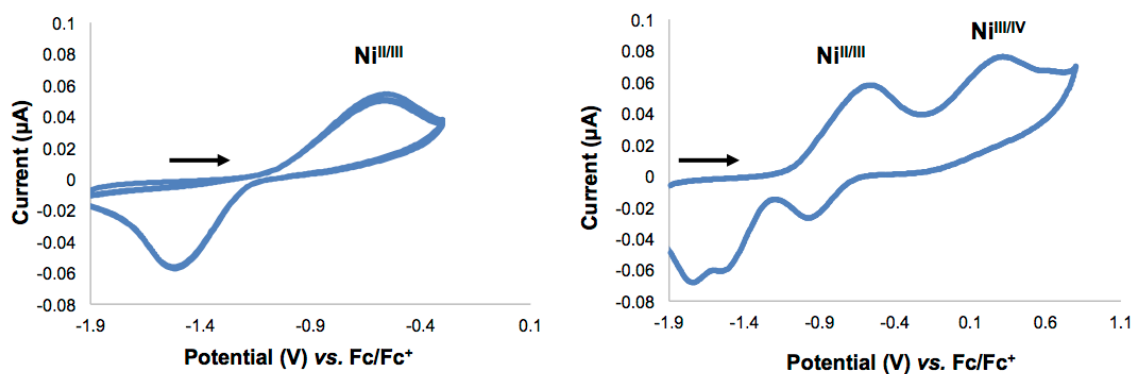
Figure 4.9. Initial Rates Plot for the C–C Coupling Event from **2a** and **3a** Conducted at 25 °C. [Ni] = 0.023 M in MeCN.



The reactivity of these high-valent Ni complexes towards carbon-heteroatom coupling reactions was next investigated. Interestingly, cyclic voltammetry studies of **1a** with tetramethyl ammonium acetate (NMe₄OAc) as the supporting electrolyte revealed dramatic differences in the reversibilities of the Ni^{II/III} and Ni^{III/IV} redox couples. As shown in Figure 4.10, the Ni^{II/III} couple is essentially unaffected by the presence of acetate. In contrast, scanning to higher potentials in NMe₄OAc/MeCN revealed complete irreversibility of the Ni^{III/IV} couple. The loss of reversibility is not observed when non-coordinating anions such as BF₄⁻ or PF₆⁻ serve as the supporting electrolyte (See Figure 4.8). Thus, these studies initially suggested that

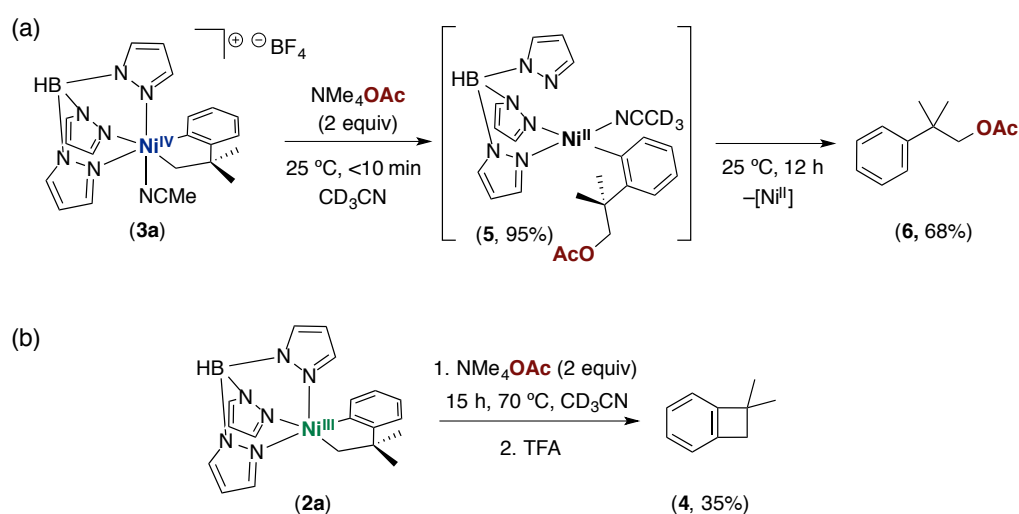
distinct reactivity between the high oxidation state complexes in the presence of nucleophilic coupling partners could be occurring.

Figure 4.10. Cyclic Voltammograms of **1a** with NMe₄OAc as the Supporting Electrolyte in MeCN. [Ni] = 0.01 M, [NMe₄OAc] = 0.1 M in MeCN, Scan rate = 100 mV/s



Based on the electrochemical analyses of **1a**, acetate was used as the nucleophile for reactivity studies. An isolated sample of Ni^{IV} complex **3a** in acetonitrile was subjected to 2 equiv of NMe₄OAc at room temperature for 10 min. Under these conditions, Ni^{II} product **5** was formed in 95% yield as determined by ¹H NMR spectroscopy (Scheme 4.11a). The Ni^{II} product **5** was not sufficiently stable for isolation and instead the σ -aryl ligand underwent protodemetalation to form the organic product **6** in 65% yield after 12 h at room temperature. Importantly, under these conditions <1% of benzocyclobutane (**4**) was detected. This result demonstrates that C(sp³)–O bond-formation occurs with high selectivity over C(sp³)–C(sp²) coupling at this Ni^{IV} center. In addition, these results corroborate our CV studies of **1a**, which initially suggested the instability of Ni^{IV} to nucleophilic anions.

Scheme 4.11. Selectivity Differences as a Function of Oxidation State Demonstrating Preferential (a) C–O Coupling from **3a** and (b) C–C Coupling from **2a** in the Presence of Tetramethyl Ammonium Acetate

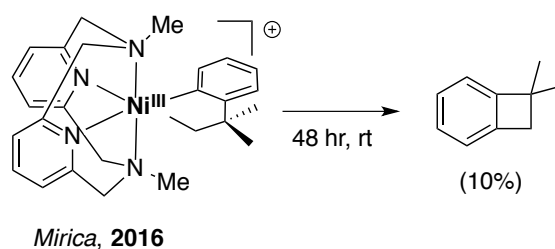


The electrochemical studies of **1a** provided initial support for the stability of the Ni^{III} center to exogenous acetate. Indeed, the reactivity of Ni^{III} complex **2a** proved to be highly complementary to that of **3a**. In the presence of 2 equiv of NMe₄OAc, no reaction was observed after 1 h at room temperature. However, after prolonged heating of the reaction mixture at 70 °C, dimethyl benzocyclobutane (**4**) was determined to be the major product by ¹H NMR spectroscopy (35%, Scheme 4.11b). Treatment of the crude reaction mixture with acid and subsequent analysis by GC/MS also did not show the formation of any products derived from C–O coupling.

The lower yields obtained for benzocyclobutane product **4** under these reaction conditions may be due to decomposition pathways caused by acetate binding to the metal center. For example, previous studies in our lab¹ have demonstrated that octahedral Ni^{III} complexes undergo low-yielding reductive eliminations when compared to related penta-coordinate species. Recent work by Mirica and co-workers have also demonstrated that the octahedral complex (N⁴)Ni^{III}(CH₂CMe₂-*o*-C₆H₄) undergoes very low yielding C–C coupling (~10% yield of 1,1-dimethylbenzocyclobutane, Scheme 4.12) when compared to five-coordinate **2a**. These studies suggest that the reactivity of octahedral Ni^{III} complexes may be

different from their five-coordinate analogues. Thus, in the present system we propose that acetate binds to complex **2a** to generate an octahedral complex, from which C–C coupling is unfavorable.¹⁷

Scheme 4.12. Recent Report by Mirica Demonstrating Low-yielding Benzocyclobutane Formation from an Octahedral Ni^{III} Center.

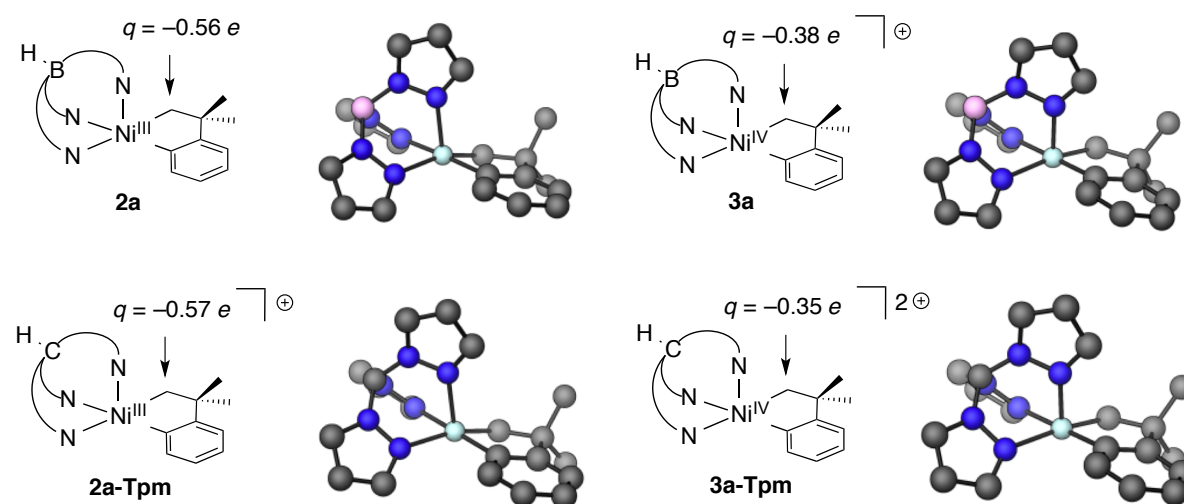


Overall, the selectivity differences observed between **2a** and **3a** demonstrate that complementary reactivity can be achieved by accessing distinct oxidation states of nickel. These results can be attributed to a number of contributing factors including: (1) the enhanced electrophilicity of a Ni^{IV}- σ -alkyl carbon, (2) favorable electrostatic interactions between the cationic Ni^{IV} center and the anionic nucleophile and (3) intrinsic properties of the high-valent metal centers. To begin probing these features, DFT calculations² were carried out to assess the point charges on the σ -alkyl carbon for **2a**, **3a**, and their tris(pyrazolyl) methane (Tpm) derivatives. As shown in Figure 4.11, the point charges on the methylene carbon in Ni^{IV} complexes **3a** and **3a-Tpm** are comparable ($-0.38 e^-$; $-0.35 e^-$), but are significantly more positive than their Ni^{III} analogues (**2a** = $-0.56 e^-$; **2a-Tpm** = $-0.57 e^-$). These data suggest that the oxidation state of the Ni center has a greater effect on the methylene carbon electrophilicity than the overall charge of the complex. We propose that this may contribute, at least in part, to the observed selectivity differences. Future work investigating the reactivity of proposed Ni

² DFT calculations were carried out by visiting research scholar Eric Bowes (University of British Columbia). NBO charges were obtained for geometries optimized at the B3LYP/6-31G(d) level of theory, using the SDD effective core potential for Ni and the PCM solvation model.

complexes **2a-Tpm** and **3a-Tpm** with neutral and anionic coupling partners will be needed to further elucidate the origin of these selectivity differences.

Figure 4.11. Atomic Point Charges on the Methylene Carbon of Complexes **2a**, **2a-Tpm**, **3a**, **3a-Tpm**



4.3. Conclusions

Studies in this chapter were aimed at investigating the synthesis, stability, and reactivity of organometallic Ni^{III} complexes and their Ni^{IV} analogues. Section 4.2.2 established that the combination of tripodal nitrogen donor ligands, electronically deactivating groups, and geometrically constrained scaffolds were effective for the stabilization of reactive Ni^{III} centers. Direct observation of C–C coupling was achieved from a crystallography characterized cycloneophyl-Ni^{III} complex, demonstrating one of the first examples of this transformation.

In section 4.2.3, the comparative reactivity of Ni^{III} and Ni^{IV} complexes was evaluated through electrochemical analyses, kinetic studies, and competition experiments. Throughout these studies, Ni^{IV} was shown to promote reductive elimination events more readily than analogous Ni^{III} complexes. In addition, selective carbon–carbon or carbon–heteroatom coupling could be achieved depending on the oxidation state of the nickel center. Overall, the

studies described herein demonstrate the feasibility of bond-forming reactions from high-valent nickel model systems and the complementary reactivity of the distinct oxidation states.

4.4. Experimental Procedures and Characterization of Compounds

4.4.1. General Procedures and Materials and Methods

General Procedures

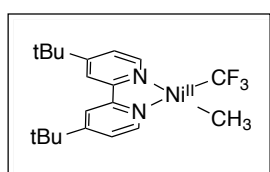
All manipulations were performed inside an N₂ filled glovebox unless otherwise noted. NMR spectra were obtained on a Varian VNMR 700 (699.76 MHz for ¹H; 175.95 MHz for ¹³C) or a Varian VNMR 500 (500.09 MHz for ¹H; 470.56 MHz for ¹⁹F; 125.75 MHz for ¹³C; 225 MHz for ¹¹B) spectrometer. ¹H and ¹³C NMR chemical shifts are reported in parts per million (ppm) relative to TMS, with the residual solvent peak used as an internal reference. ¹⁹F NMR chemical shifts are reported in ppm relative to CCl₃F. ¹¹B NMR spectra are referenced to BF₃Et₂O. Abbreviations used in the NMR data are as follows: s, singlet; d, doublet; t, triplet; q, quartet; m, multiplet; bq, broad quartet; br, broad signal. Yields of reactions that generate fluorinated products were determined by ¹⁹F NMR analysis using a relaxation delay of 12 s. Quantitative ¹¹B NMR were recorded according to the literature¹⁸ at a 90° pulse angle with a 125 s relaxation delay (longest T₁ = 23 s) and a 10 s acquisition period and were checked against a calibration curve. Magnetic susceptibilities were determined by the Evans method in CH₃CN at 23 °C on a 700 MHz spectrometer.¹⁹ Mass spectral data were obtained on a Micromass magnetic sector mass spectrometer in electrospray ionization mode. Elemental analyses were conducted by Midwest Microlabs. Cyclic voltammetry was performed using a CHI600C potentiostat from CH instruments. EPR spectra were collected at -176 °C using a Bruker EMX ESR spectrometer with a nitrogen-cooled Cryostat. X-ray crystallographic data were collected on a Bruker SMART APEX-I CCD-based X-ray diffractometer. Flash chromatography was performed using a Biotage Isolera One system with cartridges containing high performance silica gel.

Materials and Methods

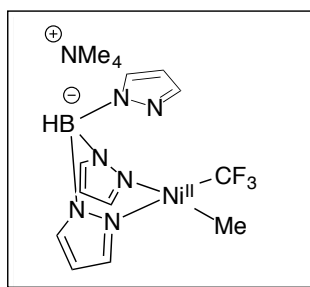
The following compounds were prepared via literature procedures: (PPh₃)₂Ni(CF₃)(OTFA),²⁰ (dtbpy)Ni(CF₃)(OTFA),^{9b} NMe₄[(Tp)Ni^{II}(CF₃)₂],^{9b} K[(Tp)Ni^{II}(CH₂CMe₂-*o*-C₆H₄)].^{9b} AgBF₄ was purchased from Strem Chemicals. 4,4'-*di-tert*-butylbipyridine (dtbpy), ZnMe₂ (1.2 M solution in toluene), and ferrocenium tetrafluoroborate (FcBF₄) were purchased from Aldrich. 4,4'-difluorobiphenyl was purchased from Oakwood Chemicals. Potassium trispyrazolyl borate (KTP) was purchased from Alfa Aesar. Electrochemical studies were performed with

electrochemical grade NBu_4BF_4 or NMe_4OAc , which were purchased from Aldrich. NBu_4BF_4 was used without further purification and NMe_4OAc was dried at $70\text{ }^\circ\text{C}$ overnight under vacuum. Pentane (Fisher), diethyl ether (EMD), and tetrahydrofuran (Fisher) were deaerated via a N_2 sparge and were purified by a solvent purification system. Acetonitrile (Acros) was sparged and used without further purification. CD_2Cl_2 , and CD_3CN were obtained from Cambridge Isotopes Laboratories and were stored over activated 4 \AA molecular sieves (EMD Millipore). Basic alumina (Aldrich) was dried for 48 h under vacuum at $210\text{ }^\circ\text{C}$. Celite was dried for 12 h under vacuum at $100\text{ }^\circ\text{C}$. Unless otherwise noted, all glassware was dried overnight in an oven at $150\text{ }^\circ\text{C}$ and cooled under an inert atmosphere before use. All commercial reagents were used without further purification/drying unless explicitly stated in the experimental section. Unless otherwise noted, all manipulations were performed under an inert atmosphere in a N_2 glovebox.

4.4.2. Synthesis and Characterization of Compounds

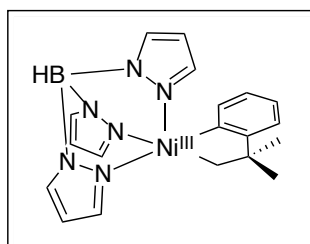


Synthesis of $[(\text{dtbpy})\text{Ni}^{\text{II}}(\text{CF}_3)(\text{Me})]$: A 150 mL round bottom flask was charged with $(\text{dtbpy})\text{Ni}^{\text{II}}(\text{CF}_3)(\text{OTFA})^{\text{9b}}$ (600 mg, 1.18 mmol, 1.0 equiv), and the yellow solid was dissolved in THF (60 mL). The resulting yellow-orange solution was cooled to $-35\text{ }^\circ\text{C}$, and then ZnMe_2 (0.55 mL of a 1.2 M solution in toluene, 0.55 equiv) was added. The reaction mixture was allowed to warm to room temperature over approximately 5 min, during which time the solution changed color from dark orange to dark red. The solution was then filtered through a 3 cm pad of basic alumina, and the pad was washed with THF (5 mL). The washes were combined, and the volatiles were removed under reduced pressure. The resulting dark red residue was triturated with pentane (10 mL), and the solids were collected by filtration. The solids were washed with additional pentane (40 mL) and then dried under reduced pressure to yield the title compound as a red solid (189 mg, 39% yield). ^1H NMR (700 MHz, CD_2Cl_2 , $23\text{ }^\circ\text{C}$): δ 8.82 (d, $J_{\text{HH}} = 6.0\text{ Hz}$, 1H), 8.45 (d, $J_{\text{HH}} = 6.0\text{ Hz}$, 1H), 7.93-7.83 (multiple peaks, 2H), 7.51-7.43 (multiple peaks, 2H), 1.42 (s, 18H), -0.01 (s, 3H). ^{13}C NMR (176 MHz, CD_2Cl_2 , $23\text{ }^\circ\text{C}$): δ 163.06, 162.56, 155.68, 153.73, 151.03, 148.07, 142.05 (Ni- CF_3 shift extracted from ^{19}F - ^{13}C HMBC spectrum) 123.59, 122.99, 117.38, 117.20, 29.91, -6.26 . ^{19}F NMR (377 MHz, CD_2Cl_2 , $23\text{ }^\circ\text{C}$): δ -24.65 (s, 3F). Elemental Analysis calcd for $\text{C}_{20}\text{H}_{27}\text{F}_3\text{N}_2\text{Ni}$, C: 58.43, H: 6.62, N: 6.81; found, C: 58.33, H: 6.28, N: 6.72.



Synthesis of $\text{NMe}_4[\text{(Tp)Ni}^{\text{II}}(\text{CF}_3)(\text{Me})]$ (1c**)** A 20 mL vial was charged with $(\text{dtbpy})\text{Ni}^{\text{II}}(\text{CF}_3)(\text{Me})$ (180 mg, 0.44 mmol, 1.0 equiv), and the red solid was dissolved in a minimal amount of acetonitrile (10 mL). A solution of NMe_4Tp (132 mg, 0.46 mmol, 1.05 equiv) in acetonitrile (3 mL) was added, and the resulting dark orange solution immediately changed color to yellow-brown. Over

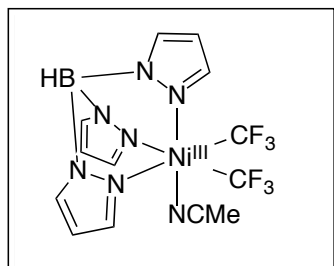
the course of approximately 5 min, 4,4'-di-*tert*-butylbipyridine (dtbpy) precipitated from solution in the form of a white crystalline solid. The solution was concentrated to approximately 3 mL, which led to further precipitation of dtbpy. The precipitate was collected on a fritted filter and washed with acetonitrile (5 mL). The filtrate was collected and concentrated under reduced pressure. The resulting brown residue was washed with diethyl ether (3 x 10 mL) and pentane (3 x 10 mL) and the remaining solids were collected to afford complex **1c** as a light tan powder (41 mg, 22% yield). ^1H NMR (700 MHz, CD_3CN , 23 °C): δ 7.88 (br, 3H), 7.58 (br, 3H), 6.17 (br, 3H), 5.10-4.43 (bq, *B-H*, 1H), 3.07 (s, 12H), -0.54 (s, 3H). ^{13}C NMR (176 MHz, CD_3CN , 23 °C): δ 140.72, 140.50 (Ni- CF_3 shift extracted from ^{19}F - ^{13}C HMBC spectrum), 134.79, 103.83, 55.88, -9.01. ^{11}B NMR (225 MHz, CD_3CN , 23 °C): δ -2.55 (d, $J_{\text{BH}} = 113$ Hz, *B-H*). ^{19}F NMR (471 MHz, CD_3CN , 23 °C): δ -23.22 (s, 3F). Elemental Analysis calcd for $\text{C}_{15}\text{H}_{25}\text{BF}_3\text{N}_7\text{Ni}$, C: 41.91, H: 5.86, N: 22.81; found, C: 41.46, H: 6.05, N: 22.59.



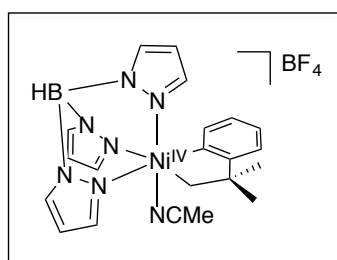
Synthesis of $[(\text{Tp})\text{Ni}^{\text{III}}(\text{CH}_2\text{CMe}_2\text{-}o\text{-C}_6\text{H}_4)]$ (2a**)** In a glovebox, a 20 mL vial was charged with $\text{K}[(\text{Tp})\text{Ni}^{\text{II}}(\text{CH}_2\text{CMe}_2\text{-}o\text{-C}_6\text{H}_4)]^{\text{9a}}$ (180 mg, 0.41 mmol, 1.0 equiv). The yellow solid was dissolved in acetonitrile (10 mL), and a solution of AgBF_4 (78 mg, 0.41 mmol, 1.0 equiv) in acetonitrile (5 mL) was added at -35 °C. The orange

solution immediately turned dark red, with concomitant precipitation of a Ag mirror. The crude reaction mixture was then filtered through a celite plug. The plug was washed with acetonitrile (5 mL), and the filtrates were combined and concentrated to approximately 3 mL. Orange crystals precipitated from the solution over the course of 10 min. These crystals were collected, washed with acetonitrile (5 mL), and dried under vacuum to afford **2a** as an orange solid (98 mg, 60% yield). Samples for elemental analysis were obtained by cooling a saturated solution of **2a** in acetonitrile to -35 °C to obtain orange-red crystals of **2a**. ^{11}B NMR (225 MHz, CD_3CN , 23 °C): δ -3.07 (br, *B-H*). Elemental Analysis calcd for $\text{C}_{19}\text{H}_{22}\text{BN}_6\text{Ni}$, C: 56.50, H: 5.49, N:

20.81; found, C: 56.63, H: 5.52, N: 20.83. HRMS-electrospray (m/z): $[M]^+$ calcd. for $C_{19}H_{22}BN_6Ni$, 403.1352; found, 403.1352.

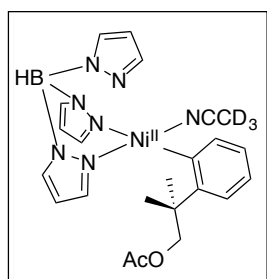


Synthesis of $[(Tp)Ni^{III}(CF_3)_2(MeCN)]$ (2b**)** In the glovebox, a 20 mL vial was charged with $(MeCN)_2Ni^{II}(CF_3)_2$ (150 mg, 0.54 mmol, 1.0 equiv). The solid was dissolved in acetonitrile (8 mL). A solution of NMe_4Tp (163 mg, 0.57 mmol, 1.05 equiv) in acetonitrile (3 mL) was added, and the yellow-brown solution immediately turned orange-brown. A solution of $AgBF_4$ (105 mg, 0.54 mmol, 1.0 equiv) in acetonitrile (2 mL) was then added to the reaction mixture at $-35\text{ }^\circ\text{C}$. The orange-brown reaction mixture immediately changed color to purple, with concomitant formation of a Ag mirror. The crude reaction mixture was removed from the glovebox and filtered through a celite plug. The celite plug was washed with acetonitrile (10 mL), and the combined filtrates were concentrated to dryness under reduced pressure. The crude purple-brown solid was purified further by flash chromatography on silica gel (mobile phase: hexanes/ethyl acetate with a gradient from 90:10 to 80:20). Compound **2b** was obtained as a purple solid (132 mg, 54% yield). ^{11}B NMR (225 MHz, CD_3CN , $23\text{ }^\circ\text{C}$): δ -14.03 (br). Elemental Analysis calcd. for $C_{13}H_{13}BF_6N_7Ni$, C: 34.64, H: 2.91, N: 21.75; found, C: 34.80, H: 2.98, N: 21.77.



Synthesis of $[(Tp)Ni^{IV}(CH_2CMe_2\text{-}o\text{-}C_6H_4)(MeCN)]BF_4$ (3a**):** In the glovebox, a 20 mL vial was charged with $K[(Tp)Ni^{II}(CH_2CMe_2\text{-}o\text{-}C_6H_4)]$ (150 mg, 0.34 mmol, 1.0 equiv). The yellow solid was dissolved in acetonitrile (10 mL), and a solution of $AgBF_4$ (134 mg, 0.69 mmol, 1.0 equiv) in acetonitrile (5 mL) was added at $-35\text{ }^\circ\text{C}$. The orange solution immediately turned dark red, with concomitant precipitation of Ag^0 . The crude reaction mixture was then filtered through a celite plug. The plug was washed with acetonitrile (5 mL), and the filtrates were combined and concentrated to approximately 2 mL. Red-orange crystals precipitated from the solution over the course of 15 min. These crystals were collected, washed with acetonitrile (5 mL), and dried under vacuum to afford **3a** as a red-orange solid (91 mg, 51% yield). 1H NMR (700 MHz, CD_3CN , $23\text{ }^\circ\text{C}$) δ 8.18 (d, $J_{HH} = 2.0$ Hz, 1H), 8.13 (d, $J_{HH} = 2.0$ Hz, 1H), 7.99 (d, $J_{HH} = 2.3$ Hz,

1H), 7.97 (d, $J_{\text{HH}} = 2.3$ Hz, 1H), 7.86 (d, $J_{\text{HH}} = 2.3$ Hz, 1H), 7.26 (t, $J_{\text{HH}} = 7.2$ Hz, 1H), 7.19 (d, $J_{\text{HH}} = 7.7$ Hz, 1H), 6.94 (t, $J_{\text{HH}} = 7.7$ Hz, 1H), 6.77 (d, $J_{\text{HH}} = 2.3$ Hz, 1H), 6.74 (d, $J_{\text{HH}} = 7.7$ Hz, 1H), 6.55 (d, $J_{\text{HH}} = 2.3$ Hz, 1H), 6.49 (s, 1H), 6.22 (s, 1H), 6.09 (d, $J_{\text{HH}} = 3.8$ Hz, 1H), 6.00 (d, $J_{\text{HH}} = 3.8$ Hz, 1H), 4.61 (bq, B-H) 2.36 (s, 2H), 1.96 (s, 3H), 1.68 (s, 3H), 1.59 (s, 3H). ^{13}C NMR (176 MHz, CD_3CN , 0 °C) δ 154.20, 151.08, 143.77, 141.80, 141.62, 138.08, 136.50, 136.07, 132.52, 128.97, 127.94, 127.49, 107.86, 107.15, 106.96, 87.40, 48.24, 31.38, 28.50. ^{11}B NMR (225 MHz, CD_3CN , 23 °C) δ -1.18 (s, BF_4), -4.38 (d, $J_{\text{BH}} = 98$ Hz, B-H). ^{19}F NMR (471 MHz, CD_3CN , 23 °C) δ -151.95. HRMS-electrospray (m/z): $[\text{M}]^+$ calcd. for $\text{C}_{21}\text{H}_{25}\text{BN}_7\text{Ni}$, 444.1612; found, 444.1613.



***In situ* generation of $[(\text{Tp})\text{Ni}^{\text{II}}(\text{CH}_2\text{CMe}_2\text{-}o\text{-C}_6\text{H}_4\text{OAc})(\text{NCCD}_3)]$ (**5**).** A 4 mL vial was charged with **3a** (5.2 mg, 0.0098 mmol, 1.0 equiv), NMe_4OAc (2.6 mg, 0.020 mmol, 2 equiv), 1,3,5-trimethoxybenzene (2.0 mg, 0.012 mmol, 1.2 equiv) as an internal ^1H NMR standard, and CD_3CN (0.5 mL). The resulting orange solution was transferred to a teflon-lined screw cap NMR tube and removed from the glovebox. The

NMR tube was analyzed by ^1H NMR spectroscopy after <10 min at room temperature which showed generation of Ni^{II} reductive elimination product **5** in 95% yield ^1H NMR (401 MHz, CD_3CN , 23 °C) δ 8.16 (d, $J_{\text{HH}} = 2.0$ Hz, 1H), 7.94 (d, $J_{\text{HH}} = 2.0$ Hz, 1H), 7.87 (d, $J_{\text{HH}} = 2.2$ Hz, 1H), 7.85 (d, $J_{\text{HH}} = 2.2$ Hz, 1H), 7.73 (d, $J_{\text{HH}} = 2.2$ Hz, 1H), 7.10 (m, 1H), 7.02-6.93 (multiple peaks, 2H), 6.85 (ddd, $J_{\text{HH}} = 8.5, 7.0, 2.0$ Hz, 1H), 6.71 (d, $J_{\text{HH}} = 2.0$ Hz, 1H), 6.43 (t, $J_{\text{HH}} = 2.2$ Hz, 1H), 6.35 (t, $J_{\text{HH}} = 2.2$ Hz, 1H), 6.08 (t, $J_{\text{HH}} = 2.2$ Hz, 1H), 4.56 (d, $J_{\text{HH}} = 6.3$ Hz, 1H), 4.29 (d, $J_{\text{HH}} = 6.3$ Hz, 1H), 1.97 (s, 3H), 1.95 (s, 3H), 1.53 (s, 3H), 1.41 (s, 3H).

4.4.3. EPR Studies

Procedure for EPR detection of complexes 2a and 2b: A 4 mL vial was charged with the appropriate Ni^{III} complex (0.005 mmol) and acetonitrile (1 mL). Four drops of this solution were added to 300 μ L of a 3:1 PrCN: MeCN solution. The sample was then flash-frozen in a septum-capped EPR tube in liquid nitrogen until analysis at 100 K.

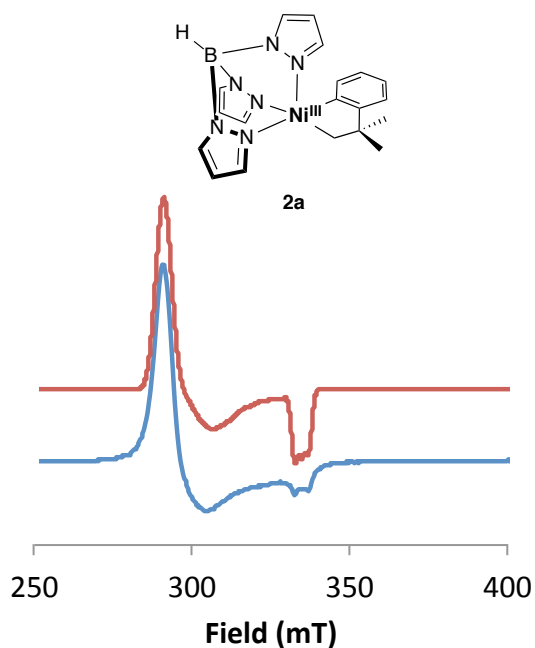


Figure 4.12. EPR Spectrum of **2a** (bottom/blue) and the Simulated Spectrum (top/red). Fit using the following parameters: $g_x = 2.29$, $g_y = 2.25$, $g_z = 2.01$, $A_n(N) = 21$ G

Procedure for the attempted detection of complex 2c: A 4 mL scintillation vial was charged with $\text{NMe}_4[\text{Ni}^{\text{II}}(\text{Tp})(\text{Me})(\text{CF}_3)]$ (**1c**) (0.005 mmol) and acetonitrile (1 mL). A separate 4 mL vial was charged with FcBF_4 (0.02 mmol) and acetonitrile (1 mL). Both solutions were then cooled to -78 $^\circ\text{C}$ in a glovebox cold well. After 10 min, 200 μ L of the FcBF_4 solution (0.004 mmol, 0.8 equiv) was added in one portion via syringe to the solution of **1c**. The vial was quickly shaken, resulting in the immediate disappearance of the blue FcBF_4 salt, indicating rapid consumption of the oxidant. Four drops of this solution were transferred to 300 μ L of a precooled (-78 $^\circ\text{C}$) solution of 3:1 PrCN:MeCN. The sample was then flash-frozen at -196 $^\circ\text{C}$ in a septum-capped EPR tube until analysis. EPR signals consistent with the formation of **2c** were not observed.

4.4.4. Cyclic Voltammetry Studies

General Experimental Procedure: Cyclic voltammetry on complexes **1a-c** was performed in a 3-electrode cell consisting of a 3 mm glassy carbon disc working electrode, a Ag/Ag⁺ reference electrode with a Ag wire in a fritted chamber containing a solution of AgBF₄ (0.01 M) and the corresponding supporting electrolyte (0.1 M) in acetonitrile, and a Pt wire counter electrode. A 2 mL solution of each complex (0.01 M) and the supporting electrolyte (0.1 M) was added to the electrochemical cell. Cyclic voltammetry scans were taken at 100 mV/s. After obtaining the CV for each complex, ferrocene was added as an internal reference.

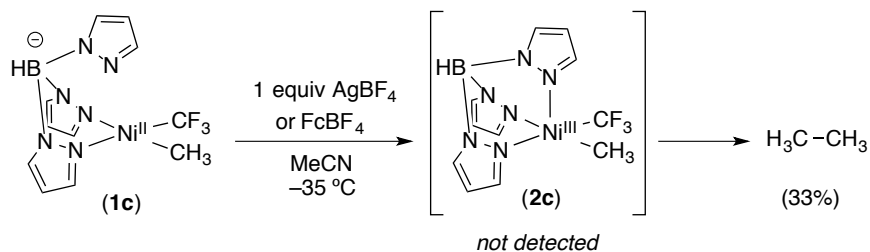
For complexes 1a-c (Ni^{II/III} couple): Supporting electrolyte = 0.1 M NBu₄PF₆ in MeCN

For complex 1a (full window): Supporting electrolyte = 0.1 M NBu₄BF₄ in MeCN

For complex 1a (Ni^{II/III} couple and full window): Supporting electrolyte = 0.1 M NMe₄OAc in MeCN.

4.4.5. Reactivity Studies

NMR oxidation studies of **1c**



Procedure for the oxidation of **1c:** A 4 mL vial was charged with **1c** (5.0 mg, 0.012 mmol, 1.0 equiv), 1,3,5-trimethoxybenzene (2.0 mg, 0.012 mmol, 1.0 equiv) as an internal ¹H NMR standard, and CD₃CN (0.5 mL). This light yellow solution was transferred to a screw cap NMR tube and cooled to -35 °C. A cooled solution of ferrocenium tetrafluoroborate (FcBF₄, 3.1 mg, 0.012 mmol, 1.0 equiv) in CD₃CN was added at -35 °C, filling the NMR tube completely. The tube was quickly capped, shaken vigorously, and was analyzed by ¹H NMR spectroscopy after 30 min at room temperature to determine the yield of ethane (33 %). A final spectrum was taken 2 h later at which point no additional ethane was observed.

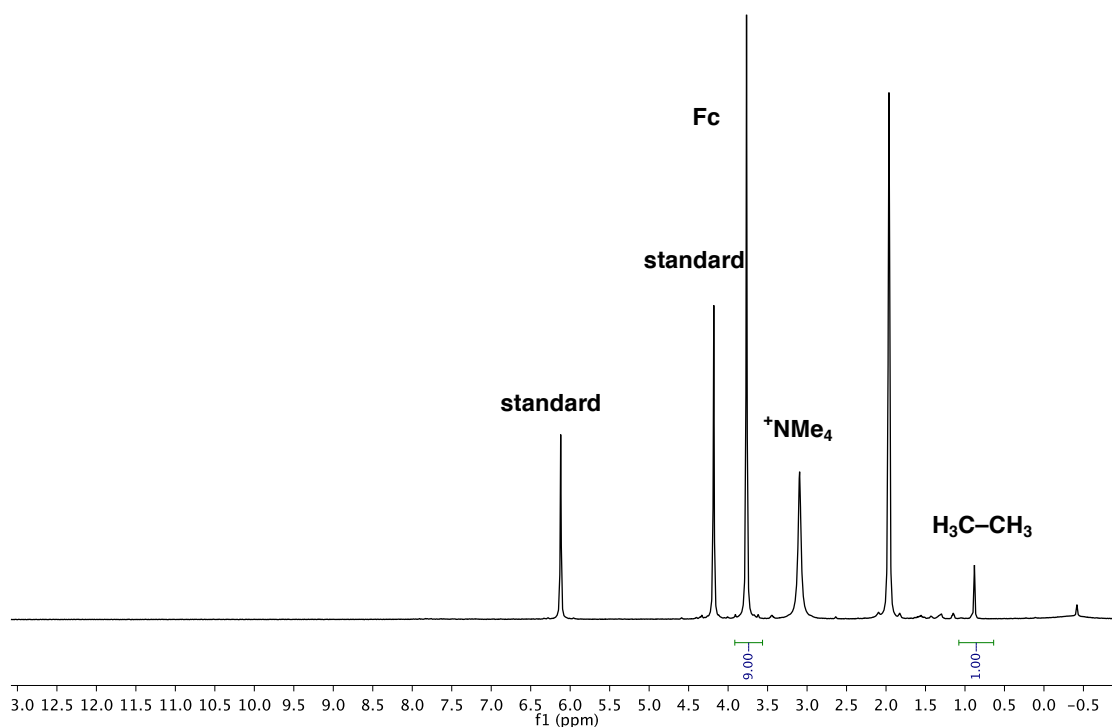
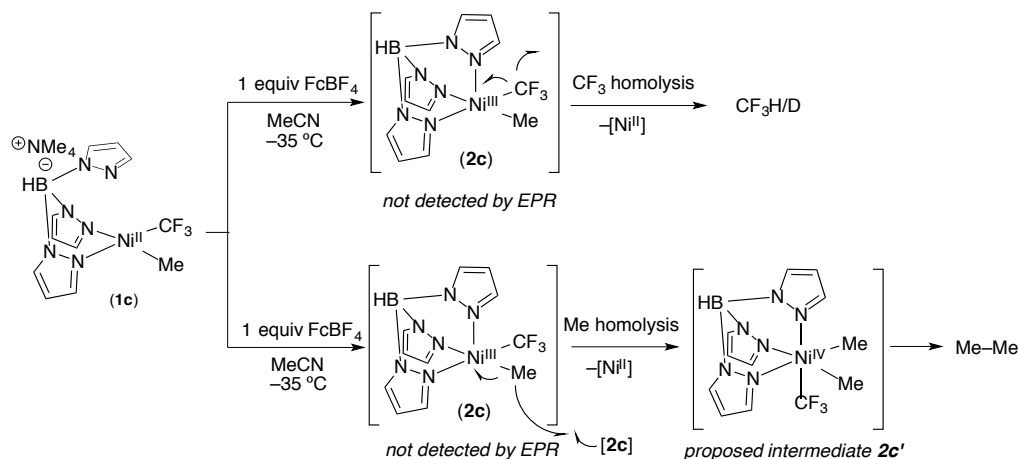


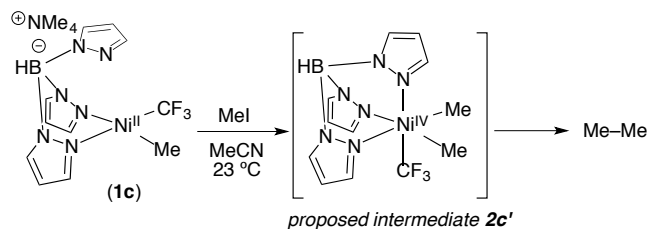
Figure 4.13. ^1H NMR Spectrum of the Crude Reaction Mixture after Oxidation of **1c** with FcBF_4 . Standard = 1,3,5-trimethoxybenzene

Evidence for $\text{Ni}-\text{CF}_3$ and $\text{Ni}-\text{CH}_3$ group homolysis from putative intermediate **2c**



Experimental Procedure: A modified procedure of the reaction described above was followed. After addition of the oxidant at $-35\text{ }^\circ\text{C}$ the sample was analyzed after <10 min at room temperature. Analysis of the crude reaction mixture by ^1H NMR and ^{19}F NMR spectroscopy revealed the formation of $\text{CF}_3\text{H/D}$ which is presumably generated via CF_3 homolysis from unstable Ni^{III} intermediate **2c**. In addition, resonances associated with a

diamagnetic Ni–CF₃ complex were also observed in low yield (10%, ¹⁹F NMR = s, –26.14 ppm; ¹H NMR (Ni^{IV}–Me) 2.61 ppm). We tentatively assign these features to Ni^{IV} complex **2c'** generated via Me group transfer from the unstable Ni^{III} to the Ni^{II} starting material **1c**.



Procedure for the oxidation of **1c with MeI:** A 4 mL vial was charged with **1c** (5.0 mg, 0.012 mmol, 1.0 equiv) and dissolved in acetonitrile (0.5 mL). An excess of MeI was added (approximately 20 equiv) and the resulting solution was transferred to an NMR tube and taken out of the glovebox. The crude reaction mixture was analyzed by ¹H NMR and ¹⁹F NMR spectroscopy. The resonances in Figure 4.14 (top spectra) correspond to proposed complex **2c'**.

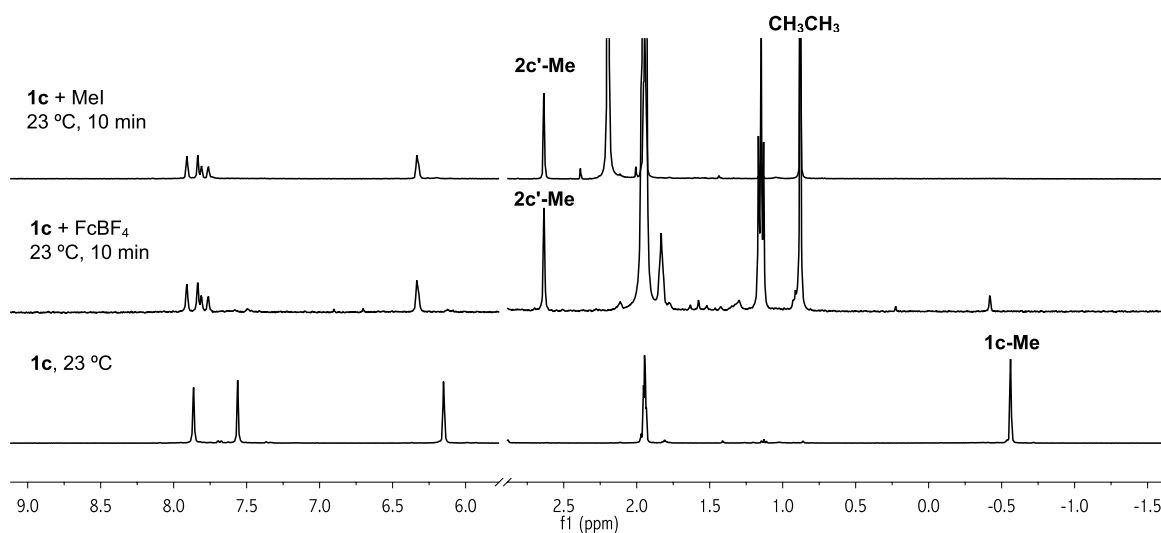
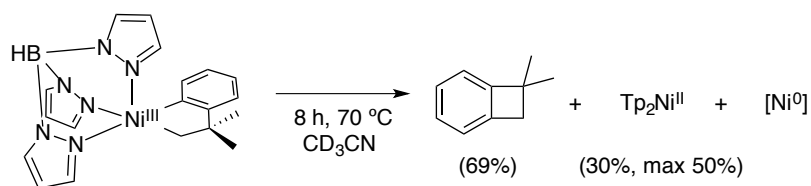


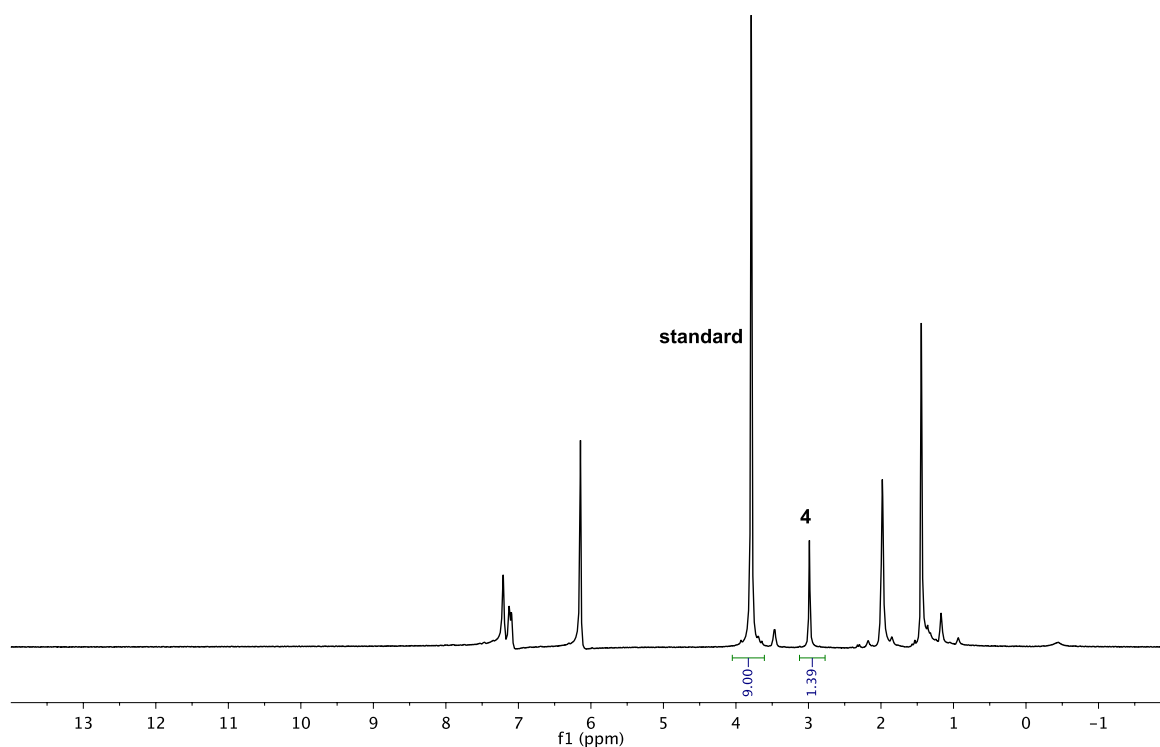
Figure 4.14. ¹H NMR Spectra Showing the Treatment of Complex **1c** with FcBF₄ and MeI, Generating Proposed Ni^{IV}–Me Complex, **2c'** in Both Experiments

Reductive Elimination Studies from 2a



Procedure for the thermolysis of 2a: A 4 mL vial was charged with **2a** (5 mg, 0.012 mmol, 1.0 equiv), 1,3,5-trimethoxybenzene (2.1 mg, 0.0124 mmol, 1.0 equiv) as an internal ¹H NMR standard, and CD₃CN (0.5 mL). The resulting orange solution was transferred to a teflon-lined screw cap NMR tube and removed from the glovebox. The NMR tube was heated in an oil bath at 70 °C for 8 h. The solution was then analyzed by ¹H NMR spectroscopy to determine the yield of 1,1-dimethylbenzocyclobutane (69% yield). The NMR tube was then brought back into the glove box. Next, NBu₄BF₄ (0.038 M in MeCN, 1.0 equiv) was added to the NMR tube as an ¹¹B NMR standard. The tube was capped, and the sample was analyzed by quantitative ¹¹B NMR spectroscopy to determine the yield of Ni^{II}Tp₂ (30% based on Ni). Representative NMR spectra are shown in Figure 4.15.

(a)



(b)

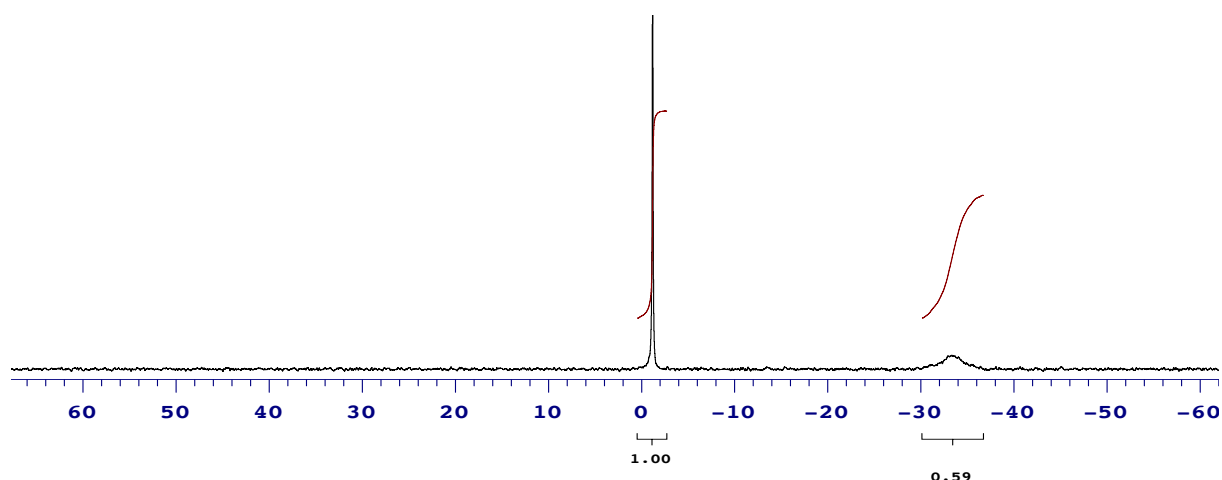
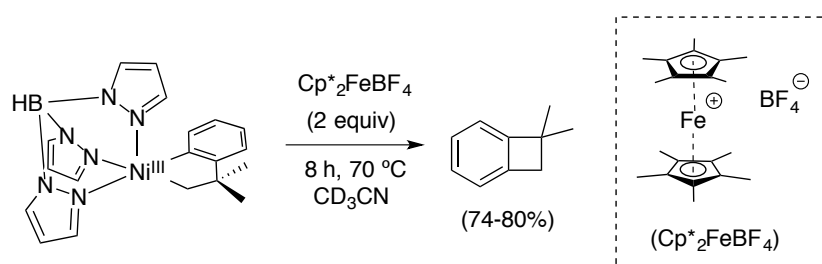


Figure 4.15. (a) ^1H NMR Spectrum of the Crude Reaction Mixture after Heating **2a** at $70\text{ }^\circ\text{C}$ for 8 h. Standard = 1,3,5-trimethoxybenzene; (b) ^{11}B NMR Spectrum of the Ni^{II} Byproduct NiTp_2 after Heating for $70\text{ }^\circ\text{C}$ for 8 h. Standard = NBu_4BF_4 .



Procedure for the thermolysis of **2a with added weak oxidant:** A 4 mL vial was charged with **2a** (5.0 mg, 0.012 mmol, 1.0 equiv), decamethylferrocenium tetrafluoroborate ($\text{Cp}^*_2\text{FeBF}_4$) (10 mg, 0.024 mmol, 2.0 equiv) 1,3,5-trimethoxybenzene (2.1 mg, 0.0124 mmol, 1.0 equiv) as an internal ^1H NMR standard, and CD_3CN (0.5 mL). The resulting green solution was transferred to a screw cap NMR tube and removed from the glove box. The sample was heated in an oil bath at $70\text{ }^\circ\text{C}$ for 8 h. The solution was then analyzed by ^1H NMR spectroscopy to determine the yield of benzocyclobutane (74-80% yield).

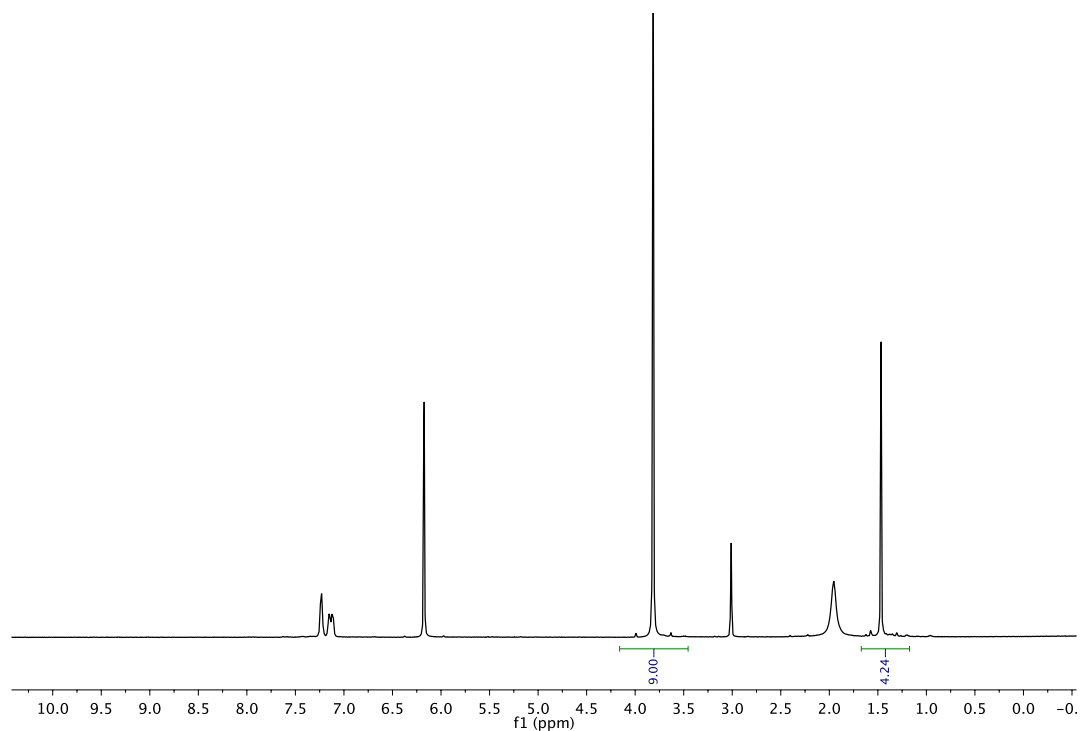
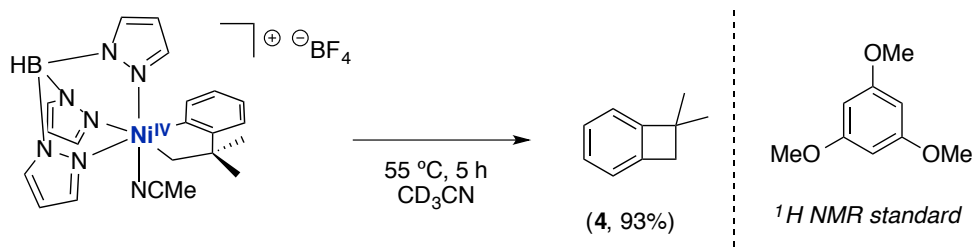


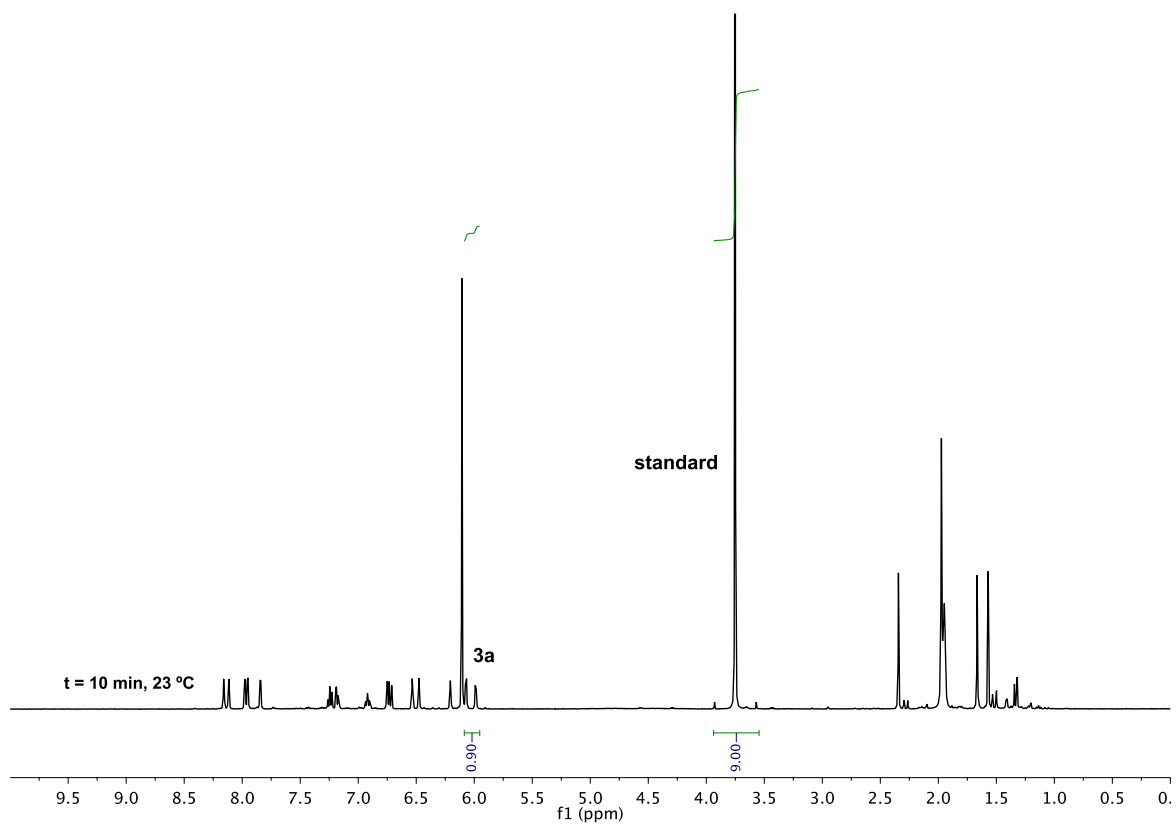
Figure 4.16. ^1H NMR Spectrum of the Crude Reaction Mixture after Heating **2a** at 70 °C for 8 h with the Additive Cp^*FeBF_4 . Standard = 1,3,5-trimethoxybenzene.

C–C Coupling from Ni^{IV} Complex **3a** at 55 °C



Experimental Procedure: A 4 mL vial was charged with **3a** (4.0 mg, 0.0075 mmol), 1,3,5-trimethoxybenzene as an internal ^1H NMR standard, and CD_3CN (0.5 mL). The resulting orange solution was transferred to a teflon-lined screw cap NMR tube and removed from the glovebox. After 5 h at 55 °C the reaction mixture was analyzed by ^1H NMR spectroscopy to determine the yield of 3,3-dimethylbenzocyclobutane (**4**, 93%).

(a)



(b)

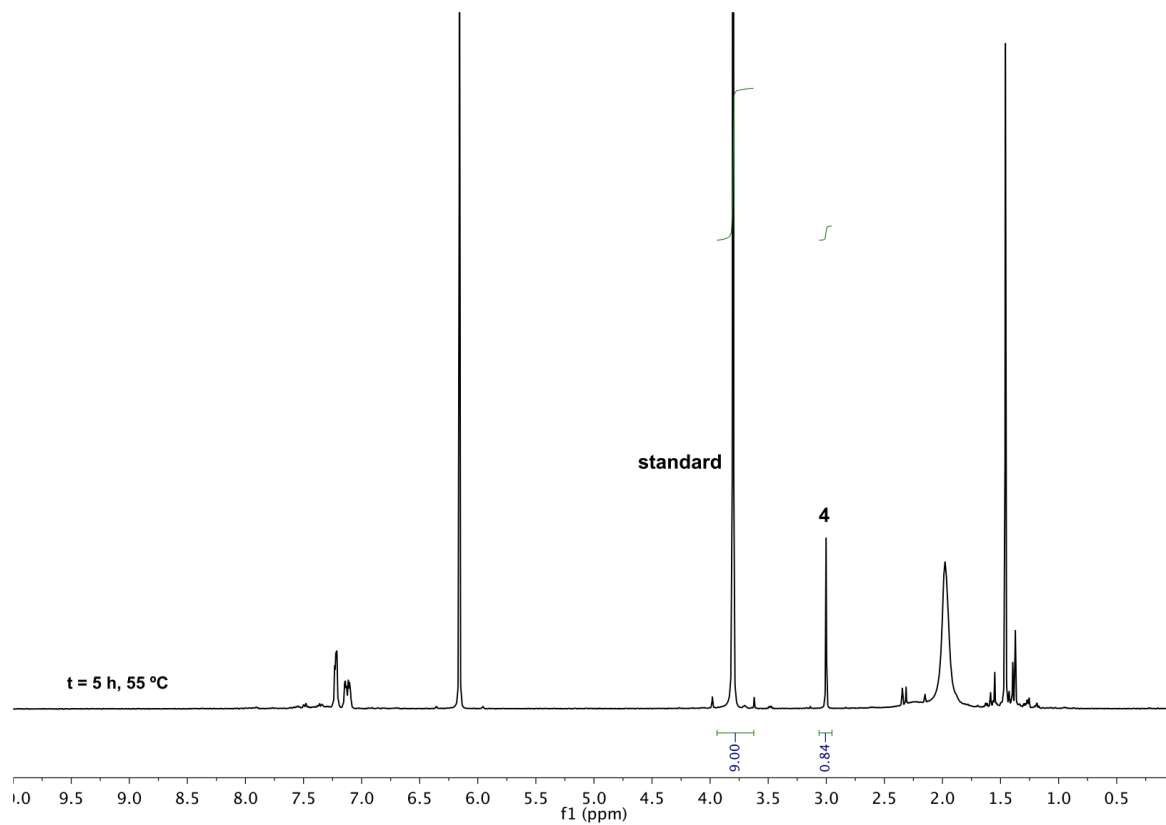
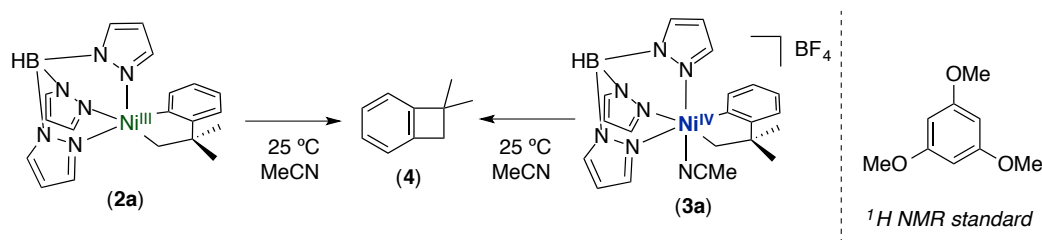


Figure 4.17. ^1H NMR Spectra of (a) Unreacted Ni^{IV} Complex **3a** and the Standard 1,3,5-trimethoxybenzene (b) Dimethyl Benzocyclobutane Formation after 5 h at $55 \text{ }^\circ\text{C}$

Determining Initial Rates for C-C Coupling Ni^{III} vs. Ni^{IV} at 25 °C



Experimental Procedure: In the glovebox, the respective Ni complex (0.0094 mmol, 1.0 equiv) was weighed into a 4 mL vial and then dissolved in CD₃CN (4.0 mL) at 25 °C. 1,3,5-trimethoxybenzene (0.0094 mmol, 1.0 equiv) was added as an internal ¹H NMR standard. The resulting solutions were transferred to J-Young valve NMR tubes equipped with an O-ring seal and taken out of the glovebox. The initial rates of reductive elimination were determined by monitoring the first 8-20% of the reaction progress by ¹H NMR spectroscopy at 25 °C. Concentration versus time data were acquired from the integration of the ¹H NMR signals of 1,1-dimethylbenzocyclobutane (4) with respect to the internal standard. Initial rate values were obtained from the slope of a linear-fit line corresponding to the formation of 4.

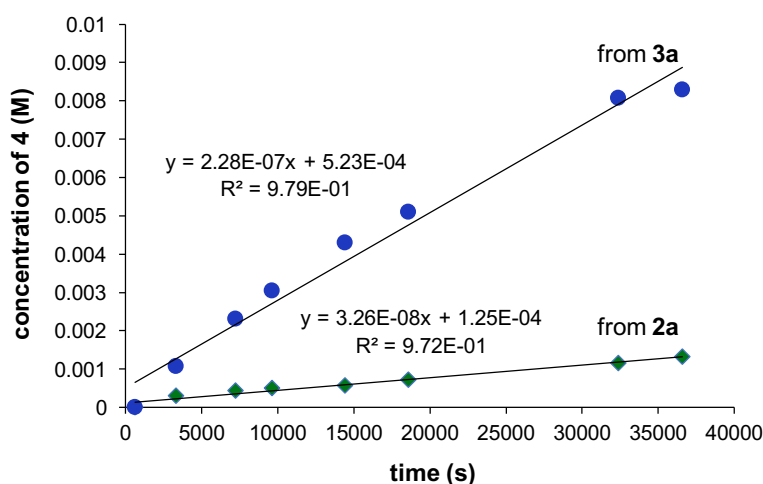
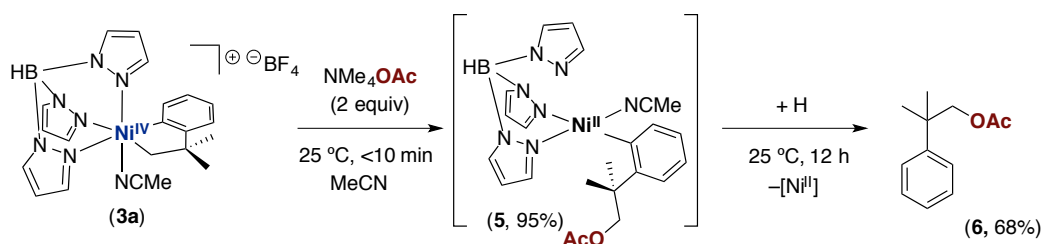


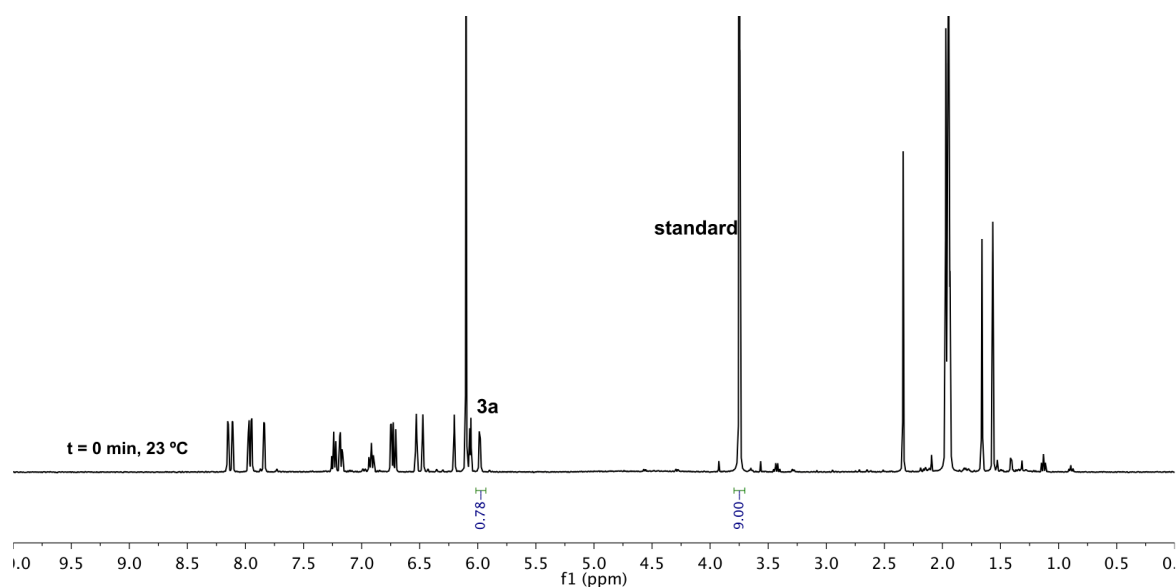
Figure 4.18. Plot of Concentration vs. Time Data for the Formation of C-C Coupled Product dimethyl benzocyclobutane from 3a and 2a. Conditions: [Ni] = 0.0023 M; T = 25 °C.

C–O vs. C–C Competition Experiments from Ni^{III} and Ni^{IV}

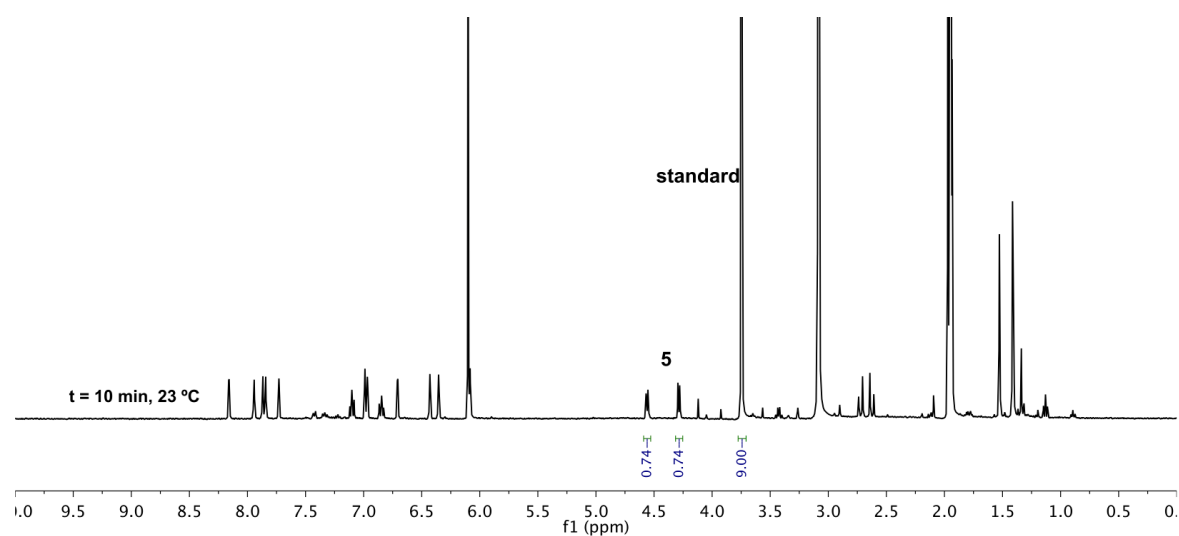


Experimental Procedure: A 4 mL vial was charged with **3a** (5.2 mg, 0.0098 mmol, 1.0 equiv), NMe₄OAc (2.6 mg, 0.020 mmol, 2 equiv), 1,3,5-trimethoxybenzene (2.0 mg, 0.012 mmol, 1.2 equiv) as an internal ¹H NMR standard, and CD₃CN (0.5 mL). The resulting orange solution was transferred to a teflon-lined screw cap NMR tube and removed from the glovebox. The NMR tube was analyzed by ¹H NMR spectroscopy after <10 min at room temperature which showed generation of Ni^{II} reductive elimination product **5** in 95% yield (Figure 4.19b). After 12 h at room temperature, this complex underwent proto-demetalation to form the organic product **6** in 68% yield (Figure 4.19c).

(a)



(b)



(c)

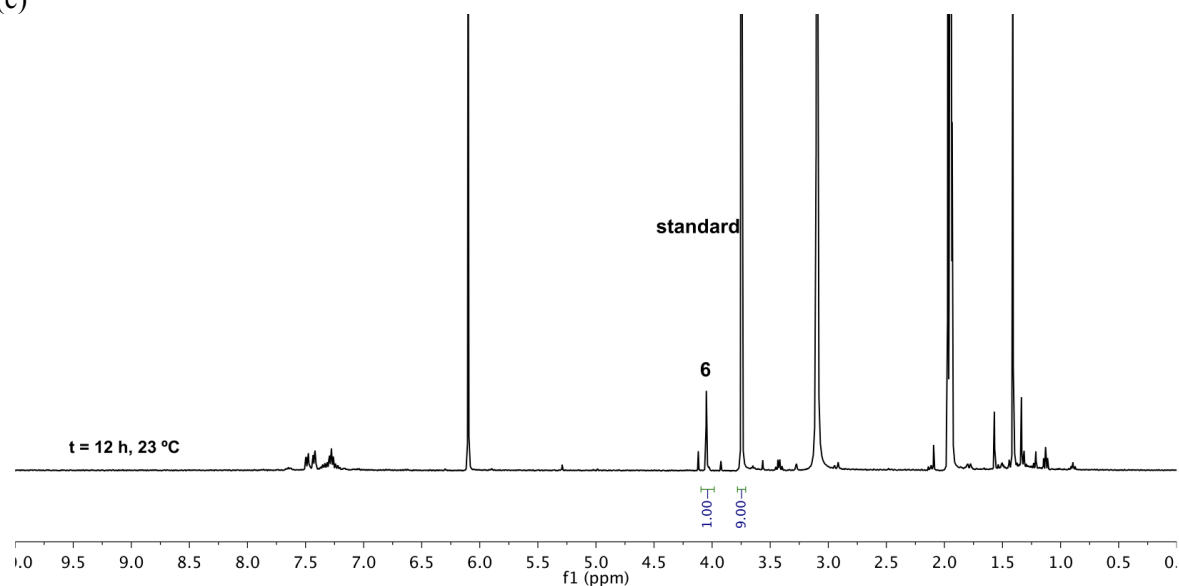
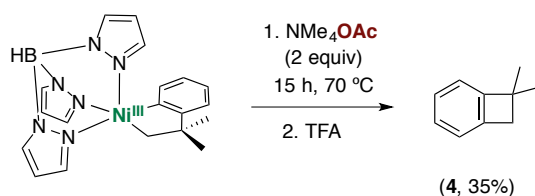


Figure 4.19. ¹H NMR Spectra of (a) Unreacted Ni^{IV} Starting Material **3a** (b) the Reaction of **3a** with 2 equiv of NMe₄OAc after 10 min at rt to Generate **5** (c) Organic Product **6** Formed after 12 h at 23 °C



Experimental Procedure: A 4 mL vial was charged with **2a** (5.5 mg, 0.014 mmol, 1.0 equiv), NMe₄OAc (3.6 mg, 0.028 mmol, 2 equiv), 1,3,5-trimethoxybenzene (2.4 mg, 0.014 mmol, 1.0 equiv) as an internal ¹H NMR standard, and CD₃CN (0.5 mL). The resulting orange solution was transferred to a teflon-lined screw cap NMR tube and removed from the glovebox. The

NMR tube was analyzed by ^1H NMR spectroscopy after 1 hr at room temperature and no reactivity of **2a** was observed. The sample was then heated in an oil bath at $70\text{ }^\circ\text{C}$ for 15 h. The solution was then analyzed by ^1H NMR spectroscopy to determine the yield of 1,1-dimethylbenzocyclobutane (**4**, 35%). Trifluoroacetic acid was added afterwards to ensure that no products of C–O coupling were attached to paramagnetic species. The NMR spectra in Figure 4.20 shows the yield of C–C coupled product after the addition of acid. The sample was also analyzed by GC/MS which only showed formation of compound **4**.

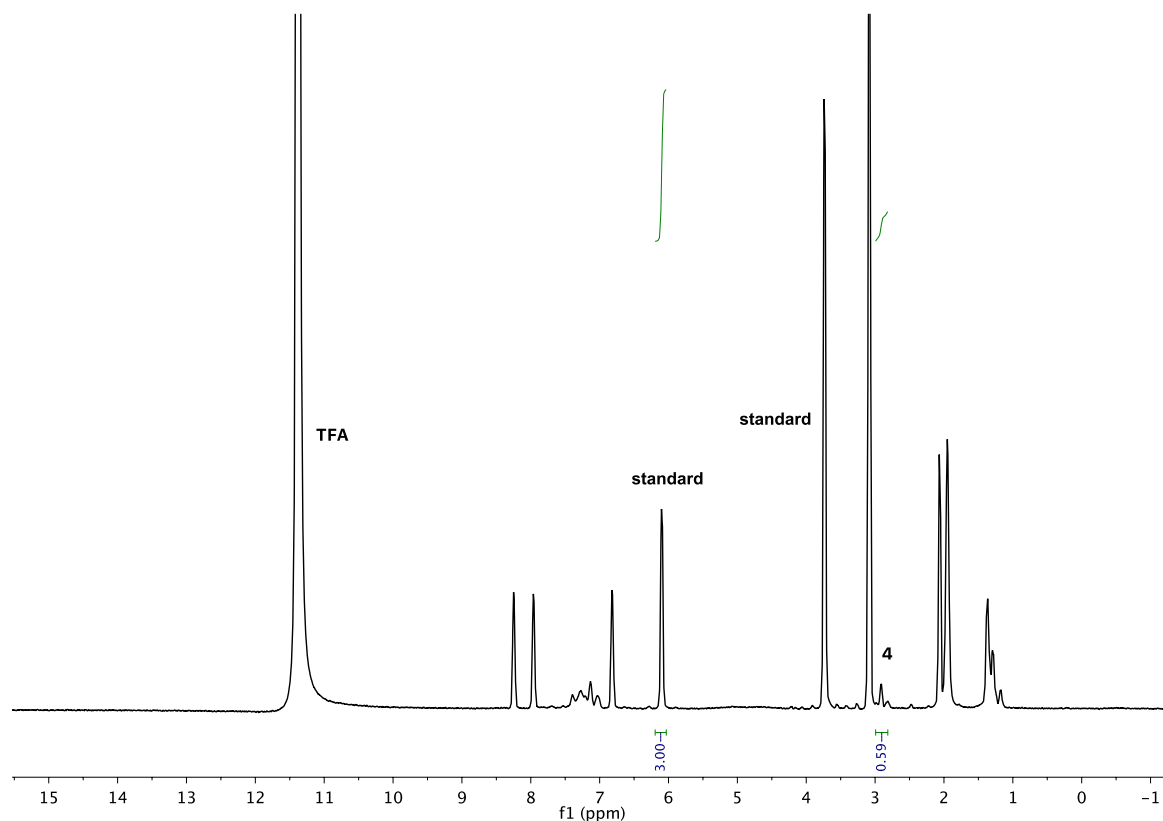
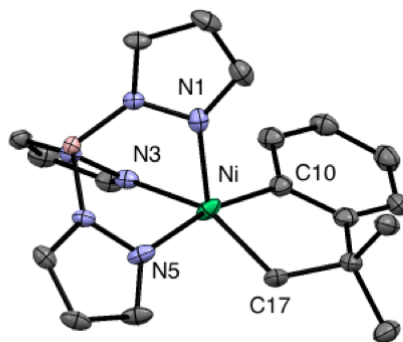


Figure 4.20. ^1H NMR Spectrum of the Reaction between **2a** and 2 equiv of NMe_4OAc after 15 h at $70\text{ }^\circ\text{C}$ and Treatment with Trifluoroacetic Acid (TFA).

4.4.6. X-ray Structural Determination

X-ray Crystallography Experimental Data of 2a



Orange plates of **2a** were grown by slow evaporation of an acetonitrile solution of the compound with a trace of added formamide at $-35\text{ }^{\circ}\text{C}$. A crystal of dimensions $0.24 \times 0.19 \times 0.02\text{ mm}$ was mounted on a Rigaku AFC10K Saturn 944+ CCD-based X-ray diffractometer equipped with a low temperature device and Micromax-007HF Cu-target micro-focus rotating anode ($\lambda = 1.54187\text{ \AA}$) operated at 1.2 kW power (40 kV, 30 mA). The X-ray intensities were measured at 85(1) K with the detector placed at a distance 42.00 mm from the crystal. A total of 2028 images were collected with an oscillation width of 1.0° in ω . The exposure times were 5 sec. for the low angle images, 30 sec. for high angle. Rigaku d*trek images were exported to CrysAlisPro for processing and corrected for absorption. The integration of the data yielded a total of 32434 reflections to a maximum 2θ value of 139.12° of which 6827 were independent and 6785 were greater than $2\sigma(I)$. The final cell constants were based on the xyz centroids 32434 reflections above $10\sigma(I)$. Analysis of the data showed negligible decay during data collection. The structure was solved and refined with the Bruker SHELXTL (version 2014/6) software package, using the space group P2(1)/c with $Z = 8$ for the formula $\text{C}_{19}\text{H}_{22}\text{BN}_6\text{Ni}$. There are two crystallographically independent complexes in the asymmetric unit. The crystal was found to be a two-component pseudo-merohedral twin. The 2-methyl-2-phenylpropyl group bonded to Ni1 is partially disordered in two orientations. All non-hydrogen atoms were refined anisotropically with the hydrogen atoms placed in idealized positions. Full matrix least-squares refinement based on F2 converged at $R1 = 0.0496$ and $wR2 = 0.1308$ [based on $I > 2\sigma(I)$], $R1 = 0.0499$ and $wR2 = 0.1315$ for all data. Acknowledgement is made for funding from NSF grant CHE-0840456 for X-ray instrumentation.

Sheldrick, G.M. SHELXTL, v. 2014/6; Bruker Analytical X-ray, Madison, WI, 2014.
 CrystalClear Expert 2.0 r16, Rigaku Americas and Rigaku Corporation (2014), Rigaku
 Americas, 9009, TX, USA 77381-5209, Rigaku Tokyo, 196-8666, Japan.
 CrysAlisPro 1.171.38.41 (Rigaku Oxford Diffraction, 2015).

Table 4.1. Selected Bond Lengths (Å) and Angles (°) for **2a**

Ni(1)-N(1)	2.032(3)	N(1)-Ni(1)-N(3)	88.4(1)
Ni(1)-N(3)	2.050(3)	C(10)-Ni(1)-C(17)	82.9(2)
Ni(1)-N(5)	2.012(3)	N(1)-Ni(1)-C(10)	101.6(1)
Ni(1)-C(17)	1.966(6)	N(1)-Ni(1)-C(17)	118.5(2)
Ni(1)-C(10)	1.926(3)	N(3)-Ni(1)-C(17)	152.5(2)

4.5. References

-
- (1) Adapted with permission from: Bour, J. R.; Camasso, N. M.; Meucci, E. A.; Kampf, J. W.; Canty, A. J.; Sanford, M. S. *J. Am. Chem. Soc.* **2016**, *138*, 16105. © American Chemical Society.
- (2) For reviews on Ni catalysis, see: (a) Meijere, A. d.; Diederich, F. *Metal-Catalyzed Cross-Coupling Reactions*; Wiley-VCH: Weinheim, 2004. (b) Hu, X. *Chem. Sci.* **2011**, *2*, 1867. (c) Rosen, B. M.; Quasdorf, K. W.; Wilson, D. A.; Zhang, N.; Resmerita, A-M.; Garg, N. K.; Percec, V. *Chem. Rev.* **2011**, *111*, 1346. (d) Ge, S.; Hartwig, J. F. *Angew. Chem. Int. Ed.* **2012**, *51*, 12837. (e) Montgomery, J. Organonickel Chemistry. In *Organometallics in Synthesis: Fourth Manual*; Lipshutz, B. H., Ed.; Wiley: Hoboken, N.J., 2013; pp 319 (f) Tasker, S. Z.; Standley, E. A.; Jamison, T. F. *Nature* **2014**, *509*, 299. (g) Ananikov, S. *ACS Catal.* **2015**, *5*, 1964.
- (3) For select examples of nickel catalyzed C–C and C–heteroatom coupling reactions invoking Ni^{III} intermediates, see: (a) Jones, G. D.; Martin, J. L.; McFarland, C.; Allen, O. R.; Hall, R. E.; Haley, A. D.; Brandon, R. J.; Konovalova, T.; Desrochers, P. J.; Pulay, P.; Vicic, D. A. *J. Am. Chem. Soc.* **2006**, *128*, 13175. (b) Zultanski, S.; Fu, G. C. *J. Am. Chem. Soc.* **2011**, *133*, 15362. (c) Joshi-Pangu, A.; Wang, C-Y.; Biscoe, M. R. *J. Am. Chem. Soc.* **2011**, *133*, 847. (d) Dudnik, A. S.; Fu, G. C. *J. Am. Chem. Soc.* **2012**, *134*, 10693. (e) Dai, Y. J.; Wu, F.; Zang, Z. H.; You, H. Z.; Gong, H. G. *Chem. Eur. J.* **2012**, *18*, 808. (f) Schley, N. D.; Fu, G. C. *J. Am. Chem. Soc.* **2014**, *136*, 16588. (g) Aihara, Y.; Tobisu, M.; Fukumoto, Y.; Chatani, N. *J. Am. Chem. Soc.* **2014**, *136*, 15509. (h) Wu, X.; Zhao, Y.; Ge, H. *J. Am. Chem. Soc.* **2014**, *136*, 1789. (i) Tellis, J. C.; Primer, D. N.; Molander, G. A. *Science* **2014**, *345*, 433. (j) Zuo, Z.; Ahneman, D. T.; Chu, L.; Terrett, J. A.; Doyle, A. G.; MacMillan, D. W. C. *Science* **2014**, *345*, 437. (k) Cornella, J.; Edwards, J. T.; Qin, T.; Kawamura, S.; Wang,

- J.; Pan, C-M.; Gianatassio, R.; Schmidt, M. A.; Eastgate, M. D.; Baran, P. S. *J. Am. Chem. Soc.* **2016**, *138*, 2174. (l) Gui, Y.-Y.; Sun, L.; Lu, Z.-P.; Yu, D.-G. *Org. Chem. Front.* **2016**, *3*, 522. (m) Shields, B. J.; Doyle, A. G. *J. Am. Chem. Soc.* **2016**, *138*, 12719.
- (4) (a) Tsou, T. T.; Kochi, J. K. *J. Am. Chem. Soc.* **1978**, *100*, 1634. (b) Tsou, T. T.; Kochi, J. K. *J. Am. Chem. Soc.* **1979**, *101*, 7547.
- (5) (a) Matsunaga, P. T.; Hillhouse, G. L.; Rheingold, A. L. *J. Am. Chem. Soc.* **1993**, *115*, 2075. (b) Koo, K.; Hillhouse, G. L. *Organometallics* **1995**, *14*, 4421. (c) Koo, K.; Hillhouse, G. L.; Rheingold, A. L. *Organometallics* **1995**, *14*, 456 (d) Koo, K.; Hillhouse, G. L. *Organometallics* **1996**, *15*, 2669. (e) Han, R.; Hillhouse, G. L. *J. Am. Chem. Soc.* **1997**, *119*, 8135 (f) Koo, K.; Hillhouse, G. L. *Organometallics* **1998**, *17*, 2924. (g) Lin, B. L.; Clough, C. R.; Hillhouse, G. L. *J. Am. Chem. Soc.* **2002**, *124*, 2890.
- (6) For select examples of structurally characterized Ni^{III} complexes, see: (a) Grove, D. M.; van Koten, G.; Zoet, R.; Murrall, N. W.; Welch, A. J. *J. Am. Chem. Soc.* **1983**, *105*, 1379. (b) Grove, D. M.; van Koten, G.; Mul, W. P.; van der Zeijden, A. A. H.; Terheijden, J. *Organometallics* **1986**, *5*, 322 (c) Grove, D. M.; van Koten, G.; Mul, P.; Zoet, R.; van der Linden, J. G. M.; Letgers, J.; Schmitz, J. E. J.; Murrall, N. W.; Welch, A. J. *Inorg. Chem.* **1988**, *27*, 2466 (d) van de Kuil, V. A.; Veldhuizen, Y. S. J.; Grove, D. M.; Zwikker, J. L.; Jenneskens, L. W.; Drenth, W.; Smeets, W. J. J.; Spek, A. L.; van Koten, G. *J. Organomet. Chem.* **1995**, *488*, 191. (e) Pandarus, V.; Zargarian, D. *Organometallics* **2007**, *26*, 4321. Castonguay, A.; Beauchamp, A.; Zargarian, D. *Organometallics* **2008**, *27*, 5723. (f) Lee, C. M.; Chen, C. H.; Liao, F. X.; Hu, C. H.; Lee, G. H. *J. Am. Chem. Soc.* **2010**, *132*, 9256. (g) Tang, F.; Rath, N. P.; Mirica, L. M. *Chem. Commun.* **2015**, *51*, 3113. (h) Yu, S.; Dudkina, Y.; Wang, H.; Kholin, K. V.; Budnikova, V.; Vicic, D. A. *Dalton Trans.* **2015**, *44*, 19443.
- (7) For select examples of stoichiometric C–C and C–heteroatom reductive elimination from Ni^{III}, see: (a) Burk, P.; Liu, M.; Miyashita, A.; Grubbs, R. H. *J. Am. Chem. Soc.* **1978**, *100*, 2418. (b) Amatore, C.; Jutand, A. *Organometallics* **1988**, *7*, 2203. (c) Jones, G. D.; McFarland, C.; Anderson, T. J.; Vicic, D. A. *Chem. Commun.* **2005**, 4211. (d) Lin, X. F.; Phillips, D. L. *J. Org. Chem.* **2008**, *73*, 3680. (e) Higgs, A. T.; Zinn, P. J.; Sanford, M. S. *Organometallics* **2009**, *28*, 6142. (f) Higgs, A. T.; Zinn, P. J.; Sanford, M. S. *Organometallics* **2010**, *29*, 5446. (g) Lipschutz, M. I.; Yang, X.; Chatterjee, R.; Tilley, T. D. *J. Am. Chem. Soc.* **2013**, *135*, 15298. (h) Breitenfeld, J.; Woodrich, M.; Hu, X. *Organometallics* **2014**, *33*, 5708. (i) Zheng, B.; Tang, F.; Luo, J.; Schultz, J. W.; Rath, N. P.; Mirica, L. M. *J. Am. Chem. Soc.* **2014**, *136*, 6499. (j) Cloutier, J.-P.; Vabre, B.; Mounang-Soumé, B.; Zargarian, D. *Organometallics* **2015**, *34*, 133. (k) Zhou, W.; Schultz, J. W.; Rath, N. P.; Mirica, L. M. *J. Am. Chem. Soc.* **2015**, *137*, 7604. (l) Zhou, W.; Rath, N. P.; Mirica, L. M. *Dalton Trans.* **2016**, *45*, 8693. (m) Xu, H.; Diccianni, J. B.; Katigbak, J.; Hu, C.; Zhang, Y.; Diao, T. *J. Am. Chem. Soc.* **2016**, *138*, 4779. (n) Schultz, J. W.; Fuchigami, K. Zheng, B. Rath, N. P.; Mirica, L. M. *J. Am. Chem. Soc.* **2016**, *138*, 12928. (o) Zhou, W.; Zheng, S. A.; Schultz, J. W.; Rath, N. P.; Mirica, L. M. *J. Am. Chem. Soc.* **2016**, *138*, 5777. (p) Watson, M. B.; Rath, N. P.; Mirica, L. M. *J. Am. Chem. Soc.* **2017**, *139*, 35.
- (8) For select studies proposing the intermediacy of Ni^{IV}, see: (a) Terao, J.; Kambe, N. *Acc. Chem. Res.* **2008**, *41*, 1545. (b) Aihara, Y.; Chatani, N. *J. Am. Chem. Soc.* **2013**, *135*, 5308. (c) Aihara, Y.; Chatani, N. *J. Am. Chem. Soc.* **2014**, *136*, 898. (d) Wu, X.; Zhao, Y.; Ge, H. *J. Am. Chem. Soc.* **2014**, *136*, 1789. (e) Yan, S.-Y.; Liu, Y.-J.; Liu, B.; Liu, Y.-H.; Zhang, Z.-Z.; Shi, B.-F. *Chem. Commun.* **2015**, *51*, 7341.
- (9) (a) Camasso, N. M.; Sanford, M. S. *Science* **2015**, *347*, 1218. (b) Bour, J. R.; Camasso, N. M.; Sanford, M. S. *J. Am. Chem. Soc.* **2015**, *137*, 8034. (c) Meucci, E. A.; Camasso, N. M.; Sanford, M. S. *Organometallics* **2017**, *36*, 247.

-
- (10) See 7n,p, also: (a) Klein, H.-F.; Bickelhaupt, A.; Jung, T.; Cordier, G. *Organometallics* **1994**, *13*, 2557. (b) Klein, H. F.; Bickelhaupt, A.; Lemke, M.; Sun, H. J.; Brand, A.; Jung, T.; Rohr, C.; Florke, U.; Haupt, H. J. *Organometallics* **1997**, *16*, 668. (c) Shimada, S.; Rao, M. L. N.; Tanaka, N. *Organometallics* **1999**, *18*, 291. (d) Dimitrov, V.; Linden, A. *Angew. Chem., Int. Ed.* **2003**, *42*, 2631. (e) Carnes, M.; Buccella, D.; Chen, J. Y. C.; Ramirez, A. P.; Turro, N. J.; Nuckolls, C.; Steigerwald, M. *Angew. Chem., Int. Ed.* **2009**, *48*, 290. (f) Martinez, G. E.; Ocampo, C.; Park, Y. J.; Fout, A. R. *J. Am. Chem. Soc.* **2016**, *138*, 4290.
- (11) Tomashenko, O. A.; Grushin, V. V. *Chem. Rev.* **2011**, *111*, 4475.
- (12) Connelly, N. G.; Geiger, W. E. *Chem. Rev.* **1996**, *96*, 877.
- (13) (a) Hegedus, L. S.; Miller, L. L. *J. Am. Chem. Soc.* **1975**, *97*, 459. (b) Tsou, T. T.; Kochi, J. K. *J. Am. Chem. Soc.* **1979**, *101*, 6319. (c) Hegedus, L. S.; Thompson, D. H. P. *J. Am. Chem. Soc.* **1985**, *107*, 5663.
- (14) Thermolysis of **2b** was also carried out in THF but did not lead to any desired coupled product.
- (15) Zhang, C.-P.; Wang, H.; Klein, A.; Biewer, C.; Stirnat, K.; Yamaguchi, Y.; Xu, L.; Gomez-Benitez, V.; Vicic, D. A. *J. Am. Chem. Soc.* **2013**, *135*, 8141.
- (16) The difference in reactivity between the two reagents could be related to the driving force of Ag^0 precipitation upon oxidation of **1a** and reduction of AgBF_4 .
- (17) An alternative path of decomposition could be undesirable side reactions of Ni^{I} with the Ni^{III} . However, the addition of $\text{Cp}_2^* \text{FeBF}_4$ leads to Ni^{IV} formation in the presence of acetate. This is consistent with the CV data using NMe_4OAc as electrolyte which shows a considerably lower Ni^{IV} onset potential (Figure 4.10).
- (18) Davis, B. L.; Rekker, B. D.; Michalczyk, R.; Garner, E. B.; Kalviri, H. R.; Baker, T. M.; Thorn, D. L.; Dixon, D. A. *Chem. Commun.* **2013**, *49*, 9095.
- (19) (a) Evans, D. F. *J. Chem. Soc.* **1959**, 2003. (b) Piguet, C. *J. Chem. Educ.* **1997**, *74*, 815
(c) Bain, G. A.; Berry, J. F. *J. Chem. Educ.* **2008**, *85*, 532.
- (20) Maleckis, A.; Sanford, M. S. *Organometallics* **2014**, *33*, 3831.

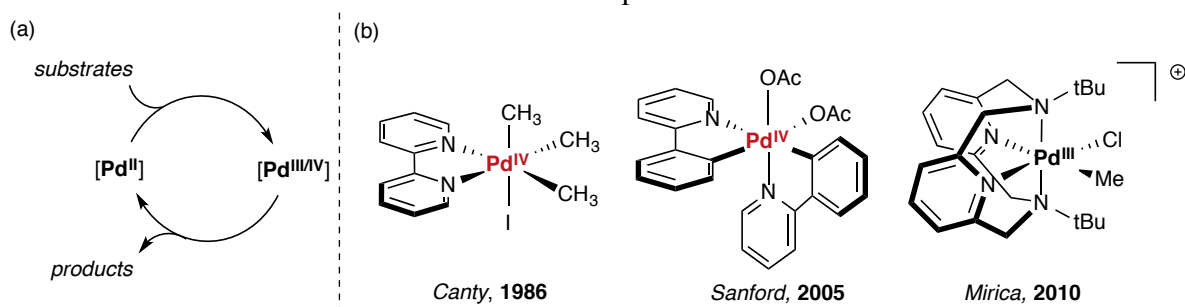
CHAPTER 5

Investigation of the Accessibility, Reactivity, and Mechanisms of High-Valent Ni and Pd Complexes

5.1. Introduction

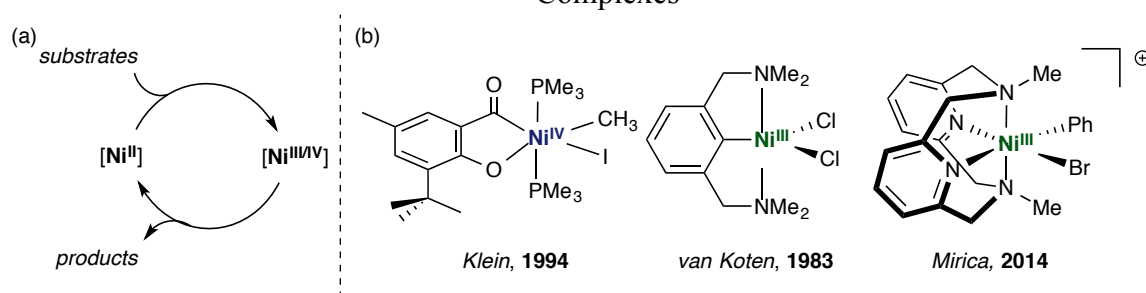
Over the past several decades, fundamental organometallic studies of high-valent Pd complexes have helped to establish Pd^{IV} as a viable and synthetically useful intermediate in catalysis (Figure 5.1).^{1,2} These studies have demonstrated that Pd^{IV} can be accessed under mild reaction conditions using a variety of 2e⁻ oxidants.^{1,2} Furthermore, they have shown that Pd^{IV} can enable challenging reductive elimination reactions that are often complementary to those occurring from more traditional Pd^{II} centers.¹⁻³ While Pd^{III} complexes are less common in the literature, studies by Ritter, Mirica, and others have demonstrated the competency of these species in mediating carbon-carbon and carbon-heteroatom bond-forming reactions.⁴ Overall, these fundamental studies have played a central role in driving the field of high-valent Pd catalysis, which is now widely used for challenging transformations such as C-H functionalization and alkene difunctionalization reactions.⁵

Figure 5.1. (a) High-Valent Pd Catalysis and (b) Representative Organometallic Pd^{III} and Pd^{IV} Complexes



In recent years, tremendous progress has been made in the field of nickel catalysis.⁶ In addition to being a sustainable and low-cost alternative to palladium, new developments in organonickel chemistry have demonstrated that the intrinsic properties of nickel enable transformations that are often not accessible with palladium (i.e., cross-coupling reactions that utilize tertiary alkyl halides⁷ or phenol derivatives⁸ as electrophiles).⁹ However, in comparison to Pd, the organometallic chemistry of high-valent Ni remains largely underdeveloped. Our lab and others have begun to investigate the synthesis and reactivity of organometallic Ni^{III} and Ni^{IV} complexes, and these investigations have provided support for their involvement in challenging bond-forming reactions (Figure 5.2).^{10,11} Despite these contributions, very little work has been done to directly compare the relative reactivity and selectivity profiles of Ni to its group 10 congener Pd.¹² A systematic comparison of the organometallic chemistry of high-valent Ni to the more established chemistry of high-valent Pd would provide insight into the similarities and differences of these systems. This, in turn, would inform the rational development of new transition metal catalyzed reactions.

Figure 5.2. (a) High-Valent Ni Catalysis and (b) Representative Organometallic Ni^{III} and Ni^{IV} Complexes



This chapter describes a direct investigation of the organometallic chemistry of high-valent Pd and Ni in order to probe several key features, including: (i) the accessibility of high-valent Pd (Pd^{IV} and/or Pd^{III}) complexes versus high-valent Ni (Ni^{IV} and/or Ni^{III}); (ii) the relative reactivity and selectivity of Pd^{IV} versus Ni^{IV} in carbon–carbon and carbon–heteroatom bond-forming reactions; and (iii) the mechanistic pathways of these transformations. Overall, these experimental and computational studies demonstrate that Ni undergoes 1e⁻ redox chemistry

more readily than Pd to access catalytically relevant Ni^{III} and Ni^{IV} species. The accessibility of these distinct oxidation states enables transformations and mechanistic pathways not seen at Pd centers.

5.2. Results and Discussion

Probing the Accessibility of High-Valent Ni and Pd: Electrochemical Oxidations

We first sought to compare the accessibility of high-valent Ni and Pd complexes by studying the electrochemistry of the M^{II} analogues **1-Ni** and **1-Pd**. Prior studies on related systems have demonstrated that tris(pyrazolyl) borate (Tp) and cyclometallated neophyl ligands are particularly stabilizing to high-valent group 10 metal complexes.^{1s,13,14} Complex **1-Ni** was prepared by ligand displacement of the precursor (PMe₃)₂Ni^{II}(CH₂CMe₂-*o*-C₆H₄) with potassium tris(pyrazolyl)borate (KTP) in 93% yield (Scheme 5.1a). Similarly, the treatment of (COD)Pd(CH₂CMe₂-*o*-C₆H₄) with 1 equiv of NMe₄Tp afforded **1-Pd** in 89% isolated yield (Scheme 5.1b).

Scheme 5.1. Synthesis of M^{II} Precursors (a) K[(Tp)Ni^{II}(CH₂CMe₂-*o*-C₆H₄)] (**1-Ni**) and (b) NMe₄[(Tp)Pd^{II}(CH₂CMe₂-*o*-C₆H₄)] (**1-Pd**)

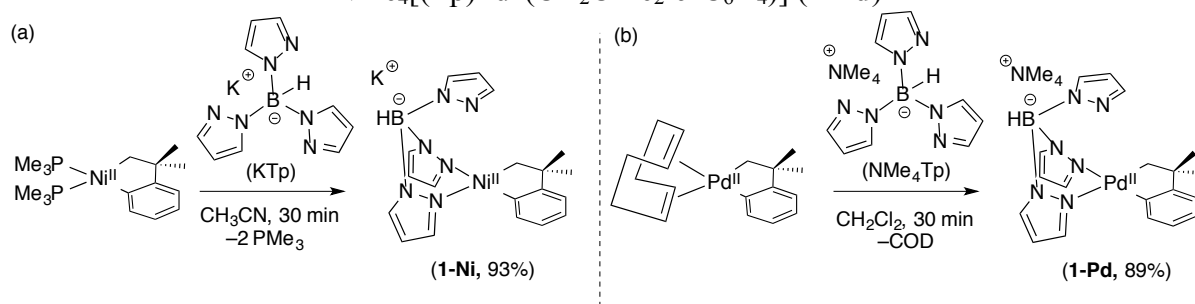
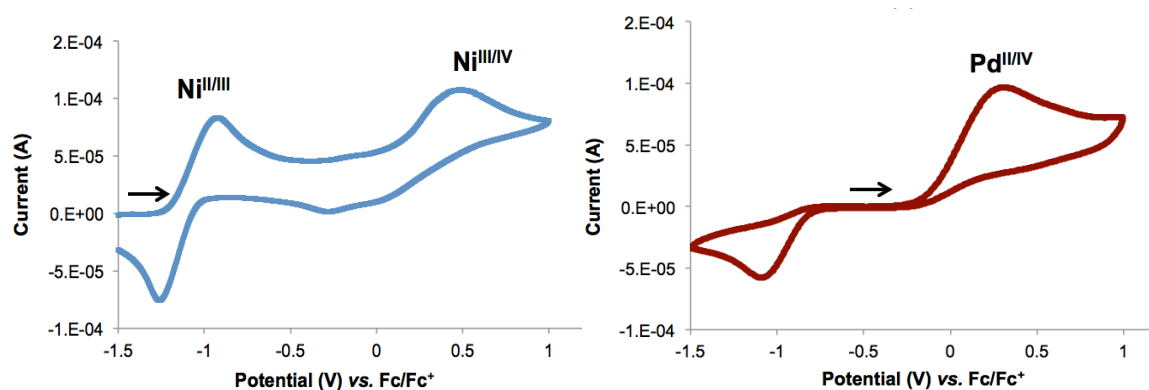


Figure 5.3 displays the cyclic voltammograms (CVs) of **1-Ni** and **1-Pd** in acetonitrile using tetrabutylammonium hexafluorophosphate (NBu₄PF₆) as supporting electrolyte. The CV of **1-Ni** reveals two quasi-reversible redox couples at approximately -1.1 V and +0.10 V vs. Fc/Fc⁺, which correspond to the Ni^{II/III} and Ni^{III/IV} couples, respectively. The onset potential associated with the Ni^{II/III} couple is among the lowest reported for an organometallic Ni complex, which is likely a result of the strong electron-donating character of the Tp and

cycloneophyl ligands. Furthermore, the distinct redox couples demonstrate the propensity of nickel to readily undergo single electron transfer chemistry. Despite the relatively low onset potentials of both couples, the large peak separation between the Ni^{III} and Ni^{IV} oxidations (approximately 1.2 V) indicates that the Ni^{III} to Ni^{IV} electron transfer is at much higher energy than the Ni^{II} to Ni^{III} process with this ligand system.

Figure 5.3. Cyclic Voltammograms of M^{II} Precursors **1-Ni** and **1-Pd**. Conditions: [Ni] = 0.01 M in MeCN, [NBu₄BF₄] = 0.1 M, Scan Rate = 100 mV/s; [Pd] = 0.005 M in MeCN/pyr, [NBu₄PF₆] = 0.1 M, Scan Rate = 100 mV/s.



In comparison, the CV of Pd^{II} complex **1-Pd** (Figure 5.3) contains a single $2e^-$ oxidation wave at -0.10 V and a corresponding reduction at -0.8 V vs. Fc/Fc⁺. We assign these features to the Pd^{II/IV} redox couple. CVs depicting net two electron transfer processes for *mer*-coordinated Pt complexes and related Pd complexes have been reported.^{15,16} The unique redox chemistry in these systems was rationalized by the anticipated instability of the corresponding M^{III} species.¹⁵ An alternative explanation for the electron transfer process in Figure 5.3 can be related to the energy cost differences between a Pd^{II} to Pd^{III} oxidation versus a Pd^{III} to Pd^{IV} oxidation. In this scenario, the energy required to remove the first electron from Pd^{II} is much larger than the energy required to remove the second electron.¹⁷ Notably, this contrasts with the trend seen at Ni, in which removal of the first electron occurs at much lower energy than that of the second.

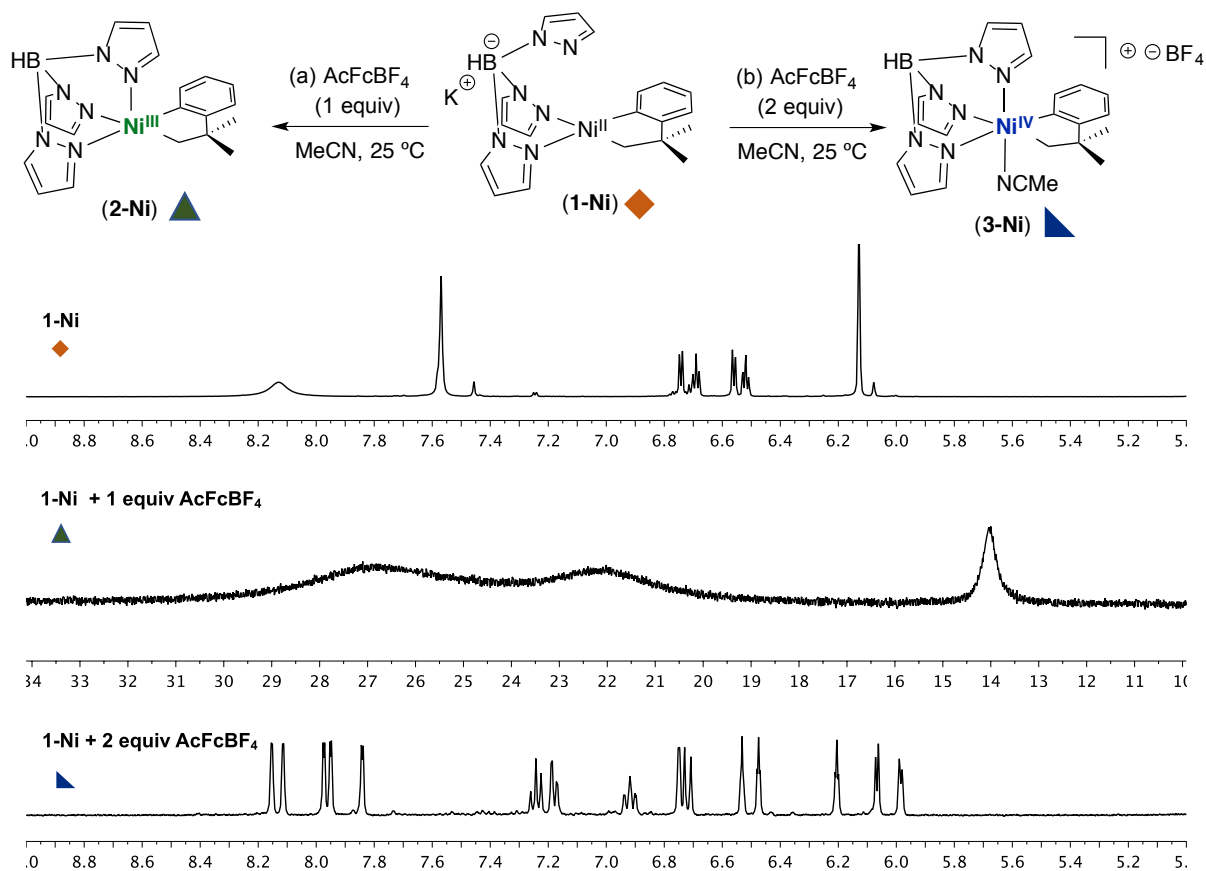
The large peak separation between the oxidation and reduction waves in both CVs shown in Figure 5.3 can be rationalized based on the large molecular reorganization that

accompanies an octahedral and square planar interconversion.^{15,16,18} This effect is more dramatic for Pd, possibly due to the comparatively more stable octahedral center. Overall, CVs of **1-Ni** and **1-Pd** suggest that while Ni can access distinct one-electron redox pathways, the analogous Pd^{II} complex preferentially undergoes two-electron redox events. Moreover, while the +4 oxidation state of Ni and Pd can be accessed at relatively similar onset potentials (+0.10 V and -0.10 V, respectively), Ni^{III} is readily accessed at a significantly lower potential (-1.1 V). The difference between the accessibilities of the high-oxidation states for nickel and palladium mirror the trends seen in the literature in which Pd^{IV} and Ni^{III} complexes are more common than their Pd^{III} and Ni^{IV} counterparts.^{1,4,10,11}

Probing the Accessibility of High-Valent Ni and Pd: Chemical Oxidations

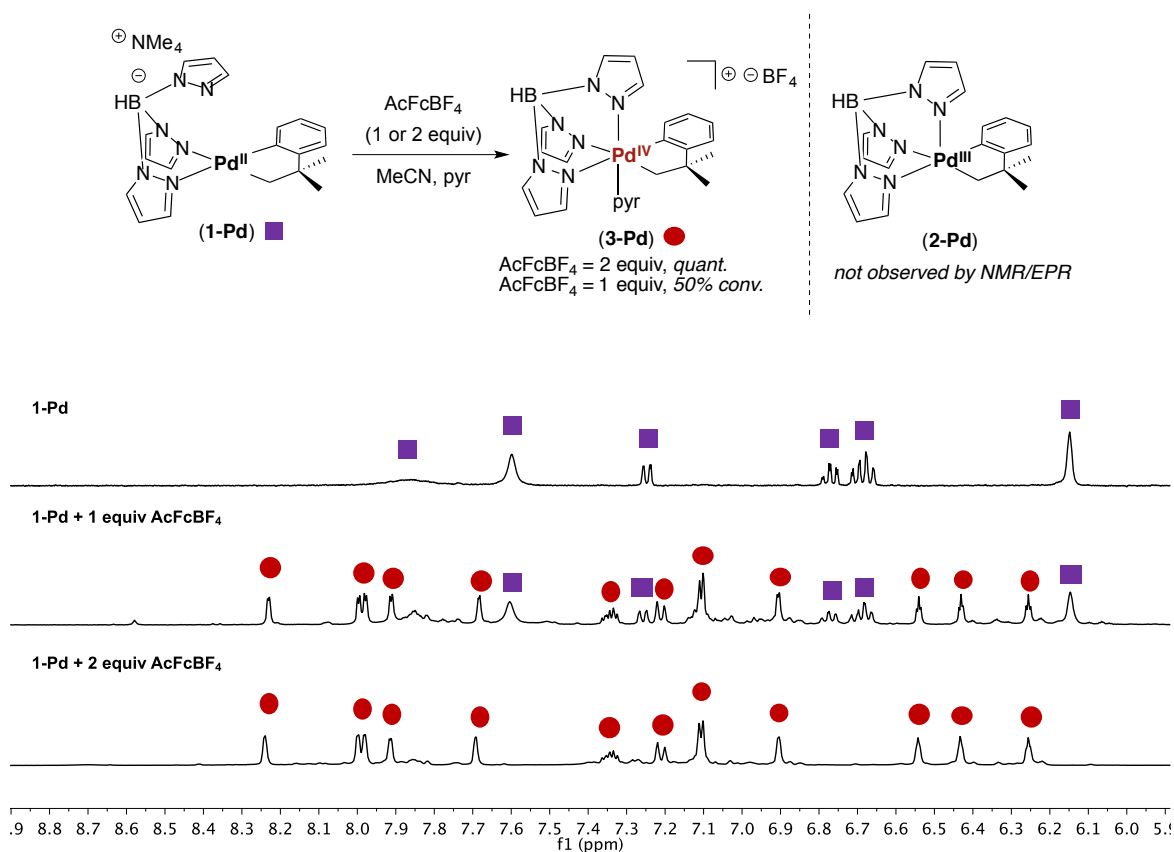
The chemical oxidation of **1-Ni** and **1-Pd** with outer-sphere $1e^-$ oxidants was next evaluated by ¹H NMR spectroscopy. These studies were conducted with acetylferrocenium tetrafluoroborate (AcFcBF₄) as the oxidant due to its suitable redox potential and solubility under the reaction conditions ($E^0 = +0.27$ V vs. Fc/Fc⁺).¹⁹ The treatment of **1-Ni** with 1 equiv of AcFcBF₄ resulted in full consumption of the diamagnetic Ni^{II} starting material and concomitant formation of paramagnetic species in the ¹H and ¹¹B NMR spectra. The observed resonances correspond to those that were previously assigned to the Ni^{III} complex **2-Ni** (Figure 5.4).²⁰ In contrast, the use of 2 equiv of AcFcBF₄ under otherwise identical conditions afforded a diamagnetic product in >95% NMR yield that we assign as the cationic Ni^{IV} complex **3-Ni** (Figure 5.4) Together with electrochemical analyses, these results support the viability of sequential $1e^-$ oxidations of **1-Ni**.

Figure 5.4. ^1H NMR Oxidation Studies of **1-Ni** with 1 or 2 equiv of AcFcBF_4 , Generating the Paramagnetic Ni^{III} Complex **2-Ni** or Diamagnetic Ni^{IV} Complex **3-Ni**



The analogous chemical oxidations of Pd^{II} precursor **1-Pd** were subsequently examined. While the Ni^{IV} complex **3-Ni** was stable in the presence of the weakly coordinating acetonitrile ligand, the treatment of **1-Pd** with 2 equiv of AcFcBF_4 in MeCN led to an unidentifiable complex mixture. However, the addition of a stronger donor ligand, pyridine- d_5 , afforded the cationic Pd^{IV} complex **3-Pd** in quantitative NMR yield (Figure 5.5). Pyridine likely increases the stability of the cationic Pd^{IV} center for detection, and the ^1H NMR spectrum of **3-Pd** is consistent with that reported in the literature.¹⁶ Interestingly, the treatment of **1-Pd** with 1 equiv of AcFcBF_4 resulted in a 50:50 mixture of Pd^{IV} complex **3-Pd** and unreacted Pd^{II} starting material **1-Pd** (Figure 5.5). No Pd^{III} products were observed by NMR or EPR spectroscopy. This observation is consistent with the electrochemical analyses of **1-Pd**, which suggest the propensity of Pd to undergo selective two-electron oxidation events.

Figure 5.5. ^1H NMR Oxidation Studies of **1-Pd** with 1 or 2 equiv of AcFcBF_4

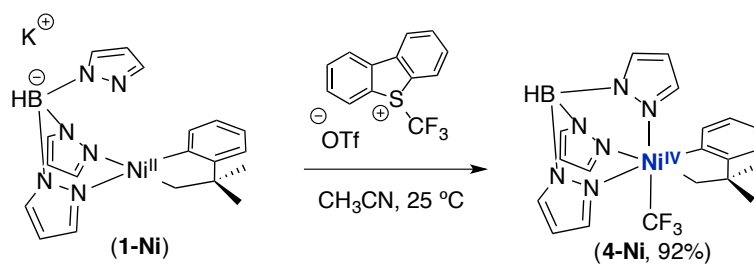


Synthetic and Mechanistic Studies at Ni^{IV} and Pd^{IV}

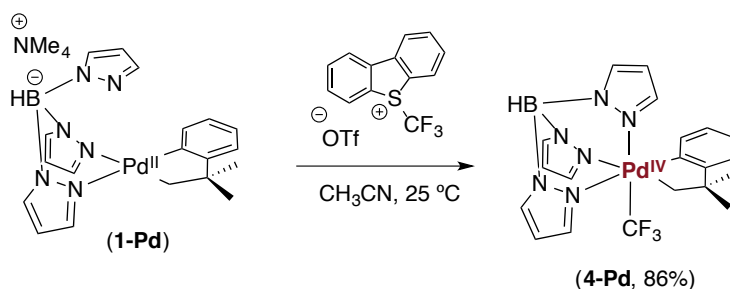
The design of high-valent metal catalyzed reactions requires not only a detailed understanding of the accessibility of the reactive intermediates, but also the impact of the metal center on the anticipated reactivity. As such, the reactivity, selectivity, and mechanistic profiles of bond-forming reactions at Ni^{IV} and Pd^{IV} centers were investigated. For these studies, we targeted isolable complexes of general structure $\text{TpM}^{\text{IV}}\text{CF}_3(\text{CH}_2\text{CMe}_2\text{-}o\text{-C}_6\text{H}_4)$ (Tp = tris(pyrazolyl)borate). We have previously shown that the trifluoromethyl ligand stabilizes the Ni^{IV} analogue **4-Ni**, thereby enabling mechanistic studies of C–C and C–heteroatom coupling reactions from that complex.^{11f} ^{11}f Ni complex **4-Ni** was prepared in 92% isolated yield following treatment of **1-Ni** with the electrophilic trifluoromethylating reagent, *S*-(trifluoromethyl) dibenzothiophenium triflate (Umemoto's Reagent), and subsequent purification by silica gel chromatography (Scheme 5.2). Similarly, the Pd analogue **4-Pd** was synthesized by the net

two-electron oxidation of Pd^{II} precursor **1-Pd** with Umemoto's Reagent in 86% isolated yield (Scheme 5.3). Both complexes were sufficiently stable for isolation, were not sensitive to water or air, and did not undergo decomposition in an acetonitrile solution over several days. These results provide ongoing support that similar design strategies can be employed for stabilizing other high-valent group 10 metal centers.^{2,13,14}

Scheme 5.2. Synthesis of TpNi^{IV}CF₃(CH₂CMe₂-*o*-C₆H₄) (**4-Ni**)

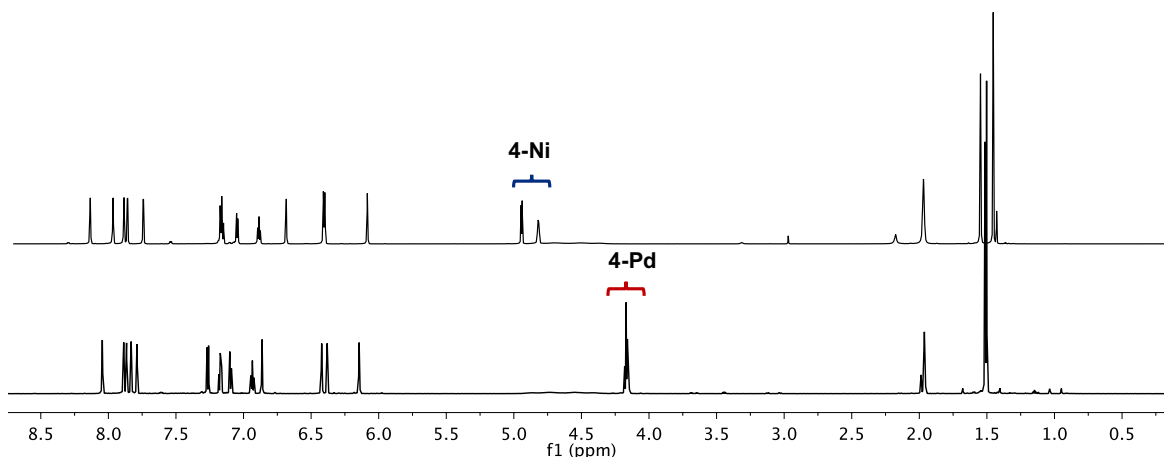


Scheme 5.3. Synthesis of TpPd^{IV}CF₃(CH₂CMe₂-*o*-C₆H₄) (**4-Pd**)



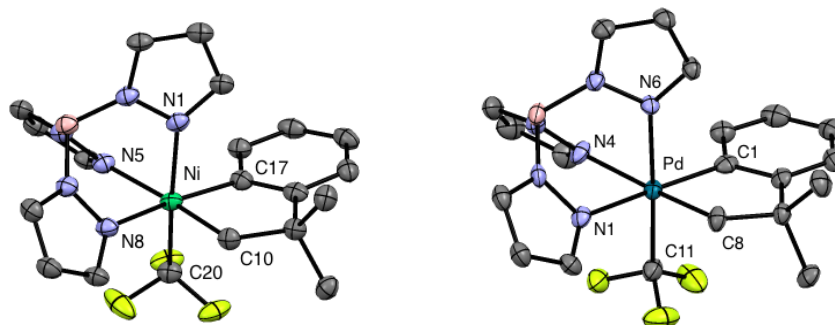
Complexes **4-Ni** and **4-Pd** were fully characterized by ¹H, ¹³C, ¹¹B, and ¹⁹F NMR spectroscopy. The ¹H NMR spectra (Figure 5.6) of these complexes are remarkably similar, and display proton resonances consistent with a κ³-tris(pyrazolyl) borate scaffold bound to an octahedral metal(IV) center. One notable distinction between the two spectra is the chemical shift of the diastereotopic methylene protons in **4-Ni** (4.7-4.9 ppm) and **4-Pd** (4.1-4.2 ppm). The greater deshielding effect of the α-protons in **4-Ni** suggests a comparatively more electrophilic M^{IV}-σ-alkyl carbon.

Figure 5.6. ^1H NMR Spectra of **4-Ni** and **4-Pd** in Acetonitrile- d_3 , Highlighting the Methylene Protons in Both Complexes



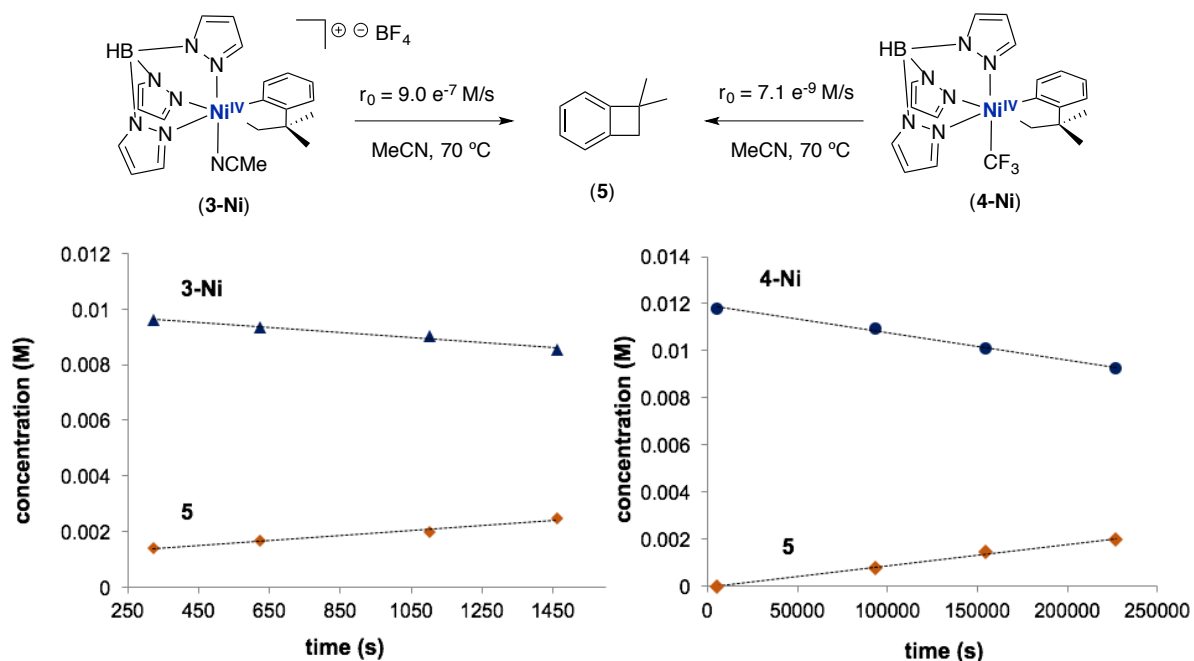
Characterization of the Ni and Pd analogues by X-ray crystallography allowed comparison of the structural features of these complexes. X-ray quality crystals of **4-Ni** were obtained by slow evaporation of a methanol solution, and colorless needles of **4-Pd** were grown from a concentrated acetone solution of the compound at room temperature. The solid-state structures of both complexes are shown in Figure 5.7. The Tp ligand binds κ^3 to both metal centers, forming the anticipated octahedral geometry. The Pd analogue exhibits significantly longer bond lengths, as might be expected for the second-row transition metal. For example, the Pd–CF₃ bond length (2.036 Å) is approximately 0.1 Å longer than that of the Ni analogue (1.941 Å), but comparable to that of related Pd^{IV}–CF₃ complexes reported in the literature.²¹ Consequently, the CF₃ group in the crystal structure of **4-Pd** is disordered, owing to its free rotation about the metal center. This is in contrast to the X-ray structure of **4-Ni** in which the shorter bond length and greater steric congestion appear to restrict rotation around the Ni^{IV}–CF₃ axis.²²

Figure 5.7. ORTEP diagrams of (a) **4-Ni** and (b) **4-Pd**. Thermal ellipsoids are drawn at 50% probability. Hydrogen atoms and disorder in the trifluoromethyl group of **4-Pd** have been omitted for clarity.

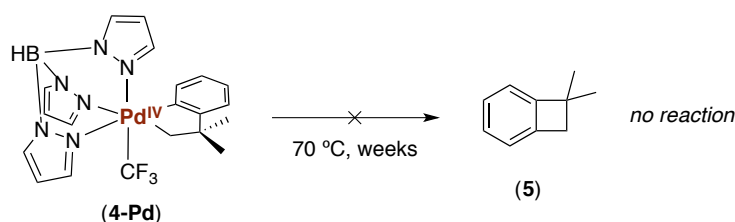


The reactivity of the Ni and Pd analogues toward bond-forming reactions was next evaluated. As shown in Figure 5.8, heating Ni^{IV} complex **4-Ni** at 70 °C in MeCN resulted in slow C(sp³)-C(sp²) bond-forming reductive elimination to afford cyclobutane product, **5** ($r_0 = 7.1e^{-9}$ M/s at 70 °C, where [Ni] = 0.011 M). This reaction is approximately 100-fold slower than from the cationic Ni^{IV} complex **3-Ni** ($r_0 = 9.0e^{-7}$ M/s at 70 °C, where [Ni] = 0.011 M). This is presumably due to stabilization of the Ni^{IV} by the CF₃ ligand. The effect was even more dramatic for palladium, with no decomposition of **4-Pd** observed at 70 °C over several weeks (Scheme 5.4). The enhanced stability of the Ni and Pd analogues allowed the reactivity and mechanisms of carbon-heteroatom couplings from these complexes to be directly compared.

Figure 5.8. Initial Rate Data for C–C Coupling from Ni^{IV}–CF₃ **4-Ni** and Cationic Ni^{IV} **3-Ni** to Form Benzocyclobutane **5** at 70 °C, Demonstrating Stabilization of the CF₃ Ligand



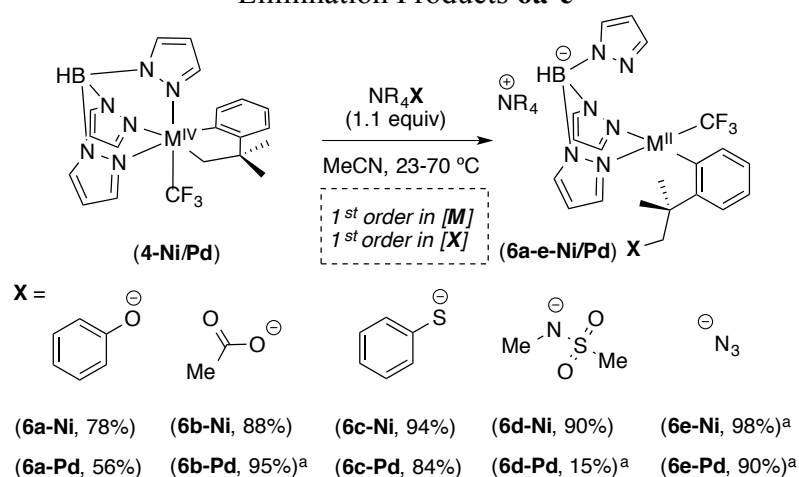
Scheme 5.4. Stability of **4-Pd** towards C–C Reductive Elimination



The treatment of **4-Ni** with O, N, and S-based nucleophiles (NMe₄X; where X = OAc, OPh, SPh, NMeMs, and N₃) led to highly selective C(sp³)-heteroatom coupling to form Ni^{II} products **6a-e-Ni** (Scheme 5.5). Kinetic studies revealed that these reactions are 2nd order overall: first order in [Ni^{IV}] and first order in [nucleophile]. Similar studies were carried out with complex **4-Pd** to compare the relative reactivity of the two metal centers. The treatment of **4-Pd** with 1.1 equiv of the respective nucleophiles led to C(sp³)-heteroatom coupled products **6a-e-Pd** in 56-84% isolated yields (Scheme 5.5).²³ No products attributed to C–C or C(sp²)-heteroatom coupling were observed under any of the conditions examined. In all cases, the reactions exhibited a first order dependence on [Pd^{IV}] and a first order dependence on [nucleophile]. Plots of the Swain-Scott nucleophilicity parameters (n_x) versus the initial rates

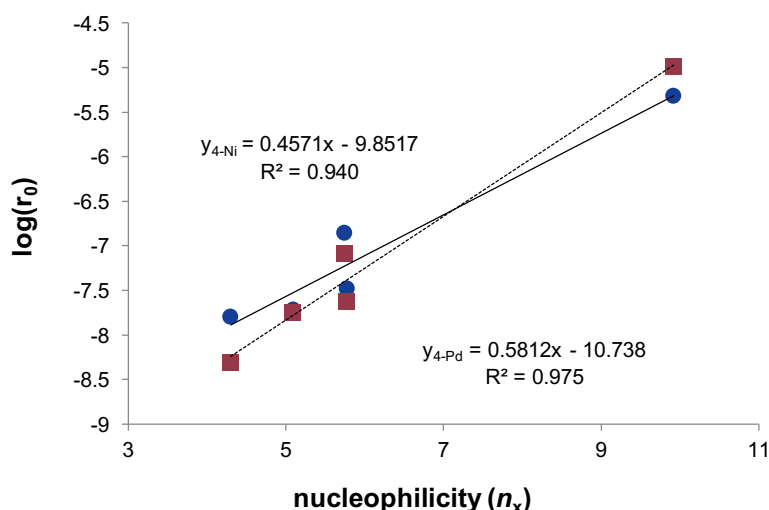
of these reactions (r_0) show a linear correlation for both Ni and Pd (0.975 and 0.940, respectively, Figure 5.9).²⁴ Overall, these data are consistent with an S_N2 -type reductive elimination pathway for both complexes, which is generally favored for $C(sp^3)$ -heteroatom couplings from high-valent group 10 metal centers.^{13c-e,25}

Scheme 5.5. $C(sp^3)$ -heteroatom Coupling from M^{IV} Complexes **4-Ni/Pd** to Form Reductive Elimination Products **6a-e**



^aRepresents crude NMR yield; reaction required 5 equiv of NR_4X to reach completion.

Figure 5.9. Swain-Scott Plot Relating the Relative Nucleophilicities (n_x) with the Initial Rate of C-Heteroatom Coupling. Starting Conditions: $[Ni] = 0.0044$ M, $[X] = 0.0054$ M, 23 °C; $[Pd] = 0.011$ M, $[X] = 0.057$ M, $T = 60$ °C



While complexes **4-Ni/Pd** exhibited the same selectivity for $C(sp^3)$ -heteroatom coupling in the presence of external nucleophiles, the rates at which these processes occurred were dramatically different. For example, in the presence of 5 equiv of NMe_4OPh , $C(sp^3)$ -O

coupling at Ni^{IV} proceeded with a significantly faster rate ($r_0 = 1.1 \times 10^{-6}$ M/s at 30 °C) than from the analogous Pd^{IV} center ($r_0 = 1.1 \times 10^{-8}$ M/s at 30 °C). The dramatic difference in reactivity between the two metal centers prompted us to investigate the mechanisms of these transformations further.

The initial rates of C(sp³)-O from **4-Ni** and **4-Pd** were examined as a function of temperature (For Ni: -10 to 40 °C; For Pd: 30 to 70 °C). The resulting Eyring plots are shown in Figure 5.10, and the activation parameters from this analysis are provided in Table 5.1. The negative entropy of activation values (ΔS^\ddagger) obtained for both Ni and Pd (-12.0 and -8.09 eu, respectively) indicate an increase in order in the transition states for these reductive elimination reactions. These results are consistent with an associative mechanism involving nucleophilic attack of ⁻OPh on the M^{IV}-alkyl carbon.^{13e,25} Overall, the Eyring parameters suggest similar mechanisms for C-O coupling at the two metal centers, with the Pd system being a significantly higher energy process.

Figure 5.10. Eyring Plot for C(sp³)-heteroatom Coupling from M^{IV} Complexes **4-Ni** and **4-Pd**. Conditions: [Ni] = 0.011 M, [NMe₄O⁻Ph] = 0.055 M, -10 to 40 °C; [Pd] = 0.011 M, [NMe₄O⁻Ph] = 0.055 M, T = 30 to 70 °C

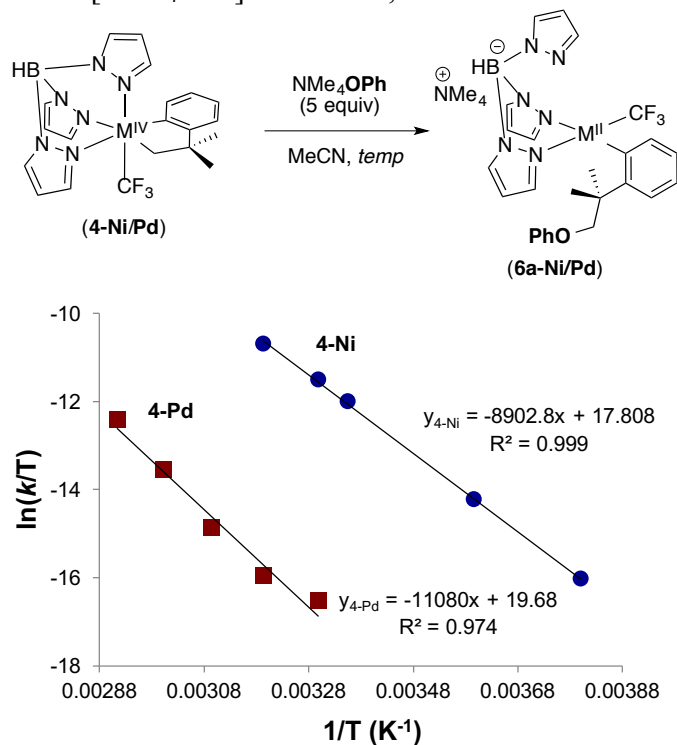


Table 5.1. Activation Parameters for C(sp³)–O Coupling from **4-Ni** and **4-Pd**

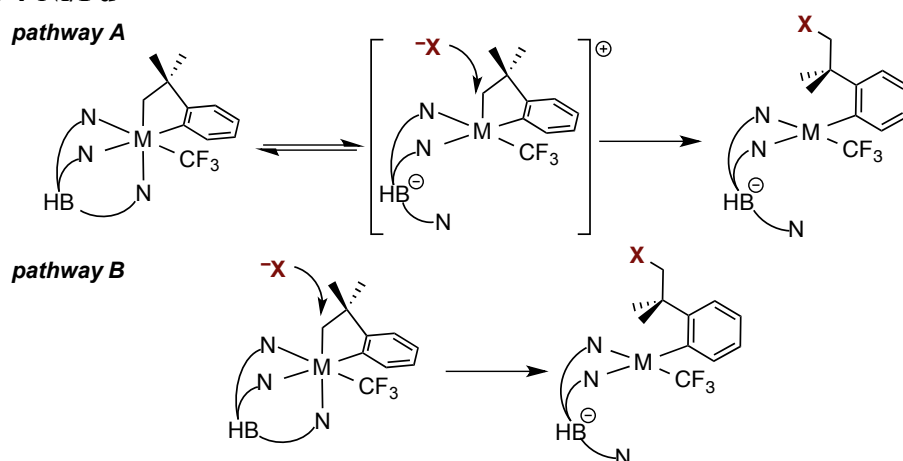
	4-Ni	4-Pd
$\Delta H^{\ddagger a}$	17.7	22.0
$\Delta S^{\ddagger b}$	-12.0	-8.09
$\Delta G_{303K}^{\ddagger a}$	21.3	24.5

^akcal/mol ^bcal/molK

Computational Details

The experimental data strongly implicate a mechanism involving S_N2-type attack by the nucleophiles on the methylene group attached to the M^{IV} center. Similar mechanisms have been proposed both experimentally and computationally for reductive elimination reactions at related cycloneophyl Pd^{IV} complexes.^{13c-e} However, in these reactions, dissociation of a ligand (typically the nucleophile, X) is often required prior to nucleophilic attack. Indeed, the vast majority of reductive elimination reactions at high-valent group 10 centers (i.e., Pd^{IV} and Pt^{IV}) are proposed to occur from five-coordinate intermediates^{1,2,13c-e,25} In the present system, C(sp³)–heteroatom coupling at M^{IV} complexes **4-Ni** and **4-Pd** could occur via dissociation of a pyrazole group (pathway A) or by direct nucleophilic attack at the six-coordinate complex (pathway B), a transformation that has much less precedence at high-valent group 10 centers (Figure 5.11).²⁶ Thus, in collaboration with Dr. Allan Canty (University of Tasmania), we utilized Density Functional Theory (DFT) to explore several key features of these processes including: (i) whether an open coordination site at M^{IV} is necessary for S_N2-type C–heteroatom coupling and (ii) how the mechanistic pathways and transition states for reductive elimination at Pd^{IV} centers compare to those at Ni^{IV}.

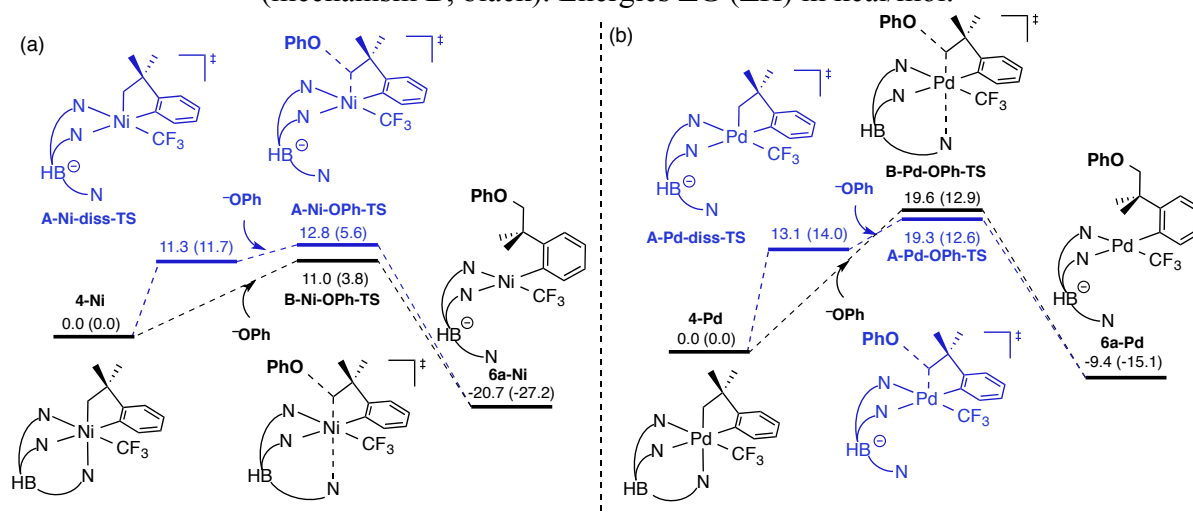
Figure 5.11. Possible S_N2 Mechanisms for Carbon–Heteroatom Coupling from M^{IV} Complexes **4-Ni/Pd**



Models¹ for S_N2 transition states for C–X coupling from complexes **4-Ni** and **4-Pd** were examined after dissociation of one pyrazole group to give a five-coordinate M^{IV} center (pathway A) as well as those formed via direct nucleophilic attack at the octahedral centers (pathway B). Computation for the Pd and Ni systems were carried out for X = OPh, OAc, SPh, and N_3 . The results with phenoxide (^-OPh) and thiophenoxide (^-SPh) are shown as representative examples in Figures 5.12 and 5.13. Energy profiles for the reaction of phenoxide with **4-Ni** and **4-Pd** are shown in Figure 5.12. The transition states for C–O bond-formation at the Pd^{IV} center (for X = OPh) via pathways A (19.3 kcal/mol) and B (19.6 kcal/mol) are substantially higher in energy than the analogous processes at Ni^{IV} (12.8 kcal/mol and 11.0 kcal/mol, respectively), consistent with our experimental studies. However, in both systems, the barriers for C–O coupling at the five-coordinate and six-coordinate centers are remarkably similar in energy (for Pd, $\Delta\Delta G^\ddagger = 0.3$ kcal/mol; For Ni, $\Delta\Delta G^\ddagger = 1.8$ kcal/mol). These calculations indicate that ligand dissociation to generate a five-coordinate intermediate is not essential for S_N2 -type coupling at Pd^{IV} and Ni^{IV} centers. This is in marked contrast to most literature examples of this type of transformation.^{2,25}

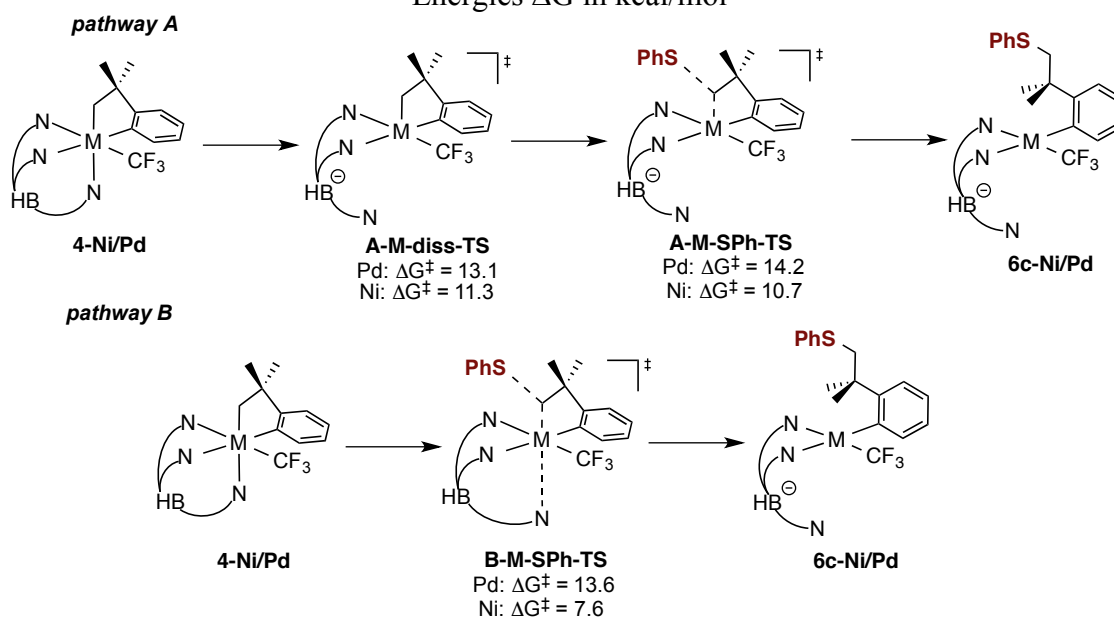
¹ Computational studies were carried out by Professor Allan Canty and Professor Alireza Ariafard at the University of Tasmania. For full computational details, see the experimental section.

Figure 5.12. Energy Profiles for the Reaction of Phenoxide with (a) **4-Ni** and (b) **4-Pd** via a Five-coordinate Intermediate (mechanism A, blue), or Direct Nucleophilic Attack (mechanism B, black). Energies ΔG (ΔH) in kcal/mol.



The transition structures and mechanistic pathways for the two complexes are more distinct when the strongest nucleophile, thiophenoxide, serves as the coupling partner ($X = \text{SPh}$). For palladium, the calculations again show similar barriers for five-coordinate ($\Delta G^\ddagger = 14.2$ kcal/mol, pathway A) and six-coordinate ($\Delta G^\ddagger = 13.6$ kcal/mol, pathway B) mechanisms. However, transition structures formed from the octahedral center via pathway B exhibit lengthened $\text{Pd}\cdots\text{N}$ distances *trans* to the site of nucleophilic attack at the methylene group ($\text{Pd}\cdots\text{N}_{\text{ax}} = 2.937$ Å, for $X = \text{SPh}$).²⁷ The very long $\text{Pd}\cdots\text{N}$ distance appears to represent a very weak bonding interaction, and thus pathway B can be considered a “five-coordinate-like” transition state in this system.

Figure 5.13. Energy Schemes for the Reaction of Thiophenoxide with **4-Ni** and **4-Pd** via a Five-coordinate Intermediate (pathway A), or Direct Nucleophilic Attack (pathway B). Energies ΔG in kcal/mol



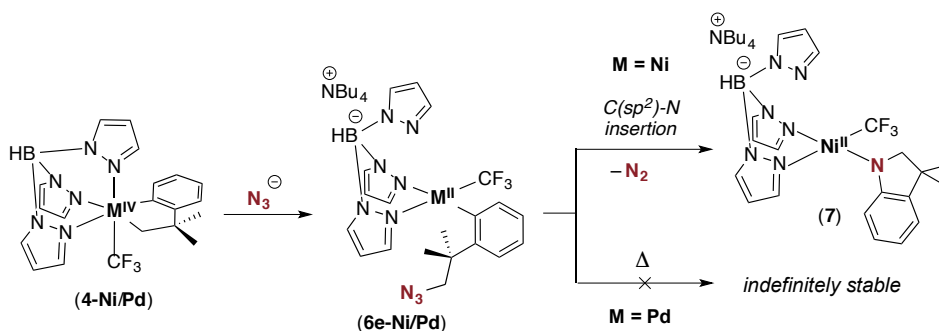
In marked contrast, for Ni, the κ^3 -Tp mechanism (pathway B, Figure 5.13) is clearly the lower energy pathway. This mechanism is favored with a $\Delta\Delta G^\ddagger$ 3.7 kcal/mol. Notably, examples of reductive elimination events occurring from six-coordinate high-valent group 10 metal centers are rare in the literature.²⁶ We attribute this unusual reaction pathway to the highly electrophilic Ni^{IV}-alkyl carbon, which renders direct nucleophilic attack of strongly nucleophilic ⁻SPh to be lower in energy than pyrazole dissociation. We anticipate that this mode of reactivity can potentially be exploited at related Ni^{IV} centers, enabling milder and more selective reaction conditions. For example, selectivity issues arising in Pd^{II/IV} catalysis could potentially be avoided with the use of a highly electrophilic/coordinately saturated Ni^{IV} intermediate.

Reactivity and Mechanism of M^{II}-Alkyl Azides

As a final set of experimental and computational studies, the distinct reactivity of the M^{IV} complexes in the presence of tetrabutylammonium azide (NBu₄N₃) was compared. As shown in Scheme 5.6, the pendant alkyl azide **6e-Ni** that results from C(sp³)-N coupling at **4-Ni**, inserts into the C(sp²)-N bond to generate Ni^{II} intermediate **7** at room temperature.²⁸ The

corresponding Pd^{II} reductive elimination product **6e-Pd**, however, does not undergo the same insertion chemistry as Ni. Instead, **6e-Pd** is remarkably stable, with no decomposition observed even upon heating at 70 °C for several weeks.

Scheme 5.6. Distinct Reactivity of M^{II}-alkyl Azides **6e-Ni** and **6e-Pd**

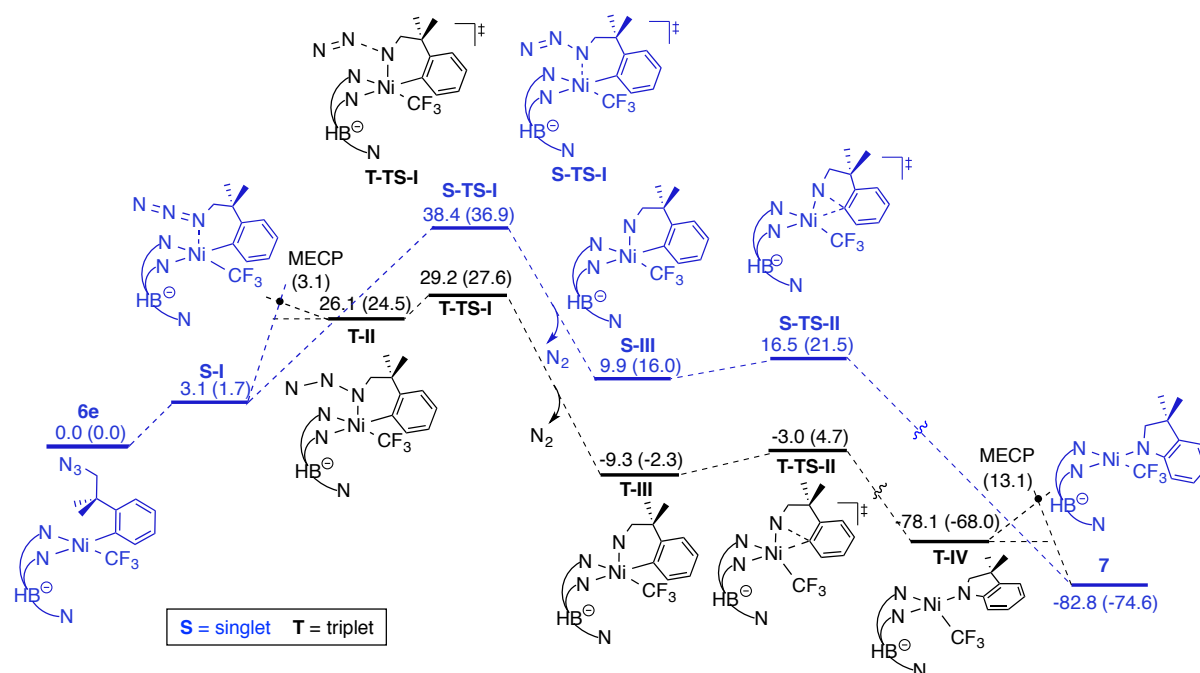


We hypothesized that the unique modes of reactivity between **6e-Ni** and **6e-Pd** could be related to the accessibility/and or reactivity of high-valent Ni and Pd intermediates. DFT calculations were therefore carried out (again in collaboration with Prof. Allan Canty) to explore the viability of such pathways. The lowest energy profiles for the Ni system were determined to be the singlet open shell pathway via a Ni^{IV}-imido intermediate (Figure 5.14, blue) and the triplet mechanism via a Ni^{III}-iminyl intermediate (Figure 5.14, black). For the singlet mechanism (blue profile, Figure 5.14), an initial weak Ni···N interaction in **S-I** leads to transition structure **S-TS-I**, resulting in formation of the Ni^{IV}-imido complex **S-III**. This species then undergoes reductive elimination to generate C(sp²)-N coupled product **7**.

Using this profile for guidance, a reaction manifold for the triplet species was obtained that was substantially lower in energy ($\Delta\Delta G^\ddagger = 9.2$ kcal/mol) (Figure 5.14, black). This pathway involves a Minimum Energy Crossing Point (MECP) from **S-I** to the initial triplet structure **T-II**. The triplet transition structure **T-TS-I** leads to Ni^{III}-iminyl intermediate **T-III** following loss of N₂. C-N coupling from this triplet species and subsequent collapse of **T-IV** to Ni product **7** occurs via a Minimum Energy Crossing Point (MECP, ΔE 13.1 kcal/mol).

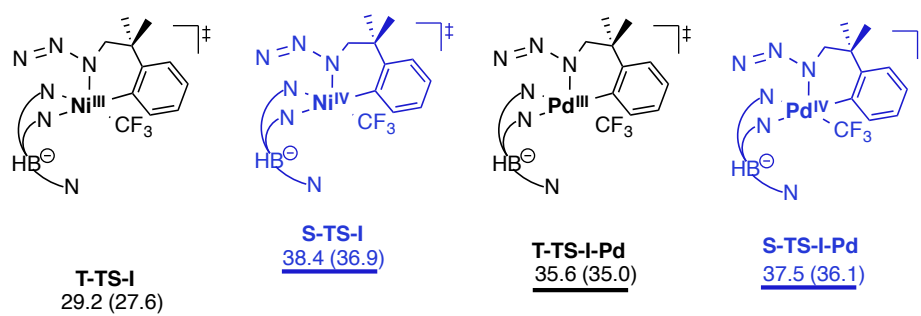
Overall, the calculations suggest that the distinct reactivity of the Ni^{II} alkyl azide **6e** can likely be attributed to a Ni^{III} mechanism.

Figure 5.14. Energy Profiles Computed for the Formation of Ni^{II} Indolinide Complexes from **6e-Ni** via Singlet (blue) and Triplet States (black). Energies ΔG (ΔH) in kcal/mol referenced to **6e**, except for the Minimum Energy Crossing Points (MECP) computed as ΔE 3.1 kcal/mol above **T-II**, and ΔE 13.1 kcal/mol above **T-IV**, at the BS1 level.



The analogous transformations at Pd were found to be substantially higher in energy than the Ni system (minimum $\Delta\Delta G^\ddagger = 6.4$ kcal/mol). This is consistent with experimental studies in which the Ni^{II} reductive elimination product **6e-Pd** did not undergo any bond-forming reactions after prolonged heating (Scheme 5.6). Interestingly, while the triplet Ni^{III}-iminyl pathway was favored over the singlet Ni^{IV}-imido mechanism ($\Delta\Delta G^\ddagger = 9.2$ kcal/mol), the two analogous processes for Pd were indistinguishable ($\Delta\Delta G^\ddagger = 1.9$ kcal/mol; Figure 5.15). These results are reminiscent of electrochemical studies of the system, which demonstrate the accessibility of Ni^{III} and, in contrast, Pd's preference for $2e^-$ pathways (Figure 5.3). Here, the ability of Ni to readily undergo single electron chemistry leads to unique reactivity that is not readily accessible at the Pd center.

Figure 5.15. Transition Structures Computed for Loss of N₂ from Ni^{II} Intermediate **6e-Ni** and Pd^{II} Complex **6e-Pd**. Energies ΔG^\ddagger (ΔH^\ddagger) in kcal/mol referenced to **6e-Ni** or **6e-Pd**.



5.3. Conclusions

The combined experimental and computational studies in this chapter reveal remarkable similarities in the chemistry of Ni^{IV} and Pd^{IV}, but a significantly enhanced role for Ni^{III} in enabling reactivity that is distinct from palladium. In particular, electrochemical analyses and chemical oxidation studies of Tp-ligated M^{II} precursors demonstrate the surprisingly comparable accessibility of the Ni^{IV} and Pd^{IV} oxidation states, despite only sporadic examples of well-defined Ni^{IV} complexes in the literature.¹¹ Reactivity and mechanistic studies of isolated Ni^{IV} and Pd^{IV} complexes showed that both species undergo selective carbon–heteroatom bond-forming reactions, with the Ni system reacting under much milder conditions.

In contrast to Pd, the +3 oxidation state for Ni is readily accessible and thus, more widely-accepted in the literature.²⁹ The propensity of Pd to undergo $2e^-$ redox chemistry and for Ni to readily promote one-electron transfer processes was highlighted in this chapter through electrochemical analyses, oxidation studies monitored by NMR spectroscopy, and distinct reactivity profiles of M^{II}-alkyl azide derivatives. Computations carried out on the latter system suggest that the Ni-mediated C(sp²)-N insertion process occurs via a transient Ni^{III}-iminyl intermediate, via a pathway that was not accessible for the analogous Pd complex. Overall, these results demonstrate the importance of metal, ligand, and oxidation state on

reactivity and selectivity as well as the potential for similar roles of Ni^{IV}/Pd^{IV} and a complementary role for Ni^{III} in organic synthesis.

5.4. Experimental Procedures and Characterization of Compounds

5.4.1. General Procedures and Materials and Methods

General Procedures

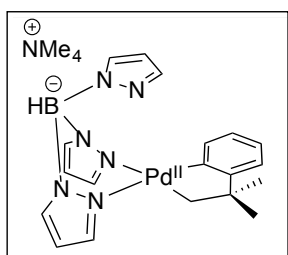
All experiments and manipulations were carried out under an inert nitrogen atmosphere using standard glovebox or Schlenk techniques unless otherwise indicated. NMR spectra were obtained on a Varian VNMR 700 (699.76 MHz for ¹H; 175.95 MHz for ¹³C), a Varian VNMR 500 (500.09 MHz for ¹H; 470.56 MHz for ¹⁹F) or a Varian VNMR 400 spectrometer (399.54 MHz for ¹H; 128.187 for ¹¹B). ¹H and ¹³C chemical shifts are reported in parts per million (ppm) relative to TMS, with the residual solvent peak as an internal reference. ¹⁹F chemical shifts and ¹¹B chemical shifts are reported in ppm and are referenced on a unified scale, where the single primary reference is the frequency of the residual solvent peak in the ¹H NMR spectrum. Abbreviations used in the NMR data: s, singlet; d, doublet; dd, doublet of doublets; t, triplet; td, triplet of doublets; m, multiplet; br, broad signal; bq, broad quartet. Cyclic voltammetry was performed using a CHI600C potentiostat from CH instruments. The electrodes were obtained from BASi. Mass spectral data were obtained on a Micromass magnetic sector mass spectrometer in electrospray ionization mode. X-ray crystallographic data were collected on a Bruker SMART APEX-I CCD-based X-ray diffractometer. Flash chromatography was conducted using a Biotage Isolera One system with cartridges containing high performance silica gel.

Materials and Methods

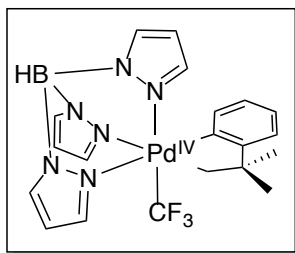
The following compounds were prepared via literature procedures: K[(Tp)Ni^{II}(CH₂CMe₂-*o*-C₆H₄)] (**1-Ni**),^{11f} Pd^{II}(CH₂CMe₂-*o*-C₆H₄)(COD),³⁰ [(Tp)Ni^{IV}(CH₂CMe₂-*o*-C₆H₄)(CF₃)] (**4-Ni**),^{11f} NMe₄SPh,^{11f} NMe₄OPh,^{13d} NMe₄N(Me)(Ms),^{11f} NMe₄Tp,^{11g} and acetylferrocenium tetrafluoroborate (AcFcBF₄).¹⁹ The spectra of complex **3-Pd** matched that reported in the literature.¹⁶ AgBF₄ was purchased from Strem Chemicals. NBu₄N₃, NMe₄OAc, *S*-(trifluoromethyl) dibenzothiophenium triflate and ferrocenium tetrafluoroborate (FcBF₄) were purchased from Aldrich. 4,4'-difluorobiphenyl was purchased from Oakwood Chemicals. Potassium trispyrazolyl borate (KTp) was purchased from Alfa Aesar. Electrochemical studies

were performed with electrochemical grade NBu_4BF_4 or NBu_4PF_6 , which were purchased from Aldrich and used without further purification. Pentane (Fisher), diethyl ether (EMD), and tetrahydrofuran (Fisher) were deaerated via a N_2 sparge and were purified by a solvent purification system. Acetonitrile (Acros) was sparged and used without further purification. Pyridine- d_6 and CD_3CN were obtained from Cambridge Isotopes Laboratories and were stored over activated 4 Å molecular sieves (EMD Millipore). Basic alumina (Aldrich) was dried for 48 h under vacuum at 210 °C. Celite was dried for 12 h under vacuum at 100 °C. Unless otherwise noted, all glassware was dried overnight in an oven at 150 °C and cooled under an inert atmosphere before use. All commercial reagents were used without further purification/drying unless explicitly stated in the experimental section. Unless otherwise noted, all manipulations were performed under an inert atmosphere in a N_2 glovebox.

5.4.2. Synthesis and Characterization of Compounds

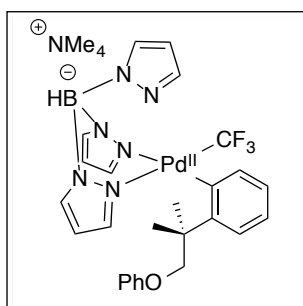


Synthesis of $\text{NMe}_4[(\text{Tp})\text{Pd}^{\text{II}}(\text{CH}_2\text{CMe}_2\text{-}o\text{-C}_6\text{H}_4)]$ (1-Pd**):** A 250 mL round bottom flask was charged with $(\text{COD})\text{Pd}(\text{CH}_2\text{CMe}_2\text{-}o\text{-C}_6\text{H}_4)^{30}$ (300 mg, 0.864 mmol, 1.0 equiv). The yellow solid was dissolved in dichloromethane (50 mL) and NMe_4Tp (260 mg, 0.907 mmol, 1.1 equiv) was added at room temperature. The light tan solution was stirred for 2 h. The crude reaction mixture was then concentrated to a tan solid, washed several times with ether (3 x 10 mL), and dried under vacuum to afford **1-Pd** as a white solid (404 mg; 89 % yield). ^1H NMR (700 MHz, CD_3CN , 23 °C) δ 8.02–7.79 (br, 2H), 7.67–7.57 (br, 2H), 7.27 (d, $J_{\text{HH}} = 7.2$ Hz, 1H), 6.80 (t, $J_{\text{HH}} = 7.2$ Hz, 1H), 6.72 (t, $J_{\text{HH}} = 7.2$ Hz, 1H), 6.69 (d, $J_{\text{HH}} = 7.2$ Hz, 1H), 6.21–6.13 (br, 1H), 4.73 (bq, B-H), 3.04 (s, 12H), 1.96 (s, 2H), 1.33 (s, 6H). ^{13}C NMR (176 MHz, CD_3CN , 23 °C) δ 168.40, 161.91, 140.44, 135.95, 134.72, 122.92, 121.46, 121.10, 103.62, 55.1, 47.31, 40.72, 33.59. ^{11}B NMR (225 MHz, CD_3CN , 23 °C) δ -1.83 (d, $J_{\text{BH}} = 112$ Hz, B-H). HRMS-electrospray (m/z): $[\text{M} - \text{NMe}_4]^+$ calcd. for $\text{C}_{19}\text{H}_{22}\text{BN}_6\text{Pd}$, 451.1034; found, 451.1067



Synthesis of [(Tp)Pd^{IV}(CH₂CMe₂-*o*-C₆H₄)(CF₃)] (4-Pd): A 20 mL vial was charged with NMe₄[(Tp)Pd^{II}(CH₂CMe₂-*o*-C₆H₄)] (1-Pd) (290 mg, 0.55 mmol, 1.0 equiv). The solid was dissolved in acetonitrile (15 mL). *S*-(Trifluoromethyl) dibenzothiophenium triflate (288 mg, 0.72 mmol, 1.3 equiv) was added at room

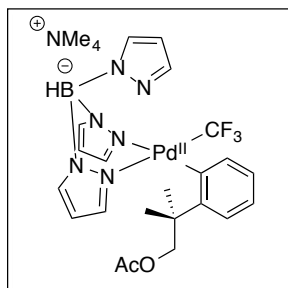
temperature and the light tan solution immediately turned orange-brown. The solvent was removed by rotary evaporation. The crude brown solid was purified by flash chromatography on silica gel (mobile phase: ethyl acetate/hexanes with a gradient from 90:10 to 70:30). The title complex was isolated as a white solid (245 mg, 86% yield). ¹H NMR (700 MHz, CD₃CN, 23 °C): δ 8.04 (d, *J*_{HH} = 1.9 Hz, 1H), 7.89 (d, *J*_{HH} = 2.3 Hz, 1H), 7.87 (d, *J*_{HH} = 2.3 Hz, 1H), 7.83 (d, *J*_{HH} = 1.9 Hz, 1H), 7.79 (d, *J*_{HH} = 2.3 Hz, 1H), 7.26 (m, 1H), 7.18 (m, 1H), 7.10 (dd, *J*_{HH} = 7.7, 1.7 Hz, 1H), 6.93 (td, *J*_{HH} = 7.7, 1.7 Hz, 1H), 6.86 (d, *J*_{HH} = 2.2 Hz, 1H), 6.42 (t, *J*_{HH} = 2.2 Hz, 1H), 6.38 (t, *J*_{HH} = 2.2 Hz, 1H), 6.14 (d, *J*_{HH} = 2.2 Hz, 1H), 4.63 (bq, **B-H**), 4.19–4.13 (multiple peaks, 2H), 1.51 (s, 3H), 1.50 (s, 3H). ¹³C NMR (176 MHz, CD₃CN, 23 °C): δ 161.23, 154.38, 141.48, 140.93, 140.40, 136.09, 136.05, 135.62, 130.95, 126.71, 126.11, 126.08, 125.85 (Pd-CF₃, shift for CF₃ group extracted from ¹⁹F–¹³C HMBC NMR spectrum), 105.96, 105.88, 105.72, 67.02, 45.94, 31.63, 31.53. ¹⁹F NMR (377 MHz, CD₃CN, 23 °C): δ –18.39. ¹¹B NMR (225 MHz, CD₃CN, 23 °C): δ –3.54 (d, *J*_{BH} = 102 Hz, **B-H**).



Synthesis of NMe₄[(Tp)Pd^{II}(C₆H₄-*o*-CMe₂CH₂OPh)(CF₃)] (6a-Pd): A 20 mL vial equipped with a magnetic stir bar was charged with [(Tp)Pd^{IV}(CH₂CMe₂-*o*-C₆H₄)(CF₃)] (4-Pd) (50 mg, 0.094 mmol, 1.0 equiv) and dissolved in acetonitrile (8 mL). NMe₄OPh (17 mg, 0.10 mmol, 1.1 equiv) was added and the resulting solution was stirred at 70 °C for 32 h. The reaction mixture was then cooled

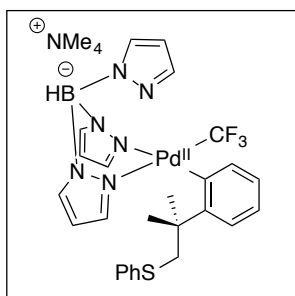
to room temperature, and solvent was removed by rotary evaporation. The resulting yellow residue was washed several times with diethyl ether (3 x 10 mL). The solids were further dried under vacuum to afford complex **6a-Pd** as a yellow solid (35 mg, 56% yield). ¹H NMR (700 MHz, CD₃CN, 23 °C) δ 7.89 (d, *J*_{HH} = 7.4 Hz, 1H), 7.77–7.66 (multiple peaks, 3H), 7.49 (d, *J*_{HH} = 2.3 Hz, 1H), 7.41 (s, 1H), 7.24 (d, *J*_{HH} = 7.9 Hz, 1H), 7.15 (t, *J*_{HH} = 7.9 Hz, 2H), 6.87 (t, *J*_{HH} = 7.5 Hz, 1H), 6.83 (t, *J*_{HH} = 7.5 Hz, 1H), 6.76 (d, *J*_{HH} = 7.8 Hz, 3H), 6.60 (s, 1H), 6.28 (s, 1H), 6.16 (s, 1H), 5.85 (s, 1H), 4.75 (bq, **B-H**), 4.35 (d, *J*_{HH} = 8.6 Hz, 1H), 4.26 (br, 1H), 3.07 (s, 12H), 1.78 (s, 3H), 1.47 (s, 3H). ¹³C NMR (176 MHz, CD₃CN, 23 °C) δ 159.80, 154.43,

150.59, 141.25, 136.98, 136.83 (Pd-CF₃, shift for CF₃ group extracted from ¹⁹F-¹³C HMBC NMR spectrum), 135.52, 135.20, 134.06, 129.07, 126.12, 122.56, 121.79, 119.65, 114.48, 103.90, 103.88, 103.61, 77.53, 55.18, 39.64, 27.03, 27.02. ¹⁹F NMR (471 MHz, CD₃CN, 23 °C) δ -18.75. ¹¹B NMR (225 MHz, CD₃CN, 23 °C) δ -2.04 (d, *J*_{BH} = 113 Hz, **B-H**). HRMS-electrospray (m/z): [M - NMe₄]⁻ calcd. for C₂₆H₂₇BF₃N₆PdO, 613.1326; found, 613.1344.



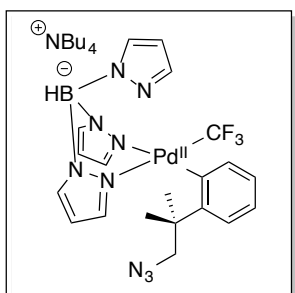
Crude Synthesis of NMe₄[(Tp)Pd^{II}(C₆H₄-*o*-CMe₂CH₂OAc)(CF₃)] (8b-Pd): A 20 mL vial equipped with a magnetic stir bar was charged with [(Tp)Pd^{IV}(CH₂CMe₂-*o*-C₆H₄)(CF₃)] (**4-Pd**) (20 mg, 0.037 mmol, 1.0 equiv) and dissolved in acetonitrile (4 mL). NMe₄OAc (24 mg, 0.19 mmol, 5 equiv) was added and the resulting solution was stirred at 70 °C for 3 weeks. The reaction mixture was

then cooled to room temperature, and solvent was removed by rotary evaporation. The resulting yellow residue was washed several times with diethyl ether (3 x 10 mL). Due to the extremely slow reactivity of NMe₄OAc and the Pd complex, this reaction required prolonged heating and excess acetate to reach only 95% conversion after the three-week time period. Complex **8b-Pd** was characterized without complete removal of excess tetramethylammonium acetate. ¹H NMR (700 MHz, CD₃CN, 23 °C): δ 7.86 (d, *J*_{HH} = 7.2 Hz, 1H), 7.83 (d, *J*_{HH} = 2.3 Hz, 1H), 7.73 (s, 1H), 7.69 (s, 1H), 7.47 (m, 1H), 7.44 (d, *J*_{HH} = 2.3 Hz, 1H), 7.14 (d, *J*_{HH} = 7.9 Hz, 1H), 6.86 (m, 1H), 6.74 (t, *J*_{HH} = 7.2 Hz, 1H), 6.56 (s, 1H), 6.30 (t, *J*_{HH} = 2.0 Hz, 1H), 6.20 (t, *J*_{HH} = 2.0 Hz, 1H), 5.93 (t, *J*_{HH} = 2.0 Hz, 1H), 4.69 (bq, **B-H**), 4.44 (d, *J*_{HH} = 10.7 Hz, 1H), 4.32 (d, *J*_{HH} = 10.7 Hz, 1H), 3.15 (s, 12H), 1.88 (s, 3H), 1.62 (s, 3H), 1.41 (s, 3H). ¹³C NMR (176 MHz, CD₃CN, 23 °C): δ 170.61, 149.85, 141.28, 137.10, 136.81 (Pd-CF₃, shift for CF₃ group extracted from ¹⁹F-¹³C HMBC NMR spectrum), 135.51, 135.09, 134.89, 134.26, 125.94, 122.53, 121.75, 103.88, 103.86, 103.58, 73.68, 55.01, 39.02, 27.11, 25.12, 20.12. ¹⁹F NMR (377 MHz, CD₃CN, 23 °C): δ -18.78. ¹¹B NMR (225 MHz, CD₃CN, 23 °C): δ -2.04 (d, *J*_{BH} = 117 Hz, **B-H**). HRMS-electrospray (m/z): [M - NMe₄]⁻ calcd. for C₂₂H₂₅BF₃N₆O₂Pd, 579.1112; found, 579.1136



Synthesis of $\text{NMe}_4[(\text{Tp})\text{Pd}^{\text{II}}(\text{C}_6\text{H}_4\text{-}o\text{-CMe}_2\text{CH}_2\text{SPh})(\text{CF}_3)]$ (6c-Pd**):** A 20 mL vial equipped with a magnetic stir bar was charged with $[(\text{Tp})\text{Pd}^{\text{IV}}(\text{CH}_2\text{CMe}_2\text{-}o\text{-C}_6\text{H}_4)(\text{CF}_3)]$ (**4-Pd**) (50 mg, 0.094 mmol, 1.0 equiv) and dissolved in acetonitrile (8 mL). NMe_4SPh (19 mg, 0.10 mmol, 1.1 equiv) was added and the resulting solution was stirred at 70 °C for 12 h. Solvent was removed by rotary evaporation.

The resulting yellow residue was washed several times with diethyl ether (3 x 10 mL). The solids were further dried under vacuum to afford complex **6c-Pd** as a yellow solid (55 mg, 84% yield). ^1H NMR (700 MHz, CD_3CN , 23 °C) δ 7.93 (d, $J_{\text{HH}} = 7.4$ Hz, 1H), 7.77 (d, $J_{\text{HH}} = 2.2$ Hz, 1H), 7.75 (s, 1H), 7.70 (s, 1H), 7.42 (d, $J_{\text{HH}} = 2.2$ Hz, 1H), 7.38 (s, 1H), 7.18 (dd, $J_{\text{HH}} = 7.9, 1.5$ Hz, 1H), 7.16–7.09 (multiple peaks, 4H), 7.03 (m, 1H), 6.86 (t, $J_{\text{HH}} = 7.2$ Hz, 1H), 6.77 (t, $J_{\text{HH}} = 7.2$, 1H), 6.60 (s, 1H), 6.29 (d, $J_{\text{HH}} = 2.2$ Hz, 1H), 6.19 (d, $J_{\text{HH}} = 2.2$ Hz, 1H), 5.84 (t, $J_{\text{HH}} = 2.2$ Hz, 1H), 4.79 (bq, *B-H*), 3.59 (d, $J_{\text{HH}} = 11.6$ Hz, 1H), 3.44 (br, 1H), 3.09 (s, 12H), 1.85 (s, 3H), 1.56 (s, 3H). ^{13}C NMR (176 MHz, CD_3CN , 23 °C) δ 154.49, 151.49, 141.31, 139.46, 137.03, 136.81 (Pd- CF_3 , shift for CF_3 group extracted from ^{19}F - ^{13}C HMBC NMR spectrum), 135.45, 133.84, 128.46, 127.42, 125.78, 124.31, 122.62, 121.68, 103.94, 103.88, 103.51, 55.17, 47.33, 39.77, 29.75, 29.12. ^{19}F NMR (471 MHz, CD_3CN , 23 °C) δ -18.78. ^{11}B NMR (225 MHz, CD_3CN , 23 °C) δ -2.04 (d, $J_{\text{BH}} = 109$ Hz, *B-H*). HRMS-electrospray (m/z): $[\text{M} - \text{NMe}_4]^+$ calcd. for $\text{C}_{26}\text{H}_{27}\text{BF}_3\text{N}_6\text{PdS}$, 629.1098; Found, 629.1116.



Crude Synthesis of $\text{NMe}_4[(\text{Tp})\text{Pd}^{\text{II}}(\text{C}_6\text{H}_4\text{-}o\text{-CMe}_2\text{CH}_2\text{N}_3)(\text{CF}_3)]$ (6e-Pd**):** A 20 mL vial equipped with a magnetic stir bar was charged with $[(\text{Tp})\text{Pd}^{\text{IV}}(\text{CH}_2\text{CMe}_2\text{-}o\text{-C}_6\text{H}_4)(\text{CF}_3)]$ (**4-Pd**) (20 mg, 0.037 mmol, 1.0 equiv) and dissolved in acetonitrile (4 mL). NBu_4N_3 (54 mg, 0.19 mmol, 5 equiv) was added and the resulting solution was stirred at 70 °C for one week. The reaction mixture was then cooled

to room temperature, and solvent was removed by rotary evaporation. The resulting yellow residue was washed several times with diethyl ether (3 x 10 mL). Due to the extremely slow reactivity of NBu_4N_3 and the Pd complex, this reaction required prolonged heating and excess azide to reach only 90% conversion after the one-week time period. Complex **6e-Pd** was characterized without complete removal of excess tetrabutylammonium azide.

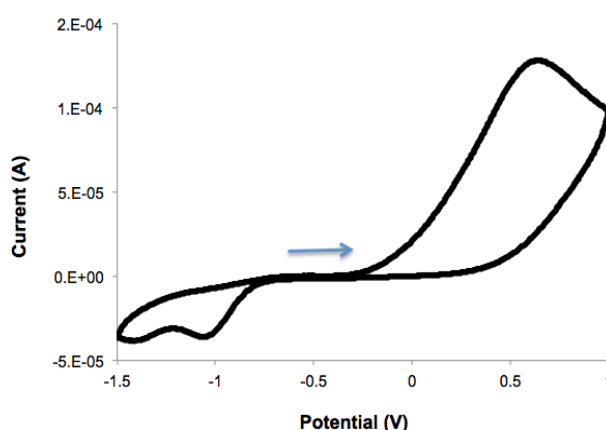
^1H NMR (700 MHz, CD_3CN , 23 °C) δ 7.97 (d, $J_{\text{HH}} = 7.4$ Hz, 1H), 7.84 (d, $J_{\text{HH}} = 2.2$ Hz, 1H), 7.81 (s, 1H), 7.66 (s, 1H), 7.49 (s, 1H), 7.35 (d, $J_{\text{HH}} = 2.2$ Hz, 1H), 7.11 (dd, $J_{\text{HH}} = 7.9, 1.5$ Hz,

1H), 6.85 (td, $J_{\text{HH}} = 7.4, 1.5$ Hz, 1H), 6.79 (td, $J_{\text{HH}} = 7.9, 1.5$ Hz, 1H), 6.52 (s, 1H), 6.33 (d, $J_{\text{HH}} = 2.1$ Hz, 1H), 6.19 (d, $J_{\text{HH}} = 2.1$ Hz, 1H), 5.94 (t, $J_{\text{HH}} = 2.1$ Hz, 1H), 4.77 (bq, **B-H**), 3.62 (d, $J_{\text{HH}} = 11.7$ Hz, 1H), 3.48 (d, $J_{\text{HH}} = 11.7$ Hz, 1H), 3.13–3.06 (m, 8H), 1.62 (overlapping peaks, 14H), 1.37 (m, 8H), 0.99 (t, $J_{\text{HH}} = 7.4$ Hz, 12 H). ^{13}C NMR (176 MHz, CD_3CN , 23 °C) δ 154.91, 149.98, 141.63, 141.08, 140.94, 136.90 (Pd- CF_3 , shift for CF_3 group extracted from ^{19}F - ^{13}C HMBC NMR spectrum), 136.84, 135.89, 135.64, 133.41, 125.91, 122.79, 121.74, 104.15, 103.80, 103.67, 62.88, 58.32, 40.06, 27.77, 27.39, 23.31, 19.32, 12.79. ^{19}F NMR (471 MHz, CD_3CN , 23 °C) δ -19.03. ^{11}B NMR (225 MHz, CD_3CN , 23 °C) δ -2.06 (d, $J_{\text{BH}} = 113$ Hz, **B-H**). HRMS-electrospray (m/z): $[\text{M} - \text{NMe}_4]^-$ calcd. for $\text{C}_{20}\text{H}_{22}\text{BF}_3\text{N}_9\text{Pd}$, 562.1078; found, 562.1093

5.4.3. Cyclic Voltammetry Studies

Experimental Procedure: Cyclic voltammetry on complex **1-Pd** was performed in a 3-electrode cell consisting of a 3 mm glassy carbon disc working electrode, a Ag/Ag^+ reference electrode with a Ag wire in a fritted chamber containing a solution of AgBF_4 (0.01 M) and NBu_4PF_6 (0.1 M) in acetonitrile, and a Pt wire counter electrode. A 2 mL solution of the complex (0.01 M) and NBu_4PF_6 (0.1 M) in acetonitrile was added to the electrochemical cell. Cyclic voltammetry scans were taken at 100 mV/s. After obtaining the CV for each complex, ferrocene was added as an internal reference.

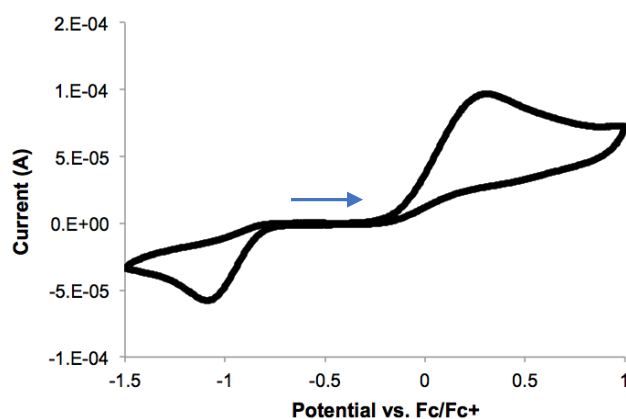
Figure 5.16. CV of **1-Pd** in the Absence of Added Pyridine. Conditions: $[\text{Pd}] = 0.01$ M in MeCN, $[\text{NBu}_4\text{PF}_6] = 0.1$ M in MeCN, Scan rate = 100 mV/s



We hypothesized that the irreversibility in the CV of complex **1-Pd** could be improved with the addition of a strong L-type ligand such as pyridine to stabilize the high-valent center. Cyclic voltammetry of complex **1-Pd** was therefore performed under the previous conditions with the

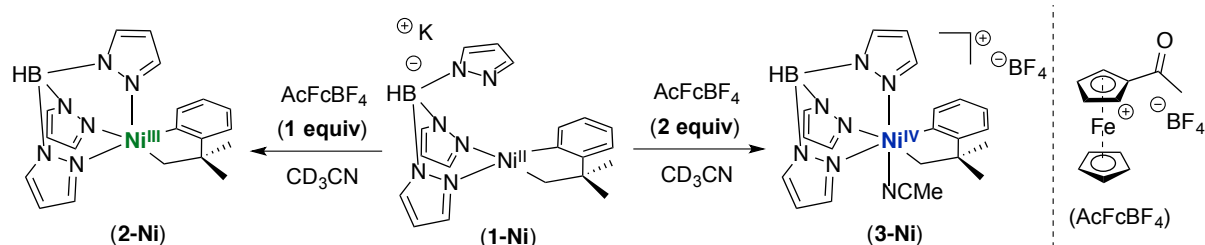
addition of 2 mL of pyridine. [Pd] = 0.005 M in a 50/50 mixture of acetonitrile/pyridine. As shown in Figure 5.17, the reversibility of the complex is improved with added pyridine.

Figure 5.17. CV of **1-Pd** with Added Pyridine. Conditions: [Pd] = 0.005 M in MeCN/pyr, [NBu₄BF₄] = 0.1 M, Scan Rate = 100 mV/s



5.4.4. NMR Oxidation Studies

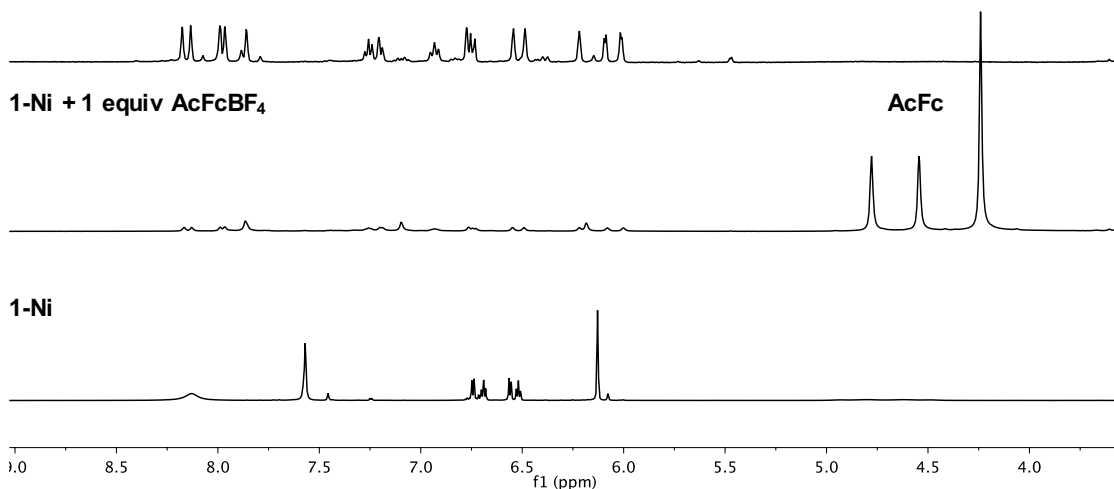
For Ni:



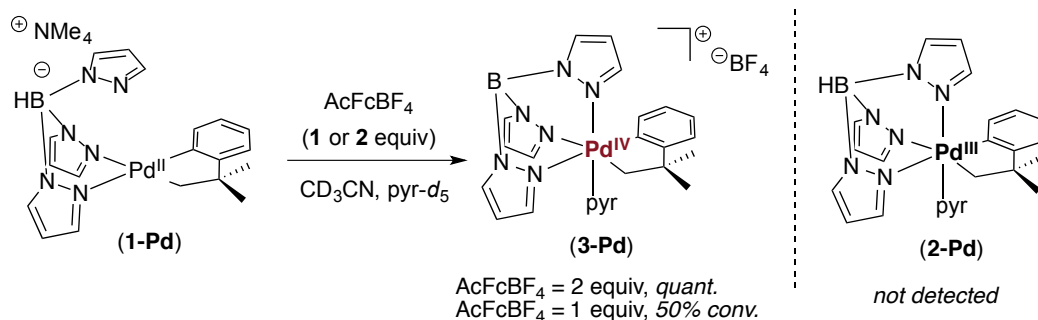
Experimental Procedure for the oxidation of 1-Ni: A 4 mL vial was charged with **1-Ni** (5.0 mg, 0.0096 mmol, 1.0 equiv) and CD₃CN (0.5 mL). This light tan solution was transferred to a screw cap NMR tube. A solution of the corresponding amount of acetylferrocenium tetrafluoroborate (AcFcBF₄; 3.0 mg, 0.0096 mmol, 1.0 equiv or 6.0 mg, 0.0192 mmol, 2 equiv) in CD₃CN was added. The tube was quickly capped, shaken vigorously, and was analyzed by ¹H NMR spectroscopy after <5 min at room temperature. In the presence of 2 equiv of AcFcBF₄, Ni^{IV} complex **3-Ni** was formed in 95% NMR yield. In the presence of 1 equiv of AcFcBF₄, analysis by ¹H NMR and ¹¹B NMR spectroscopy revealed the formation of a paramagnetic species that we previously characterized as Ni^{III} complex **2-Ni**.²⁰

Figure 5.18. ^1H NMR Spectra of **1-Ni** and the Treatment of **1-Ni** with 1 or 2 equiv of AcFcBF_4

1-Ni + 2 equiv AcFcBF_4

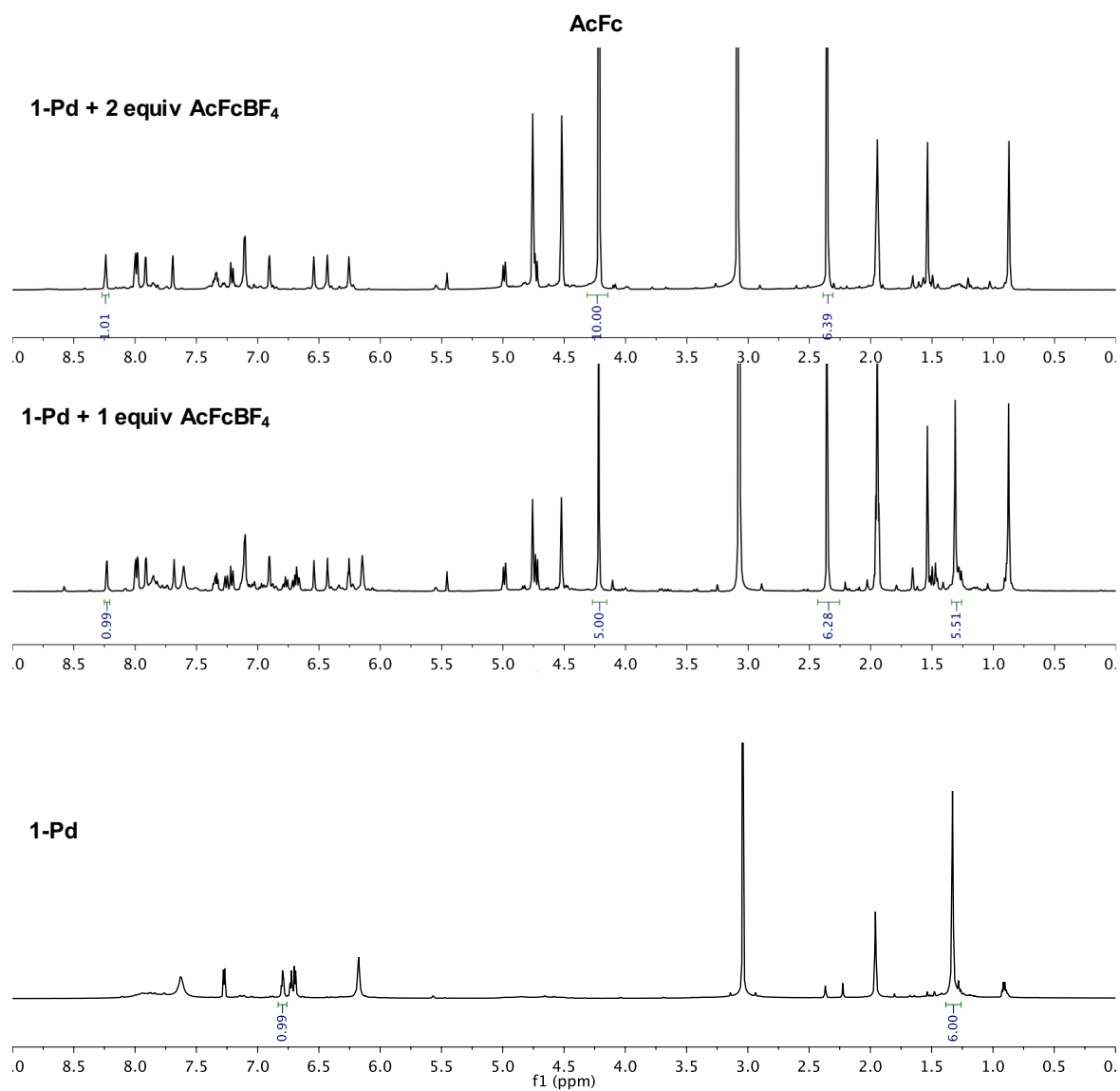


For Pd:



Experimental Procedure for the oxidation of 1-Pd: A 4 mL vial was charged with **1-Pd** (5.0 mg, 0.0096 mmol, 1.0 equiv), pyridine- d_6 (4 μL ; 0.05 mmol; 5.2 equiv), and CD_3CN (0.5 mL). This light tan solution was transferred to a screw cap NMR tube. A solution of the corresponding amount of acetylferrocenium tetrafluoroborate (AcFcBF_4 ; 3.0 mg, 0.0096 mmol, 1.0 equiv or 6.0 mg, 0.0192 mmol, 2 equiv) in CD_3CN was added. The tube was quickly capped, shaken vigorously, and was analyzed by ^1H NMR spectroscopy after <5 min at room temperature. In the presence of 2 equiv of AcFcBF_4 , Pd complex **3-Pd** was formed in approximately quantitative yield against acetylferrocene as the internal ^1H NMR standard. In the presence of 1 equiv of AcFcBF_4 Pd complex **3-Pd** was formed in approximately 50% yield against acetylferrocene as the internal ^1H NMR standard with 50% of unreacted **1-Pd** remaining.

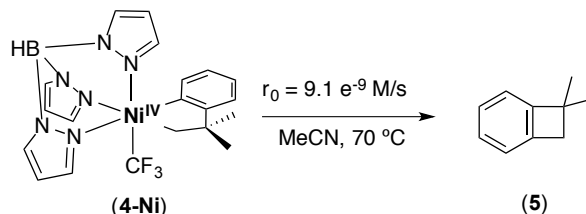
Figure 5.19. ^1H NMR Spectra of **1-Pd** and the Treatment of **1-Pd** with 1 or 2 equiv of AcFcBF_4



5.4.5. Reductive Elimination Studies

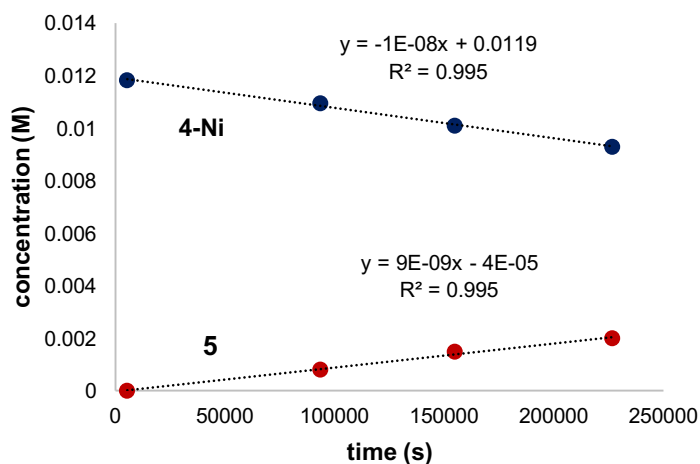
Determining Initial Rates for C–C Coupling: Ni^{IV} vs. Pd^{IV}

For Ni:

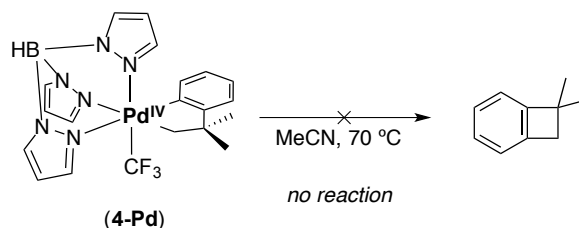


Experimental Procedure: In the glovebox, complex **4-Ni** (2.8 mg, 0.0059 mmol, 1.0 equiv) was added to a J-Young valve NMR tube equipped with an O-ring seal and then dissolved in CD₃CN (0.5 mL) at room temperature. DMSO (1.0 μL, 0.014 mmol, 2.4 equiv) was added as an internal proton standard. The NMR sample was taken out of the glovebox and analyzed by ¹H NMR spectroscopy to obtain integrations for the internal standard and complex **4-Ni**. The sample was then placed in an oil bath at 70 °C to induce reductive elimination. At various time points, the NMR sample was taken out of the oil bath and immediately cooled in an ice bath. Concentration versus time data were acquired from the integration of the methylene proton signals of **5** and **4-Ni** with respect to the internal standard. The initial rate of reductive elimination was determined by monitoring the first 10% of the reaction progress by ¹H NMR spectroscopy. Initial rate values were obtained from the slope of a linear-fit line corresponding to the growth of **5** (Figure 5.20).

Figure 5.20. Concentration vs. Time Data for Reductive Elimination of **4-Ni** to Form **5**. Starting Conditions: [Ni] = 0.011 M, T = 70 °C

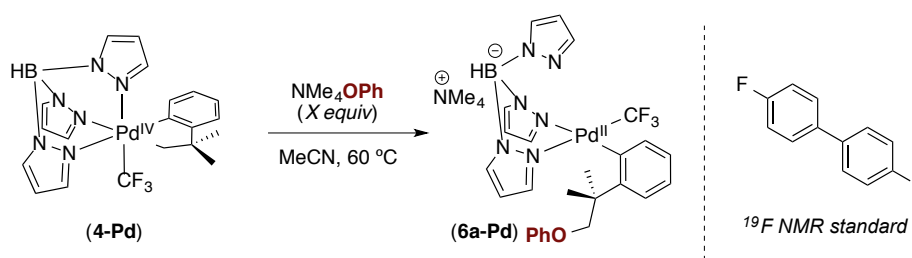


For Pd:



Experimental Procedure: In the glovebox, complex **4-Pd** (3.0 mg, 0.0059 mmol, 1.0 equiv) was added to a J-Young valve NMR tube equipped with an O-ring seal and then dissolved in CD₃CN (0.5 mL) at room temperature. DMSO (1.0 μL, 0.014 mmol, 2.4 equiv) was added as an internal proton standard. The NMR sample was placed in an oil bath at 70 °C. However, no reactivity or decomposition of **4-Pd** was observed after monitoring the reaction by ¹H NMR spectroscopy for 3 weeks.

Determining Order in Reagents for C–X Bond Formation at Pd^{IV}



Experimental Procedure: Pd^{IV} Complex **4-Pd** (3.0 mg, 0.0057 mmol, 1.0 equiv) was weighed into a J-Young valve NMR tube equipped with an O-ring seal. Various amounts of NMe₄OPh (0.0068 mmol to 0.057 mmol) and the ¹⁹F NMR standard 4,4'-difluorobiphenyl (~ 2 mg) were weighed into 4 mL vials, and the solids were dissolved in CD₃CN (0.5 mL). The resulting solution was added to the NMR tube at room temperature. The tube was then placed into an NMR spectrometer that had been pre-heated to 60 °C. The rate of reductive elimination from **4-Pd** to form **6a-Pd** was monitored by ¹⁹F NMR spectroscopy at 60 °C. Concentration versus time data were acquired by integration of the CF₃ signals of **4-Pd** and **6a-Pd** with respect to the internal standard (Figure 5.21). Initial rates were obtained from the slope of a linear-fit line monitoring the first 5-20% of the reaction progress. A plot of ln(*r*₀) vs. ln([⁻OPh]) showed that the rate of coupling is first-order in ⁻OPh (Figure 5.22).

Figure 5.21. Concentration vs. Time Data for the Reductive Elimination of **4-Pd** to Form **6a-Pd** in the Presence of 1.2, 2.5, 5, and 10 equiv of NMe_4OPh .

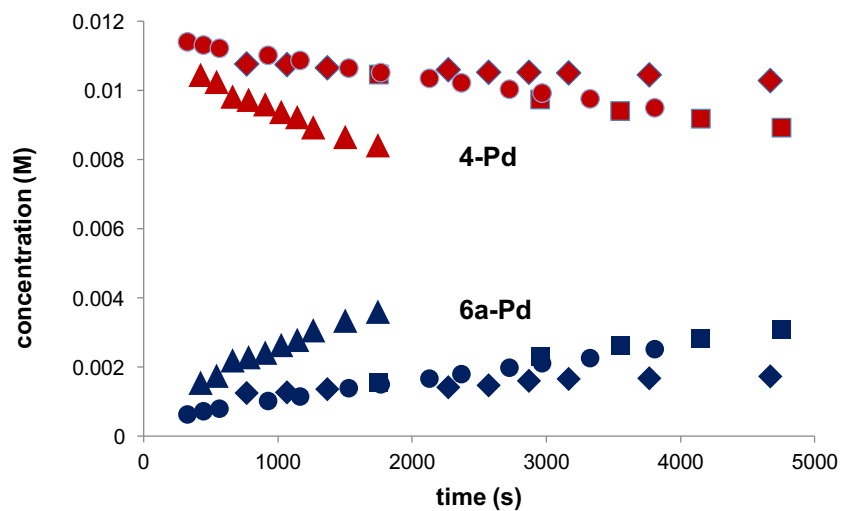
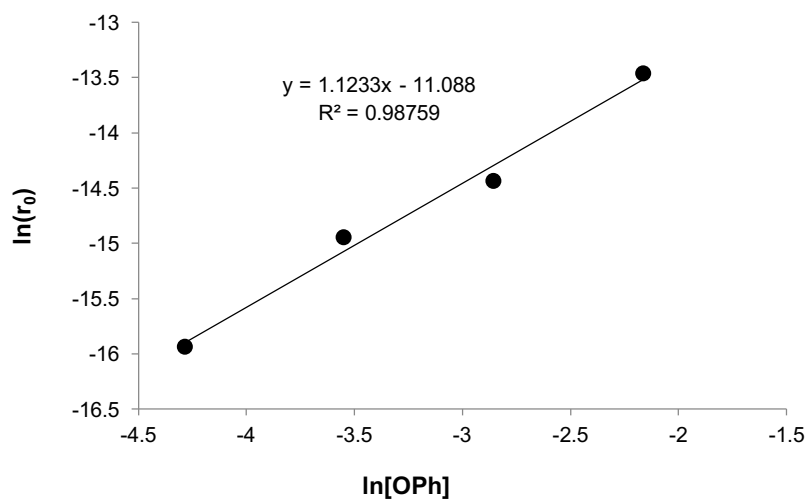
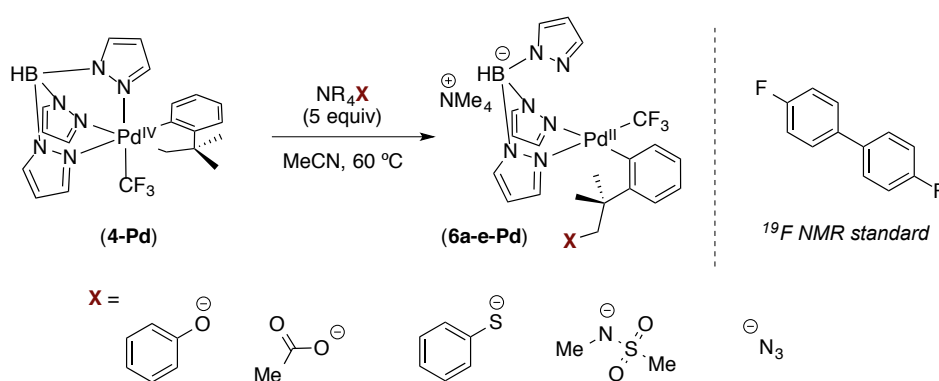


Figure 5.22. $(\ln[\text{OPh}])$ vs $(\ln[r_0])$ Plot. The slope of the line is approximately 1.



Determining Initial Rates for C-X Bond-Formation at 60 °C



Experimental Procedure: In the glovebox Pd^{IV} complex **4-Pd** (3.0 mg, 0.0057 mmol, 1.0 equiv) was added to a J-Young valve NMR tube equipped with an O-ring seal. The respective nucleophile, NR₄X, where X = OPh, OAc, SPh, N(Me)(Ms), N₃ (0.0288 mmol, 5 equiv), along with the internal standard 4,4'-difluorobiphenyl (~ 2 mg) was weighed into a 4 mL vial and then dissolved in CD₃CN (0.5 mL). The resulting solutions were added to the NMR tubes at room temperature and taken out of the glovebox. The tube was then placed into an NMR spectrometer that had been pre-heated to 60 °C. The rates of reductive elimination were determined by monitoring the first 10-40% of the reaction progress by ¹⁹F NMR spectroscopy at this temperature. Concentration versus time data were acquired from the integration of the CF₃ signals of **4-Pd** and **6-Pd** with respect to the internal standard. Initial rate values were obtained from the slope of a linear-fit line corresponding to the decay of **4-Pd**.

Figure 5.23. Concentration vs. Time Data for Reductive Elimination from **4-Pd** to Form **6a-Pd**. Starting Conditions: [Pd] = 0.011 M, [OPh] = 0.057 M, T = 60 °C

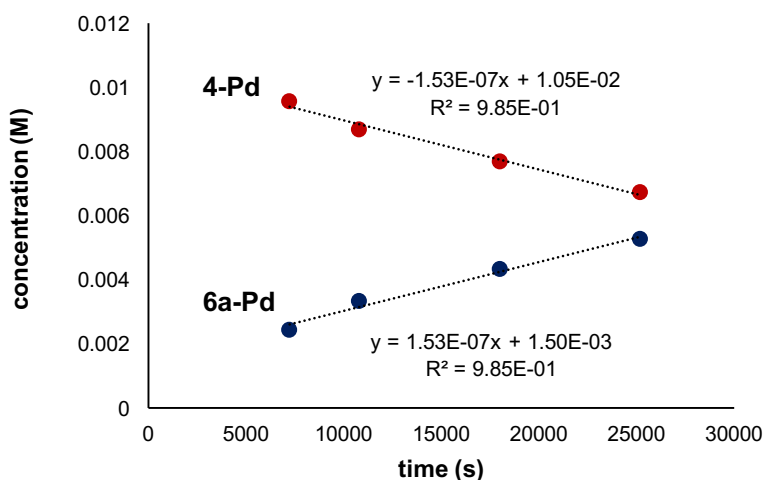


Figure 5.24. Concentration vs. Time Data for Reductive Elimination from **4-Pd** to Form **6b-Pd**. Starting Conditions: [Pd] = 0.011 M, [OAc] = 0.057 M, T = 60 °C

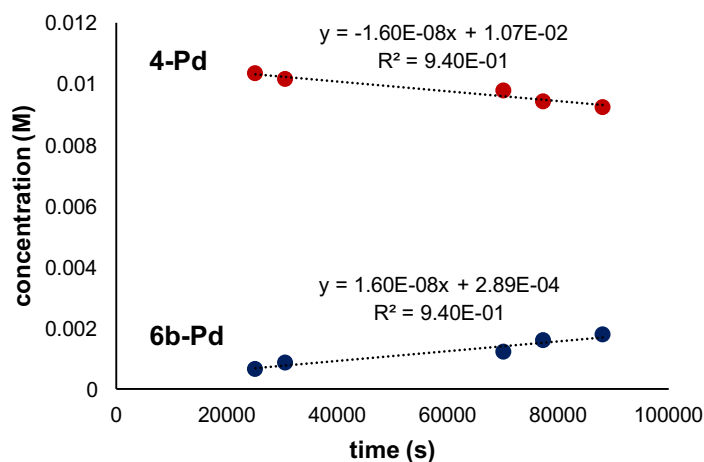


Figure 5.25. Concentration vs. Time Data for Reductive Elimination from **4-Pd** to Form **6c-Pd**. Starting Conditions: [Pd] = 0.011 M, [SPh] = 0.057 M, T = 60 °C

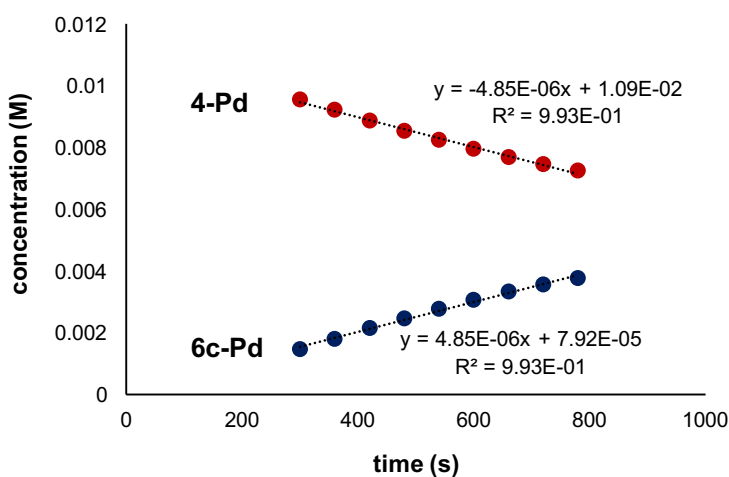


Figure 5.26. Concentration vs. Time Data for Reductive Elimination from **4-Pd** to form **6d-Pd**. Starting Conditions: [Pd] = 0.011 M, [NMeMs] = 0.057 M, T = 60 °C

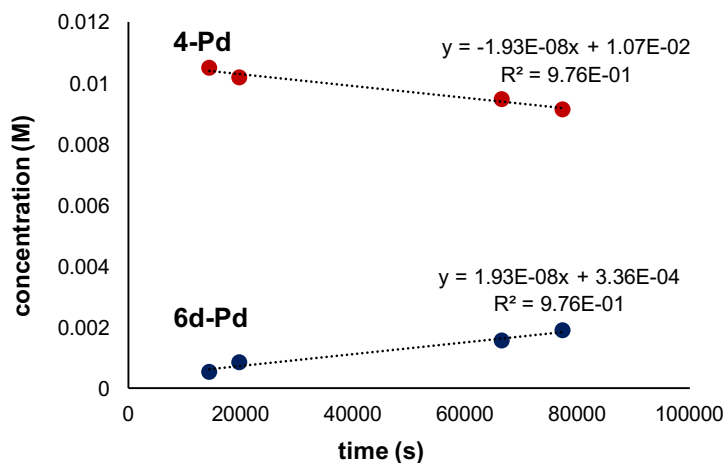
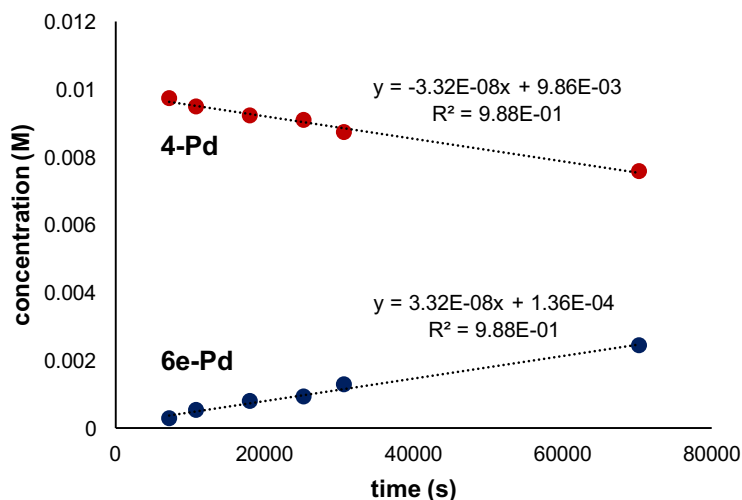


Figure 5.27. Concentration vs. Time Data for Reductive Elimination from **4-Pd** to Form **6e-Pd**. Starting Conditions: [Pd] = 0.011 M, [N₃] = 0.057 M, T = 60 °C



Nucleophilicity Values

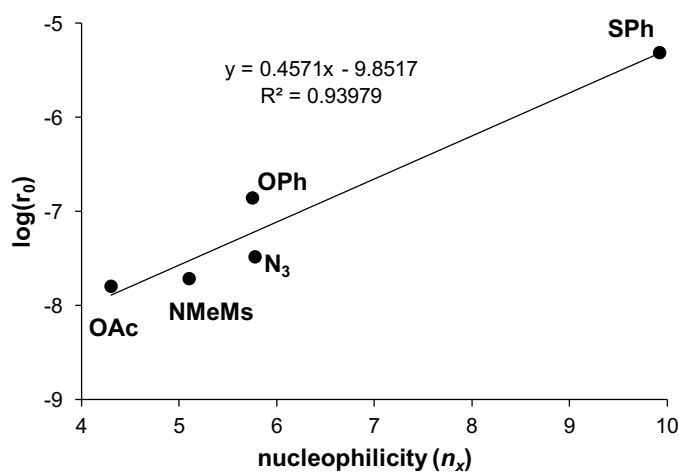
The Swain-Scott nucleophilicity parameters for the various nucleophiles (acetate, phenoxide, thiophenolate, ⁻N(Me)(Ms), and azide) were obtained from a report published by Pearson and co-workers.²⁴ The reported nucleophilicity parameters were plotted vs. experimental initial rates. The value for ⁻N(Me)(Ms) was not available and was, therefore, estimated based on the nucleophilicity value of a related sulfonamide, ⁻NHSO₂Ph.

Table 5.2. Nucleophilicity Parameters and Initial Rate Values for C–X Bond-Formation Reactions from Complex **4-Pd** to Form **6a-e-Pd**

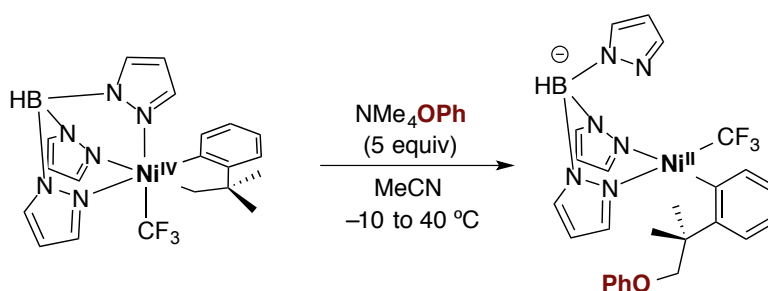
Nucleophile (X)	Nucleophilicity (<i>n_x</i>)	Initial Rate (<i>r</i> ₀) (M/s)	log(<i>r</i> ₀)
⁻ OPh	5.75	1.53e-7	-6.85
⁻ OAc	4.30	1.60e-8	-7.79
⁻ SPh	9.92	4.85e-6	-5.31
⁻ N(Me)(Ms)*	5.10	1.93e-8	-7.71
⁻ N ₃	5.78	3.32e-8	-7.45

*The nucleophilicity value for ⁻N(Me)(Ms) is an estimation based on the available *n_x* value for ⁻NHSO₂Ph.

Figure 5.28. Plot of Nucleophilicity Parameters vs. Initial Rate of C–X Coupling from **4-Pd** to form **6a-e-Pd**



Determining Activation Parameters for C–O Coupling at Ni^{IV} and Pd^{IV}

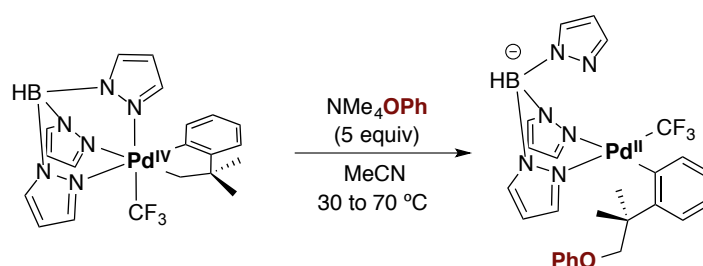


Experimental Procedure: The activation parameters for C–O coupling at Ni^{IV} were determined through an Eyring Plot in the temperature range of –10 to 40 °C. In the glovebox, complex **9** (2.6 mg, 0.0055 mmol, 1.0 equiv), NMe₄OPh (4.4 mg, 0.027 mmol, 5.0 equiv), and the ¹⁹F NMR standard 4,4-difluorobiphenyl (~2 mg) were weighed into a 4 mL vial. CD₃CN (0.5 mL) was added at –35 °C and the resulting solution was transferred to a J-Young valve NMR tube equipped with an O-ring seal at this temperature. The NMR tube was taken out of the glovebox and immediately flash frozen in an ethyl acetate/liquid nitrogen bath (–84 °C). The sample was then placed into an NMR spectrometer where the probe had been pre-set to the respective temperature (–10 to 40 °C). The rate of reductive elimination was determined by monitoring approximately the first 10% of the reaction by ¹⁹F NMR spectroscopy at –10 °C, 5 °C, 25 °C, 30 °C, and 40 °C. Concentration versus time data were acquired from the integration of the CF₃ signals of **4-Ni** and **6a-Ni** with respect to the internal standard. Initial rate values were obtained from the slope of a linear-fit line corresponding to the decay of **4-Ni**. The activation parameters for C–O coupling were extracted from the resulting Eyring Plot.

Table 5.3. Eyring Plot Data for the Reductive Elimination of **4-Ni** to Form **6a-Ni**

Temp (K)	Initial Rate (M s ⁻¹)	Rate Constant (<i>k</i>)	1/T (K ⁻¹)	ln(<i>k</i> / <i>t</i>)
263.2	1.91 x 10 ⁻⁸	2.88 x 10 ⁻⁵	0.0038	-16.02
278.2	1.22 x 10 ⁻⁷	1.84 x 10 ⁻⁴	0.0036	-14.23
298.2	1.21 x 10 ⁻⁶	1.83 x 10 ⁻³	0.0034	-12.00
303.2	2.01 x 10 ⁻⁶	3.03 x 10 ⁻³	0.0033	-11.55
313.2	4.73 x 10 ⁻⁶	7.14 x 10 ⁻³	0.0032	-10.69

For Pd:



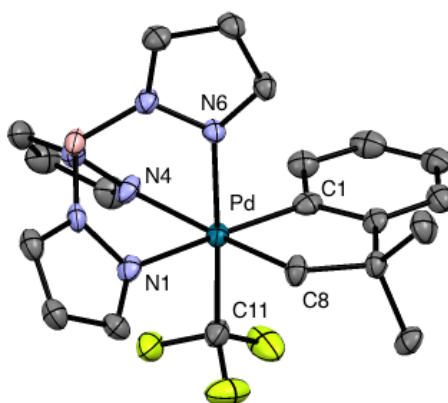
Experimental Procedure: The activation parameters for C–O coupling at Pd^{IV} were determined through an Eyring Plot in the temperature range of 30 to 70 °C. In the glovebox, complex **4-Pd** (3 mg, 0.0055 mmol, 1.0 equiv), NMe₄O^{Ph} (4.4 mg, 0.027 mmol, 5.0 equiv), and the ¹⁹F NMR standard 4,4-difluorobiphenyl (~2 mg) were weighed into a 4 mL vial. CD₃CN (0.5 mL) was added at –35 °C and the resulting solution was transferred to a J-Young valve NMR tube equipped with an O-ring seal at this temperature. The NMR tube was taken out of the glovebox and immediately flash frozen in an ethyl acetate/liquid nitrogen bath (–84 °C). The sample was then placed into an NMR spectrometer where the probe had been pre-set to the respective temperature (30 to 70 °C). The rate of reductive elimination was determined by monitoring approximately the first 10% of the reaction by ¹⁹F NMR spectroscopy at the indicated temperature. Concentration versus time data were acquired from the integration of the CF₃ signals of **4-Pd** and **6a-Pd** with respect to the internal standard. Initial rate values were obtained from the slope of a linear-fit line corresponding to the decay of **4-Pd**. The activation parameters for C–O coupling were extracted from the resulting Eyring Plot.

Table 5.4. Eyring Plot Data for the Reductive Elimination of **4-Pd** to Form **6a-Pd**

Temp (K)	Initial Rate (M s ⁻¹)	Rate Constant (<i>k</i>)	1/T (K ⁻¹)	ln(<i>k</i> / <i>t</i>)
303.2	1.31 x 10 ⁻⁸	1.98 x 10 ⁻⁵	0.0033	-16.54
313.2	2.39 x 10 ⁻⁸	3.61 x 10 ⁻⁵	0.0032	-15.97
323.2	3.34 x 10 ⁻⁸	1.11 x 10 ⁻⁴	0.0031	-14.88
333.2	2.86 x 10 ⁻⁷	4.32 x 10 ⁻⁴	0.0030	-13.56
343.2	9.33 x 10 ⁻⁷	1.41 x 10 ⁻³	0.0029	-12.40

5.4.6. X-ray Structural Determination

X-ray Crystallography Experimental Data of **4-Pd**



Colorless needles of **4-Pd** were grown from an acetone solution of the compound at 25 °C. A crystal of dimensions 0.14 x 0.12 x 0.08 mm was mounted on a Rigaku AFC10K Saturn 944+ CCD-based X-ray diffractometer equipped with a low temperature device and Micromax-007HF Cu-target micro-focus rotating anode ($\lambda = 1.54187$ Å) operated at 1.2 kW power (40 kV, 30 mA). The X-ray intensities were measured at 85(1) K with the detector placed at a distance 42.00 mm from the crystal. A total of 2028 images were collected with an oscillation width of 1.0° in ω . The exposure times were 1 sec. for the low angle images, 10 sec. for high angle. The integration of the data yielded a total of 32046 reflections to a maximum 2θ value of 136.30° of which 3856 were independent and 3643 were greater than $2\sigma(I)$. The final cell constants were based on the xyz centroids 22474 reflections above $10\sigma(I)$. Analysis of the data showed negligible decay during data collection; the data were processed with CrystalClear 2.0 and corrected for absorption. The structure was solved and refined with the Bruker SHELXTL

(version 2014/6) software package, using the space group P2(1)/c with $Z = 4$ for the formula $C_{20}H_{22}BN_6F_3Pd$. All non-hydrogen atoms were refined anisotropically with the hydrogen atoms placed in idealized positions. The $-CF_3$ group is rotationally disordered in two orientations. Full matrix least-squares refinement based on F2 converged at $R1 = 0.0573$ and $wR2 = 0.1516$ [based on $I > 2\sigma(I)$], $R1 = 0.0588$ and $wR2 = 0.1525$ for all data. Acknowledgement is made for funding from NSF grant CHE-0840456 for X-ray instrumentation.

Table 5.5. Selected Bond Lengths (Å) and Angles (°) for **4-Pd**

Pd(1)-N(1)	2.165(5)	N(1)-Pd(1)-N(4)	84.8(2)
Pd(1)-N(4)	2.217(6)	C(1)-Pd(1)-N(1)	173.4(2)
Pd(1)-N(6)	2.128(5)	C(8)-Pd(1)-N(1)	91.7(2)
Pd(1)-C(1)	2.020(6)	C(1)-Pd(1)-C(8)	82.1(2)
Pd(1)-C(8)	2.068(7)	C(1)-Pd(1)-C(11)	90.2(2)
Pd(1)-C(11)	2.036(6)	C(8)-Pd(1)-C(11)	92.1(2)

5.4.7. Computational Details

Gaussian 09^{31a} was used for DFT calculations at the B3LYP level for optimization, using the Stuttgart/Dresden ECP (SDD) basis set for Pd^{31b} and the 6-31G(d) basis set for other atoms (referred to as basis set BS1). Single point calculations were performed at the B3LYP-D3 level,^{31c,d} utilizing the quadruple- ξ valence polarized def2-QZVP^{31e} basis set on Ni and Pd along with the corresponding ECP and the 6-311+G(2d,p) basis set on other atoms (basis set BS2). All calculations were carried out for acetonitrile as solvent with the IEFPCM (SCRF) model. All thermodynamic data were calculated at the standard state (298.15 K and 1 atm) and entropy calculations were adjusted by the method proposed by Okuno.^{31f} This computational procedure has been benchmarked for palladium when applied to C \cdots C coupling from a closely related 2,2'-bipyridine (bpy) cation $[Pd^{IV}(CH_2CMe_2-o-C_6H_4-C,C')(F)(bpy-N,N')]^+$ in acetonitrile.^{13c} The triflate (OTf) salt of this cation computes as ΔG^\ddagger 24.7 kcal/mol, compared with experimental (ΔG^\ddagger 23.8 kcal/mol) and different computation procedures (ΔG^\ddagger 23.3 kcal/mol) for a sulfonamide (Tf₂N) salt.^{13e} All transition structures contained one imaginary

frequency, exhibiting atom displacements consistent with the anticipated reaction pathway. The nature of transition structures was confirmed by Intrinsic Reaction Coordinate (IRC) searches, vibrational frequency calculations, and potential energy surface scans. Natural bond order analyses³² were performed in conjunction with BS1. For studies of formation of the indolinide complex, computation for geometry optimization and single-point employed the UCAM-B3LYP and UCAM-B3LYP-D3 functionals, respectively, within the broken-symmetry unrestricted methodology to facilitate calculations for triplet and open-shell singlet configurations.

5.5. References

- (1) For select fundamental organometallic studies at Pd^{IV}, see: (a) Uson, R.; Fornies, J.; Navarro, R. *J. Organomet. Chem.* **1975**, *96*, 307. (b) Byers, P. K.; Canty, A. J.; Skelton, B. W.; White, A. H. *J. Chem. Soc., Chem. Commun.* **1986**, 1722. (c) Alsters, P. L.; Engel, P. F.; Hogerheide, M. P.; Copijn, M.; Spek, A. L.; van Koten, G. *Organometallics* **1993**, *12*, 1831. (d) Markies, B. A.; Canty, A. J.; Boersma, J.; van Koten, G. *Organometallics* **1994**, *13*, 2053. (e) van Asselt, R.; Rijnberg, E.; Elsevier, C. J. *Organometallics* **1994**, *13*, 706. (f) van Belzen, R.; Hoffmann, H.; Elsevier, C. J. *Angew. Chem., Int. Ed.* **1997**, *36*, 1743. (g) Cotton, F. A.; Gu, J.; Murillo, C. A.; Timmons, D. J. *J. Am. Chem. Soc.* **1998**, *120*, 13280. (h) Dick, A. R.; Kampf, J. W.; Sanford, M. S. *J. Am. Chem. Soc.*, **2005**, *127*, 12790. (i) Cotton, F. A.; Koshevoy, I. O.; Lahuerta, P.; Murillo, C. A.; Sanau, M.; Ubeda, M. A.; Zhao, Q. *J. Am. Chem. Soc.* **2006**, *128*, 13674. (j) Whitfield, S. R.; Sanford, M. S. *J. Am. Chem. Soc.*, **2007**, *129*, 15142. (k) Racowski, J. M.; Dick, A. R.; Sanford, M. S. *J. Am. Chem. Soc.*, **2009**, *131*, 10974. (l) Oloo, W.; Zavalij, P. Y.; Zhang, J.; Khaskin, E.; Vedernikov, A. N. *J. Am. Chem. Soc.* **2010**, *132*, 14400. (m) Vicente, J.; Arcas, A.; Julia-Hernandez, F.; Bautista, D. *Chem. Commun.* **2010**, 7253. (n) Khusnutdinova, J. R.; Rath, N. P.; Mirica, L. M. *J. Am. Chem. Soc.* **2010**, *132*, 7303. (o) Bercaw, J. E.; Durrell, A. C.; Gray, H. B.; Green, J. C.; Hazari, N.; Labinger, J. A.; Winkler, J. R. *Inorg. Chem.* **2010**, *49*, 1801. (p) Khusnutdinova, J. R.; Rath, N. P.; Mirica, L. M. *Angew. Chem. Int. Ed.* **2011**, *50*, 5532. (q) Vicente, J.; Arcas, A.; Julia-Hernandez, F.; Bautista, D. *Angew. Chem. Int. Ed.* **2011**, *50*, 6896. (r) Zhao, X.; Dong, V. M. *Angew. Chem. Int. Ed.* **2011**, *50*, 932. (s) Racowski, J. M.; Gary, J. B.; Sanford, M. S. *Angew. Chem. Int. Ed.* **2012**, *51*, 3414.
- (2) For select reviews on fundamental studies at Pd^{IV}, see: (a) Canty, A. J. *Acc. Chem. Res.* **1992**, *25*, 83. (b) Canty, A. J. *Dalton Trans.* **2009**, 10409. (c) Muñiz, K. *Angew. Chem. Int. Ed.* **2009**, *48*, 9412. (d) Xu, L. M.; Li, B. J.; Yang, Z.; Shi, Z. J. *Chem. Soc. Rev.* **2010**, *39*, 712. (e) Sehnal, P.; Taylor, R. J. K.; Fairlamb, I. J. S. *Chem. Rev.* **2010**, *110*, 824. (f) Vedernikov, A. N. *Top. Organomet. Chem.* **2010**, *31*, 101. (g) Racowski, J. M.; Sanford, M. S. *Top. Organomet. Chem.* **2011**, *35*, 61. (h) Vigalok, A. *Acc. Chem. Res.*, **2015**, *48*, 238. (i) Desnoyer, A.; Love, J. A. *Chem. Soc. Rev.* **2017**, *46*, 197.
- (3) For reviews on low-valent Pd catalysis, see: (a) Littke, A. F.; Fu, G. C. *Angew. Chem. Int. Ed.* **2002**, *41*, 4176. (b) Nicolaou, K. C.; Bulger, P. G.; Sarlah, D. *Angew. Chem. Int. Ed.* **2005**, *44*, 4442. (c) Sather, A. C.; Buchwald, S. L. *Acc. Chem. Res.* **2016**, *49*, 2146.
- (4) (a) Powers, D. C.; Ritter, T. *Nat. Chem.* **2009**, *1*, 302. (b) Powers, D. C.; Geibel, M. A. L.; Klein, J. M. E. N.; Ritter, T. *J. Am. Chem. Soc.* **2009**, *131*, 17050. (c) Khusnutdinova, J. R.; Rath, N. P.; Mirica, L. M. *Angew. Chem. Int. Ed.* **2011**, *50*, 5532. (d) Powers, D. C.; Ritter, T. *Top. Organomet. Chem.* **2011**, *35*, 129. (e) Martinez-Martinez, A.-J.; Chicote, M.-T.; Bautista, D.; Vicente, J. *Organometallics* **2012**, *31*, 3711. (f) Powers, D. C.; Lee, E.; Ariafard, A.; Sanford, M. S.; Yates, B. F.; Canty, A. J.; Ritter, T. *J. Am. Chem. Soc.* **2012**, *134*, 12002. (g) Tang, F.; Qu, F.; Khusnutdinova, J. R.; Rath, N. P.; Mirica, L. M. *Dalton Trans.* **2012**, *41*, 14046. (h) Mirica, L. M.; Khusnutdinova, J. R. *Coord. Chem. Rev.* **2013**, *257*, 299. (i) Luo, J.; Rath, N. P.; Mirica, L. M. *Organometallics* **2013**, *32*, 3343. (j) Canty, A. J.; Sanford, M. S.; Ariafard, A.; Yates, B. F. *Organometallics* **2013**, *32*, 544.
- (5) For select reviews on Pd^{IV} in catalysis, see: (a) Muniz, K. *Angew. Chem. Int. Ed.* **2009**, *48*, 9412. (b) Lyons, T.; Sanford, M. S. *Chem. Rev.* **2010**, *110*, 1147. (c) Hickman, A. J.; Sanford, M. S. *Nature* **2012**, *484*, 177. (d) Engle, K. M.; Mei, T.-S.; Wasa, M.; Yu, J.-Q.

- Acc. Chem. Res.* **2012**, *45*, 788. (e) Topczewski, J. T.; Sanford, M. S. *Chem. Sci.*, **2015**, *6*, 70.
- (6) (a) Meijere, A. d.; Diederich, F. *Metal-Catalyzed Cross-Coupling Reactions*; Wiley-VCH: Weinheim, 2004. (b) Hu, X. *Chem. Sci.* **2011**, *2*, 1867. (c) Rosen, B. M.; Quasdorf, K. W.; Wilson, D. A.; Zhang, N.; Resmerita, A-M.; Garg, N. K.; Percec, V. *Chem Rev.* **2011**, *111*, 1346. (d) Montgomery, J. "Organonickel Chemistry" in *Organometallics in Synthesis: Fourth Manual* Lipshutz, B. H. (Ed.) Wiley, Hoboken, N.J., **2013**, pp. 319-428. (e) Tasker, S. Z.; Standley, E. A.; Jamison, T. F. *Nature* **2014**, *509*, 299. (f) Everson, D. A.; Weix, D. J. *J. Org. Chem.* **2014**, *79*, 4793. (g) Ananikov, V. *ACS Catal.*, **2015**, *5*, 1964.
- (7) (a) Zultanski, S. L.; Fu, G. C. *J. Am. Chem. Soc.* **2013**, *135*, 624. (b) Iwasaki, T.; Kambe, N. *Top. Curr. Chem.* **2016**, *374*, 66. (c) Serrano, E.; Martin, R. *Angew. Chem. Int. Ed.* **2016**, *55*, 11207. (d) Chu, C. K.; Liang, Y.; Fu, G. C. *J. Am. Chem. Soc.*, **2016**, *138*, 6404.
- (8) (a) Dankwardt, J. W. *Angew. Chem. Int. Ed.* **2004**, *43*, 2428. (b) Rosen, B. M.; Quasdorf, K. W.; Wilson, D. A.; Zhang, N.; Resmerita, A-M.; Garg, N. K.; Percec, V. *Chem. Rev.* **2011**, *111*, 1346. (c) Li, B.-J.; Yu, D.-G.; Sun, C.-L.; Shi, Z.-J. *Chem. Eur. J.* **2011**, *17*, 1728. (d) Chatani, N. *Top. Curr. Chem.* **2016**, *374*, 41.
- (9) Rare example of Pd-catalyzed cross-coupling of alkyl bromides: Peacock, D. M.; Roos, C. B.; Hartwig, J. F. *ACS Cent. Sci.*, **2016**, *2*, 647.
- (10) (a) Grove, D. M.; van Koten, G.; Zoet, R.; Murrall, N. W.; Welch, A. J. *J. Am. Chem. Soc.* **1983**, *105*, 1379. (b) Grove, D. M.; van Koten, G.; Mul, W. P.; van der Zeijden, A. A. H.; Terheijden, J. *Organometallics* **1986**, *5*, 322 (c) Grove, D. M.; van Koten, G.; Mul, P.; Zoet, R.; van der Linden, J. G. M.; Letgers, J.; Schmitz, J. E. J.; Murrall, N. W.; Welch, A. J. *Inorg. Chem.* **1988**, *27*, 2466 (d) van de Kuil, V. A.; Veldhuizen, Y. S. J.; Grove, D. M.; Zwikker, J. L.; Jenneskens, L. W.; Drenth, W.; Smeets, W. J. J.; Spek, A. L.; van Koten, G. *J. Organomet. Chem.* **1995**, *488*, 191. (e) Pandarus, V.; Zargarian, D. *Organometallics* **2007**, *26*, 4321. Castonguay, A.; Beauchamp, A.; Zargarian, D. *Organometallics* **2008**, *27*, 5723. (f) Higgs, A. T.; Zinn, P. J.; Sanford, M. S. *Organometallics* **2009**, *28*, 6142. (g) Higgs, A. T.; Zinn, P. J.; Sanford, M. S. *Organometallics* **2010**, *29*, 5446. (h) Lee, C. M.; Chen, C. H.; Liao, F. X.; Hu, C. H.; Lee, G. H. *J. Am. Chem. Soc.* **2010**, *132*, 9256. (i) Lipschutz, M. I.; Yang, X.; Chatterjee, R.; Tilley, T. D. *J. Am. Chem. Soc.* **2013**, *135*, 15298. (j) Breitenfeld, J.; Woodrich, M.; Hu, X. *Organometallics* **2014**, *33*, 5708. (k) Zheng, B.; Tang, F.; Luo, J.; Schultz, J. W.; Rath, N. P.; Mirica, L. M. *J. Am. Chem. Soc.* **2014**, *136*, 6499. (l) Tang, F.; Rath, N. P.; Mirica, L. M. *Chem. Commun.* **2015**, *51*, 3113. (m) Yu, S.; Dudkina, Y.; Wang, H.; Kholin, K. V.; Budnikova, V.; Vicic, D. A. *Dalton Trans.* **2015**, *44*, 19443. (n) Cloutier, J-P.; Vabre, B.; Mounang-Soumé, B.; Zargarian, D. *Organometallics* **2015**, *34*, 133. (o) Zhou, W.; Schultz, J. W.; Rath, N. P.; Mirica, L. M. *J. Am. Chem. Soc.* **2015**, *137*, 7604 (p) Zhou, W.; Rath, N. P.; Mirica, L. M. *Dalton Trans.* **2016**, *45*, 8693 (q) Xu, H.; Diccianni, J. B.; Katigbak, J.; Hu, C.; Zhang, Y.; Diao, T. *J. Am. Chem. Soc.* **2016**, *138*, 4779. (r) Schultz, J. W.; Fuchigami, K. Zheng, B. Rath, N. P.; Mirica, L. M. *J. Am. Chem. Soc.* **2016**, *138*, 12928. (s) Zhou, W.; Zheng, S. A.; Schultz, J. W.; Rath, N. P.; Mirica, L. M. *J. Am. Chem. Soc.* **2016**, *138*, 5777. (t) Watson, M. B.; Rath, N. P.; Mirica, L. M. *J. Am. Chem. Soc.* **2017**, *139*, 35
- (11) (a) Klein, H.-F.; Bickelhaupt, A.; Jung, T.; Cordier, G. *Organometallics* **1994**, *13*, 2557. (b) Klein, H. F.; Bickelhaupt, A.; Lemke, M.; Sun, H. J.; Brand, A.; Jung, T.; Rohr, C.; Florke, U.; Haupt, H. J. *Organometallics* **1997**, *16*, 668. (c) Shimada, S.; Rao, M. L. N.; Tanaka, N. *Organometallics* **1999**, *18*, 291. (d) Dimitrov, V.; Linden, A. *Angew. Chem., Int. Ed.* **2003**, *42*, 2631. (e) Carnes, M.; Buccella, D.; Chen, J. Y. C.; Ramirez, A. P.; Turro, N. J.; Nuckolls, C.; Steigerwald, M. *Angew. Chem. Int. Ed.* **2009**, *48*, 290. (f) Camasso, N. M.; Sanford, M. S. *Science* **2015**, *136*, 12771. (g) Bour, J. R.; Camasso, N. M.; Sanford,

- M. S. *J. Am. Chem. Soc.* **2015**, *137*, 8034. (h) Martinez, G. E.; Ocampo, C.; Park, Y. J.; Fout, A. R. *J. Am. Chem. Soc.* **2016**, *138*, 4290. Schultz, J. W.; Fuchigami, K.; Zheng, B.; Rath, N. P.; Mirica, L. M. *J. Am. Chem. Soc.* **2016**, *138*, 12928. (i) Watson, M. B.; Rath, N. P.; Mirica, L. M. *J. Am. Chem. Soc.* **2017**, *139*, 35. (j) Meucci, E. A.; Camasso, N. M.; Sanford, M. S. *Organometallics* **2017**, *36*, 247.
- (12) (a) Lin, B.-L.; Liu, L.; Fu, Y.; Luo, S.-W.; Chen, Q.; Guo, Q.-X. *Organometallics* **2004**, *23*, 2114. (b) Ackerman, L. K. G.; Lovell, M. M.; Weix, D. J. *Nature* **2015**, *524*, 454.
- (13) (a) Campora, J.; Palma, P.; del Rio, D.; Lopez, J. A.; Valerga, P. *Chem. Commun.* **2004**, *13*, 1490 (b) Qu, F.; Khusnutdinova, J. R.; Rath, N. P.; Mirica, L. M. *Chem. Commun.* **2014**, *50*, 3036. (c) Pérez-Temprano, M. H.; Racowski, J. M.; Kampf, J. W.; Sanford, M. S. *J. Am. Chem. Soc.* **2014**, *136*, 4097. (d) Camasso, N. M.; Pérez-Temprano, M. H.; Sanford, M. S. *J. Am. Chem. Soc.* **2014**, *136*, 12771. (e) Pendleton, I. M.; Pérez-Temprano, M. H.; Sanford, M. S.; Zimmerman, P. M. *J. Am. Chem. Soc.* **2016**, *138*, 6049.
- (14) Pd^{IV} and Pt^{IV} tris(pyrazoyl)borate complexes: (a) O'Reilly, S. A.; White, P. S.; Templeton, J. L. *J. Am. Chem. Soc.* **1996**, *118*, 5684. (b) Canty, A. J.; Jin, H.; Roberts, A. S.; Skelton, B. W.; White, A. H. *Organometallics* **1996**, *15*, 5713. (c) Canty, A. J.; Jin, H.; Penny, J. D. *J. Organomet. Chem.* **1999**, *573*, 30. (d) Reinartz, S.; White, P. S.; Brookhart, M.; Templeton, J. L. *J. Am. Chem. Soc.* **2001**, *123*, 6425. (e) Campora, J.; Palma, P.; del Rio, D.; Carmona, E. *Organometallics* **2003**, *22*, 3345. (f) Campora, J.; Palma, P.; del Rio, D.; Lopez, J. A.; Alvarez, E. *Organometallics* **2005**, *24*, 3624. (g) Maleckis, A.; Sanford, M. S. *Organometallics* **2011**, *30*, 6617.
- (15) Jude, H.; Krause Bauer, J. A.; Connick, W. B. *J. Am. Chem. Soc.* **2003**, *125*, 3446.
- (16) Campora, J.; Palma, P.; del Rio, D.; Lopez, J. A.; Alvarez, E.; Connelly, N. G. *Organometallics*, **2005**, *24*, 3624.
- (17) (a) Albright, T. A. *Tetrahedron* **1982**, *38*, 1339. (b) Albright, T. A.; Burdett, J. K. Whangbo, M.-H. *Orbital Interactions in Chemistry*, 2nd ed.; Wiley: Hoboken, NJ, 2013; pp 401–463. (c) Miessler, G. L.; Fischer, P. J.; Tarr, D. A. *Inorganic Chemistry*, 5th ed.; Pearson/Prentice Hall: Upper Saddle River, NJ, 2014; pp 365–382.
- (18) Geiger, W. E. *Organometallics* **2007**, *26*, 5738.
- (19) Connelly, N. G.; Geiger, W. E. *Chem. Rev.* **1996**, *96*, 877
- (20) Bour, J. R.; Camasso, N. M.; Meucci, E. A.; Kampf, J. W.; Canty, A. J.; Sanford, M. S. *J. Am. Chem. Soc.* **2016**, *138*, 16105.
- (21) (a) Ye Y.; Ball, N. D.; Kampf, J. W.; Sanford, M. S. *J. Am. Chem. Soc.* **2010**, *132*, 14682. (b) Ball, N. D.; Gary, J. B.; Ye Y.; Sanford, M. S. *J. Am. Chem. Soc.*, **2011**, *133*, 7577.
- (22) The Ni^{IV}–CF₃ bond length is within the range of reported Ni^{IV}–CF₃ and Ni^{III}–CF₃ bond distances (1.920–1.965 Å), see references 10 and 11.
- (23) Complexes 6b-Pd, 6d-Pd, and 6e-Pd were characterized *in-situ* with residual tetraalkylammonium salt in the crude reaction mixture.
- (24) (a) Swain, C. G.; Scott, C. B. *J. Am. Chem. Soc.* **1953**, *75*, 141. (b) Pearson, R. G.; Sobel, H. R.; Songstad, J. *J. Am. Chem. Soc.* **1968**, *90*, 319.
- (25) For studies of C(sp³)-heteroatom reductive elimination at Pt see: (a) Luinstra, G. A.; Labinger, J. A.; Bercaw, J. E. *J. Am. Chem. Soc.*, **1993**, *115*, 3004. (b) Williams, B. S.; Holland, A. W.; Goldberg, K. I. *J. Am. Chem. Soc.* **1999**, *121*, 252. (c) Williams, B. S.; Goldberg, K. I. *J. Am. Chem. Soc.* **2001**, *123*, 2576. (d) Canty, A. J.; Denney, M. C.; van Koten, G.; Skelton, B. W.; White, A. H. *Organometallics* **2004**, *23*, 5432. (e) Vedernikov, A. N.; Binfield, S. A.; Zavalij, P. Y.; Khusnutdinova, J. R. *J. Am. Chem. Soc.* **2006**, *128*, 82. (f) Khusnutdinova, J. R.; Zavalij, P. Y.; Vedernikov, A. N. *Organometallics*, **2007**, *26*, 3466. (g) Pawlikowski, A. V.; Getty, A. D.; Goldberg, K. I. *J. Am. Chem. Soc.* **2007**, *129*, 10382. (h) Smythe, N. A.; Grice, K. A.; Williams, B. S.; Goldberg, K. I. *Organometallics*

-
- 2009**, 28, 277. (i) Khusnutdinova, J. R.; Newman, L. L.; Zavalij, P. Y.; Lam Y.-F.; Vedernikov, A. N. *J. Am. Chem. Soc.* **2008**, 130, 2174. (j) Vedernikov, A. N. *Chem. Commun.* **2009**, 32, 4781. (k) Vedernikov, A. N. *Acc. Chem. Res.* **2012**, 45, 803.
- (26) (a) K. L. Bartlett, K. I. Goldberg, W. T. Borden, *Organometallics* **2001**, 20, 2669; (b) Michel, C.; Laio, A.; Mohamed, F.; Krack, M.; Parrinello, M.; Milet, A. *Organometallics* **2007**, 26, 1241. (c) Fu, Y.; Li, Z.; Liang, S.; Guo, Q.-X.; Liu, L. *Organometallics* **2008**, 27, 3736.
- (27) Bondi, A. *J. Phys. Chem.* **1964**, 68, 441.
- (28) For intermolecular alkyl azide insertions into Ni^{II}-C bonds, see: Koo, K.; Hillhouse, G. L. *Organometallics* **1995**, 14, 4421.
- (29) For select examples of nickel catalyzed C-C and C-heteroatom coupling reactions invoking Ni^{III} intermediates, see: (a) Jones, G. D.; Martin, J. L.; McFarland, C.; Allen, O. R.; Hall, R. E.; Haley, A. D.; Brandon, R. J.; Konovalova, T.; Desrochers, P. J.; Pulay, P.; Vicic, D. A. *J. Am. Chem. Soc.* **2006**, 128, 13175. (b) Zultanski, S.; Fu, G. C. *J. Am. Chem. Soc.* **2011**, 133, 15362. (c) Hu, X. *Chem. Sci.* **2011**, 2, 1867. (d) Joshi-Pangu, A.; Wang, C.-Y.; Biscoe, M. R. *J. Am. Chem. Soc.* **2011**, 133, 847. (e) Dudnik, A. S.; Fu, G. C. *J. Am. Chem. Soc.* **2012**, 134, 10693. (f) Dai, Y. J.; Wu, F.; Zang, Z. H.; You, H. Z.; Gong, H. G. *Chem. Eur. J.* **2012**, 18, 808. (g) Schley, N. D.; Fu, G. C. *J. Am. Chem. Soc.* **2014**, 136, 16588. (h) Aihara, Y.; Tobisu, M.; Fukumoto, Y.; Chatani, N. *J. Am. Chem. Soc.* **2014**, 136, 15509. (i) Wu, X.; Zhao, Y.; Ge, H. *J. Am. Chem. Soc.* **2014**, 136, 1789. (j) Tellis, J. C.; Primer, D. N.; Molander, G. A. *Science* **2014**, 345, 433. (k) Zuo, Z.; Ahneman, D. T.; Chu, L.; Terrett, J. A.; Doyle, A. G.; MacMillan, D. W. C. *Science* **2014**, 345, 437. (l) Cornella, J.; Edwards, J. T.; Qin, T.; Kawamura, S.; Wang, J.; Pan, C.-M.; Gianatassio, R.; Schmidt, M. A.; Eastgate, M. D.; Baran, P. S. *J. Am. Chem. Soc.* **2016**, 138, 2174. (m) Gui, Y.-Y.; Sun, L.; Lu, Z.-P.; Yu, D.-G. *Org. Chem. Front.* **2016**, 3, 522. (n) Shields, B. J.; Doyle, A. G. *J. Am. Chem. Soc.* **2016**, 138, 12719.
- (30) Campora, J.; Lopez, J. A.; Palma, P.; Rio, D.; Carmona, E.; Valerga, P.; Graiff, C.; Tiripicchio, A. *Inorg. Chem.* **2001**, 40, 4116.
- (31) (a) Frisch, M. J.; et al. *Gaussian 09*, revision A.02; Gaussian, Inc.: Wallingford, CT, 2009. (b) Andrae, H.; Haussermann, U.; Dolg, M.; Stoll, H.; Preuss, H. *Theor. Chim. Acta* **1990**, 77, 123. (c) Ehrlich, S.; Moellmann, J.; Grimme, S. *Acc. Chem. Res.* **2013**, 46, 916. (d) Antony, J.; Sure, R.; Grimme, S. *Chem. Commun.* **2015**, 51, 1764. (e) Weigend, F.; Furche, F.; Aldrichs, R. *J. Chem. Phys.* **2003**, 119, 12753. (f) Okuno, Y. *Chem. Eur. J.* **1997**, 3, 212.
- (32) Glendening, E. D.; Read, A. E.; Carpenter, J. E.; Weinhold, F. *NBO*, version 3.1; Gaussian Inc.; Pittsburgh, PA, **2003**.